INFLUENCE OF NANO-TiO_2 ADDITION ON THE ENVIRONMENTAL PERFORMANCE OF CEMENTITIOUS COMPOSITES: A HOLISTIC APPROACH

by

Carlos Moro

A Dissertation

Submitted to the Faculty of Purdue University

In Partial Fulfillment of the Requirements for the degree of

Doctor of Philosophy

Lyles School of Civil Engineering

West Lafayette, Indiana

December 2021

THE PURDUE UNIVERSITY GRADUATE SCHOOL

STATEMENT OF COMMITTEE APPROVAL

Dr. Maria Mirian Velay Lizancos, Chair

Lyles School of Civil Engineering

Dr. Jan Olek

Lyles School of Civil Engineering

Dr. Brandon E. Boor

Lyles School of Civil Engineering

Dr. Ramses V. Martínez

Industrial and Biomedical Engineering

Approved by:

Dr. Dulcy M. Abraham

Dedicated to my parents, grandparents, Jorge and Miranda

ACKNOWLEDGEMENTS

I would first like to thank my mentor, advisor, and academic mother, Prof. Mirian Velay-Lizancos. I have no words to express my gratitude for convincing me to do the Ph.D. I am delighted that you pushed me to do better for the last four years. I will keep every single piece of advice that I received from you, and I hope I could be a mentor as good as you someday, or at least half of it.

Next, I would like to acknowledge my committee members, Prof. Jan Olek, Prof. Brandon Boor, and Prof. Ramses Martinez, for their invaluable supervision, support, and knowledge received during my studies. I really appreciate it.

I must express my very profound gratitude to our big family in the Lyles School of Civil Engineering at Purdue University for their support throughout my Ph.D. studies, especially my office and lab mates: Alberto, Anan, Dan, Fabian, Hyungu, Marina, Masoud. Miguel, Raikhan, and Romika. I wish you the best in your promising future.

I would also thank all my friends made along the way. I definitely had a fantastic time with all of you guys, particularly with our trattoria italo-española (Riccardo, Sara, Vito, Fabrizio and, of course, Antonio included) with our famous arguments about the most famous dessert, how to cut jamón, and a long list of etcetera. Special thanks to my big brother Vito; my door will be always opened to you.

I cannot forget all the support received from my old friends, David, Diego, Luis, Miguel, and my athletics family in Riazor Coruña (Julio, Quique, Pepe, Tere, and everybody else). In our global world, the most important thing is not how many friends you can count, but how many of those you can count on. Thank you all.

I would also like to acknowledge my family for their continuous love and support. Many thanks also to my grandparents (Elvira, Irene, Jesus and Toto) for every special moment we have spent together. And, of course, thank you Jorge, mum and dad for all these years. I would not have become the person I am today without all of you. I love you so much.

Lastly, to you, Miranda, thank you for these three and a half years of unconditional and sincere love. Thanks for your patience. I am looking forward to the first chapter of our bright future. Love you so much!

TABLE OF CONTENTS

LIST OF TABLES

LIST OF FIGURES

LIST OF ABBREVIATIONS

ADP	-	Abiotic depletion potential
AFM	-	Aluminate ferrite monosulfate
ANN	-	Artificial neural network
AP	-	Acidification potential
C_2H_4	-	Ethylene or ethene
C_3S	-	Alite or tricalcium silicate
C_2S	-	Belite or dicalcium silicate
$CaCO_3$	-	Calcium carbonate
CC	-	CO_2 curing
CFC-11	-	Trichlorofluoromethane or freon-11
CFC-114	-	1,2-Dichlorotetrafluoroethane, R-114 or cryofluorane
CH or $Ca(OH)_2$	-	Calcium hydroxide or Portlandite
CH_4	-	Methane
CIELab	-	Commission Internationale de l'Éclairage
CO	-	Carbon monoxide
CO_2	-	Carbon dioxide
CO_x	-	Carbon oxides
C-S-H	-	Calcium silica hydrate
D_c	-	Carbonation degree
DGWP	-	Dynamic global warming potential
EC	-	Energy consumption
EIA	-	U.S. Energy Information Administration
ELCD	-	European Platform on Life Cycle Assessment
EP	-	Eutrophication potential
EPA	-	U.S. Environmental Protection Agency
GGBFS	-	Ground granulated blast-furnace slag
GHG	-	Greenhouse gases
GWP	-	Global warming potential
HCl	-	Hydrogen chloride

ITZ	-	Interfacial transition zone
LCA	-	Life cycle assessment
LCI	-	Life cycle inventory
LCIA	-	Life cycle impact assessment
N	-	Nitrogen
N_2O	-	Nitrous oxide
NA	-	Natural aggregate
nano-TiO_2	-	Titanium dioxide nanoparticles
NC	-	Normal curing
NH_3	-	Ammonia
NMVOC	-	Non-methane volatile organic compound
NF	-	Normalization factor
NO_x	-	Nitrogen oxides
PO_4^{-3}	-	Phosphate
POCP	-	Photochemical ozone creation potential
ODP	-	Ozone depletion potential
OPC	-	Ordinary Portland cement
RA	-	Recycled aggregate
RE	-	Respiratory effects
RH	-	Relative humidity
RhB	-	Rhodamine B
S	-	Smog formation
SCM	-	Supplementary cementitious materials
SEM	-	Scanning electron microscope
SO_x	-	Sulfur oxides
T	-	Temperature
TEM	-	Transmission electron microscopy
TGA	-	Thermogravimetric analysis
TRACI	-	Tool for the reduction and assessment of chemical and other environmental impacts
UV light	-	Ultraviolet light
VOCs	-	Volatile organic compounds

w/b	-	Water-to-binder ratio
w/c	-	Water-to-cement ratio
WG	-	Waste generation
XRD	-	X-Ray powder diffraction
XRM	-	X-Ray microscope

ABSTRACT

Cement is one of the main compounds of concrete, the most consumed construction material globally. Cement manufacturing is responsible for around 8% of the total carbon dioxide (CO_2) emissions each year globally. Besides cement, concrete production requires a significant volume of aggregates and water. Over 8 billion m^3 of aggregates are used to produce 30 billion tons of concrete and other cementitious composites such as mortar every year. Thus, these cementitious composites have a significant environmental impact, and a small step in improving their environmental performance could lead to a giant leap in terms of global sustainability. It is known that the TiO_2 nanoparticles (nano-TiO_2) addition provides the cementitious composites the ability to reduce different pollutants concentrations (e.g., nitrogen oxides (NO_x) or volatile organic compounds (VOCs)) due to its photocatalytic activity. A preliminary study from Velay's Research group suggested that TiO_2 nanoparticles may also promote the carbonation of mortars. This preliminary data has served as the initial evidence of the potential use of nano-TiO_2 addition to promoting CO_2 capture. Besides, previous research showed that nano-TiO_2 addition may increase the compressive strength of cementitious composites. However, there is no agreement on what the optimum nano-TiO_2 percentage in terms of compressive strength enhancement is. Researchers also observed that an excess of nano-TiO_2 may reduce the strength of the composite. Understanding the mechanism and factors that may define the optimum percentage of nano-TiO_2 in terms of compressive strength would be vital in designing sustainable cementitious composites containing TiO_2 nanoparticles.

This dissertation aims to study the effect of nano-TiO_2 addition on the environmental performance of cementitious composites based on a holistic approach with three main pillars: (i) the composite performance, (ii) the impact of material production, and (iii) the effects during the service life.

Regarding material performance, this study analyzes the effect of the water-to-binder ratio (w/b) in the optimum percentage of nano-TiO_2 in terms of compressive strength. This part of the research concludes that the higher the w/b, the higher the optimum percentage of nano-TiO_2. In terms of age, the lower the age, the higher the optimum percentage of nano-TiO_2. Mixtures with high initial porosity present a dual beneficial effect of nano-TiO_2 addition due to the promotion of

hydration (nucleation effect) and the reduction of porosity (filling effect). On the other hand, an excessive nano-TiO_2 may cause a lack of space for calcium hydroxide (CH) growth, thus strength reduction.

Concerning the environmental performance of material production, this research aims to assess the combined effect of nano-TiO_2 and recycled aggregate on mortars' life cycle assessment (LCA), using *cradle-to-gate* as the system boundary. Results indicate that nano-TiO_2 addition on mortar mixtures enhances the sustainability of mortars with recycled concrete aggregates (RCA) to a greater extent than on mortars with natural aggregates. Indeed, a 0.5% nano-TiO_2 addition highly decreased the global warming potential in mortars with RCAs, particularly with 100% RCA replacement.

Furthermore, this dissertation focused on unveiling new mechanisms to increase the sustainability of cementitious composites during their service life. This research concludes that using nanoparticles to change the microstructure and modify the pore structure of the concrete's matrix can make concrete to capture greater amounts of CO_2 through both active (CO_2 curing) and passive (weathering) carbonation. In terms of passive or weathering carbonation, results show that the addition of nanoparticles to cementitious composites produce two simultaneous competing mechanism in terms of CO_2 uptake: (i) a beneficial effect due to the reduction of the CH crystals' size that makes CH more prone to be carbonated, and (ii) a detrimental effect due to the reduction of porosity, that reduces the CO_2 penetration. These two competing mechanisms may explain why nano-TiO_2 can be beneficial or detrimental for the CO_2 uptake as a function of the water-to-cement ratio (w/c). The higher the w/c, the higher the maximum level of nanoparticles that increases the CO_2 capture of cement paste. Regarding active carbonation, cement pastes with nano-TiO_2 addition increase both CO_2 uptake and compressive strength after 12-hour CO_2 curing compared to mixtures without nanoparticles cured under the same conditions. These effects may produce a significant improvement in terms of the environmental performance of cementitious composites. For instance, combining 0.5% nano-TiO_2 addition and CO_2 curing reduces net CO_2 emissions of over 20% in a cement paste with a 0.55 w/c. Another study of this dissertation assesses how CO_2 curing may influence the self-cleaning activity of cementitious composites. Results suggest that the lower porosity of cement pastes containing slag produced higher and more concentrated surface carbonation during CO_2 curing. Thus, CO_2 curing produced a higher reduction of the superficial

porosity in samples containing slag than in samples without slag. This higher reduction of the superficial porosity resulted in a higher self-cleaning enhancement after CO_2 curing; the lower penetration of pollutants makes them more exposed to the UV light, translating into higher self-cleaning activity. Results indicate that the combination of using slag cement and CO_2 curing has a synergistic effect that enables the production of photocatalytic cementitious composites with lower percentages of nanoparticles.

1. INTRODUCTION

1.1 Motivation

According to a recent report from the World Meteorological Organization, greenhouse gases (GHG) concentration has dramatically increased a 43% since 1990 [1]. As stated by the Intergovernmental Panel on Climate Change, 65% of the total GHG concentration corresponds to carbon dioxide (CO_2) [2], reaching its highest level in the last 3-5 million years [1]. Since the Industrial Revolution, the massive increase in CO_2 concentration has caused disastrous consequences (e.g., global warming and ocean acidification) [3]. Therefore, reducing the amount of this gas is vital for the environment.

Cement production is responsible for 8% of the total CO_2 emissions globally [4]. The CO_2 emissions caused by cement manufacturing are mainly derived from three processes: (i) the limestone decomposition (40%-50% of total emissions); (ii) the use of fossil fuels during the production of the clinker (40%-50% of total emissions); and (iii) the transportation of materials (8% of the total emissions) [5], [6]. In addition, cement is one of the main compounds of concrete and, according to the World Business Council for Sustainable Development, the second consumed material globally, only after water [7].

Besides cement, concrete production requires a significant volume of aggregates and water. More than 8 billion m^3 of aggregates are used every year to produce concrete [8] and other cementitious composites such as mortar. Furthermore, most of these aggregates come from natural resources and are extracted from quarries, with their corresponding effect on the environment. Therefore, besides generating 8% of the total CO_2 emissions each year, concrete plays an essential role in the depletion of natural resources. Considering these two facts, and that more than 30 billion tons of concrete are produced each year [8], a small step in the environmental impact of cementitious materials could lead to a giant leap in global sustainability due to the enormous relevance of those materials in the world.

There are several approaches to improve the sustainability of concrete. For instance, the valorization of wastes to transform them into by-products that could partially or totally replace a specific concrete compound (e.g., cement and natural aggregates). Previous studies claimed that

supplementary cementitious materials (SCM) could decrease CO_2 emissions associated with concrete production when used as a cement replacement [9]–[11]. Besides, natural aggregates can be partially or totally replaced by recycled aggregates. This replacement may possess a dual advantage since the use of recycled aggregates reduces both natural depletion and waste generation [12], [13]. However, the effect of these substitutions on the concrete performance must be considered to analyze their actual impact on concrete sustainability.

Furthermore, besides waste valorization, there are other ways to increase the sustainability of concrete. Previous studies showed that concrete with TiO_2 nanoparticles may have photocatalytic properties and may help to reduce prejudicial contaminants such as nitrogen oxides (NO_x) and volatile organic compounds (VOCs) [14], [15]. Some investigations have studied the influence of the nano-TiO_2 addition on the sustainability of photocatalytic concrete pavements [16]–[18]. Even though the nano-TiO_2 addition could increase some environmental categories like global warming or ozone depletion, the nanoparticles may decrease the total environmental impacts on other categories such as acidification or smog formation [17], [18].

Besides, a recent investigation [19] showed that the cementitious composites have sequestrated, from 1930 to 2013, almost half of the CO_2 emissions produced by the cement industry in the same period. Consequently, the carbonation of cementitious materials could represent an enormous carbon sink not previously considered. However, while the carbonation process may take decades, cement production has been accelerated over the last years [20]. Thus, the gap imbalance between CO_2 emitted, and CO_2 sequestrated has been significantly increasing in recent years.

Recent investigations with other cement types rather than ordinary Portland cement (e.g., calcium silicate-based cement (CSC)) exhibited promising results [21]–[24]. CSC cement may reduce the environmental impact of concrete since the CSC cement manufacturing process is associated with lower CO_2 emissions than ordinary Portland cement (OPC) [21]–[24]. CSC cement is a non-hydraulic cement containing low-lime calcium silicates in its composition [21], [23]. Therefore, CSC cement must be cured with CO_2 to harden [21], [23].

Several investigations showed another potential alternative to capture CO_2 by curing fresh OPC composites with CO_2 [25]–[28]. Changes in cementitious composites may facilitate a faster

rate of CO_2 uptake and/or a higher absolute CO_2 capture and, thus, a significant reduction of the environmental impact of concretes and cementitious composites.

A previous study from Velay's Research group [29] showed that the use of nano-TiO_2 made mortars more susceptible to be carbonated during TGA sample preparation (grinding) than in the case of mortars with no nanoparticles. This observation suggested that using 0.5% of nano-TiO_2 (by the total weight of cement) could promote the carbonation of mortars. Thus, this preliminary data has served as the initial evidence of the potential use of TiO_2 nanoparticles addition to promote CO_2 capture, thus reducing the environmental impact of cementitious composites.

Finally, to produce a real impact on concrete sustainability, the present research highlights the importance of adopting a holistic approach in terms of its life cycle assessment, with three main pillars that should be considered to move towards a zero-impact sustainable concrete: (i) the composite performance, (ii) the impact during production (impact of materials used and potential valorization of wastes), and (iii) the effects during the service life (such as photocatalytic and self-cleaning effect and CO_2 uptake).

1.2 Aim and objectives

This research aims to study the effect of nano-TiO_2 addition on the environmental impact of cementitious materials. To achieve it, the main objectives of the investigation are:

1. To study the influence of water-to-binder ratio and testing age in the optimum percentage of nano-TiO_2 in terms of compressive strength of cement mortars.

The effect of nano-TiO_2 on the compressive strength of cementitious composites can be critical to evaluate the nano-TiO_2 addition impact on their sustainability. The addition of nanoparticles may have a positive effect on compressive strength. As a consequence of this potential improvement, less cement content would be required to produce a cementitious composite with a given strength.

Thus, it would reduce the overall environmental impact of cementitious composites production with a required strength since it would decrease the amount of cement content needed, and cement is the compound that largely contributes to the CO_2 emissions of cementitious

composites. However, previous research did not agree on the optimum percentage of nano-TiO_2 in terms of compressive strength. This research hypothesizes that the water-to-binder ratio is a crucial factor that may affect the optimum percentage of nano-TiO_2. Besides, the variability of the optimum percentage of nano-TiO_2 as a function of the testing age will also be studied.

Understanding the role of the water-to-binder ratio in the optimum percentage of nano-TiO_2 in terms of compressive strength of cementitious composites would be vital to analyze the maximum potential effect of nano-TiO_2 on the environmental performance of cementitious composites.

2. To quantify the effect of the nano-TiO_2 in the environmental performance (at a production stage) of eco-mortars made with different percentages of recycled aggregates in comparison to the influence of the nanoparticles in the plain mortar (made with natural aggregates)

On the one hand, using recycled aggregates as a partial or total replacement of natural aggregate decreases the natural depletion associated with cementitious composites. However, its use may also reduce the compressive strength of the composite. On the other hand, nano-TiO_2 addition may increase the compressive strength of cementitious composites. Therefore, this part of the study aims to assess the combined use of nano-TiO_2 and recycled aggregates to potentially improve the environmental performance at the production stage of cementitious composites with a given compressive strength.

3. To unfold the impact of nano-TiO_2 on the CO_2 sequestration rate of cementitious composites based on its effects on the microstructure.

This part of the research pursues studying the effect of nano-TiO_2 addition on the CO_2 capture of cementitious materials. Two approaches are followed:

- Examining how the TiO_2 nanoparticle addition affects the CO_2 uptake of hardened cement pastes depending on the water-to-cement ratio and the pore structure.
- Evaluating the effect of nano-TiO_2 addition in promoting CO_2 capture during CO_2 curing of fresh cement pastes and how this type of curing may change both cement phases content and compressive strength of the studied cement pastes.

4. To study how CO_2 curing affects the self-cleaning property of cementitious materials containing nano-TiO_2.

It is well-known that the use of nano-TiO_2 provides self-cleaning properties to cementitious materials when exposed to ultraviolet (UV) light. This positive effect on the environmental performance of cementitious composites, combined with its effect on potentially promoting the CO_2 uptake during the CO_2 curing, might lead to a significant reduction of the environmental impact of the studied composites. However, how the CO_2 curing might affect the photocatalytic ability of hardened cementitious composites remains unknown. Thus, this part of the research investigates the effect of CO_2 exposure on the self-cleaning activity of cementitious composites with nano-TiO_2.

The use of supplementary cementitious materials (SCM) such as slag as partial replacement of cement is also one of the main approaches to enhancing the sustainability of cementitious composites. Previous studies showed that the addition of slag might increase the CO_2 uptake of cementitious materials during CO_2 curing. Thus, besides plain cement paste containing nano-TiO_2, this chapter also analyzes the effect of slag addition on the self-cleaning activity before and after CO_2 curing. The aim is to analyze the combination of different sustainable approaches (e.g., the addition of SCM, the use of CO_2 curing, or nanoparticles addition). Studying the interaction of those approaches may be critical to find synergies that enable us to move towards more sustainable construction.

1.3 Structure

This dissertation comprises eight chapters. Chapters 3 to 7 contain the corresponding literature review in the introduction of each chapter.

Chapter 1 encompasses the introduction specifying the motivation, the aim and objectives, and the dissertation structure.

Chapter 2 includes the materials and the general procedures employed in the study (the specific procedures of each study are described in the corresponding chapter).

Chapter 3 investigates the effect of the water-to-binder ratio and the testing age in the optimum percentage of nano-TiO_2 in terms of compressive strength of mortars.

Chapter 4 studies the effect of the addition of TiO_2 nanoparticles on the LCA (until the production stage, *cradle-to-gate*) of natural and recycled mortars using as functional unit 1 m^3 of mortar with a given compressive strength.

Chapter 5 analyzes the effect of TiO_2 nanoparticles on the CO_2 sequestration of hardened cement pastes depending on the water-to-cement ratio, exposure age, and pore structure.

Chapter 6 investigates the influence of the TiO_2 nanoparticles on compressive strength, microstructure, and CO_2 uptake after conducting an accelerated or CO_2 curing of cement pastes.

Chapter 7 examines the modification of the self-cleaning effect of the nano-TiO_2 materials after CO_2 curing in cement pastes with and without slag cement.

Chapter 8 includes the conclusions and considerations for future work.

2. MATERIALS AND GENERAL PROCEDURES

2.1 Materials

2.1.1 Ordinary Portland cement and slag cement

The Ordinary Portland cement (OPC) employed was a commercial cement type I (CEM I 52,5 N-CP2), supplied by Buzzi Unicem. This cement complied with both ASTM C150 [30] and AASHTO M85 [31] specifications, as shown in the Mill Test Certificate (Appendix A). In addition, the slag cement used meets the specifications of ASTM C989 for Grade 100 slag cement [32]. Both cement chemical compositions, obtained by a Lab X500 XRF analyzer (Hitachi, Japan), are presented in Table 2.1, the physical properties are summarized in Table 2.2.

Table 2.1. Chemical and phases composition of both cement types used.

Common name	Chemical abbreviation	OPC (%)	Slag cement (%)
Calcium Oxide	CaO or C	63.10	46.50
Silica Dioxide	SiO_2 or S	20.53	34.03
Aluminum Oxide	Al_2O_3 or A	5.21	8.62
Magnesium Oxide	SO_3 or $\bar{S}$	3.16	1.59
Sulfur Trioxide	Fe_2O_3 or F	2.82	0.66
Ferric Oxide	MgO or M	2.65	12.29
Titanium Dioxide	TiO_2	0.32	0.43
Sodium Oxide	Na_2O	0.14	0.36
Phosphorus Pentoxide	P_2O_5	0.10	<0
Zinc Oxide	ZnO	0.04	0.01
Manganese (III) Oxide	Mn_2O_3	0.04	0.50
Strontium Oxide	SrO	0.03	0.08
Chromium (III) Oxide	Cr_2O_3	0.01	0.01
Loss of ignition	LOI	2.9	-

Table 2.2. Physical properties of both cement types used.

Properties	OPC	Slag cement
Specific surface area (m^2/kg)	417	534
Specific gravity	3.15	2.9

Figure 2.1 presents the particle size distribution of both OPC and slag cement employed, obtained by a PSA 1090 Series (Anton Paar, Austria). Slag cement possesses finer particles than OPC, as shown in Figure 2.1. Whereas OPC has a D_{50} of 16.87 µm, slag cement possesses a D_{50} of 12.46 µm.

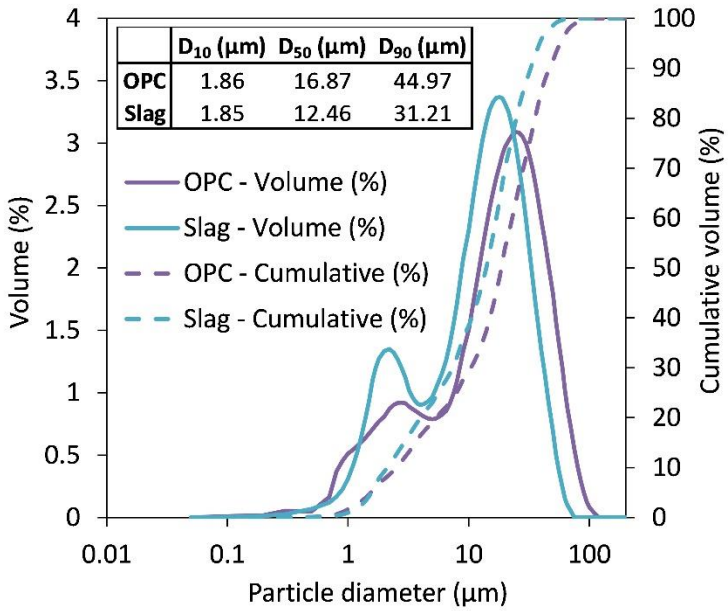

Figure 2.1. Particle size distribution of OPC and slag cement.

2.1.2 Aggregates

In the mortars prepared in these studies, two types of aggregates (shown in Figure 2.2) were used: (i) natural fine aggregates (NFA) or sand and (ii) recycled fine aggregates (RFA). The RFA (coming from construction and demolition) was supplied by a Lafayette aggregate distributor (Purdy Materials).

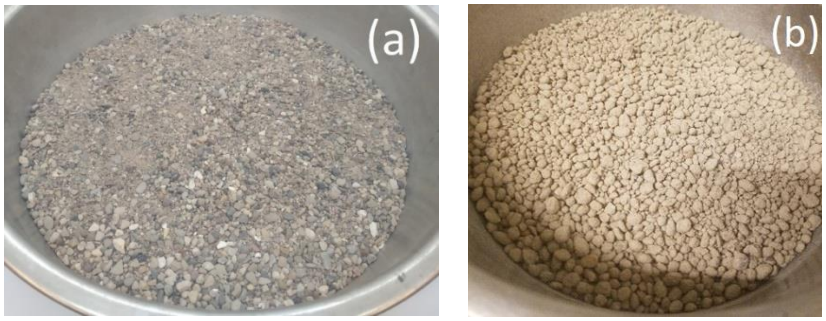

Figure 2.2. Aggregates employed. (a) NFA. (b) RFA.

Both NFA and RFA complied with the specifications for fine aggregates established by ASTM C33/C33M [33]. Following the ASTM C136/C136M specifications [34], the sieve analysis was performed for both aggregates (Figure 2.3 and Table 2.3). Besides, the ASTM C128 [35] was used to conduct the specific gravity and absorption test for both fine aggregates. The absorption test was performed to adjust the water during the mixture proportioning. The specific gravity, fineness modulus, and absorption value of both aggregates are summarized in Table 2.4.

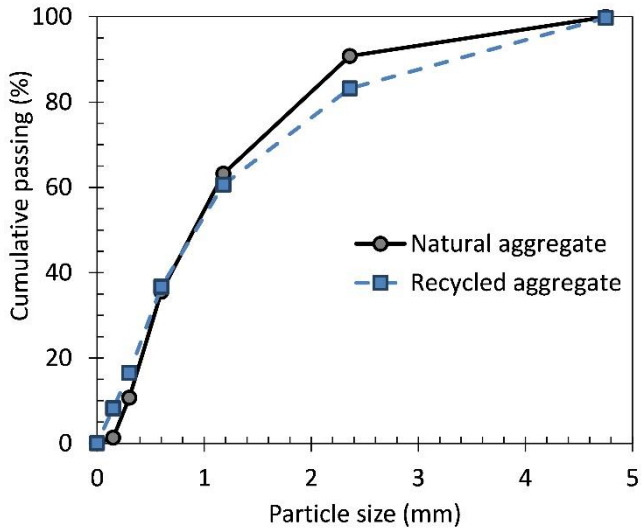

Figure 2.3. Aggregate particle size distribution curve.

Table 2.3. Particle size distribution.

Sieve	**Sieve size (mm)**	**Natural aggregate cumulative percent passing (%)**	**Recycled aggregate cumulative percent passing (%)**
3/8 in	9.50	100.00	100.00
No. 4	4.75	99.96	99.72
No. 8	2.36	90.82	83.19
No. 16	1.18	63.24	60.62
No. 30	0.60	35.53	36.71
No. 50	0.30	10.72	16.51
No. 100	0.15	1.31	8.22
Pan	0.00	0.00	0.00

Table 2.4. Physical properties of the aggregates.

Properties	NFA	RFA
Specific gravity	2.68	2.47
Fineness modulus	3.24	2.95
Absorption value (%)	1.23	8.01

2.1.3 TiO_2 nanoparticles

Sigma-Aldrich (St. Louis, MO) supplied the titanium (IV) oxide (TiO_2) nanoparticles with a crystal structure of 85% anatase and 15% rutile. The properties of the nanoparticles are shown in Table 2.5. The primary particle size (d_{50}) was obtained by transmission electron microscopy (TEM) experiment.

Table 2.5. Properties of nano-TiO_2 (supplied by Sigma-Aldrich).

Properties	Unit	TiO_2 nanoparticles
Formula weight	g/mol	79.87
Trace metal basis	%	> 99.5
Surface area	m^2/g	35 - 65
Primary particle size (d_{50})	nm	21
Density at 25 °C (lit.)	g/mL	4.26

Figure 2.4. TiO_2 nanoparticles used.

2.2 General procedures

2.2.1 Compressive strength test

A uniaxial compressive strength test was carried out according to ASTM standard C349 [36]. An MTS (Eden Prairie, MN) machine was used with a loading rate of 0.05 mm/s and a maximum load capacity of 300 kN. The test was conducted using a compression device supplied by Controls Group (Elgin, IL), which tests portions of 40 x 40 x 160 mm prisms, conforming to ASTM standard C349 [36]. In addition, the homogeneity through the samples is also checked since this standard allows to get two compressive strength measurements of each sample.

2.2.2 Thermogravimetric analysis (TGA)

The thermogravimetric analysis is a method that quantifies the mass variations of a sample over time. In the cementitious materials field, this method helps estimate the presence of different phases in the cement paste (e.g., calcium hydroxide or calcium carbonate).

At the testing age, a mortar and pestle were used to grind the specimens (Figure 2.5.b). First, samples were pretreated with a solvent (acetone) to remove the free water in the samples [37]. Each sample was then roughly ground, and 5 grams of each were soaked in a container with isopropanol (50 ml). Fifteen minutes later, the specimens were dried in an oven at 40°C to remove the excess solvent. After 10 minutes in the oven, samples were ground with a mortar and pestle and sieved using No. 200 sieve (75-µm).

Then, between 20 and 50 mg of ground powder of each sample was analyzed in a platinum pan. Thermogravimetric analysis was conducted in an atmosphere of nitrogen gas purged at a rate of 60 mL/min and delivered at a pressure of 20 psi using a Thermogravimetric Analyzer (2050, TA Instruments, New Castle, DE), shown in Figure 2.5.a. First, each specimen remained in isothermal condition for two minutes. After that, the temperature was raised until 900 °C/min, at a rate of 10 °C/min. The instrument recorded the mass loss (in %) as a function of temperature.

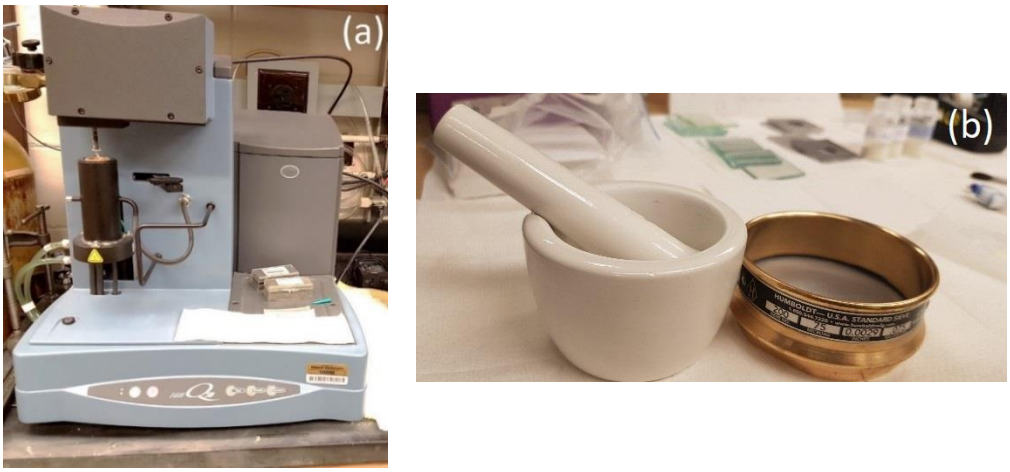

Figure 2.5. (a) Thermogravimetric analyzer. (b) Mortar, pestle and sieve used.

2.2.3 3D X-Ray Microscope (XRM)

The Zeiss Xradia 510 Versa 3D X-Ray Microscope (Figure 2.6.a) was employed to study the samples' pore structure (macroporosity). The system utilizes a two-stage magnification technique, both geometric and optical magnification (0.4X), to provide high-resolution imaging. The cylinder samples have a diameter of 3.2 cm and a height of 2.1 cm. The scans were obtained at an in-situ system temperature (~28 $^{\circ}$C), a power of 10 W, and a voltage of 150 kV. A minimum of 2401 projections was acquired per sample. The 3D X-Ray microscopy can detect pores with a nominal voxel size up to 5 µm, considering the chosen optical magnification. After the analysis, Object Research Systems (ORS) Dragonfly Pro software was employed to 3D visualize, analyze, and quantify the macroporosity and pore structure.

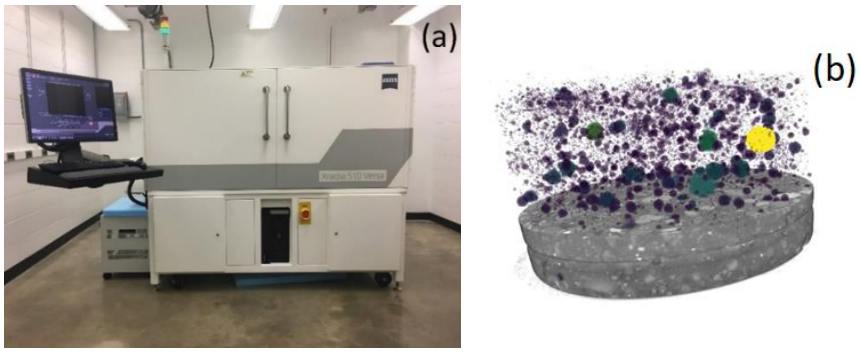

Figure 2.6. (a) Zeiss Xradia 510 Versa 3D X-Ray Microscope. (b) Example of a scanned sample.

2.2.4 X-ray powder diffraction (XRD)

X-ray powder diffraction (XRD) is a non-destructive method used to analyze the crystallographic structure.

The powdered samples used in the analysis were prepared in the same way as those used in the TGA analysis. A Siemens D500 diffractometer instrument (Figure 2.7) was used in the analysis with a 50-kV voltage and a 30-mA current. The 2θ-range of the scan was 5-65° at a 0.02°/sec scanning rate.

After the analysis, Profex software was used to perform the quantitative Rietveld refinement analysis using the program BGMN [38].

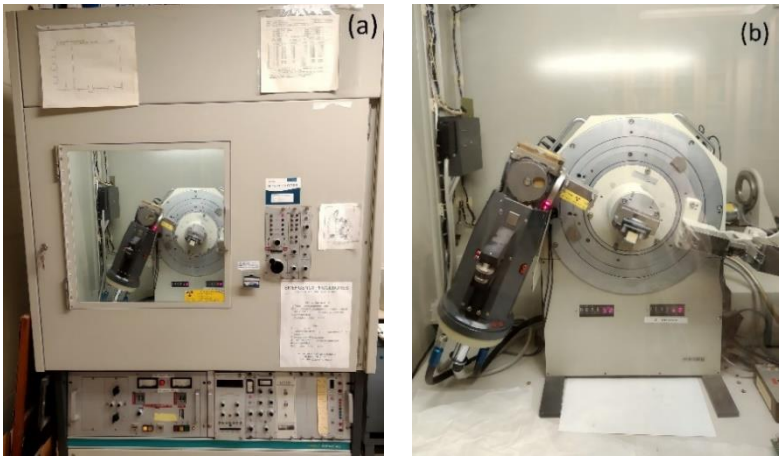

Figure 2.7. (a) Overview of the XRD machine. (b) Detail of the XRD machine.

3. INFLUENCE OF WATER-TO-BINDER RATIO ON THE OPTIMUM PERCENTAGE OF NANO-TIO_2 ADDITION IN TERMS OF COMPRESSIVE STRENGTH OF MORTARS: A LABORATORY AND VIRTUAL EXPERIMENTAL STUDY BASED ON ANN MODEL

Part of this chapter has been published as:

C. Moro, H. El-Fil, V. Francioso and M. Velay-Lizancos (2020). *'Influence of water-to-binder ratio on the optimum percentage of nano-TiO_2 addition in terms of compressive strength of mortars: A laboratory and virtual experimental study based on ANN model.'* Construction and Building Materials, vol. 275, p. 122131. https://doi.org/10.1016/j.conbuildmat.2020.120960.

3.1 Introduction

Since the discovery of the photocatalytic property of titanium dioxide nanoparticles (nano-TiO_2) at the beginning of the 21st century [39], [40], many studies have been conducted to analyze and estimate their effect on cementitious materials properties. In addition to their environmental benefits [41], [42], the inclusion of nano-TiO_2 also affects other properties. The use of nano-TiO_2 produces a decrease in both the initial and final setting time [43]–[45] due to their high specific surface. In contrast, there is no agreement about the effect of the nanoparticles on shrinkage. Some studies argued that the higher the nano-TiO_2 percentage, the higher the shrinkage [46], [47]. Other investigations claimed that shrinkage is decreased with an increase in the percentage of nano-TiO_2 [48], [49]. According to Yang et al. [49], capillary tensile forces may be an important factor because they enhance stiffness and, therefore, decrease shrinkage. Furthermore, researchers agree that TiO_2 nanoparticles modify the pore structure of cementitious materials. Several publications have revealed that the higher the percentage of nano-TiO_2, the lower the total porosity [48]–[51]. The main reasons are the nucleation effect and the filling effect, producing a denser microstructure [44], [47]. This densification of the microstructure due to the addition of nanoparticles also improves durability [52]–[56]. Even though durability could be evaluated with different properties (e.g., water absorption or chloride permeability), generally, the higher the nano-TiO_2 percentage, the higher the durability due to the enhancement of the microstructure. Researchers claimed that the chloride permeability increases with the use of nanoparticles [52]–[54]. Similarly, nano-TiO_2 decreases water absorption [54]–[56]. Despite the importance of other properties, compressive

strength is one of the main requirements of cementitious materials structures. Consequently, numerous studies have attempted to explain the influence of nano-TiO_2 in the compressive strength of cementitious materials [43], [44], [57]–[61].

The effect of the nanoparticles on the compressive strength was widely analyzed throughout the literature. Figure 3.1 shows the relative change of compressive strength at 7 and 28 days in samples with different percentages of TiO_2 nanoparticles compared to the compressive strength of the sample with no nano-TiO_2 of previous studies. Several studies have reported that nano-TiO_2 rises the compressive strength of cementitious materials up to 5% of addition [43], [44], [47], [54], [57], [58]. Those studies indicated different potential reasons. Noorvand et al. [57] stated that the reason beyond could be the restriction in the calcium hydroxide (CH) size, causing the densification of the microstructure. The acceleration of the hydration due to the nucleation effect made by the nanoparticles may also be a potential explanation [43], [44]. Other investigations [47], [54] argued that the reason for the improvement could be a combination of both effects (quicker hydration and reduction of CH size).

In contrast, Meng et al. [60] claimed that the improvement of strength could not be related to increased hydration products. Instead, they explained that a modification of the orientation index due to the nucleation effect of the nanoparticles might be the main reason. Ren et al. [58] argued that the nanoparticles could improve the interfacial transition zone (ITZ) between the cement paste and the aggregate by decreasing the CH size. Nevertheless, some studies reported a decrease in compressive strength due to the poor dispersion of the nanoparticles [59], [62]. The accumulation could be produced because of an excess of nanoparticles used or an inappropriate mixing process.

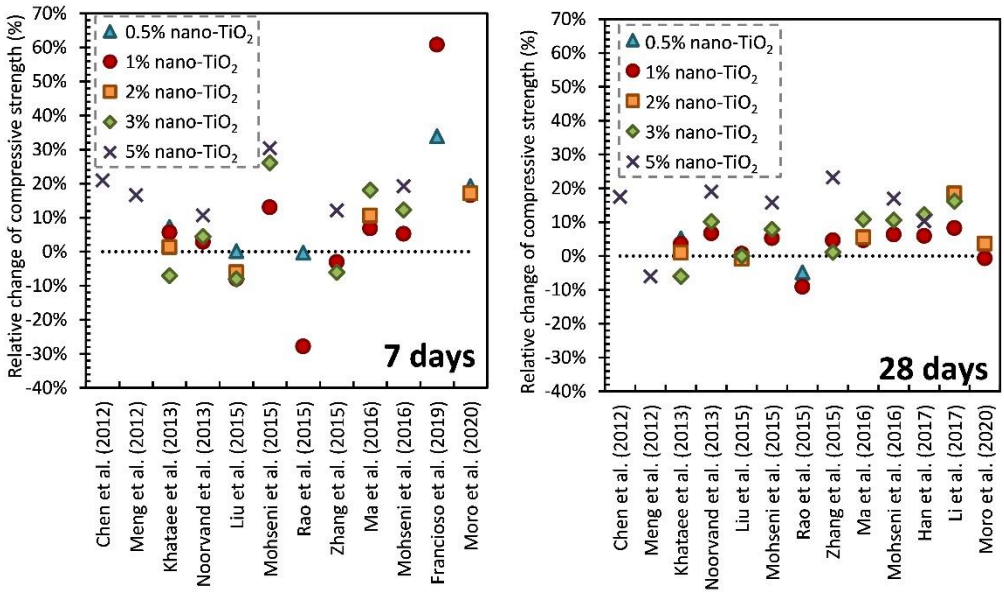

Figure 3.1. Relative change of compressive strength at 7 and 28 days compared to the compressive strength of the sample with no nanoparticles as a function of the percentage of nano-TiO_2. Data obtained from [29], [43], [44], [47], [54], [57], [60]–[67].

Previous research has indicated that there may be an optimum percentage of nano-TiO_2 for each mixture in terms of compressive strength. Therefore, higher percentages of nanoparticles than this optimum would produce a decrease in the compressive strength. Throughout the literature, there are some potential explanations for this fact. On the one hand, a bad dispersion could lead to the agglomeration of the nanoparticles due to their large surface area [58], [61]. On the other hand, the excess of nano-TiO_2 may react with the free lime producing an excess of silica. Thus, this reaction would replace part of the hydration products, decreasing strength [68].

Numerous authors investigating the effect of nanoparticles on the compressive strength have shown a different optimum percentage of nano-TiO_2 [43], [44], [48], [63], [69], [70]. Therefore, the effect of nano-TiO_2 on compressive strength may be affected by the mixture proportioning. Researchers are currently exploring advanced techniques such as artificial neural networks (ANN) to predict the key mechanical properties of concretes. In the field of construction materials, several studies used machine learning to predict the properties of concrete [71]–[75]. For instance, a new study [71] used ANN to predict the compressive strength of semi lightweight concretes containing ground granulated blast-furnace slag (GGBFS). The authors concluded that the ANN is the most promising method for the prediction of compressive strength. A recent study

[72] applied an adaptive boosting approach using machine learning-based compressive strength prediction for concrete. They used a 1030-point set of data to train the model, and they reached an accuracy of 98%. A recent study [73] predicted the compressive strength of ultra-high-performance concrete containing supplementary cementitious materials. They concluded that the developed ANN model has high accuracy and can be used to predict the compressive strength of ultra-high-performance concrete (UHPC) with the inclusion of supplementary cementitious materials. Golafshani et al. [74] predicted the compressive strength of normal and high-performance concretes using ANN and adaptive neuro-fuzzy inference system (ANFIS) hybridized with grey wolf optimizer (GWO). They obtained reliable and accurate models for the prediction of the compressive strength of concretes. Besides, according to a study conducted, NDT data prove to be useful in predicting the concrete strength [75]. This investigation predicted concrete strength with P-, S-, R-wave velocities by support vector machine (SVM) and ANN. They concluded that both techniques successfully model the relationship between the mechanical wave velocities and the concrete compressive strength.

To the best of our knowledge, no previous studies exist that use ANN to predict the compressive strength of concretes or mortars with the inclusion of TiO_2 nanoparticles, or to predict the optimal percentage of nano-TiO_2 required for improved compressive strength. Besides, no previous research has investigated how the mixture proportioning may modify the effect of nano-TiO_2 on the compressive strength of cementitious-based composites. Therefore, this chapter aims to study how the water-to-binder (w/b) ratio affects the optimum percentage of nano-TiO_2 in terms of compressive strength enhancement and to develop an ANN model that would accurately predict the compressive strength of cementitious materials made with the nano-TiO_2, combining both laboratory and virtual experimental approaches. These effects will be studied and explained based on the impact of nano-TiO_2 on hydration products content and porosity. Understanding the influence of the w/b on the optimum percentage of nano-TiO_2 in terms of compressive strength will contribute to determining the best use of these nanoparticles to enhance the performance during the service life of cementitious materials. It will also set a new step towards new guidelines for mixture proportioning of cementitious composites with nano-TiO_2. Besides, it could help to reduce the cement content needed to produce a cementitious composite with a target compressive strength by using nano-TiO_2 more effectively and efficiently.

3.2 Materials and methods

3.2.1 Artificial Neural Network

Artificial neural networks were employed in this chapter to study the effect of the w/b on the optimum percentage of nano-titanium dioxide in terms of compressive strength.

The artificial neural network (ANN) was first developed by McCulloch and Pitts [76]**.** It is a type of artificial intelligence (AI) system that aids in solving non-linear problems quickly and with a high degree of accuracy. In ANN, training data is used to develop the model. ANN learns the training data pattern and develops different outputs based on the learning process [77]. The architecture of an ANN model is based on the number of neurons and layers chosen. These neurons can be linked together by various methods, such as the feed-forward (FF) - back-propagation (BP) method, which has been successfully used in many research studies [78]–[81]. This method (FF-BP), as its name suggests, consists of two stages: the forward and the backward stage. Inputs are forwarded through each layer during the forward stage, and corresponding weights are assigned to each neuron. In the backward stage, errors of the pre-assigned weights are computed. The error is obtained by finding the difference between the predicted values and target values. The network then backpropagates and re-assigns weights to minimize the error.

Table 3.1 summarizes the main parameters of the mixtures collected from previous studies that investigated the effect of nano-TiO_2 on the compressive strength of mortars. These parameters include: % of nano-TiO_2, water-to-binder ratio (w/b), aggregate-to-binder ratio (a/b), and testing age. To build the ANN model, selection criteria were applied to eliminate outliers or extreme cases that may show different behavior than the average mortars. The selection criteria consist of excluding mixtures with very low w/b (<0.35) or very high w/b (>0.55). Besides, mixtures with percentages of nano-TiO_2 higher than 3% were also excluded since previous literature suggests that high percentages of nano-TiO_2 will have a negative effect on compressive strength [61], [66], [82]. This chapter is focused on examining how the w/b changes the optimum percentage of nano-TiO_2 in terms of compressive strength, and therefore, selecting up to 3% of nano-TiO_2 mixtures is a reasonable range. The range of ages selected for the model is from 3 days to 28 days. As a result, the dataset used to build the ANN model has a total of 194 data points, out of which a random 70%

was used for training, and the remaining points were used for validating and testing the model (15% each).

Table 3.1. Summary data from previous literature.

Reference	**% of nano-TiO_2**	**w/b**	**a/b**	**Testing Age (days)**
Chen et al. [44]	0%, 5%, 10%	0.485	2.75	3, 7, 28
Francioso et al. [29]	0%, 0.25%, 0.5%, 1%	0.5	3	7
Han et al. [83]	0%, 1%, 3%	0.3	1.1	28
Khataee et al. [61]	0%, 0.5%, 1%, 1.5%, 2%, 2.5%, 3%	0.5	3	3, 7, 28
Li et al. [66]	0%, 1%, 2.5%, 4%	0.375	1.38	3, 28
Liu et al. [67]	0%, 0.5%, 1%, 2%, 3%	0.29	1.1	3, 7, 28
Ma et al. [43]	0%, 1%, 2%, 3%	0.5	3	3, 7, 28, 90
Meng et al. [60]	0%, 5%, 10%	0.5	3	3, 7, 28
Mohseni et al. [54]	0%, 1%, 3%, 5%	0.4	[2.30-2.35]	3, 7, 28, 90
Mohseni et al. [63]	0%, 1%, 3%, 5%	0.4	[1.67-1.83]	7, 28, 90
Moro et al. [64]	0%, 0.5%, 1%, 2%	0.5	3	7, 28
Moro et al. [82]	0%, 0.5%, 1%, 2%	0.55	3	90
Noorvand et al. [57]	0%, 0.5%, 1%, 1.5%	0.35	2.75	7, 28, 90
Rao et al. [62]	0%, 0.5%, 0.75%, 1%	0.43	1, 2	7, 28, 90
Salman et al. [84]	0%, 0.25%, 0.75%, 1.25%, 1.75%	0.5	3	7, 28
Zhang et al. [47]	0%, 1%, 3%, 5%	0.4, 0.6	3	3, 7, 28

This chapter develops an ANN model using the Levenberg-Markvart (LM) learning function in a MATLAB environment. The architecture of the model is shown in Figure 3.2.

The model has four layers: an input layer, two hidden layers with 20 neurons each, and an output layer. Five input features feed into the input layer as shown in Figure 3.2, which are: (1) % of nano-TiO_2, (2) testing age, (3) a/b, (4) w/b, and (5) cement content (in kg/kg of mortar). The model outputs the predicted compressive strength (CS). Since the artificial neural network (ANN) is a method that learns the pattern of the training data, its algorithms highly depend on the number of data points available to create a robust model. While other parameters may affect the compressive strength, these five input features were selected considering the amount of data available and the relevance of each input value in terms of the influence in compressive strength. Besides the data of the five input features, the actual corresponding compressive strength of each

of the 194 collected data points was fed into the model to train and validate it. Table 3.2 shows a statistical summary of the input data used to develop the model and their corresponding compressive strength.

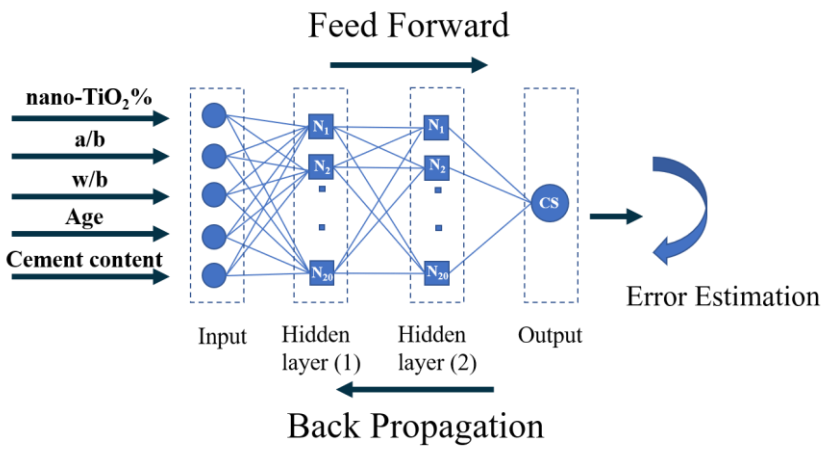

Figure 3.2.Architecture of the ANN model.

Table 3.2. Statistical summary of the input data used to develop the ANN model and the target feature.

Input feature	Range			Mean	Median
% nano-TiO_2	0.0	-	3.0	1.115	1.0
Water-to-binder ratio (w/b)	0.35	-	0.50	0.453	0.50
Agreggate-to-binder ratio (a/b)	1.0	-	3.0	2.643	3.0
Testing age (days)	3	-	28	14.98	7
Cement content (kg/kg of mortar)	0.149	-	0.319	0.209	0.215
Target feature	**Range**			**Mean**	**Median**
Actual compressive strength (MPa)	11.21	-	118.50	41.86	37.66

ANN algorithms are typically sensitive to the distribution of data points. Skewed and widely ranged datasets can result in less robust and less accurate algorithms. In addition, it can mislead or distort the results of the training procedure. Skewness and outliers can be detected through graphical means such as boxplots or scatterplots (Figure 3.3). Outliers are the points that lie outside the 1.5 × IQR margin, where IQR is defined as the 'Inter Quartile Range,' which is the difference between the 75th and 25th quartiles. Empty circles in Figure 3.3 represent outliers. The boxplot for the target value category is shown in Figure 3.3.a. The target data (measured

compressive strength) has a mean of 41.86 and a median of 37.66. The mean is greater than the median, implying that the data is skewed to the right, and outliers are detected, as shown in Figure 3.3.a. A potential solution for solving the problem of skewness is variable transformation. Transforming the data could be performed by several means. Examples of non-linear transformation include taking the square root or logarithm of the data to minimize the extreme values. In this chapter, the transformation method took the natural logarithmic (ln) of the target data. This method was chosen based on a trial and error process. Figure 3.3.b indicates a box plot of the transformed data; the transformed data is relatively equally distributed around the median (red line), i.e., the median and the mean are 3.63 and 3.64, respectively. Consequently, the data is no longer as skewed as it were.

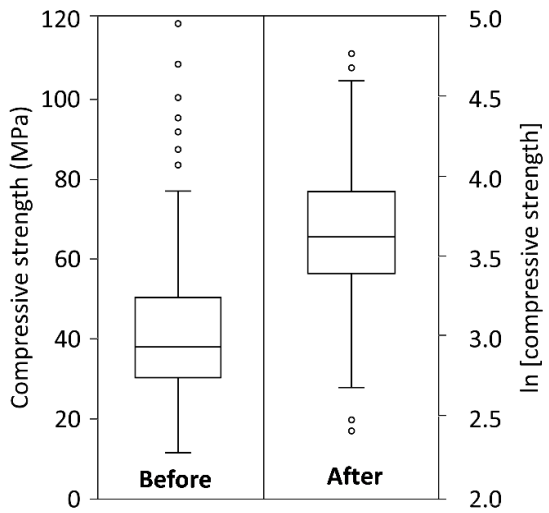

Figure 3.3. Boxplots for the target data (measured compressive strength) before and after transformation.

3.2.2 Virtual experimental campaign

A virtual experimental campaign is performed to study the impact of the w/b and testing age on the optimum percentage of nano-TiO_2 in terms of compressive strength for a set of synthetic input combinations by applying the ANN model. The synthetic data combination considers typical mortar mixture designs with w/b of 0.38-0.42 and testing ages of 3, 7, and 28 days. First, a binder content "*b*" of 0.23 kg/kg of mortar was chosen. Since binder content was fixed, for each w/b, the a/b ratio can be computed using Eq. 3.1.

$$\frac{a}{b} = \frac{1}{b} - 1 - \frac{w}{b} \qquad 3.1$$

The cement content in kg of cement per kilogram of mortar was also computed for each point by taking the difference between the total binder (0.23 kg/kg of mortar) and the weight of nano-TiO_2 (kg/kg of mortar). This approach results in a unique mixture proportioning (model input) for a given w/b, nano-TiO_2 content, and testing age.

Mixtures with a total of 5 different w/b (from 0.38 to 0.42, and intervals of 0.01) were investigated. For each studied w/b, a total of 3001 different percentages of nano-TiO_2 (from 0% to 3% with increments of 0.001%) were used. Three ages (3, 7, and 28 days) were used for this virtual experimental campaign. Combining the studied w/b (5), testing ages (3), and percentages of nano-TiO_2 (3001), a total of 45015 case scenarios were studied. These 45015 synthetic mixture designs were inputted into the trained and validated ANN model. Inputting these synthetic mixture designs into the trained and validated ANN model, a total of 45015 case scenarios were studied, and therefore, a total of 45015 estimated compressive strength results were acquired. For instance, Table 3.3 shows the synthetic data generated for mortar testing age of 3 days and w/b=0.38.

Table 3.3. Synthetic input data used for the virtual experimental campaign for w/b=0.38 and testing age of 3 days.

nano-TiO_2 (%)	**w/b**	**a/b**	**Age (days)**	**Cement content (kg/kg mortar)**
0	0.38	2.9678	3	0.2300
0.001	0.38	2.9678	3	0.2299977
⋮	⋮	⋮	⋮	⋮
0.25	0.38	2.9678	3	0.229425
⋮	⋮	⋮	⋮	⋮
3	0.38	2.9678	3	0.2231

3.2.3 Laboratory experimental campaign

The materials used to prepare the cement pastes of the experimental laboratory campaign are explained in *Chapter 2: Materials and general procedures*.

A total of 8 mixtures were studied, with four different percentages of nanoparticles (0%, 0.5%, 1%, 2%) and two w/b (0.38 and 0.42). Three cubes of each mixture were prepared. A total

of 24 cubes with dimensions 2 x 2 x 2 in. were prepared. The samples were prepared using the procedure for cement pastes shown in ASTM standard C305 [47]. Cement and nano-TiO_2 (if applicable) were mixed together in dry conditions for 30 seconds using a mixer bowl. Then, water was added, and the mixture was left for 30 s for the absorption of water. Then, the mixture was blended for 30 s at a slow speed. After that, the inside of the bowl was scraped to mix in any paste stuck to the sides. Finally, the paste was blended for 60 s at a medium speed. For the first 24 hours, specimens were kept in molds covered at room temperature. After one day, they were moisture-cured in an environmental room (95 ± 5% RH and 25 ± 1 °C) for seven days until testing. Cement pastes proportions are listed in Table 3.4.

Table 3.4. Mixture proportions of cement pastes.

Mixture	**w/b**	**Cement (g)**	**nano-TiO_2 (g)**	**Water (g)**
P0 (0.38)	0.38	1409.7	0.0	535.7
P0.5 (0.38)	0.38	1402.7	7.0	535.7
P1 (0.38)	0.38	1395.6	14.1	535.7
P2 (0.38)	0.38	1381.5	28.2	535.7
P0 (0.42)	0.42	1333.3	0.0	560.0
P0.5 (0.42)	0.42	1326.6	6.7	560.0
P1 (0.42)	0.42	1319.9	13.3	560.0
P2 (0.42)	0.42	1306.6	26.7	560.0

Uniaxial compressive strength tests (explained in *Chapter 2: Materials and general procedures*) were carried out, following the ASTM C349 [36], on samples of each mixture at seven days. After the compressive strength test, the ground powder of each sample was employed to conduct thermogravimetric analysis, following the procedure explained in *Chapter 2: Materials and general procedures*. Considering a recent study that claims that nano-TiO_2 promotes the carbonation of the CH during the samples preparation process [29], a modified equation (Eq. 3.2) was used to consider the amount of calcium carbonate that comes from the carbonation of the CH, following the method proposed by Kim and Olek [85]. Each term can be graphically seen in Figure 3.4.

$$\mathrm{CH} = 100\left\{\frac{74.1}{18.0}\cdot\frac{1}{\mathrm{M_c}}\cdot\left[\left(\mathrm{M_{start}^{CH}} - \mathrm{S_{start}^{CH}}\left(\mathrm{T_{inf}^{CH}} - \mathrm{T_{start}^{CH}}\right)\right) - \left(\mathrm{M_{end}^{CH}} - \mathrm{S_{end}^{CH}}\left(\mathrm{T_{end}^{CH}} - \mathrm{T_{inf}^{CH}}\right)\right)\right] + \right.$$
$$\left. + \frac{74.1}{100.1}\left[\frac{100.1}{44.0}\cdot\frac{1}{\mathrm{M_c}}\cdot\left[\left(\mathrm{M_{end}^{CH}} - \mathrm{S_{end}^{CH}}\left(\mathrm{T_{inf}^{CA}} - \mathrm{T_{end}^{CA}}\right)\right) - \left(\mathrm{M_{end}^{CA}} - \mathrm{S_{end}^{CA}}\left(\mathrm{T_{end}^{CA}} - \mathrm{T_{inf}^{CA}}\right)\right)\right] - \mathrm{CA_{ini}}\right]\right\} \quad 3.2$$

where:

- CH is the amount of calcium hydroxide in g/100 g of anhydrous cement.
- $\mathrm{M_C}$ is the initial (anhydrous) mass (g) of the cement in the TGA sample.
- $\mathrm{M_{start}^{CH}}$, $\mathrm{M_{end}^{CH}}$ and $\mathrm{M_{end}^{CA}}$ are the masses, in g, of the sample at the start and endpoint for CH decomposition and the endpoint for the $CaCO_3$ decomposition, respectively.
- $\mathrm{T_{start}^{CH}}$, $\mathrm{T_{inf}^{CH}}$, $\mathrm{T_{end}^{CH}}$, $\mathrm{T_{end}^{CA}}$ and $\mathrm{T_{inf}^{CA}}$ are the temperatures (°C) of the start point, the mass inflection point, the endpoint for the CH decomposition, the endpoint, and the inflection point for the $CaCO_3$ decomposition, respectively.
- $\mathrm{S_{start}^{CH}}$, $\mathrm{S_{end}^{CH}}$ and $\mathrm{S_{end}^{CA}}$ are the slopes of the tangential lines of the start and endpoint for the CH decomposition and the endpoint for the $CaCO_3$ decomposition, respectively.
- $\mathrm{CA_{ini}}$ is the initial content of $CaCO_3$ in g/g of anhydrous cement.
- 74.1/18, 74.1/100.1, and 100.1/44.0 are the molar weight ratios of CH to H_2O, CH to $CaCO_3$, and $CaCO_3$ to CO_2, respectively.

Besides, additional samples with higher w/b (0.45 and 0.55) and two different percentages of nano-TiO_2 (0% and 1%) were tested at 14 days to further discuss the chapter results.

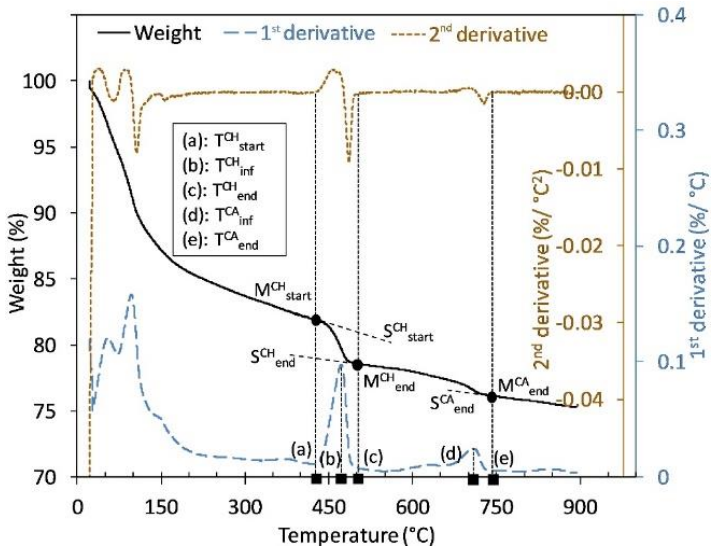

Figure 3.4. Modified method for CH calculation.

Furthermore, 3D X-Ray microscopy was employed to scan and analyze the internal structure of additional specimens. A total of four samples were 3D scanned at 14 days using a 3D X-Ray Microscope (3D XRM). Two percentages of nanoparticles (0% and 1%) and two w/b (0.45 and 0.55) were used to prepare the samples. The parameters of the scans are specified in *Chapter 2: Materials and general procedures*.

3.3 Results and discussion

3.3.1 ANN Model

A plot of the actual and predicted compressive strength is shown in Figure 3.5.a. Its performance was examined to study the model's accuracy. Figure 3.5.b presents a plot of the mean squared error (MSE) of the training, testing, and validation phases as a function of training iterations (epochs). The MSE is computed using Eq. 3.3.

$$\mathrm{MSE} = \frac{1}{n}\sum_{1}^{n}(y_i - \hat{y}_i)^2 \qquad 3.3$$

Where n is the number of data points; y_i is the actual value (measured compressive strength); $\hat{y}_i$ is the predicted value (predicted compressive strength).

The MSE for all three phases, i.e., training, testing, and validation, decreases as the number of epochs increases. It can be seen that the best validation error occurs at epoch 2 with an MSE value of 0.013, implying that the model provides high accuracy.

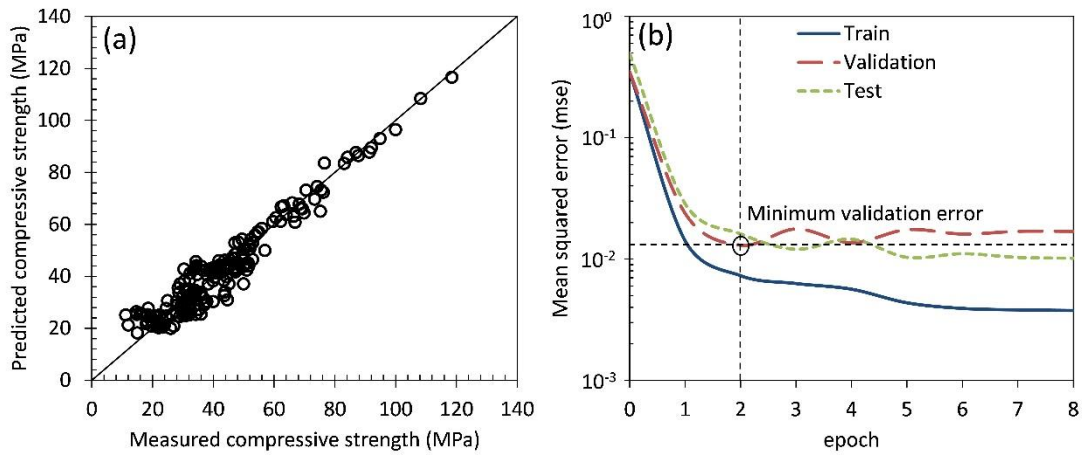

Figure 3.5. (a) Predicted compressive strength versus measured compressive strength (MPa). (b) Mean squared error (MSE) versus epoch.

3.3.2 Virtual experimental campaign

The estimated compressive strength was obtained from the virtual experiment described in section 3.2.2 using the ANN model validated in section 3.3.1. Figure 3.6.a shows the predicted compressive strength as a function of nano-TiO_2 percentage for w/b between 0.38-0.42 at a testing age of 3 days. It can be observed that for all w/b, the predicted compressive strength increases as the nano-TiO_2 percentage increases until it reaches a peak at a certain nano-TiO_2 percentage, i.e., optimum percentage of nano-TiO_2. Results suggest that the higher w/b, the higher the optimum percentage of nano-TiO_2. Similar trends are observed for testing ages 7 and 28 days, Figure 3.6.b and Figure 3.6.c, respectively.

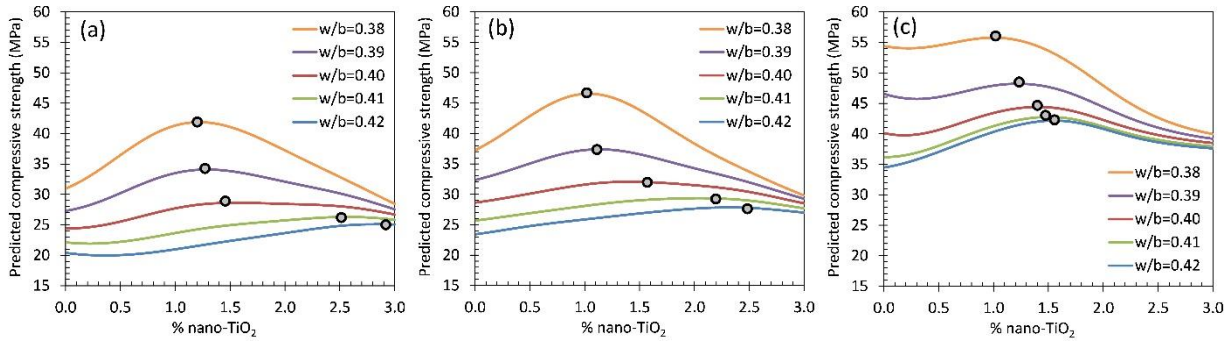

Figure 3.6. Predicted compressive strength (MPa) of the virtual experiment as a function of w/b and percentage of nano-TiO_2. (a) 3 days. (b) 7 days. (c) 28 days.

Figure 3.7 summarizes the results of the optimum percentage of nano-TiO_2 from Figure 3.6 as a function of the w/b for each testing age (3, 7, and 28 days). Figure 3.7.b presents a trend contour plot of the optimum percentage of nano-TiO_2 as a function of testing age and w/b. It indicates a clear trend observed for all testing ages: as the w/b increases, the optimum percentage of nano-TiO_2 increases. Moreover, results present another general trend: the lower the testing age, the higher the optimum percentage of nano-TiO_2 required.

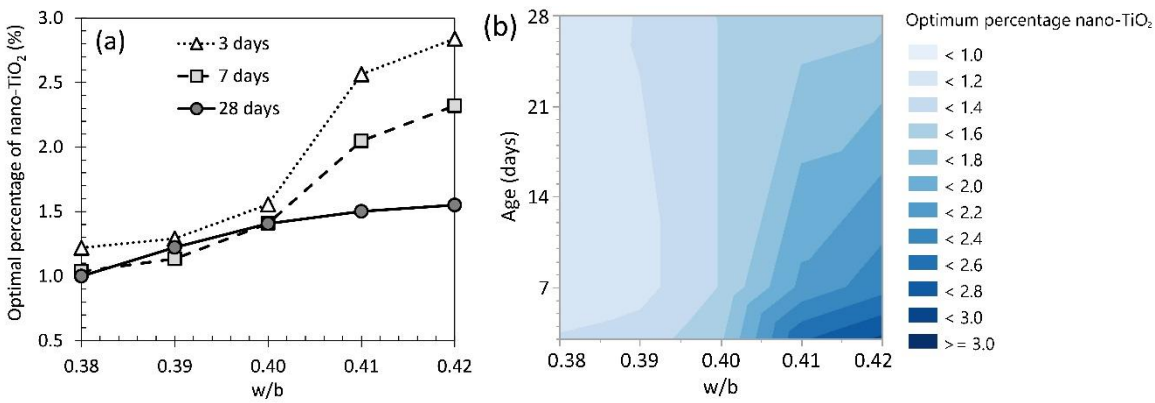

Figure 3.7. Optimal percentage of nano-TiO_2 as a function of w/b and age. (a) Based on data from Figure 3.6. (b) Trend contour plot.

3.3.3 Laboratory campaign results

Compressive strength results

Figure 3.8 exhibits the compressive strength results at seven days for all studied mixtures. The solid lines, represented in Figure 3.8, show the average value of the tested samples, whereas the shaded area refers to the range of results observed for each mixture. As expected, the lower the w/b, the higher the compressive strength observed. In both w/b, the compressive strength increased with the nanoparticles' addition until a 1% of nano-TiO_2. In mixtures with a low w/b (0.38), the compressive strength clearly reached a peak with 1% of nanoparticles, and a higher percentage reduced the strength (compared to 1% addition). However, with a higher w/b (0.42), it is not clear if the optimum percentage of nanoparticles is within the range of study, and higher percentages could have a more significant positive effect on the compressive strength of these cement pastes. The w/b=0.38 samples presented a higher variation in the compressive strength due to the nano-TiO_2 addition than samples with a high w/b for the studied range of nano-TiO_2 addition.

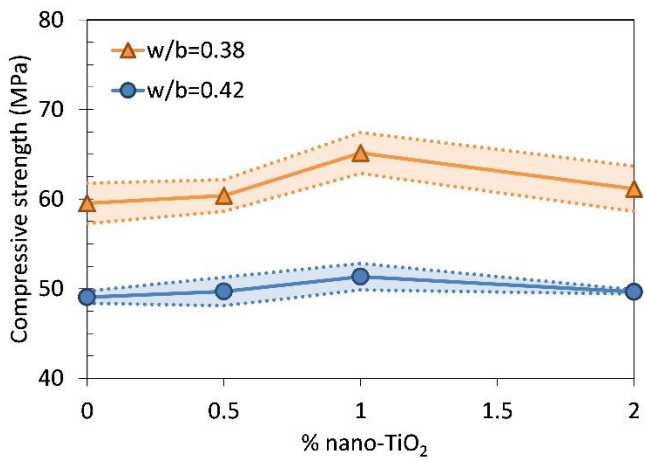

Figure 3.8. Compressive strength (MPa) at 7 days as a function of w/b and percentage of nano-TiO_2.

TGA results

Figure 3.9.a shows the CH content at seven days for all studied mixtures. With a low w/b (0.38), the CH content uniformly decreased with the use of nanoparticles up to 1% of replacement. Beyond that, a higher content of nanoparticles (2%) produced an increase in the CH content compared to the specimen with 1% of nano-TiO_2, but still lower than the CH content of the

reference sample (no nano-TiO_2). This trend can appear to be counter-intuitive in light of the compressive strength results. However, besides changes in hydration products content due to the use of nano-TiO_2, other effects of nano-TiO_2, such as the filling effect and the changes in the size of CH, may affect the porosity and, therefore, the strength. On the other hand, even though, for a high w/b (0.42), a 0.5% addition produced a slight decrease in the CH content, a higher addition of nanoparticles (1%, 2%) increased the CH content in comparison to the specimen with no nano-TiO_2. Therefore, the nanoparticles' addition may promote the growth of hydration products with a high w/b (0.42). Assessing both w/b, the CH content was lower in w/b=0.38 than 0.42. This could be related to the lower hydration degree with a higher w/b [86]–[88]. Besides, the lower the w/b, the higher the percentage of nano-TiO_2 with the lowest CH content. Figure 3.9.b presents an example of TGA curves of samples with two w/b (0.38 and 0.42) and two nano-TiO_2 percentages for each case (0% and 1%). The total amount of hydration products in the samples can be estimated with the weight loss from 105 °C up to 500 °C, where the main hydration products are decomposed (e.g., calcium silica hydrate (C-S-H), CH, and ettringite). With a low w/b, the use of 1% nano-TiO_2 had a negative impact on the total hydration products content since the reference sample (no nano-TiO_2) possesses a higher amount. With a higher w/b (0.42), the same level of nanoparticles (1%) increased the hydration products content compared to the specimen with the same w/b and no nanoparticles. TGA curves of the other studied percentages of nano-TiO_2 (0.5% and 2%) can be found in Appendix B (Figure B.1).

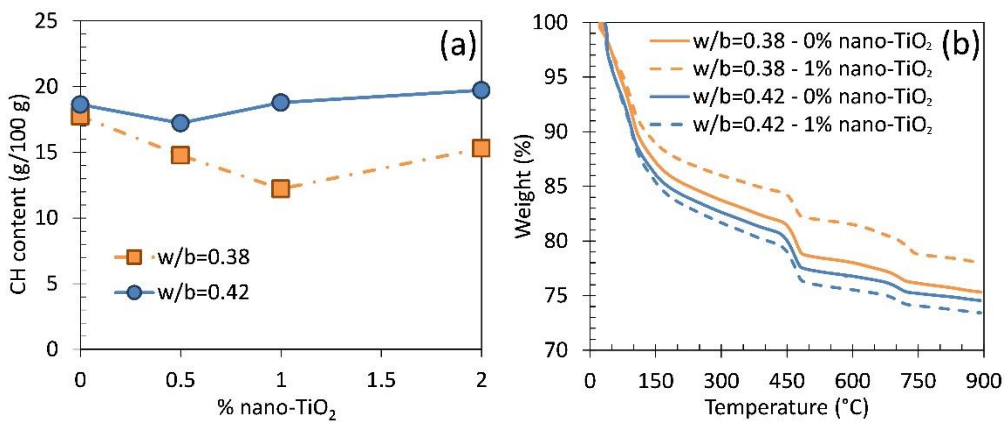

Figure 3.9. (a) CH content (g/100 g) at 7 days. (b) TGA curves at 7 days of cement pastes with two percentages of nano-TiO_2 (0% and 1%) and two w/b (0.38 and 0.42).

3.4 Discussion

3.4.1 Main effects of nano-TiO_2 modifying compressive strength of cement pastes

On the one hand, the use of nano-TiO_2 produced an increase in 7-day compressive strength in samples with a 0.38 w/b (Figure 3.8), as opposed to the specimens with no nanoparticles' inclusion. On the other hand, samples with nano-TiO_2 and a w/b of 0.38 showed a lower CH content at seven days (Figure 3.9) than the references cement pastes (no nanoparticles).

These results suggest that the increase of compressive strength at seven days is not only related to an increase of hydration products (in fact, there is a decrease of hydration products due to the use of nano-TiO_2).

It is well-known that two main factors affect the compressive strength of cement pastes: hydration products and porosity [88]. However, the porosity influences the compressive strength to a greater extent [88]. Indeed, plain cement pastes with lower w/b (lower porosity) may show higher compressive strength with lower CH content [89]. This observation can be noticed in the results of the reference sample (0% of nano-TiO_2); the higher the w/b, the higher the CH content, and the lower the compressive strength.

Therefore, results suggest that the increase of compressive strength observed at 7 days, for samples with w/b of 0.38 and nano-TiO_2 (compared to its reference mixture), is primarily related to a decrease of porosity resulting from the addition of nano-TiO_2. Also, results indicate that in the case of a low w/b, the use of nano-TiO_2 did not enhance the hydration products content. It is well-known that the hydration process may be stopped due to the lack of space for hydration products to grow (due to low porosity) [90]. This may explain why samples with lower CH content exhibited higher compressive strength with a 0.38 w/b, since previous studies observed a 50% porosity reduction due to the use of 0.5% nano-TiO_2 [29], and in the case of 0.38 w/b, the porosity of samples without nano-TiO_2 is expected to be already very low. Results also show that CH content changes cannot be used to predict changes in compressive strength produced by the use of nano-TiO_2 since the nanoparticles modify the pore structure, thus reducing the size of the big pores due to the filling effect. It may affect the compressive strength to the extent that changes in strength due to the use of nano-TiO_2 do not correlate with the corresponding changes of CH content.

Conversely, with high w/b, nano-TiO_2 may have a double positive effect on compressive strength. In addition to reducing the porosity and enhancing the overall pore structure, nano-TiO_2 may increase the hydration product content when the initial porosity of the reference cement paste is high (due to the high w/b). Since mixtures with a high w/b present high porosity, the reduction of porosity due to the use of nano-TiO_2 will not be enough to limit the growth of the CH particles. Besides, the use of nanoparticles can promote the hydration process serving as nucleation sites [43], [44]. Therefore, the higher the w/b, the higher the percentages of nano-TiO_2 that may present this dual positive effect on compressive strength.

An excess of nano-TiO_2 may limit the space available for the CH particles to grow up, eventually stopping the hydration. Results suggest that the higher the w/b (higher porosity), the higher the optimum percentage of nano-TiO_2 in terms of compressive strength. This agrees with the conclusions of the virtual experimental campaign.

3.4.2 Study of the effect of nano-TiO_2 on porosity using 3D X-Ray Microscope results and its relation to changes in hydration products

Furthermore, Figure 3.10 displays the 3D pore structure of additional samples with higher w/b (0.45 and 0.55) than the studied ones, and 0% or 1% of nano-TiO_2 at 14 days. These samples have a total volume of 16,626.34 mm^3. Figure 3.10 also presents TGA curves for the additional cement pastes prepared. As mentioned in the previous section, the total amount of hydration products in the samples can be calculated with the weight loss from 105 °C up to 500 °C, where the main hydration products are decomposed (e.g., C-S-H, CH, and ettringite). Results show that the use of 1% of nano-TiO_2 increased the hydration products content compared to each reference sample (no nanoparticles) for both w/b. Nonetheless, the nanoparticles produced a higher increase of the hydration products content in the samples with a higher w/b (0.55).

In samples with a 0.45 w/b, the use of 1% of nano-TiO_2 reduced the porosity by 5.29% (compared to the reference sample with no nano-TiO_2), and increased the CH content by 8.59%. On the other hand, specimens with a higher w/b (0.55) exhibited a 12.04% decrease in porosity (compared to the sample with no nano-TiO_2) and the CH content increased by 11.66% due to the use of 1% of nanoparticles. Therefore, the higher the w/b, the higher the porosity reduction and

the increase of the CH content for the same percentage of nanoparticles (1%). Consequently, results suggest that the higher the w/b, the higher the positive effect of 1% nano-TiO_2.

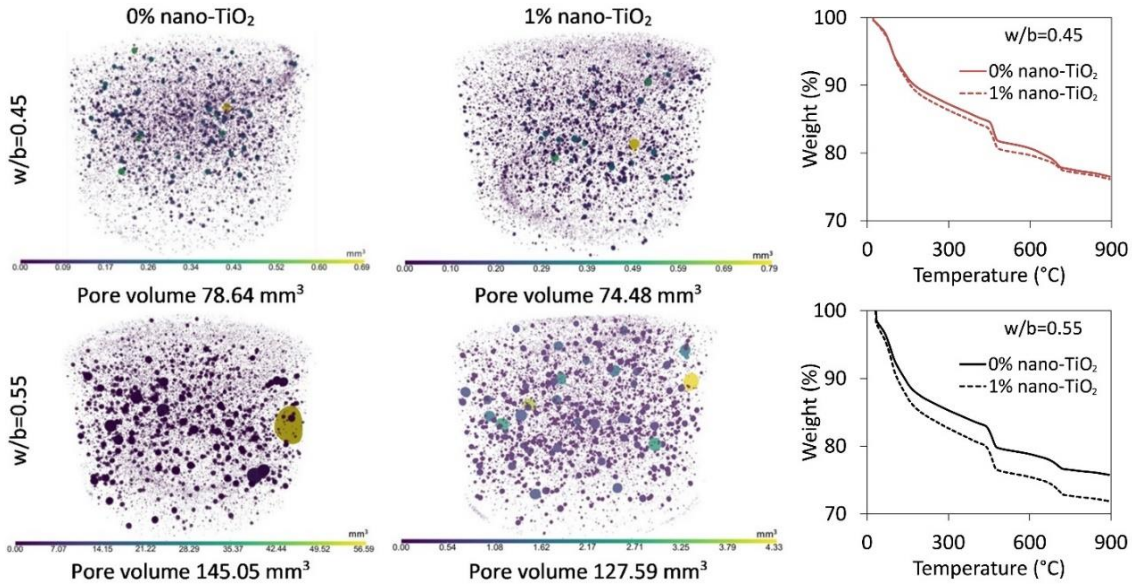

Figure 3.10. Pore structure and TGA curves of cement pastes at 14 days with two percentages of nano-TiO_2 (0% and 1%) and two different w/b (0.45 and 0.55).

Table 3.5 summarizes the changes in CH content and porosity due to the addition of nanoparticles of samples with two w/b (0.45 and 0.55) and two percentages of nanoparticles (0% and 1%) at 14 days of curing.

Table 3.5. Comparison of pore volume and CH content of samples with 0% and 1 % of nano-TiO_2

w/b	**% of nano-TiO_2**	**Pore volume (mm^3)**	**Variation due to the use of nano-TiO_2 (%)**	**CH content (%)**	**Variation due to the use of nano-TiO_2 (%)**
0.45	0%	78.64	-5.29	13.38	+8.59
	1%	74.48		14.53	
0.55	0%	145.05	-12.04	14.49	+11.66
	1%	127.59		16.18	

3.4.3 Impact of w/b on the effect of the nano-TiO_2 on compressive strength

Considering these observations, Figure 3.11 summarizes the potential effects of nano-TiO_2 on compressive strength as a function of the w/b compared to the reference cement paste (no nanoparticles). Three potential scenarios can be drawn depending on the w/b: (i) very low w/b, (ii) intermediate w/b, and (iii) high w/b:

- With a low w/b, the initial porosity of the reference sample (no nano-TiO_2) is very low. Therefore, the small potential reduction of porosity due to the use of nanoparticles will not have a significant impact on the compressive strength. However, this porosity reduction may imply a stop of the hydration process due to the lack of space for hydration products to grow. Therefore, the degree of hydration would be lower than in the reference mixtures (no nano-TiO_2). Thus, the cement pastes could negatively affect compressive strength due to the combination of both effects.
- With an intermediate w/b, the use of nanoparticles would reduce the porosity of the cement paste, increasing the compressive strength. However, the degree of hydration would still be lower than that of reference mixtures (no nanoparticles) if this porosity reduction produced a lack of space for CH to grow. As aforementioned, porosity reduction due to the nanoparticles' addition may overcome the potential adverse effect on the hydration product content, resulting in greater compressive strength than in reference mixtures.
- With a high w/b, nano-TiO_2 would also produce a higher porosity decrease. Besides, the hydration products content will increase because there is space available for them to grow up. In this case, both effects may produce a synergy and, therefore, the compressive strength may be highly increased.

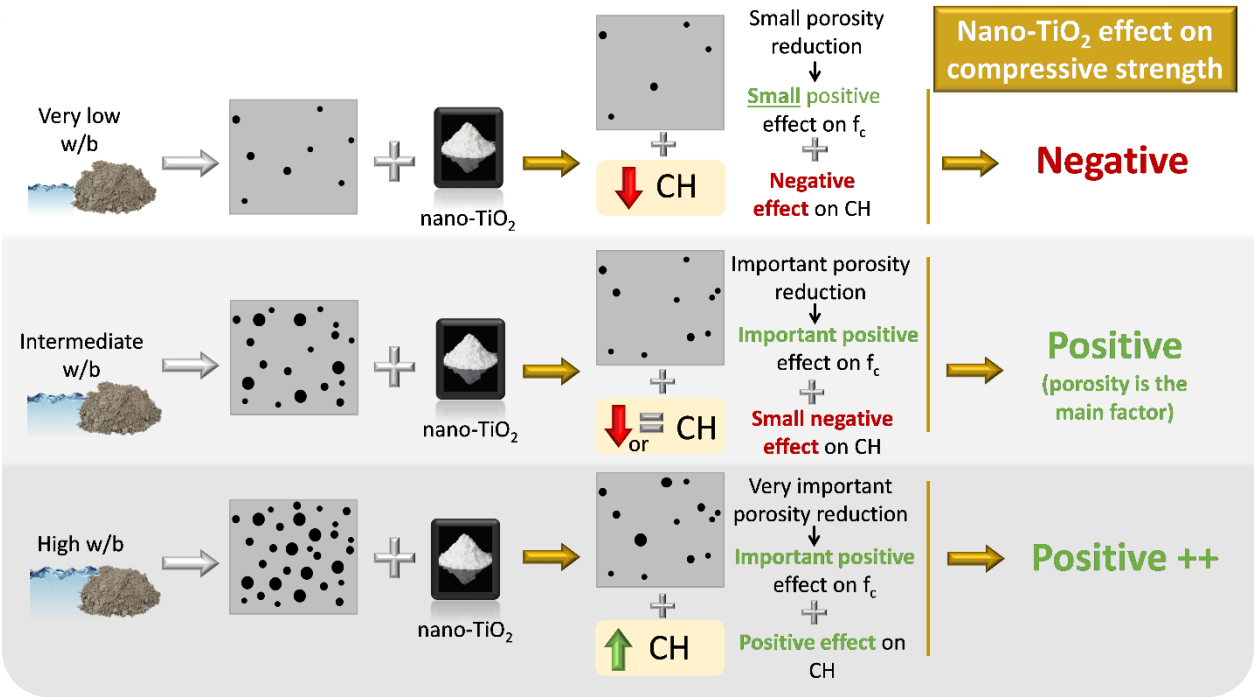

Figure 3.11. Schematic explaining why a given amount of nano-TiO_2 may cause different effects on compressive strength as a function of w/b.

3.5 Conclusions

Based on the results for this chapter, the following conclusions can be drawn:

ANN results suggest that, in general, the higher the w/b and the lower the age, the higher the optimum percentage of nano-TiO_2 in terms of compressive strength for all studied ages. Experimental results of compressive strength performed in this chapter agree with these trends, and TGA and 3D X-Ray results have been used to find the explanation of these trends.

Results indicate that changes in CH content produced by the use of nano-TiO_2 cannot be used to predict changes in compressive strength since the nanoparticles modify the pore structure, and this modification changes the compressive strength to a greater extent than changes in CH content.

The potential effects of the addition of nano-TiO_2 on compressive strength depend on the w/b:

With high w/b, the use of nano-TiO_2 may increase the compressive strength due to the synergy effect of two phenomena: (i) the reduction of the porosity due to the filling effect and

enhancement of the pore structure; and (ii) the increase of the hydration products content due to the nucleation site effect (because there is no limitation in the space available for them to grow since initial porosity is high due to the high w/b).

However, when the w/b of reference mixtures is very low, the use of nano-TiO_2 may reduce the hydration products content due to the lack of space for the CH to grow. Additionally, since the initial porosity was already very low, the porosity reduction due to the use of nano-TiO_2 would be low and could not be enough to overcome the potential negative effect on hydration. Therefore, it may lead to a decrease in the compressive strength of mortars. These results explain the dependence of the optimum percentage of nano-TiO_2 on w/b and age. Both w/b and age affect the porosity of the reference mixtures, and the effect of nano-TiO_2 depends on the initial porosity of the cement paste.

4. TIO_2 NANOPARTICLES INFLUENCE ON THE ENVIRONMENTAL PERFORMANCE OF NATURAL AND RECYCLED MORTARS: A LIFE CYCLE ASSESSMENT

Part of this chapter has been published as:

C. Moro, V. Francioso, M. Schager and M. Velay-Lizancos (2020). *'TiO_2 nanoparticles influence on the environmental performance of natural and recycled mortars: A life cycle assessment.'* Environmental Impact Assessment Review, vol. 84, p. 106430. https://doi.org/10.1016/j.eiar.2020.106430.

4.1 Introduction

Carbon oxides (CO_X), sulfur oxides (SO_X), nitrogen oxides (NO_X), and volatile organic compounds (VOCs) are toxic gases present in large quantities in the atmosphere around the world [91]–[94]. The Air Quality Index (AQI) is an indicator that quantifies the health hazard of those pollutants [91]. Many cities, particularly in Asia, show a high AQI, being potentially dangerous for human health [95], [96]. Nonetheless, the sources are diverse. While VOCs are related to indoor places [97], CO_X, SO_X, and NO_X are caused by traffic or industries [98]. Outdoor air pollutants are responsible for increasing global warming and acid rain [99]. They may also lead to diseases such as asthma or cancer [100], [101] reducing life expectancy. According to the World Health Organization (WHO), in 2016, pollution caused more than 4 million premature deaths worldwide. The principal organization fighting against climate change is the United Nations Framework Convention on Climate Change (UNFCCC). They have made several agreements, including the Kyoto Protocol [102] or the Paris Agreement [103]. However, the measures adopted are still insufficient to counter climate change [104], [105]. The World Meteorological Organization (WMO) has recently reported that greenhouse gases (GHG) have reached their highest level since 3-5 million years ago. According to the Intergovernmental Panel on Climate Change (IPCC), carbon dioxide (CO_2) had 65% of the global greenhouse gas emissions in 2014.

Cementitious composites, such as concretes and mortars, are responsible for a significant percentage of CO_2 emissions due to the cement industry. In 2016, cement production caused 8% of the total world's CO_2 emissions [4]. Some approaches that have been suggested during the last

years might help to reduce the environmental impact of the cementitious composites: (i) using cement replacements such as supplementary cementitious materials (SCM); (ii) producing a photocatalytic material capable of capturing pollutants from the environment (e.g., TiO_2 concrete); or (iii) using materials with the ability of sequestrating CO_2 such as recycled aggregate (RA). In addition to cement, cementitious composites are made of aggregates, among others. Aggregates significantly impact the sustainability of structures since they represent around 60-70% of the total concrete volume. The extraction of raw materials produced more than 70% of building energy consumption in China [106]. Due to urbanization and industrialization, the construction industry has increased the number of concrete structures built. Therefore, the amount of raw materials required is higher. Nevertheless, waste products from old structures can be used as a replacement for natural aggregate (NA) to reduce their environmental impacts [12], [13].

Consequently, using RA instead of NA could add a tremendous environmental value in terms of abiotic depletion and waste generation. RAs from construction and demolition waste are classified into two main groups [107]: (i) recycled concrete aggregates (RCA), which comes from crushed concrete, and (ii) mixed recycled aggregates (MRA), which contains ceramics and concrete. Depending on the type used, its influence on the properties of the new concrete may change. Previous research showed that RA decreases the strength of concrete [13], [108], [109]. In terms of durability, the higher the RA percentage, the lower the durability [110]. Besides, they increase concrete porosity leading to a reduction in resistance to chemical attack [51], [110]. A reduction in porosity may lead to an improvement in the durability and strength of recycled concretes. A possible alternative to decrease porosity would be using TiO_2 nanoparticles as a cement replacement.

Previous literature showed that TiO_2 nanoparticles addition reduced total porosity in cement blends at room temperature (20-25 °C) [29], [44], [47], [111]. Another study using scanning electron microscope (SEM) found that 3% wt. TiO_2 increased the particle packing density and the homogenous quality of the interfacial transition zone (ITZ) in mortars at 28 days with 20% rice husk ash [43]. These could be two potential explanations of why TiO_2 nanoparticles addition (up to 5% replacement by weight of cement) can improve compressive strength [43], [44], [57], [63], [112]–[114]. Besides, TiO_2 can accelerate the hydration of cement and restrict the growth of

calcium hydroxide (CH), leading to a denser microstructure [115]. As a result, the microstructure is refined, increasing chloride penetration resistance [116].

Moreover, TiO_2 could decrease contamination levels since this material is a well-known photocatalytic activator [17], [40]–[42]. Hazardous pollutants (NO_x, SO_x, CO_x, VOC_s) may be captured in the presence of light [14], [15]. Last year, Baral et al. [18] have reported an improvement in the environmental impacts of concrete pavements due to the incorporation of TiO_2. They stated that removing NO_x, SO_x, and toluene could enhance different impact categories (e.g., eutrophication, acidification, respiratory effects, or smog formation) [18]. Even though it could be a potential solution to decrease total emissions, estimating the environmental impacts during its production should be considered.

Over the past few decades, sustainable construction has been developed to protect the environment and its natural resources for future generations. Nowadays, the construction industry is responsible for the depletion of natural resources (half of the global consumption), energy use (40% of the total), and waste generation (50% of the total) [117]. Life cycle assessment (LCA) was developed to evaluate the environmental effect of human activities [118]. The LCA methodology quantifies the environmental performance during a given part of the life, for example, focusing on the production (*cradle-to-gate* approach) or evaluating the impacts during the whole life cycle (from *cradle-to-grave*). In the last 15 years, there has been an increase in the literature about the life cycle assessment of building materials [119]–[123]. Several studies have been focused on quantifying the environmental impact of using RA as a substitution of NA [124]–[127]. RA may show a higher total environmental impact depending on the functional unit used [126]. For instance, if the functional unit is defined as 1 m^3 of concrete with a given strength and durability, using recycled aggregate would require a higher cement content than using natural aggregate. The increase in cement content will increase CO_2 emissions [128]. However, quantifying the CO_2 uptake during the crushing process would highly decrease the CO_2 emissions of RA concrete [127].

Whereas several studies on the effect of the use of RA in environmental impact, the effect of TiO_2 nanoparticles on the sustainability of cementitious materials is still not clear. Even though some investigations evaluate the life cycle assessment of cementitious materials made with TiO_2 nanoparticles [16], [18], [129], those studies were focused on photocatalytic concrete made with

natural aggregates. No previous research has studied the influence of nano-TiO_2 on the LCA of mortars made with recycled aggregates. Two of the effects of recycled aggregate use on mortars and concretes (i) increase of porosity [51], [110] (ii) lower strength in the ITZ due to the poor adhesion between the old cement past and the new cement paste [130]. Based on that and considering that the addition of nano-TiO_2 reduces the porosity and the size of the CH [115], its use may have a different effect on natural aggregate mortars and recycled aggregate mortars. Therefore, the combined use of nano-TiO_2 and recycled aggregate and its effect on LCA should be studied.

Consequently, this chapter aims to study how the use of TiO_2 nanoparticles affects the environmental performance of eco-mortars with different percentages of recycled aggregate and its comparison to the nano-TiO_2 effect on the LCA of the standard mortar with natural aggregate.

4.2 Materials and methods

4.2.1 Materials

The material characterization of the cement, natural fine aggregates, recycled fine aggregates and nano-TiO_2 used in this chapter is exhibited in *Chapter 2: Materials and general procedures*.

4.2.2 Methods

Experimental program

An experimental program was performed to evaluate the combined effects of recycled aggregate and nano-TiO_2 on the compressive strength of mortars. These variations on strength could affect the LCA of mortars if the functional unit is defined as a unit volume of mortar with a given compressive strength. Therefore, the objective of the experimental campaign is to estimate the change in the cement content required to achieve the same compressive strength when different percentages of recycled aggregate and nano-TiO_2 are used.

In this chapter, twelve different mortars with the same water-to-cement (w/c) ratio (0.50) were designed. Three percentages of RA substitution (0%, 50%, and 100%) and four percentages,

by the total mass of cement, of nano-TiO_2 (0%, 0.5%, 1%, and 2%) substitution were used. The nomenclature of samples was MX-Y, where 'X' is the percentage of RA replacement, and 'Y' is the percentage of nano-TiO_2 substitution. The mixture proportions of each mortar are listed in Table 4.1.

Table 4.1. Mixture proportions of mortar mixtures.

Mixture	**Cement (kg/m^3)**	**NA (kg/m^3)**	**RA (kg/m^3)**	**nano-TiO_2 (kg/m^3)**	**Water (kg/m^3)**	**w/c**
M0-0	516.7	1550.2	0.0	0.0	258.4	0.5
M0-0.5	514.1	1550.2	0.0	2.6	257.1	0.5
M0-1	511.6	1550.2	0.0	5.2	255.8	0.5
M0-2	506.4	1550.2	0.0	10.3	253.2	0.5
M50-0	516.7	775.1	712.1	0.0	258.4	0.5
M50-0.5	514.1	775.1	712.1	2.6	257.1	0.5
M50-1	511.6	775.1	712.1	5.2	255.8	0.5
M50-2	506.4	775.1	712.1	10.3	253.2	0.5
M100-0	516.7	0.0	1424.3	0.0	258.4	0.5
M100-0.5	514.1	0.0	1424.3	2.6	257.1	0.5
M100-1	511.6	0.0	1424.3	5.2	255.8	0.5
M100-2	506.4	0.0	1424.3	10.3	253.2	0.5

Compressive strength is one of the most common project requirements in the construction industry. Therefore, it should be considered in the life cycle assessment. The functional unit chosen was a 1 m^3 of mortar with the same compressive strength as the reference mortar (M0-0 (0.50)). To estimate the variation of cement content needed to achieve the common target compressive strength for each mixture, plain mortars with different w/c (maintaining the same amount of aggregate) were designed and studied (Table 4.2). The nomenclature of these samples was MX-Y (Z), where 'X' is the percentage of RA replacement, 'Y' is the percentage of nano-TiO_2 substitution, and 'Z' is the w/c.

Table 4.2. Mixture proportions of additional mortar mixtures used for functional unit evaluation.

Mixture	Cement (kg/m^3)	NA (kg/m^3)	RA (kg/m^3)	nano-TiO_2 (kg/m^3)	Water (kg/m^3)	w/c
M0-0 (0.50)	516.7	1550.2	0.0	0.0	258.4	0.50
M0-0 (0.55)	486.9	1550.2	0.0	0.0	287.0	0.55
M0-0 (0.60)	460.4	1550.2	0.0	0.0	295.4	0.60

The mixing was conducted using a mortar pan mixer. First, dry aggregates (NA or RA, correspondingly) were mixed alone at low speed for 30 seconds. Next, absorption water was incorporated and mixed with aggregates for another 30 seconds. The mixture was left for 10 minutes allowing aggregates to absorb the water. Then, cement and TiO_2 (if applicable) were added and mixed at low speeds for 1 minute. Afterward, the effective water was added, and the materials were mixed for another three minutes. After that, the inside of the container was scraped to mix in any material stuck to the sides, and the mixture was mixed for one more minute.

Three prisms with dimensions 40 x 40 x 160 mm for each mixture were cast to comply with the ASTM C349 [36]. At the end of the mixing, the mortar was poured into the molds and leveled with a trowel. Next, the molds filled with mortar were put on a vibration table for 60 seconds to help the mortar settle and consolidate. Subsequently, they were wrapped in plastic film and left for 24 hours at 23 °C. After the first day, the samples were demolded and submerged in water at the same controlled temperature until testing. After 28 days of curing, each half of a sample was used for the compressive strength test (defined in *Chapter 2: Materials and general procedures*), testing a total of six samples of each mortar.

Life cycle assessment (LCA)

The LCA methodology is based on the international standards ISO 14040 [131] and ISO 14044 [132]. It is a four-step method (Figure 4.1): (i) goal and scope definition, (ii) life cycle inventory (LCI) creation and analysis, (iii) life cycle impact assessment (LCIA), and (iv) interpretation of results.

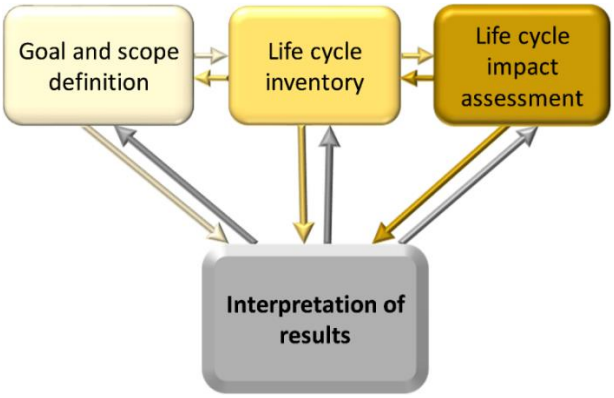

Figure 4.1. Life cycle assessment framework. Adapted from [131].

Goal and scope

The chapter aims to assess the environmental impact of TiO_2 nanoparticles' addition in both mortars with natural aggregates (natural mortars) and mortars with recycled aggregates (recycled mortars). Twelve mixes with three different percentages of RA substitution (0%, 50% and 100%) and four percentages, by total mass of cement, of nano-TiO_2 (0%, 0.5%, 1%, 2%) substitution were studied.

The chosen system boundary was a *cradle-to-gate* approach. This boundary allows quantifying the embodied environmental impacts of the material since it includes the stages from raw materials extraction (*cradle*) to mortar production (gate*)*. The functional unit (FU) chosen was 1 m^3 of mortar with the same compressive strength as the reference mixture (M0-0 (0.50)).

In order to compare the environmental impact of the studied mortars (Table 4.1), a calibration curve exhibiting the development of compressive strength as a function of cement content of the reference mortar (M0-0 (0.50), additional mortar mixtures are shown in Table 4.2) was used. This curve served to estimate the variations in the cement content to achieve the same compressive strength when RA and/or nano-TiO_2 are added.

Life cycle inventory (LCI)

As a first step, each material production's inputs (energy and materials) and outputs (emissions and wastes) should be collected. This stage is called the life cycle inventory (LCI).

Since there is no unique global database, the data was taken from different sources depending on the availability and reliability.

Table 4.3 shows the source from where the data of the life cycle inventory was taken. Production of cement, NA, nano-TiO_2, and total transportation impact (assuming a lorry of 22 t) data were obtained from the European Platform on Life Cycle Assessment (ELCD). The information about the production of RA was found in a previous study [133]. The environmental impact of mixing of mortar was assumed to be the same as that of mixing of concrete and thus data available in the literature for concrete [133] were used when assembling the LCI. This assumption was made based on two factors: (i) extensive and more reliable concrete production data than mortar production, (ii) both concrete and mortars are made mainly of aggregates, cement, and water. The main difference between concrete and mortar is the size of the aggregates (mortars contain just fine aggregate), and the mixing process is very similar.

Additionally, transport distances were collected from the life cycle inventory of Portland cement concrete [134]. However, there was no available data for TiO_2 nanoparticles transportation. Therefore, a safety factor was assumed by equalizing its transport distance to the highest value (cement).

Table 4.3. Sources of the life cycle inventory of each material or process.

Process	**Source**
Cement production	European Platform on Life Cycle Assessment (ELCD)
Natural aggregate	European Platform on Life Cycle Assessment (ELCD)
Recycled aggregate	Marinkovic et al. (2017) [133]
nano-TiO_2 production	European Platform on Life Cycle Assessment (ELCD)
Mortar mixing	Marinkovic et al. (2017) [133]
Transportation emissions	European Platform on Life Cycle Assessment (ELCD)
Transportation distances	Marceau et al. (2007) [134]

Furthermore, a previous study [135] estimated the CO_2 uptake during RA's demolition and crushing process. They quantified the CO_2 absorbed in 10.8 kilograms per ton. Consequently, this value is subtracted from the CO_2 produced during RA production to consider this beneficial effect. LCI data is presented in Table 4.4. The estimation of waste generation is made considering the

density of the studied mortars. The average density of all studied samples was 2156 kg/m^3 (with a standard deviation lower than 2.5%).

Table 4.4. Life inventory data used in this chapter.

	Cement (kg) [ELCD]	NA (kg) [ELCD]	RA (kg) [133]	nano-TiO_2 (kg) [ELCD]	Mortar mixing (m^3) [133]	Transport lorry 22t (t*km) [134]
Inputs: Fossil fuels (kg)						
Diesel	3.56E-02	3.29E-04	6.50E-04	2.91E-01	2.00E-02	2.06E-02
Gas	8.53E-03	1.24E-04	3.95E-05	6.82E-01	5.30E-02	1.13E-03
Soft coal	2.67E-02	3.13E-04	2.90E-05	7.60E-02	5.25E+00	7.31E-05
Hard coal	4.83E-02	2.18E-04	4.04E-05	8.19E-01	4.01E-02	9.01E-05
Outputs: Emissions to air (kg)						
CO_2	8.85E-01	2.34E-03	1.77E-03	2.60E+00	4.59E+00	6.40E-02
CO	2.14E-03	4.19E-06	6.62E-06	4.47E-02	8.81E-04	1.10E-04
CH_4	5.80E-04	3.72E-06	9.09E-07	8.20E-04	2.19E-03	6.25E-05
C_2H_4	3.95E-10	9.24E-12	2.06E-09	8.61E-06	7.36E-08	3.70E-10
CFC-11	5.22E-09	1.75E-10	6.75E-17	2.71E-08	2.09E-15	6.08E-11
CFC-114	5.35E-09	1.79E-10	1.44E-12	2.78E-08	3.67E-09	6.23E-11
SO_x	1.05E-03	9.49E-06	1.27E-06	1.34E-04	5.34E-02	3.41E-05
NO_x	1.79E-03	1.52E-05	2.23E-05	1.10E-02	8.01E-02	5.39E-04
N_2O	2.22E-06	3.81E-08	6.73E-08	1.73E-04	2.20E-05	7.32E-07
NH_3	3.91E-02	7.24E-09	1.82E-08	3.71E-05	3.27E-07	4.00E-07
NMVOC	2.26E-01	1.37E-06	2.64E-06	6.98E-04	9.20E-05	3.20E-05
HCl	1.99E-02	1.80E-07	3.91E-09	1.05E-04	4.00E-04	8.20E-08
N (water)	1.16E-04	4.23E-09	2.86E-09	6.88E-05	4.81E-06	2.35E-07
PO_4^{-3} (groundwater)	5.14E-07	1.23E-08	1.67E-07	1.54E-04	3.85E-03	5.88E-07

Life cycle impact assessment (LCIA)

The life cycle impact assessment (LCIA) phase aims to evaluate the importance and relevance of potential environmental impacts based on the LCI flow results. In this chapter, the *"Tool for the Reduction and Assessment of Chemical and other Environmental Impacts*" (TRACI) methodology (mid-point approach, by US EPA) was used to estimate the total environmental impact of the mixtures. Seven categories included in TRACI methodology were used to analyze the environmental impact of the studied mortars: (i) global warming potential (GWP), (ii) ozone depletion potential (ODP), (iii) eutrophication potential (EP), (iv) acidification potential (AP), (v) smog formation (S), (vi) respiratory effects (RE), and (vii) energy consumption (EC). Nevertheless,

the ecotoxicity category was excluded since there is no evidence of ecotoxicity of the main compounds of mortars [136]–[138].

Besides, another mid-point approach called CML methodology (methodology of the Centre for Environmental Studies of the University of Leiden) was employed to compare the differences between a European (CML) and an American (TRACI) methodology. In case of the adapted CML methodology, the categories analyzed were: (i) GWP, (ii) ODP, (iii) EP, (iv) AP, (v) photochemical ozone creation potential (POCP), and (vi) EC. This last category (EC) is usually called "abiotic depletion (fossil fuel)" CML methodology. To compare TRACI and CML, the CML category "abiotic depletion (fossil fuel)" was renamed as EC since it is related to the energy consumption defined in TRACI methodology.

Moreover, despite TRACI and CML are well-known LCA methodologies, in the case of cementitious composites, two extra categories, waste generation (WG) and abiotic depletion potential (ADP), should be included in the LCA to consider the potential reduction of raw materials due to the use of recycled aggregates.

As both categories are used in the analysis, an explanation of how they are modeled should be included:

- ✓ The waste generation (WG) estimates the kilograms of material used that can become a waste in the future. Considering that using recycled aggregate reduces the waste produced, the kilograms of recycled aggregate used are subtracted from the kg of total mortar made of each mixture.
- ✓ The abiotic depletion potential (ADP) is defined as the mass of new raw materials used. When recycled aggregate is used, lower amount of natural aggregate is required to make a cubic meter of mortar and, therefore, the ADP is reduced.

The LCI data is converted into a standard unit, depending on the category indicator. The characterization factors, which estimate the relative contribution of each substance to each impact category, were used. Those factors are obtained from databases made by the U.S. Environmental Protection Agency (EPA) and Leiden University in the case of TRACI [139] and CML [140], respectively.

Interpretation of results

The analysis was conducted following several approaches:

(i) Analysis of each single impact category. Every single category's results were discussed to understand the potential implications of the addition of nano-TiO_2 and/or RA.

(ii) Normalization and weighting process. The environmental impacts are usually presented in different units for each category. Therefore, a normalization step should be made to compare the results. In this chapter, two approaches were followed to analyze the results:

Approach 1: The use of normalization factors (NFs) is recommended to convert the results into a common unit. Ryberg et al. [141] collected the NF for TRACI methodology in the United States (USA, 2008). In the case of CML, the NFs were obtained from a database made by Leiden University (World, 2000) [142]. The results were reported in Table 4.7 as *"impact per year"*. Since the NFs were specifically related to each methodology, there was no data for neither waste generation (WG) nor abiotic depletion potential (ADP), which were added categories. Consequently, the NFs were used to quantify total impacts per year without considering those categories. Since the NFs convert the environmental impact of each category on impact per year in a common unit, after normalization, the values are added with uniform weight.

Approach 2: In order to introduce ADP and WG in the analysis, no standard normalization factors are applied, but a normalization using as reference the values of each category of the reference mortar (M0-0(0.50)) has been performed (Eq. 4.1). It was assumed that every impact category had the same importance in the final results regarding weighting. Therefore, for both CML and TRACI methodologies, the evaluation was made using the same weights for all categories. After the quantification, the results were displayed in parts per unit (Table 4.7).

Comparing both approaches could help to understand the influence of ADP and WG as impact categories.

(iii) Comparison of both methodologies (TRACI and CML). The results from both approaches were estimated in terms of the reference mortar (M0-0 (0.50)). Therefore, each result was divided by the value of M0-0 (0.50), as shown in Eq. 4.1. Consequently, the higher the value, the lower the sustainability of the mixture.

$$\overline{I_i} = \frac{I_i}{I_{M0-0}} \qquad 4.1$$

where:

- $\overline{I_i}$ is the value of the ith parameter modified.
- I_i is the value of the ith parameter.
- I_{M0-0} is the value of the mixture M0-0 (0.50).

(iv) Discussion about the influence of functional unit and transportation in total environmental impacts.

4.3 Results and discussion

4.3.1 Experimental campaign

Compressive strength results

Table 4.5 displays the compressive strength results of studied mortars. Those results showed a well-known trend reported in the literature, namely that addition of RA causes a reduction of compressive strength. In terms of the nano-TiO_2 effect, results suggested that the addition of nanoparticles may enhance compressive strength. This could be related to the reduction of porosity and the densification of the microstructure when nanoparticles are used [113]. Besides, the higher the percentage of RA, the higher the optimum percentage of nano-TiO_2. While the use of nanoparticles had a negligible influence on the compressive strength in natural mortars, M50 and M100 mixtures showed an increase in compressive strength by adding 0.5% nano-TiO_2. However, this improvement was not increased by adding a higher percentage of nanoparticles. The reason could be the reduction in porosity made by TiO_2 addition. Since mortars with recycled

aggregate have a higher porosity, there is more potential for improvement based on the reduction of porosity produced by nanoparticles.

Estimation of cement content due to the use of RA and/or nano-TiO_2 to achieve the same compressive strength

The functional unit (FU) chosen to perform the LCA was 1 m^3 of mortar with the same compressive strength as the reference mortar (M0-0 (0.50)). Additional mixtures were studied in a secondary experimental campaign to perform the LCA, considering the effect of both RA and nano-TiO_2 on compressive strength. This secondary experimental campaign aims to estimate the variation of cement content required to equalize the compressive strength to the compressive strength of the reference mortar (M0-0(0.5)). Figure 4.2 displays the compressive strength of mortars made with natural aggregate and no nanoparticles (M0-0) as a function of the cement content. This graph was used for estimating the cement content required to obtain the same compressive strength as the reference mortar (M0-0 (0.50)). The estimation procedure was:

- First, the compressive strength of each mixture was introduced in the graph to estimate the binder content needed to have that compressive strength if the mortar was made with natural aggregate and no nanoparticles.
- The difference between this estimated binder content and the initial binder content was calculated. Then, this variation was added to (or subtracted from) the initial content. The result is the estimated binder content required to achieve the same compressive strength as the reference mortar (M0-0 (0.50)). In mixtures with nano-TiO_2, the binder content was split in cement and nano-TiO_2 content, if applicable maintaining the corresponding nano-TiO_2 percentage. The results obtained are displayed in Table 4.5.

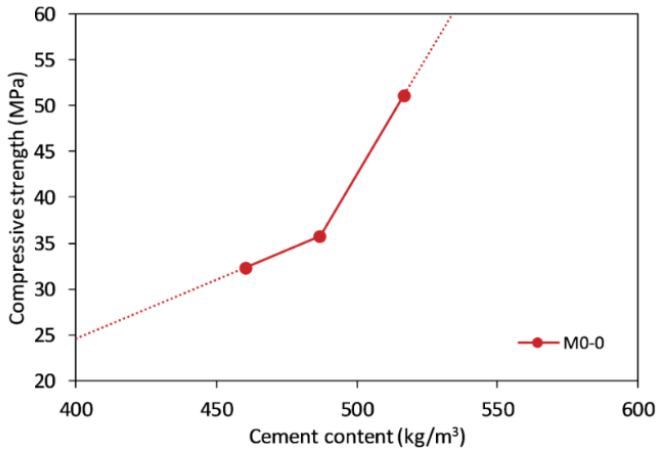

Figure 4.2. Compressive strength at 28 days as a function of cement content (M0-0).

Table 4.5 shows both initial and required binder content to achieve the same compressive strength as the reference mortar (M0-0(0.50)) at 28 days when RA and nano-TiO_2 are used. The binder content was split in cement and nano-TiO_2 content in mixtures with nanoparticles, maintaining the corresponding nano-TiO_2 percentage.

Table 4.5. Cement content required to have the same compressive strength than M0-0 (0.50) at 28 days.

Mixture	**Compressive strength at 28 days (MPa)**	**Initial binder content (kg/m^3) [*Cement- nano-TiO_2*]**	**Predicted required binder content (kg/m^3) [*Cement- nano-TiO_2*]**
M0-0 (0.50)	51.06	516.7 [*516.7-0.0*]	516.7 [*516.7-0.0*]
M0-0.5	51.70	516.7 [*514.1-2.6*]	515.5 [*512.9-2.6*]
M0-1	50.73	516.7 [*511.5-5.2*]	517.4 [*512.2-5.2*]
M0-2	52.93	516.7 [*506.4-10.3*]	513.1 [*502.8-10.3*]
M50-0	39.41	516.7 [*516.7-0.0*]	539.3 [*539.3-0.0*]
M50- 0.5	43.59	516.7 [*514.1-2.6*]	531.2 [*528.6-2.7*]
M50-1	42.13	516.7 [*511.5-5.2*]	534.1 [*528.7-5.3*]
M50-2	41.86	516.7 [*506.4-10.3*]	534.6 [*523.9-10.7*]
M100-0	32.39	516.7 [*516.7-0.0*]	572.5 [*572.5-0.0*]
M100-0.5	34.25	516.7 [*514.1-2.6*]	558.0 [*555.2-2.8*]
M100-1	34.45	516.7 [*511.5-5.2*]	556.4 [*550.9-5.6*]
M100-2	34.32	516.7 [*506.4-10.3*]	557.4 [*546.3-11.1*]

4.3.2 Life cycle assessment

Single categories

Global warming potential (GWP) quantifies the rising surface temperature of the Earth due to the increase in GHG emissions. The increase in GHG emissions could produce severe damages in both the aquatic and terrestrial biosphere. Figure 4.3.a exhibits GWP results showing the contribution of each material production separately. In general, most of the GWP value was related to cement production due to its high CO_2 emissions. Even though aggregates represent 60-70% of total volume, they have almost no influence on total GWP results (2-3% of the total). In contrast, nano-TiO_2 produced a non-negligible percentage considering the low amount added. Mixtures with nano-TiO_2 produce higher CO_2 emissions than non-modified mortars despite reducing the cement content. This result may suggest that, in terms of GWP, the use of nano-TiO_2 is even worse than using plain cement in mortar production. Figure 4.3.b presents the effect of materials transportation on GWP as a separate factor from the materials themselves. As expected, transportation influenced the total results. However, its contribution was not comparable to the contribution of cement. While transportation contributed around 3-4% of the total GWP, cement was responsible for more than 90%. Additionally, the higher the RA replacement, the lower the increase of total CO_2 emissions due to the nano-TiO_2 addition. This effect is related to the fact that nano-TiO_2 produces a higher enhancement of compressive strength and, therefore, a higher decrease of the required cement content in recycled mortars than in natural mortars.

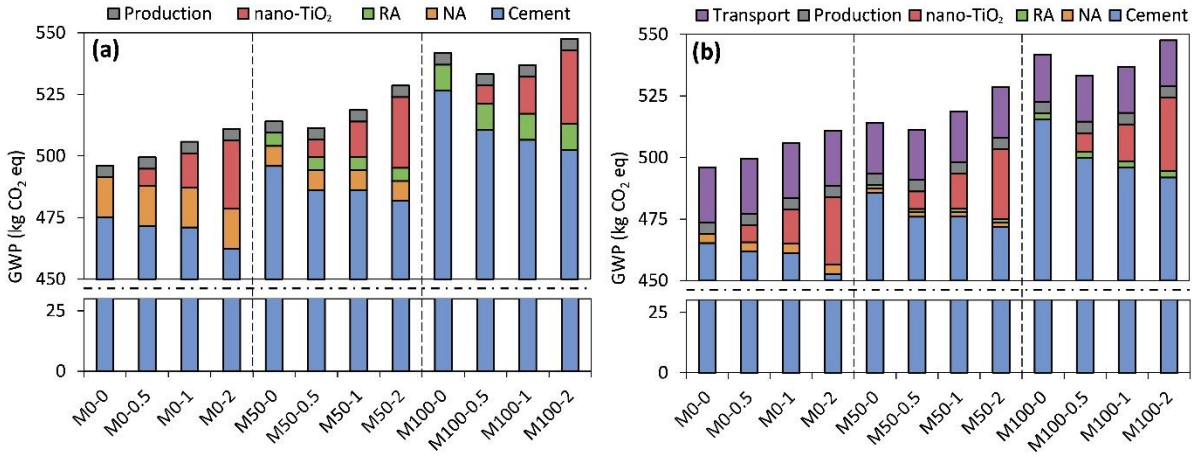

Figure 4.3. Contribution to the GWP of each material and mortar mixing production. (a) Transport included in each material impact. (b) Transport as an independent category.

The energy consumption (EC) impact category refers to the use of energy during the process. In TRACI methodology, results are expressed in megajoules surplus. According to the U.S. Energy Information Administration (EIA), surplus energy is the "energy generated beyond the immediate needs of the producing system." Figure 4.4 displays EC results. Almost every material has a significant contribution to EC. NA and RA possessed a not negligible proportion of total consumption (approximately 15% and 10%, respectively).

Moreover, nano-TiO_2 production required a significant amount of energy despite the low amount used. The higher the nano-TiO_2 addition, the higher the energy consumed. Finally, it should be noted that transportation had a strong influence on EC (Figure 4.4.b). Consequently, transport distances could modify the results. In contrast, mortar production had a minimal contribution to total results.

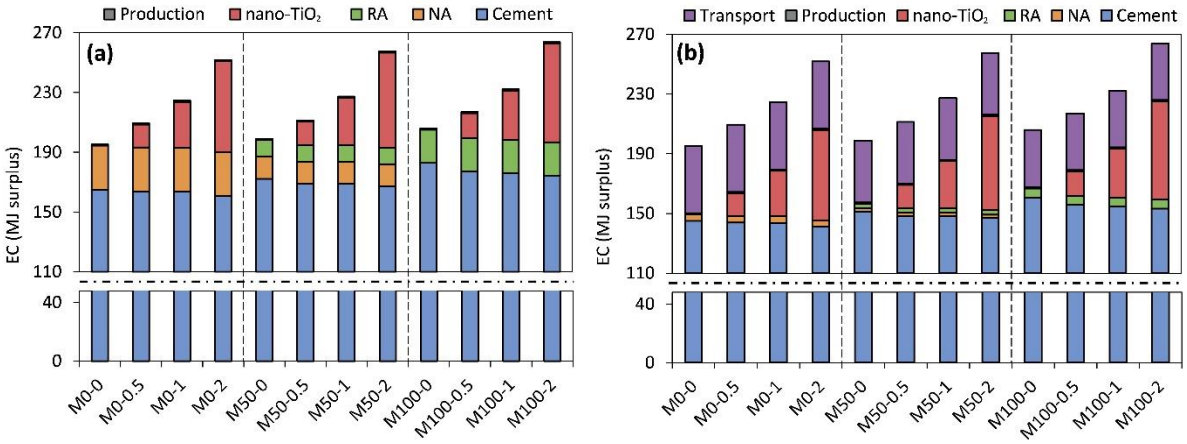

Figure 4.4. Contribution to the EC of each material and mortar mixing production. (a) Transport included in each material impact. (b) Transport as an independent category.

Since the amount of nano-TiO_2 used is very small, the transportation distance of both nano-TiO_2 and cement was assumed to be the same. Table 4.6 shows the negligible difference between assuming: (i) the same distance for both cement and nano-TiO_2 and (ii) transportation distance of nano-TiO_2 is over three times the transportation distance of cement.

Table 4.6. Effect of assuming different transportations distances for nano-TiO_2.

Mixtures	GWP (kg CO_2 eq)		EC (MJ surplus)	
	Distance nano-TiO_2 (292 km= cement)	**Distance nano-TiO_2 (1,000 km)**	**Distance nano-TiO_2 (292 km= cement)**	**Distance nano-TiO_2 (1,000 km)**
M0-0(0.50)	496.03	496.03	195.31	195.31
M0-0.5	499.46	499.58	209.39	209.64
M0-1	505.79	506.03	224.58	225.06
M0-2	510.88	511.36	251.80	252.76
M50-0	514.04	514.04	198.95	198.95
M50-0.5	511.28	511.41	211.28	211.53
M50-1	518.65	518.89	227.26	227.76
M50-2	528.61	529.11	257.49	258.49
M100-0	541.73	541.73	205.95	205.95
M100-0.5	533.32	533.45	216.99	217.25
M100-1	536.80	537.06	232.07	232.59
M100-2	547.64	548.15	263.76	264.81

Ozone depletion potential (ODP) results are shown in Figure 4.5. Cement content strongly contributed to increasing chlorofluorocarbons gases (85-90% of the total), which cause ozone depletion. While NA had a non-negligible percentage of total emissions (around 10%), RA would help to decrease those levels due to its low contribution (0.30% in the case of M100). However, this effect may be compensated by the higher amount of cement required. Besides, each 1% of TiO_2 addition produced a 5% percent increase in CFC emissions. Production of mortar and transportation (Figure 4.5.b) had almost no effect on ODP.

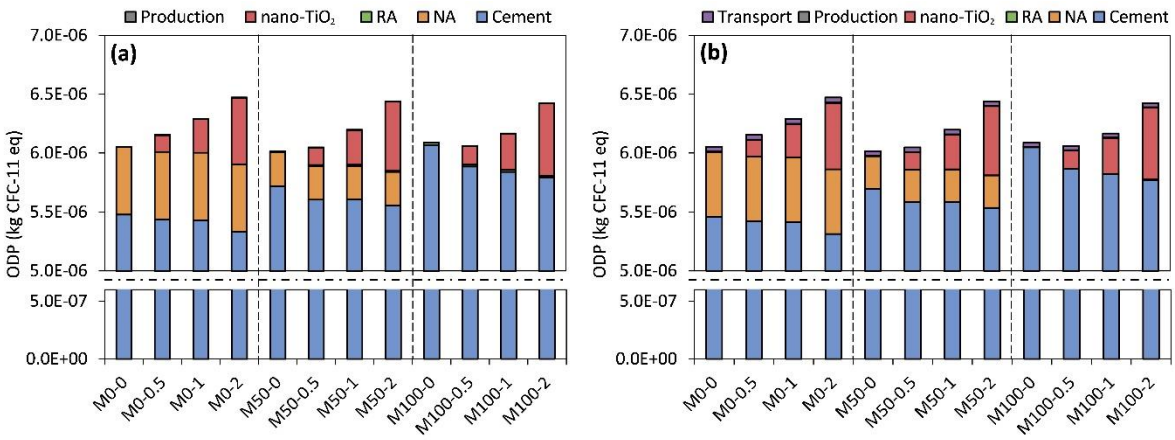

Figure 4.5. Contribution to the ODP of each material and mortar mixing production. (a) Transport included in each material impact. (b) Transport as an independent category.

Figure 4.6 presents the acidification potential (AP) results. Like GWP and ODP, cement content had the highest contribution. It exhibited a higher influence (around 99%) than in the previous categories. Any of the other materials had a negligible effect on the total results. Figure 4.6.b shows that transportation did not affect total results (0.3%). It is remarkable that the higher the nano-TiO_2 percentage, the lower the AP. The reasons are the decrease in the cement content and the low contribution of TiO_2 production to those gases.

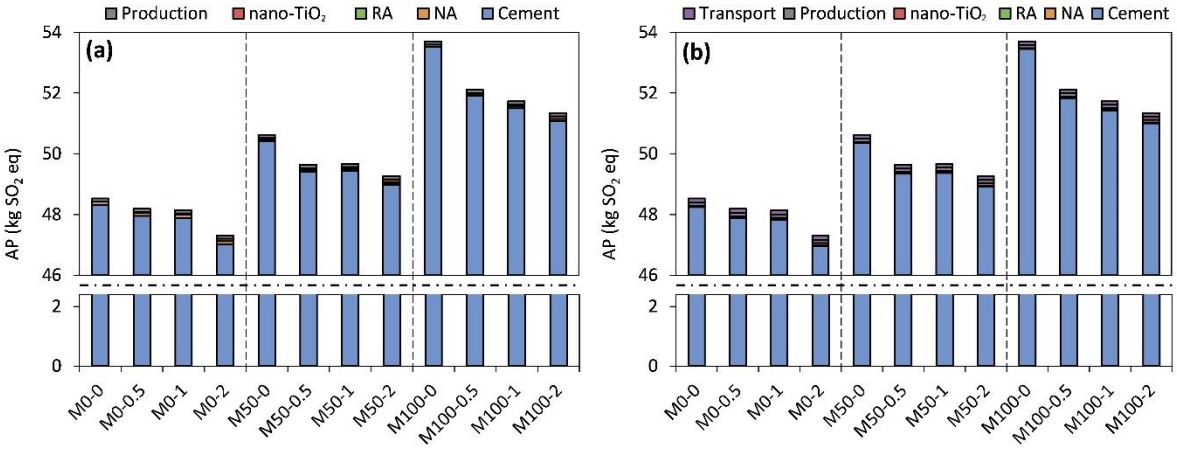

Figure 4.6. Contribution to the AP of each material and mortar mixing production. (a) Transport included in each material impact. (b) Transport as an independent category.

Figure 4.7 exhibits the results of the eutrophication potential (EP). These results were similar to AP because both are related to water pollution. Cement production was the highest contributor in EP, with around 99% of the total. In contrast, neither TiO_2 nor aggregates influenced total results. Like AP results, EP was reduced with the increase of the TiO_2 percentage due to the lower cement content.

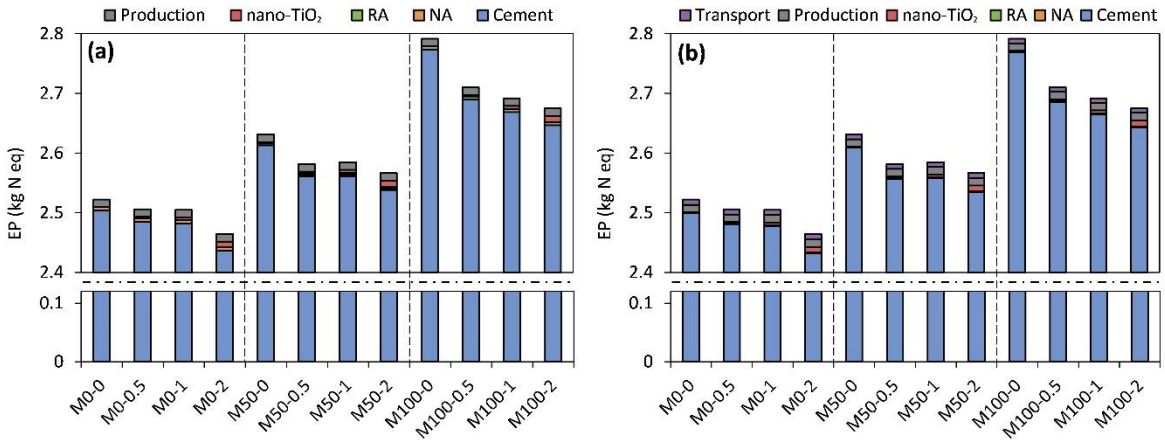

Figure 4.7. Contribution to the EP of each material and mortar mixing production. (a) Transport included in each material impact. (b) Transport as an independent category.

Influence of LCIA methodology

Considering the results of every category analyzed, Figure 4.8 shows the overview of environmental performance depending on the LCIA methodology used. The lower the value reported, the lower the environmental impact. Both results exhibited similar trends in shared categories since the characterization factors had almost no variation between methodologies. The differences between TRACI and CML are the impact categories considered in the assessment. For instance, the CML methodology considers neither smog nor respiratory effects. Those categories could estimate the risk of health diseases due to pollution. Both figures indicate that the main advantage of using RA instead of NA is decreasing the number of quarries and the waste in landfills, related to ADP and WG, respectively. In terms of nano-TiO_2, the addition of nanoparticles produced an increase in EC and photochemical ozone creation potential (POCP).

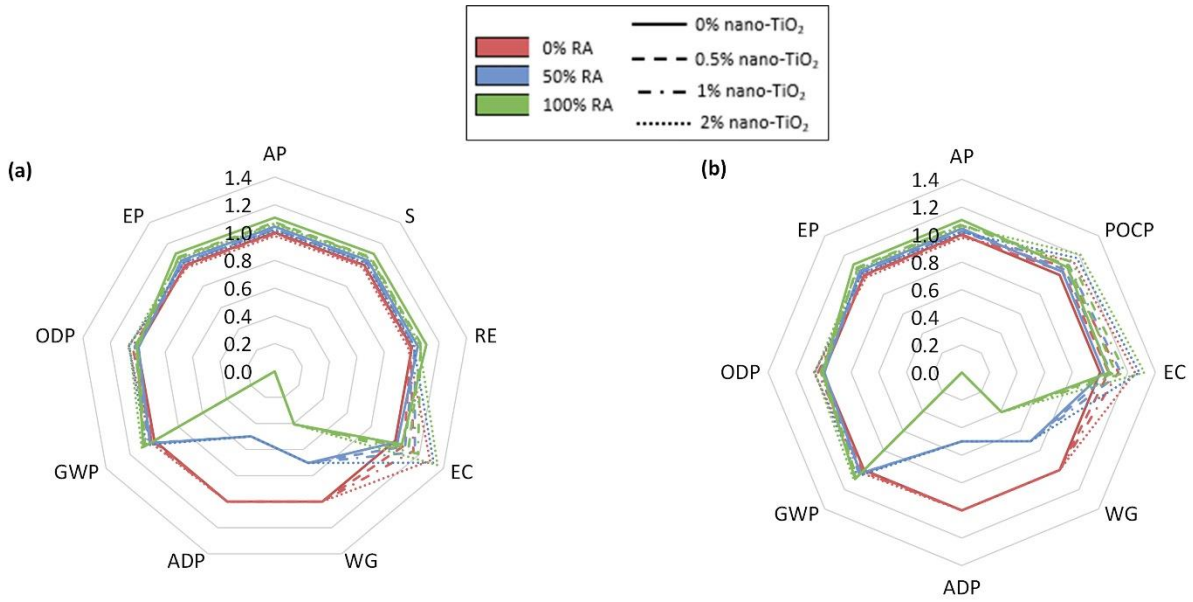

Figure 4.8. Overview of the assessment of both methodologies. (a) TRACI. (b) CML. [Global warming potential (GWP), ozone depletion potential (ODP), eutrophication potential (EP), acidification potential (AP), smog formation (S), respiratory effects (RE), photochemical ozone creation potential (POCP), energy consumption (EC), waste generation (WG), and abiotic depletion potential (ADP)].

Previous results considered both ADP and WG categories in the assessment. However, TRACI and CML do not include those categories in their default analysis. Figure 4.9 shows the comparison between including or not those categories in the analysis. While approach 2 includes WG and ADP, the normalization factors (approach 1) alternative estimates the impacts per year without considering them. As expected, the environmental impact of recycled mortars was higher when using approach 1 since WG and ADP were not considered. In contrast, when WG and ADP are considered (approach 2), results showed decreased environmental impact due to RA's use. Results also suggested that nano-TiO_2 addition could harm environmental performance without depending on the approach used.

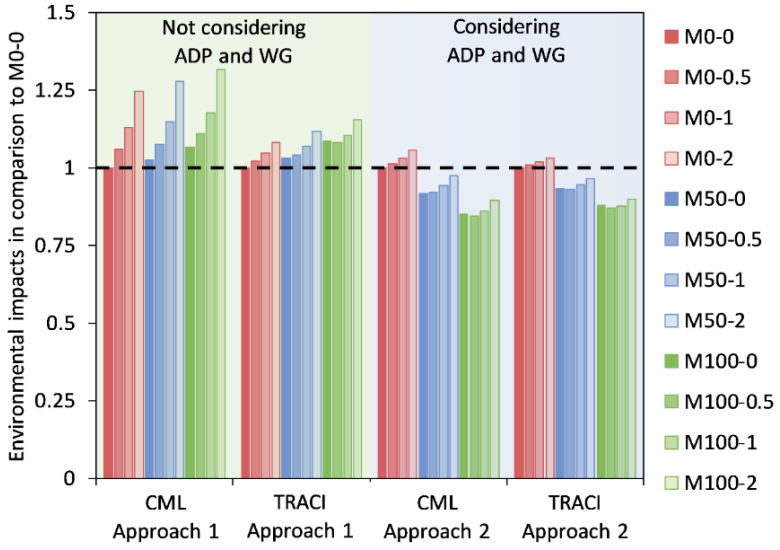

Figure 4.9. Overview of the environmental impacts considering two different approaches.

Table 4.7 presents the total results using the two methods explained in the chapter and the two chosen methodologies.

Table 4.7. Total results for both methodologies approaches analyzed.

Mixtures	TRACI Approach 1 (impacts per year)	CML Approach 1 (impacts per year)	TRACI Approach 2 (parts per unit)	CML Approach 2 (parts per unit)
M0-0	4.90E+13	8.52E+15	1.00	1.00
M0-0.5	5.00E+13	9.04E+15	1.01	1.01
M0-1	5.12E+13	9.61E+15	1.02	1.03
M0-2	5.30E+13	1.06E+16	1.03	1.06
M50-0	5.06E+13	8.73E+15	0.94	0.92
M50-0.5	5.10E+13	9.17E+15	0.93	0.93
M50-1	5.24E+13	9.77E+15	0.95	0.95
M50-2	5.47E+13	1.09E+16	0.97	0.98
M100-0	5.31E+13	9.09E+15	0.89	0.86
M100-0.5	5.30E+13	9.46E+15	0.88	0.85
M100-1	5.41E+13	1.00E+16	0.88	0.87
M100-2	5.65E+13	1.12E+16	0.91	0.90

Influence of aggregate transportation and functional unit

Previous research showed the importance of aggregate transportation on environmental performance [143], [144]. As mentioned, transport distances have a non-negligible influence on GWP and EC results. In addition, researchers have indicated that the environmental benefits of using RA in concrete production could be influenced by its transport distance [125], [126].

Figure 4.10 presents both GWP and EC results as a function of aggregate transport distance. The breaking point distance is defined as the distance from which recycled mortars have a lower environmental impact than mortars made with NA, regardless of RA transport distance. Results demonstrated high breaking point distances in the case of GWP, with values over 250 kilometers. Consequently, recycled mortars would have lower environmental performance (in terms of GWP) than mixtures made with NA assuming a maximum transport distance of 250 km for NA. Even though the effect of the nanoparticles was low, up to 1% of nano-TiO_2 addition may reduce the breaking point distance.

In terms of EC, results show a decrease in the breaking point distance compared to GWP results. According to PCA [134], the average round trip transportation distance in the U.S. for NA can be assumed as 122 km. The results showed a much lower breaking point distance than the average distance for NA regardless of the nano-TiO_2 percentage. Therefore, in an ideal situation (where RA has no transport), recycled mortars would possess higher environmental performance than mortars made by NA in terms of energy consumption. Nevertheless, nano-TiO_2 addition may have a negative effect on EC. The higher the nano-TiO_2 percentage, the higher the breaking point distance.

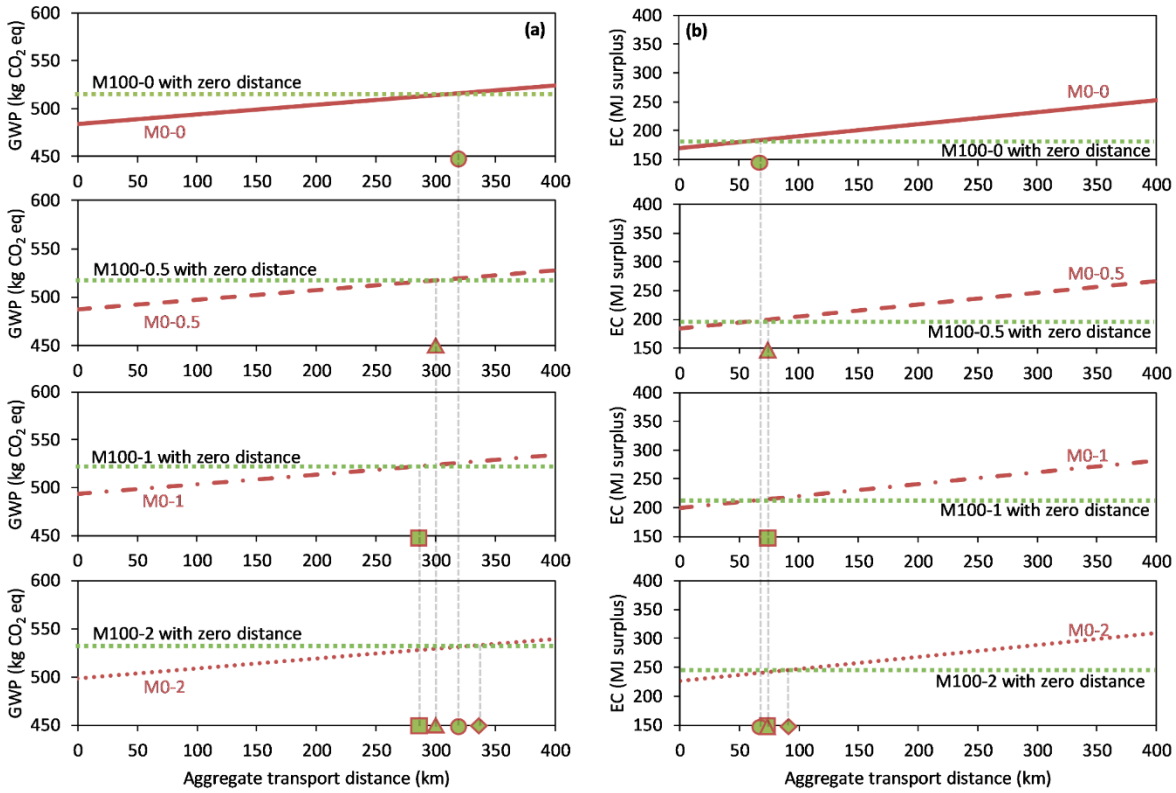

Figure 4.10. Breaking point distance of NA transportation. (a) Regarding GWP. (b) Regarding EC.

Two FU were analyzed: (i) FU1, which is 1 m^3 of mortar, and (ii) FU2, which is 1 m^3 of mortar with the same compressive strength as the reference mixture (M0-0 (0.50)). The difference was the binder content in the mixture design. While in FU1 binder contents were obtained from Table 4.1, FU2 values were taken from Table 4.5. Figure 4.11 presents the influence of the FU on environmental results. Implementing one FU rather than another changes the final output: results using FU1 showed that the utilization of RA slightly reduces CO_2 emissions (<1%). However, when the compressive strength factor is considered (FU2), the utilization of RA increases the total CO_2 emissions. The reason is the higher cement content required to compensate for the lower compressive strength due to RA. Considering the compressive strength factor (FU2), mortars with 100% RA increased 6% in GWP results due to the increase of cement content. Likewise, the other impact categories showed a similar trend. FU2 is more suitable than FU1 because cementitious materials with the same compressive strength could be used for the same application. Using FU1,

the effects on compressive strength are overlooked, and the environmental impact of the cementitious material may be underestimated.

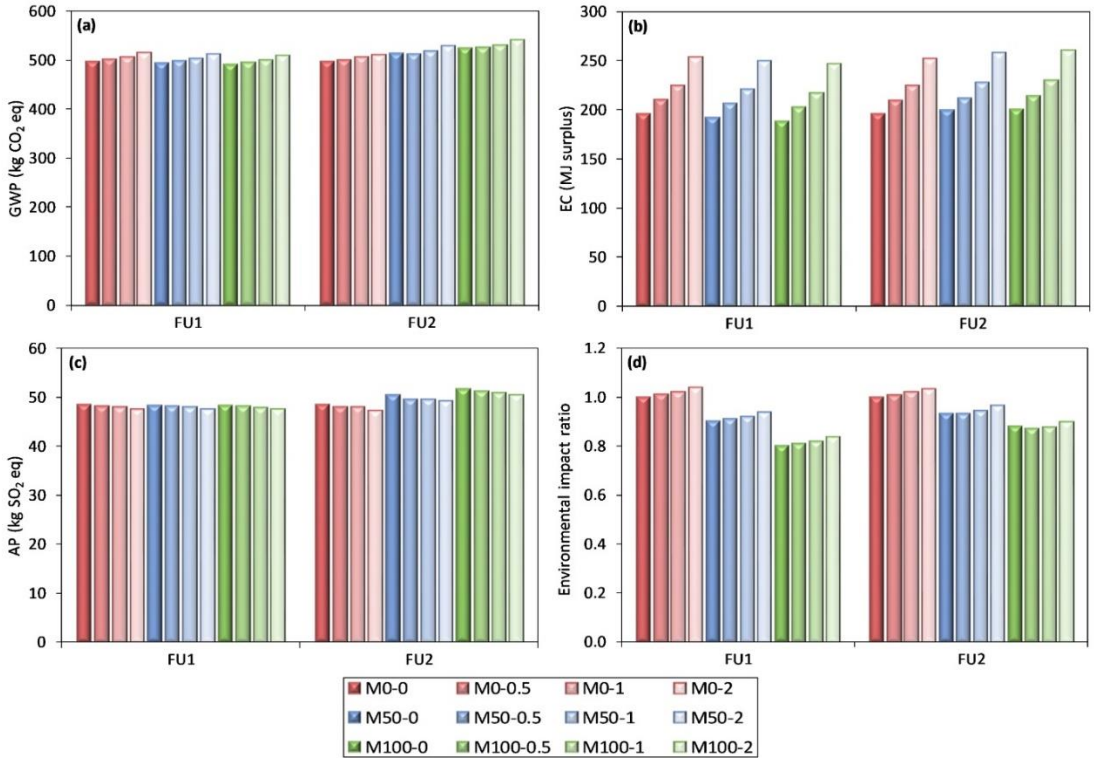

Figure 4.11. Influence of functional unit used in the assessment. (a) GWP. (b) EC. (c) AP. (d) TRACI – Approach 2.

4.3.3 Discussion

As stated previously, the use of nano-TiO_2 increased the environmental impact during mortar production. Even though this chapter is focused on mortar production, the results may be extrapolated to concrete production. On the one hand, concrete and mortars are similar materials since they possess the same main compounds (cement, water, and aggregates). On the other hand, nano-TiO_2 affects the cement paste properties, which, in this case, is the matrix of mortar, and cement paste would also be the matrix of the composite in the case of concrete. Consequently, the effect of nano-TiO_2 on the compressive strength of concretes may show similar trends than the observed on mortars and, therefore, it may show a similar trend on the effect on the environmental impact. However, further research focused on the effect of nano-TiO_2 on the concrete properties with recycled aggregates would be needed to confirm this potential trend. Nonetheless, nano-TiO_2

addition may benefit the environmental performance of mortar and concrete constructions when a holistic approach (*cradle-to-cradle*) is considered. The influence of nano-TiO_2 on durability and its proactive effects during service life could enhance emissions and other environmental impacts.

Previous research showed that nano-TiO_2 addition could decrease chloride permeability, electrical resistivity, and water absorption in mortars and concretes by making a denser microstructure and, therefore, improving its durability [52], [55], [56], [63], [145].

In terms of proactive effects during service life, it is well-known that nano-TiO_2 could highly reduce pollution levels due to its photocatalytic property [40]–[42]. Previous research was mainly focused on NO_X degradation, concluding that the higher the nano-TiO_2 percentage, the higher the NO_X degradation [146]–[149]. Nano-TiO_2 could also decompose other pollutants such as SO_X or VOCs [150], [151]. Moreover, a recent study [29] suggested that nano-TiO_2 may increase carbonation. In the case of applications with a high volume of concrete without steel reinforcement, carbonation of concrete, rather than being problematic in terms of durability, could have positive effects: (i) this potential acceleration of the carbonation rate (due to the more reactive CH) may be an opportunity to transform cementitious materials into a more effective carbon sink (natural CO_2 sequestration), and, (ii) the consumption of CH through carbonation may increase the resistance of concrete to chemical attacks reducing, for instance, the potential of calcium oxychloride formation [152].

In order to test whether nano-TiO_2 promotes the CO_2 sequestration and how RA affects this promotion, the phenolphthalein test was performed on the fresh fractured samples. Phenolphthalein is a chemical compound used as an indicator of the pH in concretes and mortars. The test consists of applying a phenolphthalein solution on the fractured surface. After a given time, a visual analysis of the samples can be made. The lighter the color, the higher the carbonation (lower pH). Figure 4.12 shows the results of this test after 30 minutes. Nano-TiO_2 addition increased the carbonation of both natural and recycled mortars. Likewise, the potential initial carbonation of the recycled aggregates can be observed by comparing the images of the reference sample (0% RA) with the 100% RA sample (both without nano-TiO_2). Despite that, carbonation was promoted due to the use of nano-TiO_2 to a greater extent when RA is used. Samples with 100% of RA and 2% of nano-TiO_2 showed the highest carbonation. A potential explanation is that

recycled mortars have a higher porosity, promoting higher and much faster carbonation than samples made with natural aggregates.

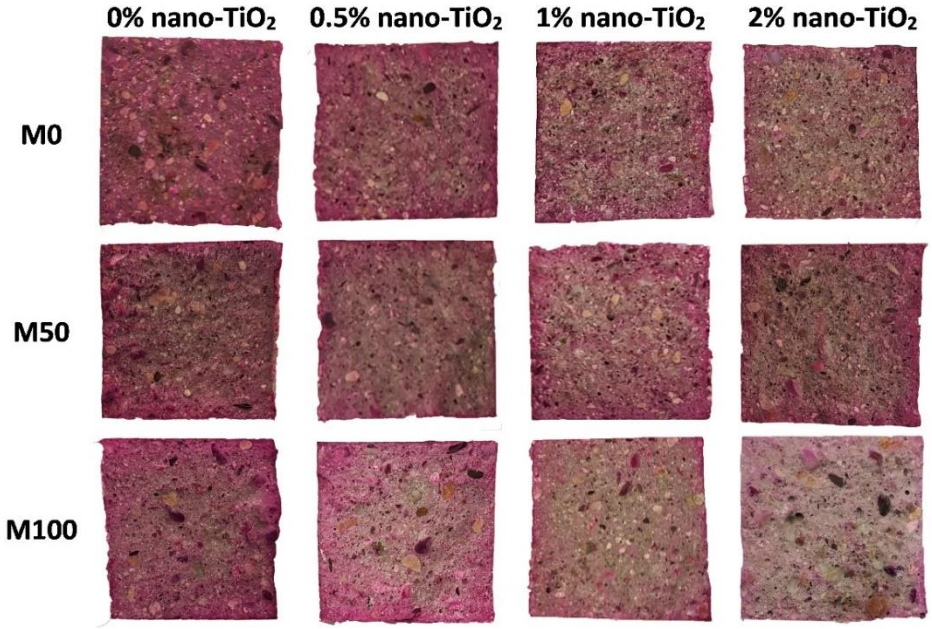

Figure 4.12. Phenolphthalein test at 28 days of mixtures with w/c=0.50.

Figure 4.13 summarizes the potential strategies for improving the sustainability of cementitious materials. In order to decrease their environmental impact, three different approaches could be followed: their composition, performance, and lifetime. Regarding materials, using supplementary cementitious materials (SCM) as a cement replacement could decrease emissions. Likewise, the use of RA instead of NA could reduce the depletion of natural resources and waste generation. On the other hand, increasing durability is equivalent to extending the lifetime of structures. This extension would reduce the number of materials and energy to employ as a function of time, enhancing sustainability. In terms of influence during service life, photocatalytic properties of nano-TiO_2 [40]–[42] could cause a significant decrease in emissions due to depolluting the environment. Besides, cementitious materials can sequestrate CO_2 during their lifetime. This effect could overcome the negative environmental implications of cement production. Using RA combined with the addition of nano-TiO_2 in concretes and mortars could promote and accelerate the CO_2 uptake, leading to an enormous benefit for the planet.

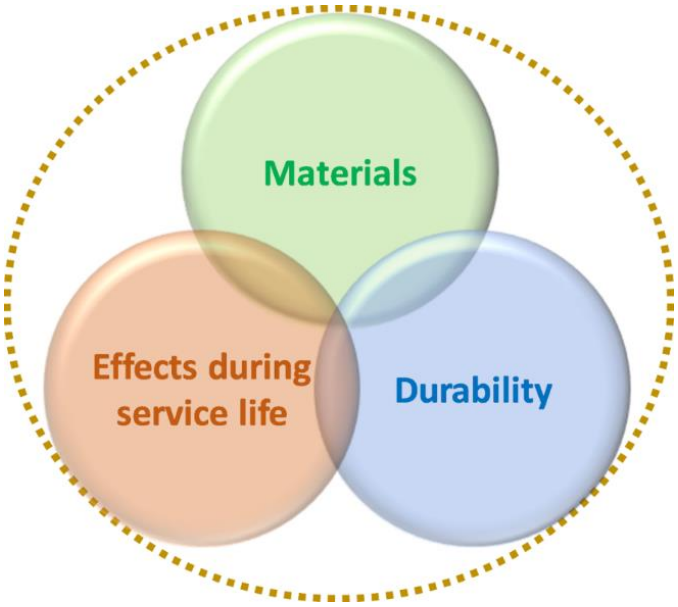

Figure 4.13. Possible sources of sustainability in cementitious materials.

Furthermore, considering the beneficial effects of the nanoparticles during service life, nano-TiO_2 could reduce the concentration of pollutants in the atmosphere. Therefore, those uptakes would overcome the negative environmental impact of nano-TiO_2 previously explained. Figure 4.14 presents an analysis to estimate how much CO_2 would need to be sequestrated to have the same environmental performance as the mortars without nanoparticles. For this purpose, the total environmental impacts of mortars with and without nano-TiO_2 are compared, using the TRACI results (Approach 2) shown in Figure 4.9. Then, an estimation on how much kg of CO_2 eq (in terms of GWP) should be increased or decreased in each mortar with nanoparticles to have the same total impact as the reference mortar (0% of nano-TiO_2) was done. The results are shown in kilograms of CO_2 per m^3 of concrete. M50-0.5, M100-0.5, and M100-1 exhibited better performance than their respective references. Thus, their proactive effects during service life would enhance sustainability on top of the actual benefits observed during the production process of those mixtures. Results summarized in Figure 4.14 exhibited that the higher the RA replacement, the lower the amount of required CO_2 uptake to compensate for the nano-TiO_2 environmental impact that affects the sustainability of the production stage. In contrast, the CO_2 uptake needed during the service life increases with higher nano-TiO_2 percentages. Nonetheless, since the results showed that nano-TiO_2 may increase the CO_2 uptake (Figure 4.12) and previous literature reported

that it could reduce several pollutants (e.g., NO_X, SO_X, and VOCs) and increase the durability, the environmental performance of mortars with nanoparticles could be highly improved.

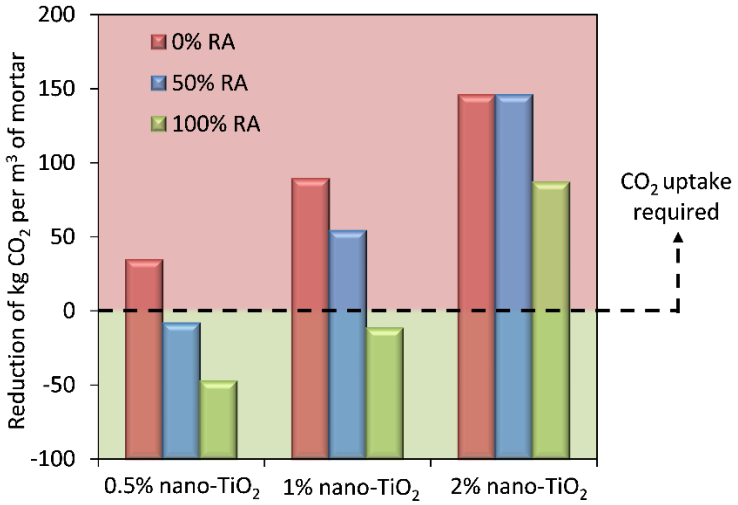

Figure 4.14. Required CO_2 reduction made by nano-TiO_2 to have the same environmental performance as the non-modified mortars (0% nano-TiO_2).

4.4 Conclusions

Considering the life cycle assessment made, the following conclusions can be drawn:

The use of nanoparticles on natural mortars produced an increase in GWP. However, a small percentage of nano-TiO_2 (0.5%) showed a significant reduction in GWP in mortars with recycled aggregates, especially in mortars with 100% RA. The use of recycled aggregates instead of natural aggregates increased GWP during mortar production since recycled mortars need more cement to achieve the same compressive strength.

The results suggested that whereas recycled aggregate could be beneficial considering waste generation and abiotic depletion, nano-TiO_2 addition may negatively impact the production of mortars. However, the system boundary of this chapter was the *cradle-to-gate* approach (extraction and transport of raw materials and manufacturing). The benefits of nano-TiO_2 nanoparticles are related to their effects during service life and durability. Considering a holistic approach, improving both durability and depollution would decrease the total environmental impact during the whole life cycle.

Finally, an estimation of the CO_2 uptake required to equalize environmental performances between mixtures was made. A 0.5% of nano-TiO_2 addition produced a reduction in the required CO_2 to be sequestrated on mortars with partial and total replacement of recycled aggregate. Higher percentages of nano-TiO_2 showed higher required CO_2 uptake than 0.5% nano-TiO_2. Considering the beneficial mechanisms of nano-TiO_2 during service life, the reduction of the environmental impact may be even higher for higher percentages of nano-TiO_2. The results suggest that using recycled aggregate combined with the addition of nano-TiO_2 in concretes and mortars could promote and accelerate the CO_2 uptake, leading to an enormous benefit for the planet.

5. MODIFICATION OF CO_2 CAPTURE AND PORE STRUCTURE OF HARDENED CEMENT PASTE MADE WITH NANO-TIO_2 ADDITION: INFLUENCE OF WATER-TO-CEMENT RATIO AND CO_2 EXPOSURE AGE

Part of this work has been published as:

C. Moro, V. Francioso and M. Velay-Lizancos (2021). *'Modification of CO_2 capture and pore structure of hardened cement paste made with nano-TiO_2 addition: Influence of water-to-cement ratio and CO_2 exposure age.'* Construction and Building Materials, vol. 275, p. 122131. https://doi.org/10.1016/j.conbuildmat.2020.122131.

5.1 Introduction

Over the last thirty years, the United Nations Framework Convention on Climate Change (UNFCCC) has been working in preventing "dangerous anthropogenic interference with the climate system" [153]. However, despite some agreements, like the Kyoto Protocol [102] or the Paris Agreement [103], the measures taken were not enough to reduce climate change or even mitigate its increase [104], [105]. In a recent report, the World Meteorological Organization claimed that the concentration of greenhouse gases (GHG) was the highest of the last 3-5 million years. Carbon dioxide (CO_2) represents a considerable percentage of the total amount; in fact, in 2014, the Intergovernmental Panel on Climate Change (IPCC) estimated its contribution as 65% of the total GHG emissions. On the other hand, the World Health Organization reported 4 million premature deaths worldwide due to pollution in 2016 [154]. In addition to the clear effect of high CO_2 emissions on global warming and health issues, those levels also promote ocean acidification. The oceans absorb CO_2 from the atmosphere, which reacts with the water and the carbonate ions. The consumption of carbonate ions impeded calcification and increased acidity by 30% from the last industrial revolution [3]. Therefore, the reduction of CO_2 emissions is vital for the future of our planet and our health.

Regrettably, the cement industry is one of the principal sources of CO_2 emissions. Around 8% of the total CO_2 emissions were produced by cement manufacturing in 2016 [4]. Between 40% and 50% of these emissions come from the limestone decomposition during the production of the clinker (the main component of cement)**,** while another 40%-50% of the cement industry emissions

are caused by the use of fossil fuels in the kiln to achieve the 1450 °C required to produce the clinker [5], [6]. Finally, a small percentage of this 8% is related to the transportation of materials [5], [6]. However, a study published [19] concluded that, between 1930 and 2013, cementitious materials have captured (through natural carbonation) the 43% of the CO_2 emitted during the cement production due to the limestone decomposition for the same period. This study concluded that the carbonation of cement hydration products represents a substantial carbon sink that is not currently considered in emissions inventories.

The theoretical basis is that carbonation of concrete occurs due to the reaction of two compounds: (i) CO_2 from the atmosphere and (ii) the calcium hydroxide ($Ca(OH)_2$, also designated with shorthand notation as CH) from cement paste. First, CO_2 dissolves in the water of the pores forming carbonate ions [155]–[157]. Then, these carbonate ions can react with the Ca ions of the pore solution, leading to calcium carbonate ($CaCO_3$) precipitation. The carbonation reaction is shown in Eq. 5.1 [25], [156].

$$\mathrm{Ca(OH)_2 + CO_2 \rightarrow CaCO_3 + H_2O} \qquad 5.1$$

Likewise, the calcium silicate hydrate (C-S-H) gel can also be carbonated through a complex decalcification–polymerization process where C-S-H can be decalcified and the free lime (CaO) can react with the carbonate ions previously created, forming calcium $CaCO_3$ [155]. Eq. 5.2 exhibits an overview of the decalcification–polymerization reaction.

$$\mathrm{(CaO)_x(SiO_2)_y(H_2O)_z + xCO_2 \rightarrow xCaCO_3 + y(SiO_2)(H_2O)_t + (z - yt)H_2O} \qquad 5.2$$

Two facts need to be highlighted: (i) the carbonation is a prolonged process (it could take decades) and (ii) the world annual cement production per capita during the last 30 years has been multiplied by 3 [8], while the population has been multiplied by 2 in the same period. Just as an illustrative example, China has used more cement between 2011 and 2013 than the U.S.A. in the whole 20th century [158]. Considering these two facts jointly, the debt created with the environment (CO_2 emissions) is too high and is being paid so slowly (CO_2 uptake).

Previous research showed two different carbonation processes (active and passive) [159]. The passive or weathering carbonation consists in exposing cementitious materials to CO_2 in the

atmosphere. The active or accelerated carbonation exposes fresh cementitious composites to a high CO_2 concentration to speed up the carbonation process.

Cementitious composites are exposed to weathering or natural carbonation during their lifetime. This type of carbonation is a slow process since the atmosphere has a low CO_2 concentration (0.0415% or 415 ppm) [160]. The weathering carbonation is usually analyzed by the carbonation depth test [161]. Previous research showed that the carbonation depth is increased when cementitious materials are exposed to CO_2 [162], [163].

The active or CO_2 curing allows to speed up the CO_2 capture in the fresh cementitious composite. Even though the use of CO_2 for curing cementitious materials was suggested in the 1970s, recent research found that this type of carbonation may possess significant benefits [164]. Many researchers have examined the potential applicability of curing fresh cement composites with CO_2 [22], [25]–[28], [164]–[166]. The chemistry beyond that process is the carbonation of the dicalcium silicate (C_2S) and tricalcium silicate (C_3S) [25], [165], [167]. This mechanism would promote CO_2 sequestration of cementitious materials for both OPC concrete and concrete with supplementary cementitious materials [26], [168], [169]. Besides, it may increase concrete durability without steel reinforcement [170]–[173] and the compressive strength compared to specimens with standard curing [25], [167], [174], [175]. Rostami et al. [172] showed an increase in both the sulfate and freeze-thaw resistance and the electrical resistivity after the early carbonation. They suggest that this result could be related to the modification of the microstructure of cement pastes. Another study found that the chloride penetration was reduced after the carbonation curing [171]. Therefore, this would help to prevent issues in cementitious composites exposed to marine environments.

Even though this would highly reduce the environmental impact of cementitious composites such as concrete (the most widely used construction material in the world), nowadays, it is not technically feasible for many construction field applications.

Since hardened cementitious composites can still absorb CO_2 during their whole service life through the carbonation process [19]. Nevertheless, the carbonation process is prolonged, and the production of cement increases year by year. Therefore, accelerating the process of CO_2 sequestration of hardened cementitious composites may have significant environmental benefits.

Previous research suggested that mortars with 0.5% of nano-TiO_2 (by the total weight of cement) exhibited higher carbonation than plain mortars during the grinding of the samples for thermogravimetric analysis sample preparation [29]. However, despite this observation, no research was found that studies the effect of nano-TiO_2 on CO_2 sequestration of hardened cementitious materials. Based on that, the main objective of this chapter is to study how nano-TiO_2 may affect the CO_2 uptake of hardened cement paste as a function of its w/c and pore structure.

5.2 Materials and methods

5.2.1 Materials and mixture procedure

The material characterization of the cement and nano-TiO_2 used in this chapter is exhibited in *Chapter 2: Materials and general procedures*.

Twelve cement paste mixtures were made with four different percentages of nano-TiO_2 (0%, 0.5%, 1%, 2%). Even though previous research showed an enhancement of the compressive strength with percentages higher than 2% [43], [44], [63], from a prospective use of nano-TiO_2 on cementitious composites at a large scale, higher percentages of nano-TiO_2 might increase the price to an unacceptable level. The nano-TiO_2 was added as a replacement of the cement by mass. Besides, three water-to-cement (w/c) ratios (0.45, 0.50, 0.55) were employed in this chapter. The different w/c were chosen to study the changes in the effect of the nanoparticles depending on the initial porosity of the paste. The mixture proportions of each cement paste are shown in Table 5.1.

Twelve samples of each mixture were cast in plastic molds with a diameter of 1 1/4” (3.175 cm) and a height of 2.1 cm. All the samples were mixed using a blender at high speed. First, cement and nano-TiO_2, if applicable, were mixed in dry conditions. Then, the water was added to the mixture in a mixer bowl. The mixture was then blended at high speed for 60 seconds. After that, the bowl's walls were scraped to mix in any paste stuck to the sides. Finally, the mixture was blended for 90 seconds more at high speed. During the first 24 hours, all samples were cured at 23 ± 0.5 °C covered with plastic to prevent water evaporation. After 24 hours, samples were demolded and left inside an environmental chamber under controlled conditions (temperature of 23 °C and humidity higher than 95%) until the testing day.

During the curing process, the samples may experience slight natural carbonation. However, significant carbonation during the first 28 days under the standard curing conditions described is not expected since carbonation is a slow process, and samples were stored in a closed chamber with controlled conditions. Nonetheless, any difference of carbonation in the samples during the curing process would be detected with the tests performed in the non-exposed samples. Important changes in the calcium carbonate content on non-exposed samples of different mixtures would indicate that samples were naturally carbonated to a different extent during the curing process. In contrast, minor variations in the calcium carbonate content on non-exposed samples would indicate that the potential carbonation of samples during the curing process affects all tested samples to the same extent. Comparing the calcium carbonate content before and after the CO_2 exposure will indicate both the extent and the relative significance of the natural carbonation during the curing process versus the carbonation produced due to the CO_2 exposure. In this chapter, the CO_2 exposure consisted in a 24-hour cycle (100% concentration) with a purity higher than 99.5%. The temperature and relative humidity during the CO_2 exposure were 21 ± 0.5 °C and 25 ± 2%, respectively. Further explanation of curing conditions and CO_2 exposure can be found in section 2.2.1.

Table 5.1. Mixture proportions of cement paste mixtures.

Mixture	**w/c**	**Cement (g)**	**nano-TiO_2 (g)**	**Water (g)**
P0 (0.45)	0.45	260.0	0.0	117.0
P0.5 (0.45)	0.45	258.7	1.3	117.0
P1 (0.45)	0.45	257.4	2.6	117.0
P2 (0.45)	0.45	254.8	5.2	117.0
P0 (0.50)	0.50	260.0	0.0	130.0
P0.5 (0.50)	0.50	258.7	1.3	130.0
P1 (0.50)	0.50	257.4	2.6	130.0
P2 (0.50)	0.50	254.8	5.2	130.0
P0 (0.55)	0.55	260.0	0.0	143.0
P0.5 (0.55)	0.55	258.7	1.3	143.0
P1 (0.55)	0.55	257.4	2.6	143.0
P2 (0.55)	0.55	254.8	5.2	143.0

5.2.2 Methods

CO_2 uptake

The CO_2 uptake of each mixture after 24 hours of CO_2 exposure was estimated following two steps:

(i) CO_2 exposure

Two samples of each mixture were exposed to a saturated CO_2 environment for 24 hours at two different ages and tested after the exposure (at 14 and 28 days). Both ages were selected considering that ordinary Portland cement (OPC) Type I was used in this chapter. For cement paste made with OPC Type I, 28 days is a reasonable and representative age to show an almost fully hydrated cement paste. Besides, 14 days was chosen to study how the CO_2 exposure may affect when the cement paste is hardened but not still completely hydrated.

Previously, a pre-curing process was conducted to control the moisture of the samples. This step is critically important to avoid excessive water content that could limit the CO_2 uptake by the samples [164]. Previous research showed that between 4 and 8 hours of pre-curing are enough to ensure around 60% of relative humidity in the samples [164], [174].

In this chapter, the samples were pre-cured for five hours in a controlled chamber with T = 23 °C and RH=50%, right before the exposure. After that, samples were placed inside a pressure chamber (Figure 5.1). A pump was turned on to vacuum the system (until the pressure was 1 atm). The CO_2 tank (> 99.5% purity) was then opened to fill the chamber with CO_2 until the pressure inside the chamber was 0 atm. After 24 hours of CO_2 exposure, the chamber valve was opened to release CO_2, and the specimens were removed from the pressure chamber.

An unexposed sample (S0) of each mixture was placed in the pre-curing chamber with the exposed samples (S1). However, instead of being placed inside the CO_2 chamber after 5 hours of pre-curing, the S0 samples were kept in the controlled chamber during the exposure time (24 hours). Figure 5.1 shows the curing procedure diagram for both exposed and non-exposed samples.

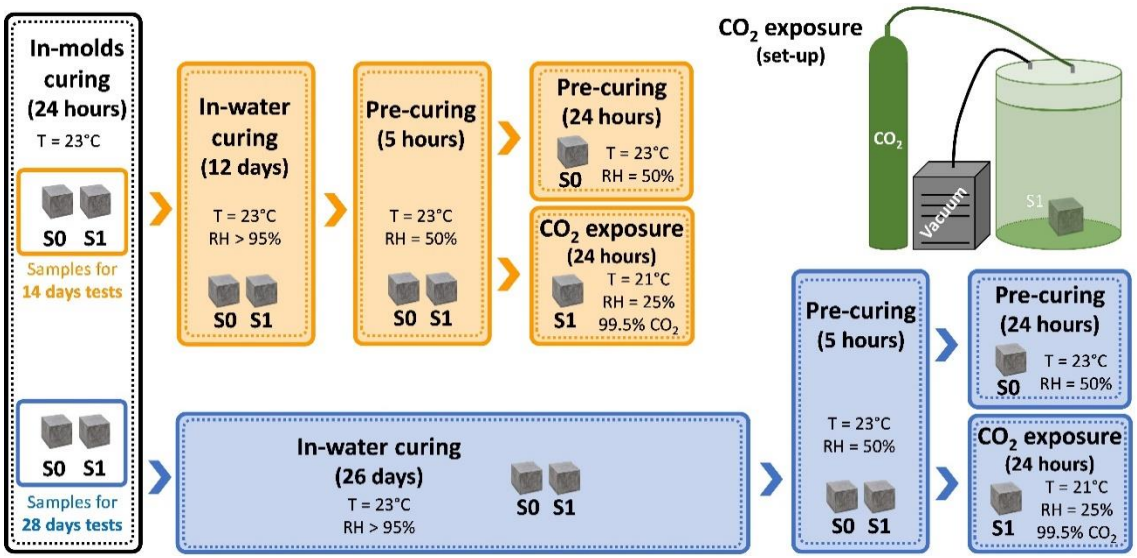

Figure 5.1. Method for quantification of CO_2 uptake. Set-up of carbonation exposure and curing procedure diagram.

(ii) Estimation of CO_2 uptake using Thermogravimetric Analysis (TGA)

After the CO_2 exposure was completed, TGA was performed for both exposed (S1) and unexposed samples (S0) to calculate the CO_2 uptake. Thus, a total of 48 samples were tested using TGA.

To prepare the samples for the thermogravimetric analysis, the hydration was stopped using a solvent exchange procedure [37]. First, 5 g of rough ground cement paste was mixed with 50 ml of isopropanol and left for 15 minutes to remove the free water. After that, the mixture was put in an oven at 40 °C for 10 minutes to remove any excess of isopropanol. Each paste was then finely ground with a mortar and pestle and sieved (No. 200, 75-µm).

TGA was conducted using the parameters explained in *Chapter 2: Materials and general procedures*. TGA can estimate the content of the different hydration products considering the approximate ranges of decomposition temperatures and using both first and second derivatives [29]. Previous research exhibited several components (e.g., calcium silica hydrate (C-S-H), ettringite, carboaluminate hydrates or calcium aluminate hydrate) decomposed between 100 °C and 400 °C [176]–[180]. After that, the decay of the calcium hydroxide (CH), one of the main hydration products in Portland cement, usually occurs between 410 °C and 520 °C, as previous

investigations suggested [57], [85], [178]–[181]. Lastly, the calcium carbonate ($CaCO_3$) content can be estimated using the mass loss between 630 °C and 830 °C [85], [178]–[180].

CO_2 uptake was obtained based on the difference between the $CaCO_3$ content of the non-exposed sample (S0) and the exposed specimen (S1). First, the content of $CaCO_3$ of each sample was calculated using Eq. 5.3.

$$\mathrm{CaCO_3}\ (\mathrm{g/100\ g}) = 100 \cdot \frac{100.1}{44.0} \cdot \frac{1}{\mathrm{M_c}} \cdot \left[\left(\mathrm{M_{start}^{CaCO_3}}\right) - \left(\mathrm{M_{end}^{CaCO_3}}\right)\right] \qquad 5.3$$

where:

- $CaCO_3$ is the amount of calcium carbonate in g/100 g of anhydrous cement.
- 100.1/44.0 is the molar weight ratio of $CaCO_3$ to CO_2.
- $\mathrm{M_C}$ is the initial (anhydrous) mass (g) of the cement in the TGA sample.
- $\mathrm{M_{start}^{CaCO_3}}$ and $\mathrm{M_{end}^{CaCO_3}}$ are the masses (g) of the sample at the start and endpoint for $CaCO_3$ decomposition, respectively.

Considering the $CaCO_3$ content of both exposed and non-exposed samples, CO_2 uptake can be obtained using Eq. 5.4.

$$\mathrm{CO_2}\ \text{uptake}\ (\mathrm{g/100\ g}) = \left[\left(\mathrm{CaCO_3^{exp,sample}}\right) - \left(\mathrm{CaCO_3^{nonexp,sample}}\right)\right] \cdot \frac{44.0}{100.1} \qquad 5.4$$

where:

- CO_2 uptake is the amount of carbon dioxide in g/100 g of anhydrous cement.
- 44.0/100.1 is the molar weight ratio of CO_2 to $CaCO_3$.
- $CaCO_3^{exp,sample}$ and $CaCO_3^{nonexp,sample}$ are the contents of the exposed and non-exposed sample, respectively (obtained by Eq. 5.3).

However, the CO_2 uptake could have different sources. As abovementioned, part of the CO_2 uptake comes from the carbonation of CH. Therefore, estimating the CH reduction during the exposure could quantify how much CO_2 uptake comes from the carbonation of CH. For that purpose, the CH content of both exposed and non-exposed samples are obtained. The content of CH of each sample was obtained using Eq. 5.5.

$$\mathrm{CH}\ (\mathrm{g}/100\ \mathrm{g}) = 100 \cdot \frac{74.1}{18.0} \cdot \frac{1}{\mathrm{M_c}} \cdot \left[\left(\mathrm{M}_{\mathrm{start}}^{\mathrm{CH}}\right) - \left(\mathrm{M}_{\mathrm{end}}^{\mathrm{CH}}\right)\right] \qquad 5.5$$

where:

- CH is the amount of calcium hydroxide in g/100 g of anhydrous cement.
- 74.1/18 is the molar weight ratio of CH to H_2O.
- $\mathrm{M_C}$ is the initial (anhydrous) mass (g) of the cement in the TGA sample.
- $\mathrm{M}_{\mathrm{start}}^{\mathrm{Ca(OH)_2}}$ and $\mathrm{M}_{\mathrm{end}}^{\mathrm{Ca(OH)_2}}$ are the masses (g) of the sample at the start and endpoint for CH decomposition, respectively.

Then, knowing the CH consumed due to the CO_2 exposure, the amount of $CaCO_3$ generated from the CH carbonations can be calculated using Eq. 5.6.

$$\mathrm{CaCO_3^{CH}}\ (\mathrm{g}/100\ \mathrm{g}) = \left[\mathrm{CH}^{\mathrm{nonexp.sample}} - \mathrm{CH}^{\mathrm{exp.sample}}\right] \cdot \frac{100.1}{74.1} \qquad 5.6$$

where:

- $CaCO_3^{CH}$ is the total amount (in g/100 g) of $CaCO_3$ coming from the carbonation of CH.
- $CH^{nonexp,\ sample}$ is the total amount (in g/100 g) of CH in the non-exposed sample (obtained by Eq. 5.5).
- $CH^{exp,\ sample}$ is the total amount (in g/100 g) of CH in the exposed sample (obtained by Eq. 5.5).
- 100.1/74.1 is the molar weight ratio of $CaCO_3$ to CH.

Due to the uncertainties of estimating the amount of other hydration products (e.g., C-S-H, AFm, and ettringite) since they are decomposed in the similar temperature range [176]–[180], it was assumed that the rest of the $CaCO_3$ content (not related to the CH carbonation), came from the carbonation of other components of the cement paste. The $CaCO_3$ from the carbonation of these hydration products (C-S-H, AFm, and ettringite) and/or anhydrous silicates and aluminates phases can be obtained using Eq. 5.7.

$$\mathrm{CaCO_3^{Other\ phases}} = \left[\mathrm{CaCO_3^{exp,sample}} - \mathrm{CaCO_3^{nonexp,sample}}\right] - \mathrm{CaCO_3^{CH}} \qquad 5.7$$

where:

- $CaCO_3^{Other\ phases}$ is the amount (in g/100 g) of $CaCO_3$ coming from the carbonation of other hydration products besides CH (C-S-H, AFm, and ettringite) and/or the carbonation of anhydrous silicates and aluminates phases.
- $CaCO_3^{exp,\ sample}$ is the total amount (in g/100 g) of $CaCO_3$ in the exposed sample (obtained by Eq. 5.3).
- $CaCO_3^{nonexp,\ sample}$ is the total amount (in g/100 g) of $CaCO_3$ in the non-exposed sample (obtained by Eq. 5.3).
- $CaCO_3^{CH}$ is the total amount (in g/100 g) of $CaCO_3$ coming from the carbonation of CH (obtained by Eq. 5.6).

Furthermore, Appendix C the reliability and repeatability of the TGA. Results showed that the procedure used to perform TGA is reliable and repeatable for both non-exposed and exposed samples.

3D X-ray microscope characterization of pore structure

3D X-ray microscopy was employed to investigate the effect of nano-TiO_2 and w/c on the pore structure changes of cement pastes due to the CO_2 exposure. To study these effects, four samples were 3D scanned before and after CO_2 exposure at 14 days (a total of eight 3D X-Ray scans have been performed). The specimens tested include two different percentages of nano-TiO_2 (0% and 1%) and two different water-to-cement ratios (0.45 and 0.55). The parameters of the experiment are described in *Chapter 2: Materials and general procedures*.

5.3 Results and discussion

5.3.1 TGA results: CH reduction and $CaCO_3$ formation

Figure 5.2.a and Figure 5.2.b present the CH reduction due to the CO_2 exposure on the studied pastes at two different ages (14 and 28 days), calculated from the TGA results. Figure 5.2.c and Figure 5.2.d present the relative CH reduction due to CO_2 exposure calculated using Eq. 5.8.

$$\text{Relative CH change (\%)} = 100 \cdot \frac{\mathrm{CH}^{\mathrm{nonexp.sample}} - \mathrm{CH}^{\mathrm{exp.sample}}}{\mathrm{CH}^{\mathrm{nonexp.sample}}} \qquad 5.8$$

Table 5.2 lists the CH content for all exposed and non-exposed samples at both ages (14 days and 28 days) with the corresponding CH change (in percentage) due to the CO_2 exposure. These CH changes can be attributed to the CH reactivity since they show the percentage of CH reduction in the exposed samples compared to the value in each non-exposed sample.

Table 5.2. CH content of all studied non-exposed samples (14 days and 28 days).

		CH content (g/100 g)					
Mixture	**w/c**	**14 days**			**28 days**		
		Non-exposed	**Exposed**	**% change**	**Non-exposed**	**Exposed**	**% change**
P0 (0.45)	0.45	13.4	12.9	3.7%	14.6	14.2	2.5%
P0.5 (0.45)	0.45	13.9	12.7	8.3%	15.2	14.9	1.4%
P1 (0.45)	0.45	14.5	13.7	5.7%	15.7	15.6	0.5%
P2 (0.45)	0.45	14.4	14.4	0.0%	14.7	14.7	0.3%
P0 (0.50)	0.50	15.0	12.5	16.5%	14.7	13.4	9.2%
P0.5 (0.50)	0.50	14.7	11.1	24.6%	15.5	13.8	11.2%
P1 (0.50)	0.50	15.4	11.4	26.0%	15.6	14.6	6.8%
P2 (0.50)	0.50	15.5	14.1	8.9%	16.6	15.5	6.5%
P0 (0.55)	0.55	14.5	10.3	28.7%	17.6	16.2	7.9%
P0.5 (0.55)	0.55	15.3	10.0	34.7%	16.9	15.1	11.0%
P1 (0.55)	0.55	16.8	10.7	36.4%	16.5	14.8	10.5%
P2 (0.55)	0.55	16.0	11.9	25.3%	17.7	15.9	10.0%

At 14 days (Figure 5.2.a), the use of nano-TiO_2 up to 1% promotes the CH reduction; samples with up to 1% of nanoparticles experiment a higher reactivity with the CO_2 than the reference ones (Figure 5.2.c). Moreover, the results show that the higher the water-to-cement (w/c) ratio, the higher the CH reduction. Likewise, for each w/c, there is a maximum percentage of nano-TiO_2 from which the CH reduction starts to decrease. Results suggest that the higher the w/c, the higher the optimum percentage of nano-TiO_2 in terms of CH reduction.

At 28 days, the results have a similar trend (Figure 5.2.b) in terms of CH reduction as a function of the w/c; the higher the w/c, the higher the CH reduction for each nano-TiO_2 level. The use of 0.5% nanoparticles in pastes with a high w/c (0.50 and 0.55) increases the CH reduction. Higher percentages reduce the CH reduction with a 0.5 w/c, while it does not significantly change with a higher ratio (0.55). However, in pastes with a low w/c (0.45), the use of nano-TiO_2 (even with just 0.5%) reduces the CH reactivity with CO_2 after the exposure at 28 days (Figure 5.2.d). It suggests that an excessive reduction of the porosity caused by the combination of (i) low w/c, (ii) higher age, and (iii) use of nanoparticles, may difficult the carbonation of the CH. This reduction of carbonation can be beneficial for steel-reinforced concrete (since avoiding carbonation of CH keeps the PH high). It is known that CH reduction through carbonation could negatively affect some concrete applications since it will lower the pH (reducing the protection of steel reinforcement against corrosion) [35].

However, for other types of cementitious composites such as mortars, plasters, and concretes without steel reinforcement, the increase of the CH reduction can be beneficial for sustainability (increasing CO_2 uptake). Besides, the reduction of both the porosity and the CH content may also be beneficial for durability. The porosity reduction will decrease the easiness of chloride-based salts and other sulfates to penetrate the material [52]. The reduction of CH will reduce the CH content available to react with chloride-based salts and other sulfates, reducing the potential formation of calcium oxychloride [53], among other harmful reactions. Thus, it could increase the durability of concrete pavements without fibers, among any other applications.

Summarizing, Figure 5.2 indicates four interesting trends: (i) there is a maximum percentage of nano-TiO_2 from which the CH reduction starts decreasing; (ii) this maximum percentage depends on the w/c, and the higher the w/c, the higher the maximum level of

nanoparticles that contributed to an increase of CH reduction; (iii) the CH reduction is highly influenced by the w/c and, (iv) the lower the age of the paste when the CO_2 24-hour exposure occurs, the higher the CH reduction in each studied mixture.

Since w/c and age change the porosity of the sample at the time of the CO_2 exposure, these observations suggest that the porosity could play a key role in the CH reduction. On the other hand, the use of nano-TiO_2 (to a certain level) may promote CH reduction despite reducing the porosity due to potential changes in the microstructure.

Figure 5.2.e presents the TGA results of the mixture that exhibited the highest CH reduction (P1 with w/c 0.55). All TGA curves are shown in Appendix D.

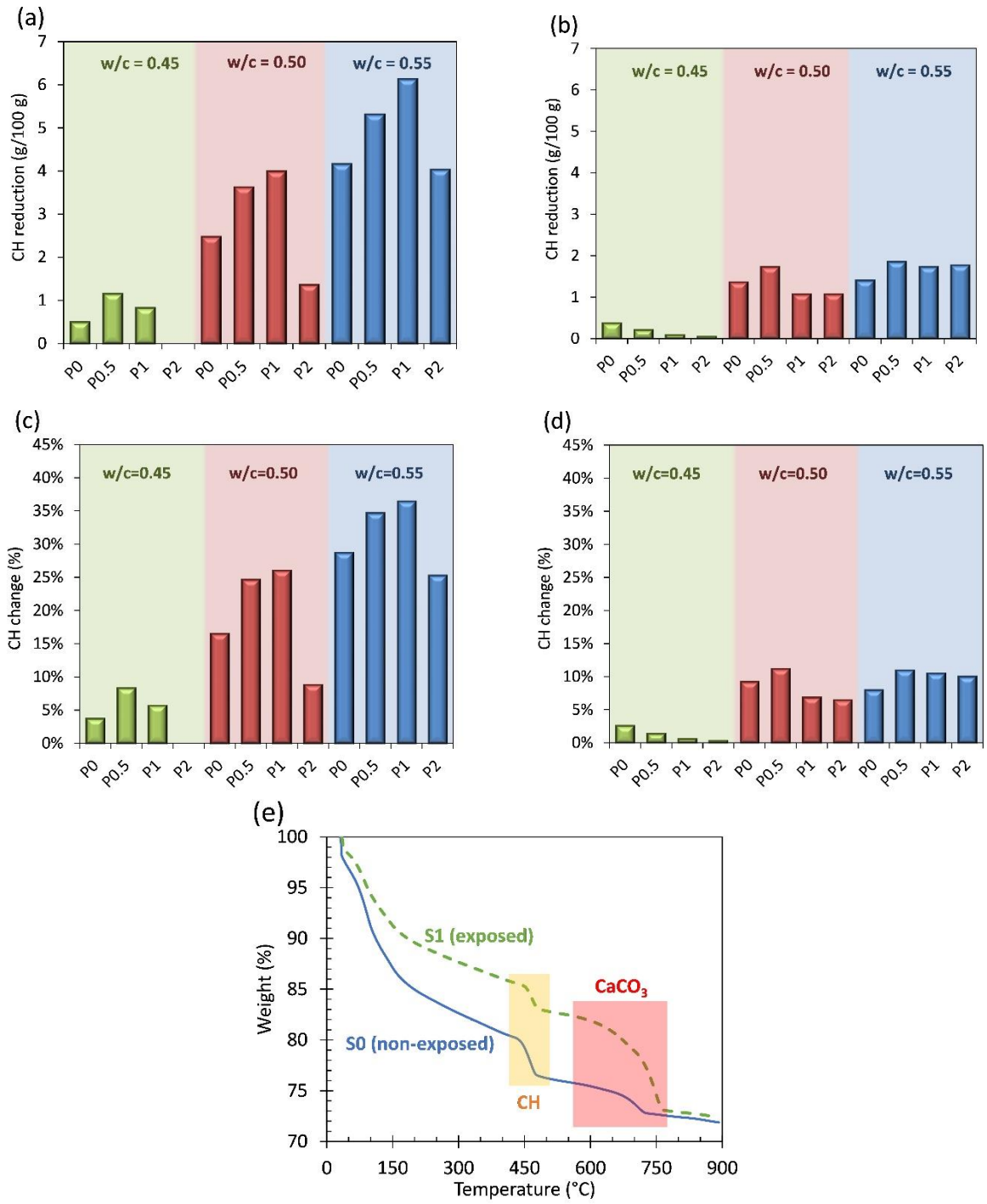

Figure 5.2. CH reduction and relative CH change due to the CO_2 exposure (g/100 g). (a) CH reduction at 14 days. (b) CH reduction at 28 days. (c) Relative CH change (%) at 14 days. (d) Relative CH change (%) at 28 days. (e) TGA curves for P1 with w/c=0.55 before and after exposure.

Figure 5.3 presents the $CaCO_3$ content of all studied samples at two different ages (14 and 28 days) before and after the 24-hour CO_2 exposure. For each mixture, while the left (red) column symbolizes the $CaCO_3$ content present in the non-exposed sample (obtained by Eq. 5.3), the right column shows the $CaCO_3$ content in the exposed sample, divided into three different parts, from top to bottom: (i) the $CaCO_3$ coming from the CH carbonated (obtained by Eq. 5.6); (ii) the $CaCO_3$ coming from the carbonation of other hydration products (e.g., C-S-H or ettringite) and/or anhydrous silicates and aluminates phases (obtained by Eq. 5.7); and (iii) the pre-existing $CaCO_3$ before the exposure (obtained by Eq. 5.3).

At 14 days (Figure 5.3.a), the initial $CaCO_3$ content (unexposed samples) does not present significant variations between samples with different levels of nano-TiO_2. It indicates that the natural carbonation produced during the curing process affects all samples to the same extent. It was expected since the carbonation process is slow in a normal environment due to the low CO_2 concentration in the atmosphere (0.0415% or 415 ppm) [160]. Therefore, since the natural carbonation of the samples is very low under these conditions, the potential changes in carbonation due to the different compositions of the mixtures will not be detected in such a short period (less than 28 days) in samples cured as described.

In addition, the percentage of $CaCO_3$ from CH carbonation (compared to the total $CaCO_3$ increase after the exposure, which is the sum of both green columns) is higher with the increase of the w/c at 14 days. After the 24-hour CO_2 exposure, the higher the w/c, the higher the $CaCO_3$ content at both studied ages. At both ages, whereas the use of nano-TiO_2 with a high w/c (0.55) increases the $CaCO_3$ content after exposure, samples with nanoparticles and low w/c (0.45) show a decrease in the $CaCO_3$ content of exposed samples in comparison to the non-modified specimens. These results agree with the results presented in Figure 5.2. Considering that nano-TiO_2 reduces the porosity [48]–[51] and that the lower the w/c, the lower the porosity [88], a potential explanation could be that cement pastes with nano-TiO_2, and low w/c (0.45) presents such a low porosity that almost inhibits the carbonation process. As mentioned for the CH reduction results, each mixture may have a maximum nano-TiO_2 percentage from which there is no increase in terms of $CaCO_3$ content after exposure. This percentage varies depending on either the w/c or the age at the 24-hour exposure. Likewise, the increase of $CaCO_3$ content during the 24-hour exposure is higher at lower age (14 days).

These results suggest two possible mechanisms modifying the CH reduction and $CaCO_3$ formation through carbonation due to 24-hour CO_2 exposure: (i) reduction of porosity (that reduces the CH reduction) and (ii) changes in the microstructure and hydration products that lead to an increase of CH reduction and $CaCO_3$ formation. This will be evaluated in the following sections.

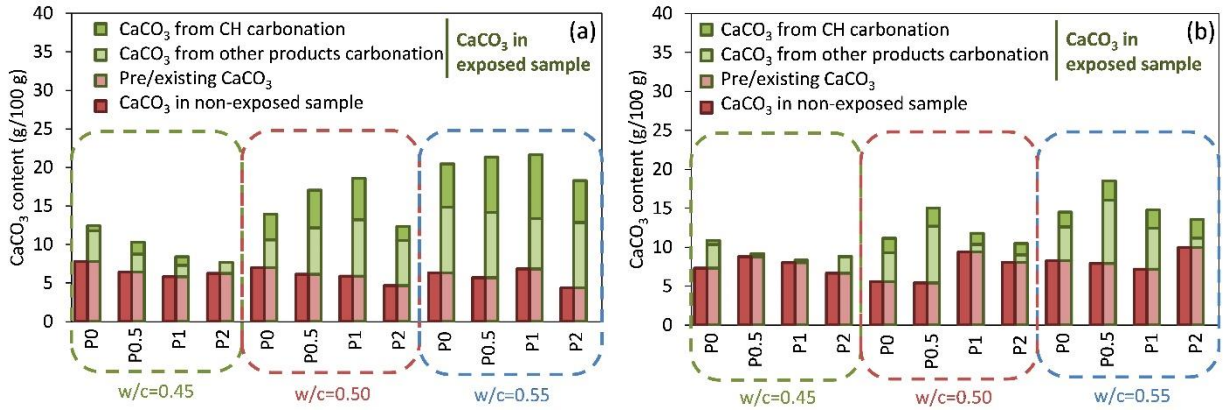

Figure 5.3. $CaCO_3$ content (g/100 g). (a) At 14 days. (b) At 28 days.

5.3.2 CO_2 uptake

Figure 5.4 shows the CO_2 uptake after CO_2 24-hour exposure at two different ages (14 and 28 days) as a function of w/c and nano-TiO_2 percentage. At both ages, the higher the w/c, the higher the CO_2 uptake. The increase of porosity due to a rise in the w/c can explain the higher CO_2 uptake observed; the higher the porosity, the easier for the CO_2 to penetrate the cement paste. Nevertheless, the CO_2 uptake after the 24-hour exposure is lower at 28 days than at 14 days. This trend also can be explained due to changes in porosity since the porosity decreases with an increase in the curing age [88]. As aforementioned, there is a maximum percentage of nanoparticles in all mixtures from which the CO_2 uptake starts to be reduced. This percentage varies depending on either the w/c or the age at the 24-hour exposure.

The optimum percentage of nano-TiO_2 (in terms of CO_2 uptake) for all w/c when 24-hour exposure occurs at 14 days is higher than when it happens at 28 days (Figure 5.4.b). Likewise, the higher the w/c, the higher the maximum percentage of nanoparticles to increase the CO_2 uptake. It is already known that nano-TiO_2 reduces the porosity of cementitious materials [29], [44], [47]. In addition, the lower the w/c, the lower the porosity [88]. Consequently, with a low w/c (0.45), the cement pastes with nano-TiO_2 have too low porosity (or space available) to carbonate the hydration

products and transform them into $CaCO_3$ since the molar volume of $CaCO_3$ is higher than portlandite (CH) or C-S-H phases among others [182]. Therefore, the lack of space available could be why samples with nano-TiO_2 showed lower CO_2 uptake than specimens with no nanoparticles when the initial porosity was already low (low w/c). In contrast, the use of nano-TiO_2 with high w/c (0.55) increases the CO_2 uptake. This can seem counter-intuitive since the use of nano-TiO_2 reduces the porosity and may reduce the penetration of CO_2 into the cement paste. However, besides reducing porosity, the use of nano-TiO_2 has other effects on the microstructure of cement pastes that may increase the CO_2 sequestration rate. It is known that the nanoparticles reduce the size of the CH [44], [115], [183]. This size reduction could make the CH more prone to be carbonated. In fact, a recent study observed that, during sample preparation for TGA (grinding with mortar and pestle), samples with nano-TiO_2 showed higher CH carbonation than reference samples without nano-TiO_2 [29].

Thus, the combination of both effects (porosity reduction and increment of CH reactivity) could explain why the use of nano-TiO_2 may be beneficial or detrimental for the CO_2 uptake as a function of w/c and age (since both of them affect the initial porosity of the mixtures).

Since samples with a high w/c possess high porosity, the reduction of porosity due to the use of nano-TiO_2 would not produce a lack of space enough to limit the carbonation process. Thus, the CH reactivity produced by the nano-TiO_2 would be reflected in a higher CO_2 uptake.

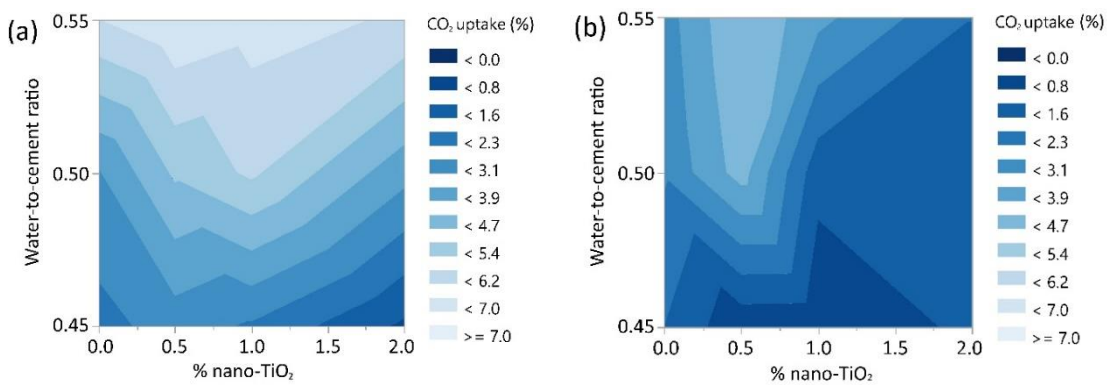

Figure 5.4. CO_2 uptake (% per cement mass) after the 24-hour exposure (g/100 g). (a) At 14 days. (b) At 28 days.

5.3.3 Pore structure

Figure 5.5 shows the pore structure of samples with 0% and 1% of nano-TiO_2 and w/c of 0.45 before and after exposure at 14 days, obtained through a 3D X-Ray microscope scanner. Based on that, Table 5.3 summarizes the data of the total volume of macropores for each mixture before and after exposure. As expected, the use of nano-TiO_2 reduces the porosity since the sample with no nanoparticles exhibits a higher porosity than the specimen with 1% of nano-TiO_2. The reason for this porosity reduction could be the refinement in the microstructure made by the nanoparticles due to their nucleation effect and the filling effect [44], [47], [65], [66]. Nevertheless, the effect of the nanoparticles is more pronounced in the specimen before exposure (~5%) than in the sample after exposure (~2%).

Regarding the porosity variation due to the 24-hour exposure, samples before exposure exhibit higher porosity than specimens after exposure as expected, since $CaCO_3$ possesses higher molar volume than portlandite (CH) or C-S-H phases, among others [182]. This evidences that (i) the carbonation process occurred during the CO_2 exposure, and (ii) the changes due to the exposure were captured by the 3D scans. In terms of changes in porosity due to the CO_2 exposure, while samples with 1% of nano-TiO_2 show a decrease of the pore volume below 2%, specimens with no nanoparticles the pore reduction is around 4%, as summarized in Table 5.3. As mentioned in previous sections, the lack of space available due to the reduction of porosity produced by nano-TiO_2 in a mixture with already low porosity (low w/c) could be the reason why the carbonation process was reduced in comparison to the specimens with no nanoparticles.

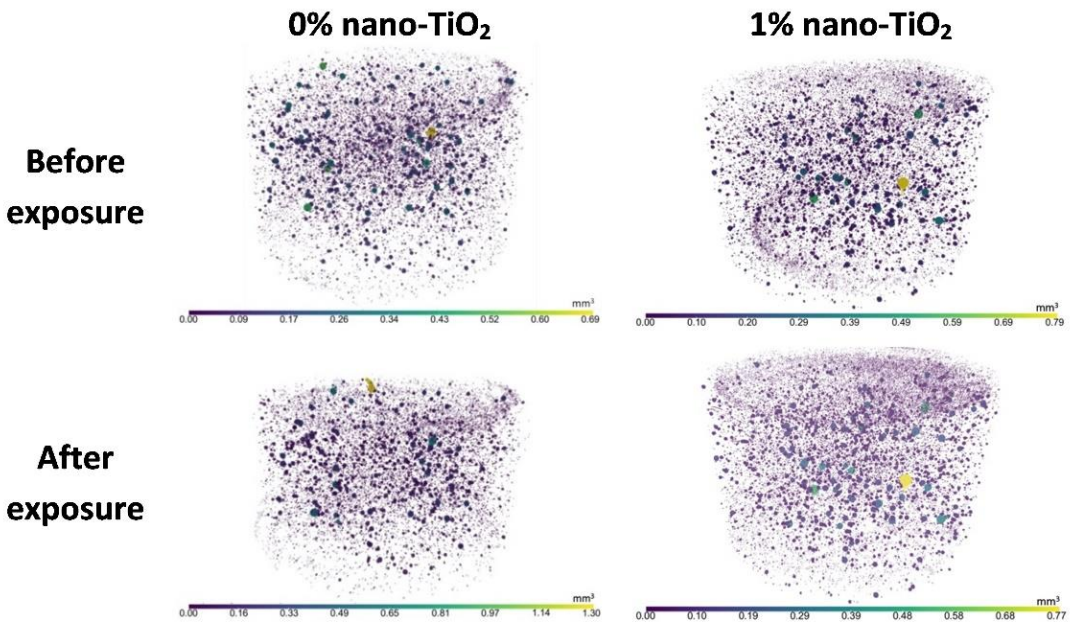

Figure 5.5. Pore structure (macropores) of samples before and after exposure at 14 days (w/c=0.45).

In contrast, in the case of 0.55 w/c, the impact of using nano-TiO_2 in the carbonation during CO_2 exposure is different. Figure 5.6 shows the pore structure of samples with a w/c of 0.55 before and after exposure at 14 days. As expected, samples with 0.55 w/c present higher porosity than samples with a low w/c (0.45). With a high w/c (0.55), the use of 1% of nano-TiO_2 decreased the porosity a 12% (in comparison to samples with no nanoparticles) in unexposed samples, while after the CO_2 exposure, the use of the same percentage of nano-TiO_2 reduced the porosity a 14% (in comparison to exposed samples with no nanoparticles).

Regarding the effect of the exposure, samples with nanoparticles presented a greater porosity reduction during the exposure than reference specimens. In samples with 1% of nano-TiO_2 and w/c 0.55, the CO_2 exposure produced a 7% reduction of porosity. In contrast, samples with no nanoparticles presented a decrease of 5% of their porosity due to the CO_2 exposure.

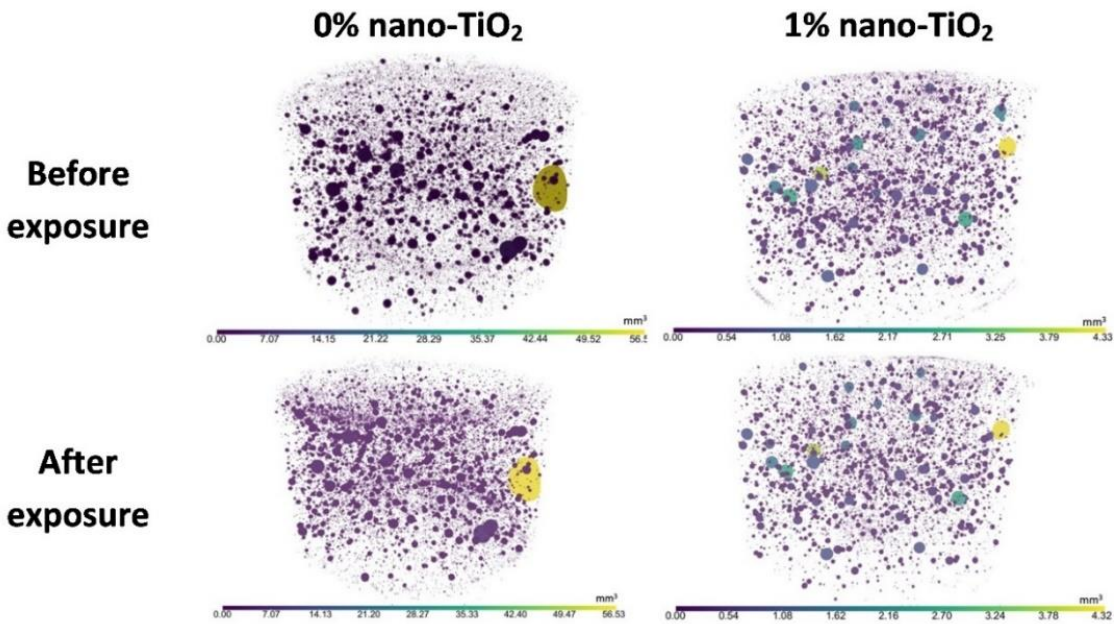

Figure 5.6. Pore structure (macropores) of samples before and after exposure at 14 days (w/c=0.55).

Table 5.3 presents the comparison between the pore volume and the CO_2 uptake of the samples with 0% and 1% of nano-TiO_2 before and after exposure at 14 days. The total volume of the sample is 16,626.34 mm^3.

The reduction in porosity due to the exposure is related to the CO_2 uptake; the higher the CO_2 uptake, the higher the porosity reduction. As previously noted, $CaCO_3$ possesses a higher molar volume than portlandite (CH) or C-S-H phases, among others [182]. Therefore, the higher the carbonation (higher CO_2 uptake), the higher the expected porosity reduction due to the CO_2 exposure.

Table 5.3. Comparison of pore volume (macropores) and CO_2 uptake of samples with 0% and 1% of nano-TiO_2.

w/c	% of nano-TiO_2	Pore volume (mm^3) of macropores		Decrease due to the exposure (%)	CO_2 uptake (%)	Reduction due to the use of nano-TiO_2 (%)	
		Before exposure	After exposure			Before exposure	After exposure
0.45	**0%**	78.64	76.47	4.41	2.04	5.29	2.27
	1%	74.48	73.46	1.37	1.14		
0.55	**0%**	145.44	138.04	5.16	6.21	12.04	13.93
	1%	127.59	118.40	7.20	6.52		

Figure 5.7 shows the pore volume histogram of the samples with w/c=0.45 before and after the CO_2 exposure at 14 days. Each column refers to the total cumulative volume of pores (macropores) for each range of pore sizes. Both graphs show a decrease in the size of the pores after exposure. This reduction is related to the carbonation process; each pore reduces its size due to the formation of calcium carbonate. This data suggests that with low w/c (0.45), the use of 1 % of nano-TiO_2 does not promote CO_2 uptake. These observations agree with the results presented in Figure 5.4.

Moreover, P0 (0.45) shows a higher cumulative pore volume in the lowest size range after exposure. Even though it can seem counter-intuitive, the explanation could be that the smallest pores of the unexposed samples can suffer a porosity reduction during the carbonation. Therefore, after exposure, part of these initially small pores may be completely filled due to the calcium carbonate formation or becoming negligible in terms of volume. This may reduce the total cumulative volume pores in the lowest range of pore volume size. The pore size reduction due to carbonation is more remarkable in larger pores.

In contrast, P1 (0.45) exhibits an increase in the volume of the lowest range due to the pores size reduction of larger pores over the CO_2 exposure (Figure 5.7.b).

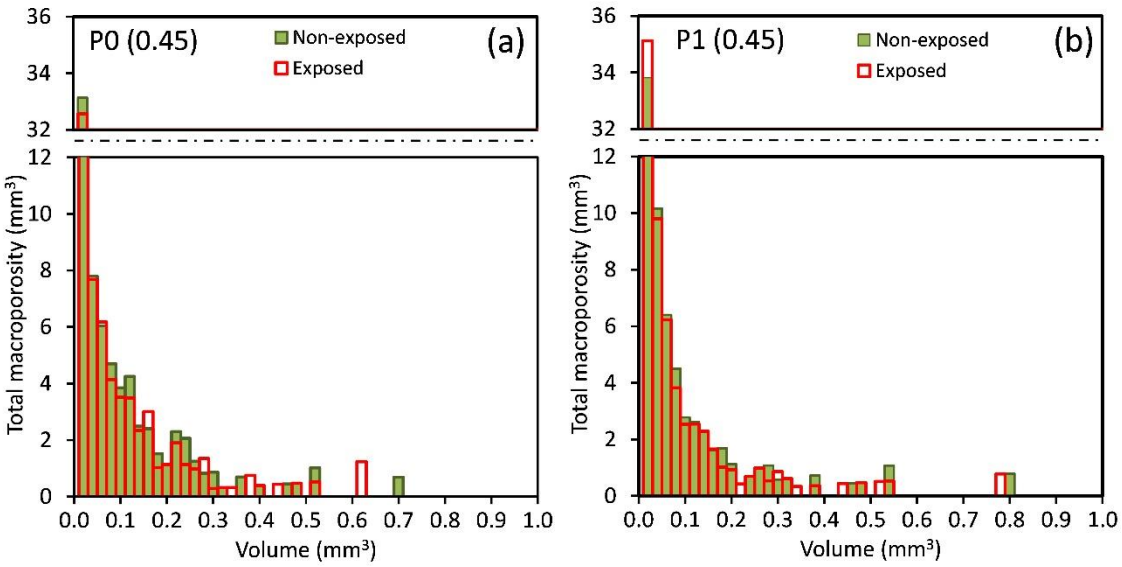

Figure 5.7. Histogram of the pore volume of w/c=0.45. (a) P0. (b) P1.

Figure 5.8 displays the pore volume histogram of the samples with a 0.55 w/c before and after the exposure at 14 days. While Figure 5.8.a and Figure 5.8.c present the sample results with no nanoparticles, Figure 5.8.b and Figure 5.8.d show the pore volume of the sample with 1% of nano-TiO_2. The graphs show that samples with 0.55 w/c present a higher maximum pore size and higher cumulative volume of pores than 0.45 w/c samples. The results show a decrease in the pore size for both 0% and 1% nano-TiO_2 samples, with 0.55 w/c, due to the exposure. As a result, most of the cumulative volume pores are observed in the lowest pore volume ranges, and a reduction of the cumulative pore volume in larger size ranges. This reduction is more pronounced in the sample with 1% nano-TiO_2 (Figure 5.8.b and Figure 5.8.d) than in the reference mixture. It suggests that nano-TiO_2 may promote carbonation in samples with a high w/c since a high porosity reduction during the CO_2 exposure indicates high carbonation.

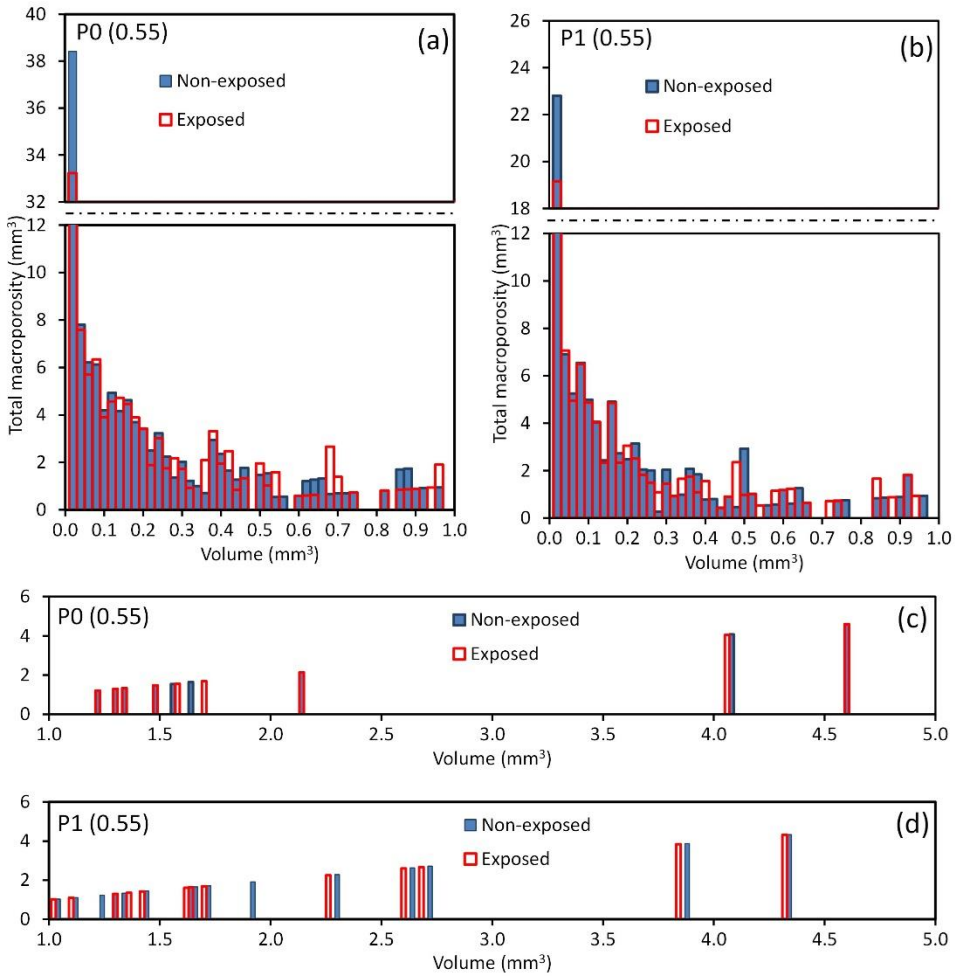

Figure 5.8. Histogram of the pore volume of w/c=0.55. (a) P0 (<1mm^3). (b) P1 (<1mm^3). (c) P0 (1-5mm^3). (d) P1 (1-5mm^3).

Figure 5.9 displays the pore volume histogram of the samples with a 0.45 w/c at 14 days and two different percentages of nano-TiO_2 (0% and 1%). To analyze the effect of nano-TiO_2 on the pore structure, samples cured under the same conditions were compared. Figure 5.9.a presents a comparison between the pore volume histogram of samples with and without nano-TiO_2 under normal curing conditions (unexposed samples), while Figure 5.9.b shows the same data, but for samples exposed to CO_2. Each column refers to the total cumulative volume of pores for each range of pore sizes. Results show that, in general, the use of 1% of nano-TiO_2 decreases the pore volume in non-exposed samples (Figure 5.9.a). The filling effect of nano-TiO_2 on both exposed and unexposed samples affects a wide range of pores, but it significantly reduces the volume of pores between 0.1 mm^3 and 0.25 mm^3.

Moreover, results suggest that the carbonation process and the nanoparticles might have a different filling effect. While the carbonation process (Figure 5.7) affects more to pores with a volume between 0.25 and 0.5 mm^3, the use of 1% of nano-TiO_2 (Figure 5.9) produces a more remarkable modification of ranges with lower volume (0.1-0.25 mm^3). Consequently, the pores affected by the filling effect of nano-TiO_2 are smaller than the pores affected by the filling effect of the carbonation. Figure 5.10 shows similar trends for samples with a 0.55 w/c.

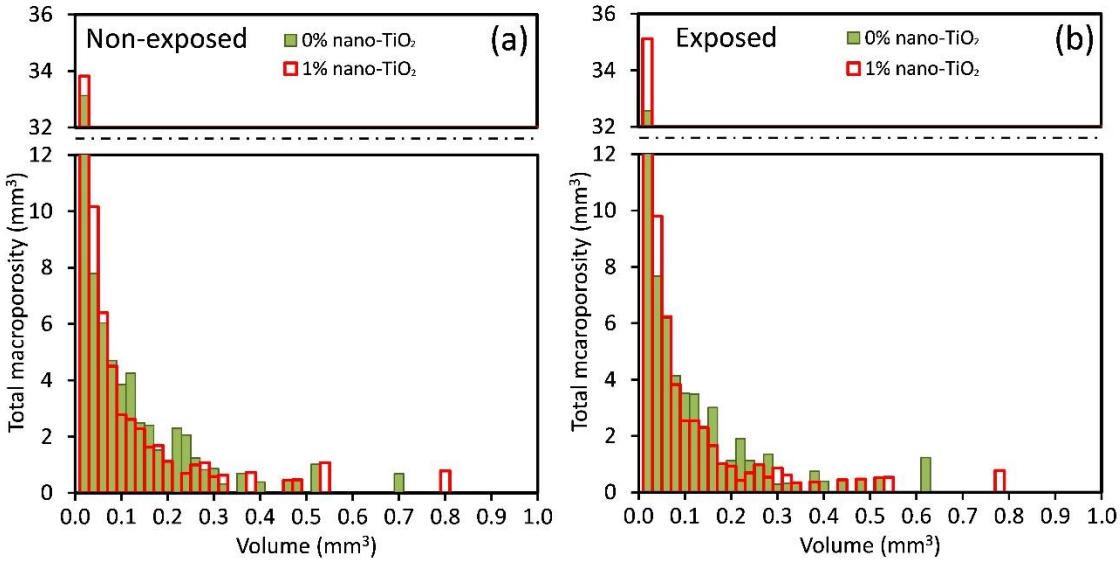

Figure 5.9. Histogram of the pore volume of w/c=0.45. (a) Non-exposed. (b) Exposed.

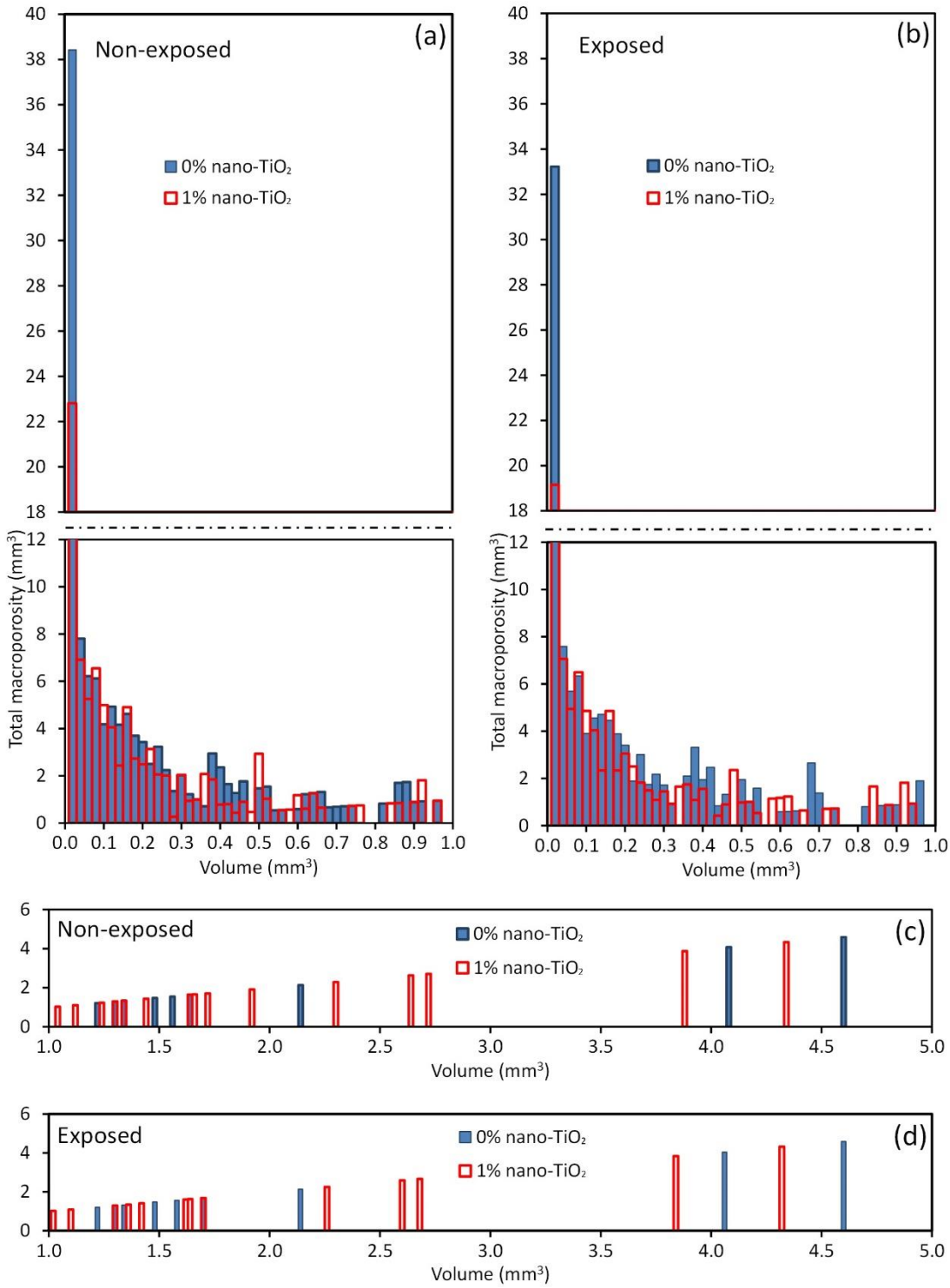

Figure 5.10. Histogram of the pore volume of w/c=0.55. (a) Non-exposed (<1mm^3). (b) Exposed (<1mm^3). (c) Non-exposed (1-5mm^3). (d) Exposed (1-5mm^3).

Reducing the pore size on a given range of pore volume sizes may increase the porosity on lower ranges (refinement of the pore structure). In samples with a high w/c (0.55), the filling effect of nano-TiO_2 (Figure 5.10) was primarily observed on pore volume sizes up to 0.7 mm^3, especially for ranges between 0.38 and 0.46 mm^3. Thus, with a 0.55 w/c, an increase in porosity in smaller pore volume ranges due to the filling effect would be expected on ranges smaller than 0.38 mm^3. However, in samples with a 0.45 w/c, the pores affected by the filling effect of nano-TiO_2 (Figure 5.10) are mainly in the range of 0.1-0.25 mm^3. Therefore, an increase of porosity in ranges of smaller sizes would be expected on ranges smaller than 0.1 mm^3, producing a higher increase of porosity on the lowest size range compared to the same effect on samples with a 0.55 w/c. It may explain why in non-exposed samples with 1% nano-TiO_2 addition (Figure 5.7.b and Figure 5.8.b), samples with higher w/c showed a lower porosity in the lowest range of pore volume, while in non-exposed samples and no nano-TiO_2 addition (Figure 5.7.a and Figure 5.8.a), the porosity in the lowest range of pore volume increases with the w/c.

Therefore, the pore structure analysis, done using the 3D X-ray, may validate the potential explanation stated in the previous sections, based on the thermal analysis results, about the effect of the nanoparticles as a function of the w/c. With a 0.45 w/c, the sample with 1% nano-TiO_2 produces a lower porosity reduction than the reference specimen (no nanoparticles) after the 24-hour CO_2 exposure at 14 days. In contrast, the sample with 1% nanoparticles and a higher water-to-cement ratio (0.55) presents a higher porosity decrease than the specimen with no nano-TiO_2. Therefore, these results correlate with the observations noted regarding CO_2 uptake using thermal analysis.

5.3.4 Relevance to cementitious composites

The findings of this chapter might also be relevant for cementitious composites such as mortar and concrete. It is known that (i) cement is the main compound of the cementitious composite matrix, and (ii) cement is the concrete compound that contributes to most to the CO_2 footprint of concretes and mortar. Thus, even though this chapter was focused on the effect of nano-TiO_2 on the CO_2 uptake of cement pastes, the results suggest that the use of nano-TiO_2 on cementitious composites would clearly affect its environmental footprint. While this chapter is focused on studying the effect of nano-TiO_2 addition on the CO_2 uptake of cement pastes, from a

practical point of view, cost-benefit studies would be required in the future to analyze the potential uses of nano-TiO_2 addition on cementitious composites such as concrete or mortars. Furthermore, the cost-benefit analysis may vary from country to country since they are a wide range of prices of nano-TiO_2 from one region to another.

5.4 Conclusions

The present chapter was designed to study the effect of nano-TiO_2 on the CO_2 uptake of cement paste.

Based on the thermal analysis results, three remarkable conclusions can be drawn: (i) the effect of nano-TiO_2 on the CH reduction, $CaCO_3$ formation, and CO_2 uptake due to the CO_2 exposure is highly influenced by both exposure age and the water-to-cement ratio of the cement pastes; (ii) the use of nanoparticles is beneficial for CO_2 uptake until a certain percentage from which the improvement starts to decrease; (iii) the maximum nano-TiO_2 percentage that increases the CO_2 uptake depends on water-to-cement ratio and age of CO_2 exposure.

The higher the w/c, the higher the maximum level of nanoparticles that increases the CO_2 uptake and CH reduction of cement paste. In the same way, the lower the 24-hour CO_2 exposure age, the higher the CO_2 uptake and the CH reduction in each studied mixture.

Since w/c and exposure age change the porosity, the results obtained suggest that porosity could play a key role in the CH reduction, $CaCO_3$ formation, and CO_2 uptake due to the CO_2 exposure. On the other hand, the use of nano-TiO_2 (up to a certain level) promotes the CO_2 uptake despite reducing the porosity. Since the use of nano-TiO_2 may reduce the CH size, it could make the CH more prone to be carbonated during the CO_2 exposure, promoting the CO_2 uptake of cement paste. Thus, the combination of these two competing mechanisms (porosity reduction and increment of CH reactivity) could explain why the use of nano-TiO_2 may be beneficial or detrimental for the CO_2 uptake as a function of w/c and age (since both of them affect the initial porosity of the mixtures).

Due to the high porosity of mixtures with high w/c, the effect of nano-TiO_2 on porosity (that would lead to a reduction of the CO_2 penetration) could not overcome the increase of carbonation due to more reactive hydration products when initial porosity is high.

The pore structure analysis, done using 3D X-ray microscopy, agrees with the conclusions based on the thermal analysis. Samples before the 24-hour CO_2 exposure exhibit higher porosity than specimens after exposure, as expected, since $CaCO_3$ possesses higher molar volume than portlandite (CH) or C-S-H phases, among others. The use of 1% nanoparticles with a low w/c produced a lower porosity reduction over the CO_2 exposure. It suggests that the sample with 1% of nano-TiO_2 and 0.45 w/c evidenced lower carbonation than the reference sample. In contrast, with a high w/c (0.55), using 1% of nano-TiO_2 produces a higher decrease of porosity during the CO_2 exposure than the specimen with no nanoparticles. Consequently, these results agree with the thermal analysis conclusions. Besides, carbonation reduced the pore size, especially on the larger pores, improving the pore structure.

6. IMPACT OF NANO-TiO_2 ADDITION ON THE REDUCTION OF NET CO_2 EMISSIONS OF CEMENT PASTES AFTER CO_2 CURING

Part of this work has been published as:

C. Moro, V. Francioso and M. Velay-Lizancos (2021). *'Impact of nano-TiO_2 addition on the reduction of net CO_2 emissions of cement pastes after CO_2 curing.'* Cement and Concrete Composites, vol. 123, p. 104160. https://doi.org/10.1016/j.cemconcomp.2021.104160.

6.1 Introduction

The cement industry is one of the main carbon dioxide (CO_2) emitters, with around 8% of each year's total emissions [4]. However, cementitious materials are well-known to react with CO_2. Xi et al. [19] claimed that cementitious materials captured 43% of the total CO_2 emitted by the cement industry in the period 1930-2013. Therefore, cementitious composites could be an important carbon sink that should be considered due to the sequestration of almost half of their total CO_2 emissions.

The carbonation of cementitious materials can be classified into two different types (passive or active) depending on several properties (e.g., exposure time or CO_2 concentration) [159]. Passive carbonation involves the exposure of the cementitious materials for a long time in a low CO_2 concentration environment. All cementitious materials present this type of carbonation during their lifetime since the atmosphere possesses a low CO_2 concentration (0.0415% or 415 ppm) [160]. During the exposure, atmospheric CO_2 reacts with the hydration products (e.g., calcium hydroxide (CH or $Ca(OH)_2$) or calcium silica hydrate (C-S-H or $(CaO)_x \cdot (SiO_2)_y \cdot (H_2O)_z$)) of the cement paste producing calcium carbonate as shown in Eq. 6.1 and 6.2 [25], [156], [184], [185].

$$Ca(OH)_2 + CO_2 \rightarrow CaCO_3 + H_2O \qquad 6.1$$

$$(CaO)_x(SiO_2)_y(H_2O)_z + xCO_2 \rightarrow xCaCO_3 + y(SiO_2)(H_2O)_t + (z - yt)H_2O \qquad 6.2$$

Nevertheless, while worldwide cement production has been increasing rapidly over the last decades [20], the passive or natural carbonation of cementitious materials is a slow process.

Therefore, those materials do not have enough time to partially compensate the CO_2 emitted by the cement industry. An acceleration of the carbonation process may help reduce the net CO_2 emissions of cementitious composite materials in a shorter time.

The active or accelerated carbonation consists of increasing the CO_2 concentration for a short time to promote the quicker reaction of the different phases of the cement paste with the CO_2 present [25], [164]. Thus, in addition to the hydration products, the principal phases of anhydrous cement (alite, C_3S or $3(CaO)\cdot SiO_2$, and belite, C_2S or $2(CaO)\cdot SiO_2$) could react with the CO_2 as exhibited in Eq. 6.3 and 6.4 [164].

$$3CaO \cdot SiO_2 + (3 - x)CO_2 + yH_2O \rightarrow xCaO \cdot SiO_2 \cdot yH_2O + (3 - x)CaCO_3 \qquad 6.3$$

$$2CaO \cdot SiO_2 + (2 - x)CO_2 + yH_2O \rightarrow xCaO \cdot SiO_2 \cdot yH_2O + (2 - x)CaCO_3 \qquad 6.4$$

Previous research showed the beneficial effects of accelerated (or CO_2) curing [28], [170]–[172]. Cementitious materials may improve the microstructure [167], [175], [186], [187], the strength [174], [188]–[192], or the durability [171], [172], [193] after CO_2 curing. Some authors argued that the refinement of the microstructure and the reduction of porosity could be the reason beyond the enhancement of strength [167], [175] and durability [171], [172], [193]. The accelerated curing promotes the carbonation of the hydration products [185] and, therefore, the porosity is reduced due to the higher molar volume of the $CaCO_3$ in comparison to other phases (e.g., CH or C-S-H) [182]. However, the bigger pores (micropores and mesopores) may increase due to the leaching of the C-S-H gel [193], [194]. Another potential explanation for the compressive strength improvement could be the rapid cement dissolution [190], [191]. Either way, the carbonation of cementitious materials could decrease total net CO_2 emissions while improving the material properties. Thus, it would be a potential double positive effect.

Traditionally, the hydration products content and the porosity have been identified as the significant factors contributing to the compressive strength of cement pastes [88]. Nonetheless, the porosity affects the compressive strength to a greater extent [88]. Numerous studies showed that the use of TiO_2 nanoparticles might decrease the total porosity of cementitious materials [29], [44], [47], [111]. Besides, the nanoparticles may enhance the interfacial transition zone (ITZ) of mortars due to the particle packing density [43], [82]. Nano-TiO_2 may restrict the CH crystals size

increasing its reactivity and leading to a denser microstructure [44], [47], [115] and, therefore, improving both strength and durability [47], [52]–[56]. In terms of CO_2 sequestration, recent studies showed that nano-TiO_2 addition modifies the CO_2 capture of hardened cement pastes [29], [195]. Francioso et al. [29] suggested that the use of 0.5% of nano-TiO_2 (by the total weight of cement) may promote natural carbonation (carbonation due to the exposure of the sample to the atmospheric CO_2) of powdered mortar samples at seven days. In addition, a recent investigation found that nano-TiO_2 addition increased the CO_2 capture of hardened cement paste after a weathering carbonation [195].

However, the effect of nano-TiO_2 on CO_2 sequestration by CO_2 curing was not studied. Previous studies focused on CO_2 sequestration of plain cement pastes showed the benefits of CO_2 curing compared to the carbonation of hardened cement paste [164], [171], [196]. Besides, there is a lack of investigation regarding the effect of TiO_2 nanoparticles on cementitious materials' properties after CO_2 curing. Therefore, the main objective of this investigation is to evaluate the potential effect of nano-TiO_2 addition on net CO_2 emissions related to CO_2 cured cement pastes. In addition, it also studies the impact of the curing procedure on both hydration products and the compressive strength of cement pastes made with different levels of TiO_2 nanoparticles.

6.2 Materials and Methods

6.2.1 Materials and mixture procedure

The material characterization of the cement and nano-TiO_2 used in this chapter is exhibited in *Chapter 2: Materials and general procedures*.

Cement paste mixtures were made with four different percentages of nano-TiO_2 (0%, 0.5%, 1%, 2%) and water-to-cement ratio of 0.55. The mixture proportions of each cement paste are listed in Table 6.1. A total of 12 samples of each mixture were cast in steel molds with 16x4x4 cm dimensions, meeting the standard ASTM C349 [36] for compressive strength tests. After 12 hours, samples were demolded and left inside an environmental chamber under controlled conditions (temperature of 23 °C and humidity of 50%) for 12 more hours. At 24 hours of age, while six specimens remained inside the environmental chamber to be used as a reference (normal curing (NC) samples), the other six samples of each mixture were placed in a carbonation chamber with

20% of CO_2 and a temperature of 23 °C for 12 hours. Those samples were exposed to CO_2 curing (CC). After carbonation, these samples were placed again in the environmental chamber with the NC samples for 12 more hours until testing. Thus, all NC and CC samples were tested at 48 hours. Figure 6.1 shows the curing procedure diagram for normal cured and CO_2 cured samples.

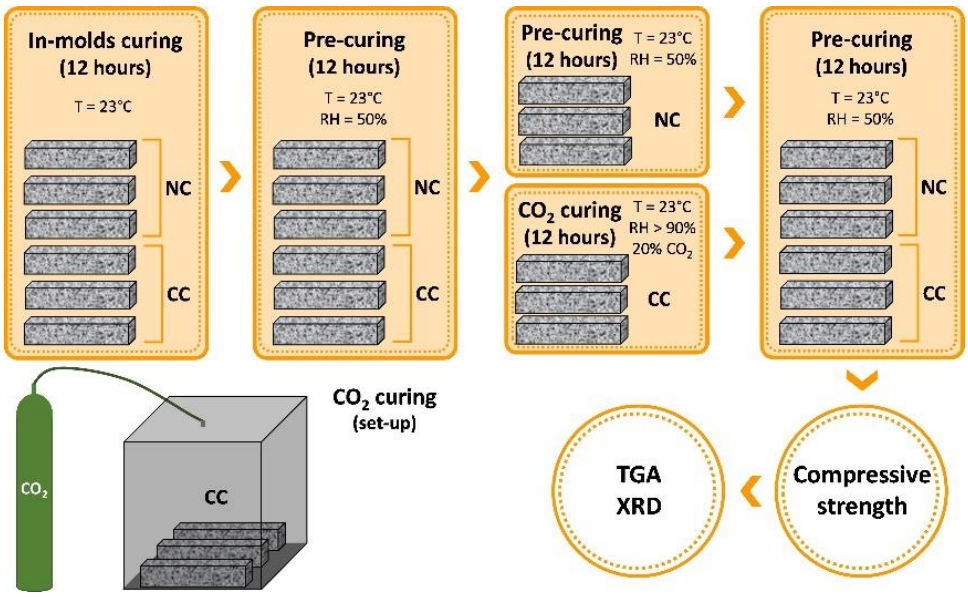

Figure 6.1. Curing procedure diagram and experimental campaign of this chapter.

Table 6.1. Mixture proportions of cement paste mixtures.

Mixture	w/c	Cement (g)	nano-TiO_2 (g)	Water (g)
P0	0.55	2213.4	0.0	1217.3
P0.5	0.55	2202.3	11.1	1217.3
P1	0.55	2191.2	22.1	1217.3
P2	0.55	2169.1	44.3	1217.3

While NC samples were naturally carbonated with atmospheric CO_2 during the whole 48 hours, CC samples were naturally carbonated with atmospheric CO_2 for 24 hours, then intentionally carbonated with 20% CO_2 concentration for another 12 hours, and after that, naturally carbonated again with atmospheric CO_2 for 12 more hours. In this chapter, the carbonation of NC and CC samples was compared to analyze the effectiveness of the 12-hour CO_2 curing in the CO_2 chamber for each mixture (with and without nano-TiO_2).

6.2.2 Methods

Compressive strength test

An MTS (Eden Prairie, MN) machine was used for the uniaxial compressive strength test. The parameters of the test are specified in *Chapter 2: Materials and general procedures*. A total of six samples of each mixture were tested.

X-ray powder diffraction (XRD)

After the compressive strength test, the broken pieces were used for TGA and XRD analysis. All the exterior parts of the sample were discarded. The specimens used were obtained 5-6 mm from the top surface of the sample (in its center). Each sample was prepared using a solvent exchange procedure to remove the free water [37]. The roughly ground sample was placed in a container with isopropanol. After 15 minutes, the sample was placed for 10 minutes in an oven at 40 °C to remove the excess of isopropanol. Each specimen was then ground (using a mortar and pestle) and sieved (with a No. 200 sieve, 75-µm). The parameters of the test are specified in *Chapter 2: Materials and general procedures*.

Thermogravimetric analysis (TGA)

Another sample from the same ground specimens used for the XRD test was employed for TGA. The parameters of the tests are specified in *Chapter 2: Materials and general procedures*.

The CO_2 captured for each sample due to the accelerated carbonation was calculated based on the difference between the $CaCO_3$ content of the normal cured (NC) specimens and the CO_2 cured (CC) samples. The $CaCO_3$ content of each sample was obtained using Eq. 6.5.

$$\mathrm{CaCO_3\ (g/100\ g)} = 100 \cdot \frac{100.1}{44.0} \cdot \frac{1}{\mathrm{M_c}} \cdot \left[\left(\mathrm{M_{start}^{CaCO_3}}\right) - \left(\mathrm{M_{end}^{CaCO_3}}\right)\right] \qquad 6.5$$

Where $CaCO_3$ is the content (g/100 g) of calcium carbonate of anhydrous cement; 100.1 and 44.0 are the molar weight ratios of $CaCO_3$ and CO_2, respectively; M_C is the initial mass (g) of the anhydrous cement in the sample; and $M_{start}^{CaCO_3}$ and $M_{end}^{CaCO_3}$ are the masses (g) of the sample at the start and endpoint for $CaCO_3$ decomposition, respectively.

Then, the CO_2 uptake can be calculated based on the difference of $CaCO_3$ content between the NC and the CC samples using Eq. 6.6.

$$\mathrm{CO_2\ uptake\ (g/100\ g)} = \left[\left(\mathrm{CaCO_3^{CC,sample}}\right) - \left(\mathrm{CaCO_3^{NC,sample}}\right)\right] \cdot \frac{44.0}{100.1} \qquad 6.6$$

Where CO_2 uptake is the content (g/100 g) of carbon dioxide of anhydrous cement; 44.0 and 100.1 are the molar weight ratios of CO_2 and $CaCO_3$ respectively; and $CaCO_3^{CC,sample}$ and $CaCO_3^{NC,sample}$ are the contents (g/100 g) of the CC and NC sample, respectively.

During the sample preparation (grinding), NC samples may be more naturally carbonated with atmospheric CO_2 than CC samples due to the higher content of unreacted CH available on NC samples. Besides, previous literature [29] suggested that nano-TiO_2 may promote the natural carbonation of ground mortars. Considering this, CO_2 uptake of pastes with nanoparticles, calculated based on the difference between $CaCO_3$ content of CC samples vs. NC samples, may be underestimated because of two reasons: (i) in NC samples, mixes with nanoparticles would present higher passive carbonation than mixes without nanoparticles during grinding and, (ii) intentionally carbonated with 20% CO_2 concentration or CO_2 cured (CC) samples of all mixes are expected to have less CH available to naturally carbonate with atmospheric CO_2 during grinding than non-actively carbonated with atmospheric CO_2 samples (NC) of the corresponding mixes.

Therefore, the CO_2 uptake calculated based on the difference between the $CaCO_3$ content of CC samples and NC samples of pastes may be slightly under-predicted due to the natural carbonation during sample preparation; since NC samples contain more CH available to be carbonated, the natural carbonation during sample preparation would affect NC samples to a higher degree than CC samples. Nonetheless, CO_2 capture results, obtained in this chapter, remain on the conservative side since the real CO_2 uptake would be higher, especially for samples with nano-TiO_2.

The CH reduction during CO_2 curing is defined as the difference between the CH content of the NC specimens and the CC samples of each mixture. It is well-known that part of the CO_2 uptake comes from the carbonation of the CH [184], [185], [197], [198]. Thus, the results of CH

reduction could relate the CO_2 uptake with the CH consumed during the CO_2 curing of each mixture. Eq. 6.7 estimates the CH content of each sample using a modification of the traditional or stepwise method [37]. That method corrects the presence of hydration products (e.g., C-S-H) in the CH decomposition area (400-500 °C) [37]. If this correction were not made, the CH content would be overestimated [37].

$$\mathrm{CH}\left(\frac{\mathrm{g}}{100\ \mathrm{g}}\right) = \frac{100}{\mathrm{M_c}} \cdot \frac{74.1}{18.0} \cdot \left[\left(\mathrm{M}^{\mathrm{CH}}_{\mathrm{start}} - \mathrm{S}^{\mathrm{CH}}_{\mathrm{start}}\left(\mathrm{T}^{\mathrm{CH}}_{\mathrm{inf}} - \mathrm{T}^{\mathrm{CH}}_{\mathrm{start}}\right)\right) - \left(\mathrm{M}^{\mathrm{CH}}_{\mathrm{end}} + \mathrm{S}^{\mathrm{CH}}_{\mathrm{end}}\left(\mathrm{T}^{\mathrm{CH}}_{\mathrm{end}} - \mathrm{T}^{\mathrm{CH}}_{\mathrm{inf}}\right)\right)\right] \qquad 6.7$$

Where CH is the content (g/100 g) of calcium hydroxide of anhydrous cement; 74.1 and 18.0 are the molar weight ratio of CH and H_2O, respectively; M_C is the initial mass (g) of the anhydrous cement in the sample; M^{CH}_{start} and M^{CH}_{end} are the masses (g) of the sample at the start and endpoint for CH decomposition, respectively; S^{CH}_{start} and S^{CH}_{end} are the slopes (%/°C) of the tangential lines of the start and endpoint for the CH; and T^{CH}_{start}, T^{CH}_{inf}, T^{CH}_{end} are the temperatures (°C) of the start point, the mass inflection point, the endpoint for the CH decomposition, respectively. Figure 6.2 shows a qualitative example of a TGA result, including first and second derivative and the modified CH calculation procedure.

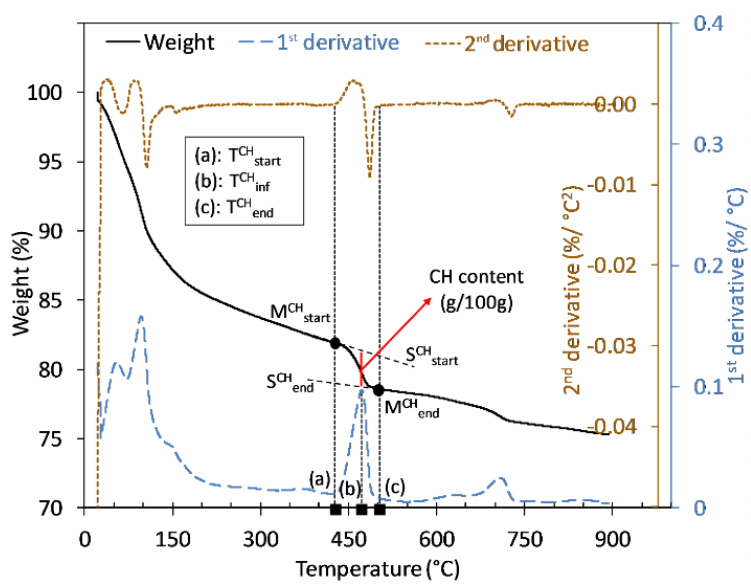

Figure 6.2. Modified method for the CH calculation.

Scanner Electro-Microscope (SEM)

SEM analysis was performed to evaluate microstructure changes during CO_2 curing with and without nanoparticles. Samples with 0% and 0.5% nano-TiO_2 were prepared to consider the effect of the nanoparticles. For each nano-TiO_2 percentage (0% and 0.5%), a CO_2 cured and a normal cured sample were prepared.

The sample preparation is defined as follows. First, the hydration of the samples was stopped using a solvent exchange procedure [37]. Then, after dry cutting a sample of each mixture using a saw, a vacuum epoxy impregnation method was applied to them. Then, samples were dried in an oven for eight hours at 70 °C. Later, samples were lapped and polished. Lapping was performed using Hillquist (Denver, Colorado, USA) mesh flat diamond laps (45, 30, and 15 μm). Next, polishing was carried out with Buehler (Lake Bluff, Illinois, USA) microclothes with different grit sizes (9 μm, 6 μm, 3 μm, 1 μm, and 1/4 μm), lubricated with diamond pastes. Finally, after applying a palladium sputter-coated on the top surface to prevent electrostatic charge accumulation, SEM analysis was performed using the ASPEX personal SEM, equipped with the energy dispersive x-ray (EDX) analyzer, at 15 keV of accelerated voltage.

Estimation of CO_2 emissions

Considering cement production produces around 8% of the global CO_2 emissions each year [4], decreasing the net CO_2 emissions would be a key factor in improving the environmental performance of cementitious materials. It is well-known that cementitious materials may sequestrate CO_2 during their service life [19]. Therefore, the potential CO_2 uptake of those materials should be included in the estimation of the net CO_2 emissions. To quantify these emissions, life cycle inventory data of cement production and nano-TiO_2 (Table 6.2) were obtained from the European Platform on Life Cycle Assessment (ELCD).

Table 6.2. Life inventory data used.

	Cement (kg)	nano-TiO_2 (kg)
Diesel	3.56E-02	2.91E-01
Gas	8.53E-03	6.82E-01
Soft coal	2.67E-02	7.60E-02
Hard coal	4.83E-02	8.19E-01
CO_2	8.85E-01	2.60E+00
CO	2.14E-03	4.47E-02
CH_4	5.80E-04	8.20E-04
C_2H_4	3.95E-10	8.61E-06
CFC-11	5.22E-09	2.71E-08
CFC-114	5.35E-09	2.78E-08
SO_x	1.05E-03	1.34E-04
NO_x	1.79E-03	1.10E-02
N_2O	2.22E-06	1.73E-04
NH_3	3.91E-02	3.71E-05
NMVOC	2.26E-01	6.98E-04
HCl	1.99E-02	1.05E-04
N (water)	1.16E-04	6.88E-05
PO_4^{-3} (groundwater)	5.14E-07	1.54E-04

Panesar et al. [123] showed that the CO_2 emissions associated with each mixture could be different depending on the functional unit used. Three functional units were used in this chapter to estimate the total CO_2 emissions:

- Functional unit 1 (FU1): Quantification of the total CO_2 emissions of each mixture per m^3 of cement paste.
- Functional unit 2 (FU2): Quantification of the total CO_2 emissions of each mixture per m^3 of cement paste with a given compressive strength.
- Functional unit 3 (FU3): Quantification of the total CO_2 emissions of each mixture per m^3 of cement paste with a given compressive strength and considering the CO_2 captured during the CO_2 curing process (from age 24 hours to 36 hours).

FU2 and FU3 use compressive strength as a factor to analyze CO_2 emissions. Thus, these functional units require to modify the binder content (cement + nano-TiO_2, if applicable) of the pastes to equalize the compressive strength of each mixture with the compressive strength of the cement paste with no nanoparticles (P0) and normal curing (NC). Note that the compressive strength of the paste P0-NC is considered as reference strength in this chapter. Besides, the compressive strength at early ages (48 hours) was chosen as a limiting factor. When the early strength is not a requirement, the results could be affected.

Samples with CO_2 curing and/or with nano-TiO_2 addition will present a different strength. Thus, it will be required to estimate the modification of binder content per m^3 of cement paste needed to achieve the reference strength. For example, if P0-CC presents a higher strength than the reference one (P0-NC), the amount of binder required to achieve the reference strength would be lower than the binder content of the reference mixture (P0-NC).

To estimate the variations of binder content required to achieve the reference strength, extra mixtures with normal curing and no nano-TiO_2 were prepared, based on the results of the range of strength observed for mixtures with CC and/or nano-TiO_2. The supplementary material contains a further explanation of the procedure and results of the estimations.

Table 6.3 summarizes the mixture proportions (fixing the total volume) per m^3 of cement paste of the two reference mixtures (cement paste with no nano-TiO_2). Then, using those compressive strength values of the reference mixtures (P0 with NC and water-to-cement ratios of 0.50 and 0.55), a calibration curve can be obtained to estimate the variation of compressive strength as a function of the binder content. The estimation procedure was:

- The compressive strength values of all studied mixtures are introduced in the calibration curve to estimate the binder content required to obtain the same compressive strength, in case the mixture used was the reference with no nanoparticles (P0).
- The difference (in percentage) between the initial binder content and the estimated binder content was obtained and subtracted from the initial binder content to calculate the binder content required to achieve the same compressive strength as P0-NC. Then, the binder content was split into cement and nano-TiO_2 content depending on the percentage of nanoparticles used (0%, 0.5%, 1%, and 2%).

Table 6.3. Mixture proportions per m^3 of reference cement pastes (no nano-TiO_2) used for the calibration curve.

Mixture	w/c	Cement (kg/m^3)	nano-TiO_2 (kg/m^3)	Water (kg/m^3)
P0 (0.50)	0.50	1223.3	0.0	611.7
P0 (0.55)	0.55	1152.8	0.0	634.0

6.3 Results and discussion

6.3.1 Compressive strength

Figure 6.3 displays the compressive strength results of normal curing (NC) and CO_2 curing (CC) samples. The shaded areas represent the dispersion of the results for all studied specimens. The homogeneity through the samples (dispersion between the two compressive strength values of the same sample) was also checked, being lower than 1.8 MPa for all the samples.

In NC samples, the use of nano-TiO_2 was beneficial in terms of compressive strength. The higher the nanoparticles percentage, the higher the compressive strength, as expected. Whereas adding 0.5% nano-TiO_2 in NC pastes produced an 8.4% increase in the compressive strength, 1% of nano-TiO_2 increased 15.3% the compressive strength of NC samples taking as reference the compressive strength of the NC paste without nano-TiO_2 (P0-NC). However, percentages higher than 1% of nano-TiO_2 (P2) did not produce important variations in compressive strength enhancement of NC samples compared to P1-NC.

In contrast, CC samples did not show the same trend. Samples with nano-TiO_2 showed higher compressive strength than samples without nano-TiO_2 for all studied percentages. Samples with 0.5% of TiO_2 nanoparticles presented the highest enhancement in terms of the compressive strength of CC pastes compared to the reference CO_2 cured mixture (P0-CC). The compressive strength of the CC samples with higher dosages of nanoparticles (1% and 2%) was lower than in P0.5-CC results.

A potential explanation for this variation of the optimum percentage of nanoparticles could be related to the porosity. It is known that the carbonation curing reduces the porosity since the $CaCO_3$ possesses a higher molar volume than other cement phases such as C-S-H or CH [182].

Previous research also showed that nano-TiO_2 densifies the microstructure of cementitious materials leading to improved compressive strength [43], [44], [47], [54].

Consequently, the higher the percentage of nano-TiO_2, the lower the initial porosity before the CO_2 curing process. This is relevant since the increase of compressive strength due to carbonation is related to reducing porosity. The lower the initial porosity before CO_2 curing, the lower the maximum potential improvement of compressive strength due to carbonation. Besides, a high porosity reduction at a very early age may stop the hydration due to a lack of space for the hydration products to grow [29], [199]. This may explain why the optimum percentage of nano-TiO_2 (in terms of compressive strength) is lower for CO_2 cured samples than for normal cured samples.

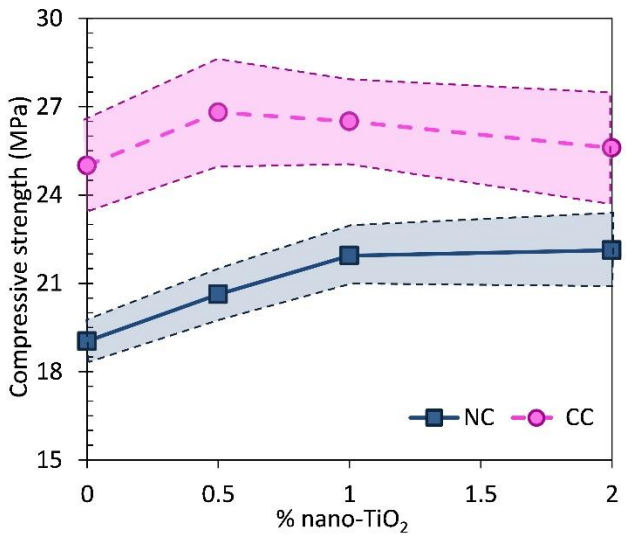

Figure 6.3. Compressive strength results for NC and CC samples.

6.3.2 X-ray diffraction results (XRD)

Figure 6.4 shows the XRD patterns of normal cured samples with the studied percentages of nano-TiO_2. The most prominent peaks present in those XRD patterns are related to the CH since, along with C-S-H, the CH is the main hydration product in hydrated cement pastes. Other cement phases as alite (C_3S), belite (C_2S), or ettringite were also present in XRD patterns of NC samples. XRD patterns suggest that the use of the nanoparticles produced an acceleration in the hydration of NC samples since the ettringite peaks, formed in the first hours of the hydration process, were more pronounced in samples with nano-TiO_2 than in the reference specimen (no nanoparticles).

The peak at a diffraction angle (°2θ) around 25 is also relevant since it refers to the presence of TiO_2 nanoparticles in those samples. XRD patterns for NC samples showed that the higher the nano-TiO_2 percentage, the higher the peak (Figure 6.4). This was also observed in the CC samples (Figure 6.5).

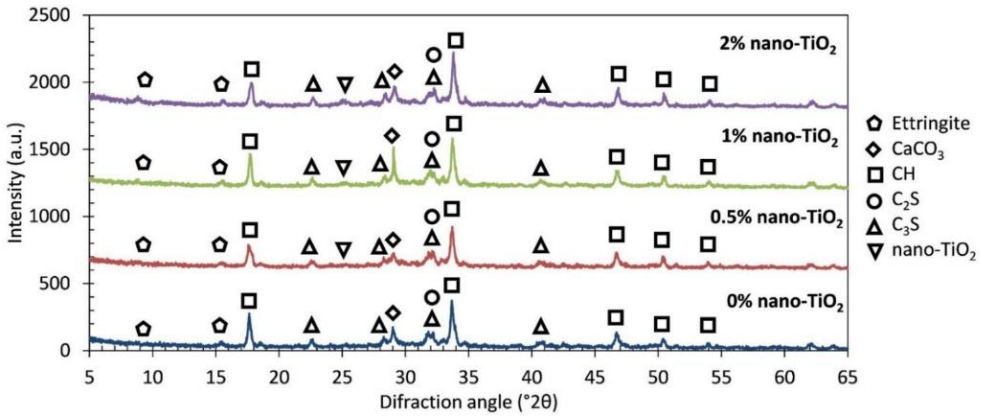

Figure 6.4. XRD pattern of mixtures with normal curing and with different percentages of nano-TiO_2 (0%, 0.5%, 1%, 2%).

Figure 6.5 exhibits the XRD patterns of the CO_2 cured samples with different percentages of nano-TiO_2. In contrast to the results of normal cured samples (Figure 6.4), most of the peaks in those XRD patterns are related to the $CaCO_3$ due to the carbonation process (Figure 6.5). Comparing the results of NC and CC samples, it is observed that the prominent peaks of CH in XRD of NC samples were remarkability decreased in the case of CC samples. It suggests an important degree of carbonation of CH during CO_2 curing. Besides, results showed that ettringite was carbonated during the CO_2 curing since XRD patterns of CC samples did not show any peaks related to ettringite. Results also suggest that the belite was carbonated during CO_2 curing producing $CaCO_3$ since the peak intensities of C_2S have decreased in the CC samples compared to the results of NC samples.

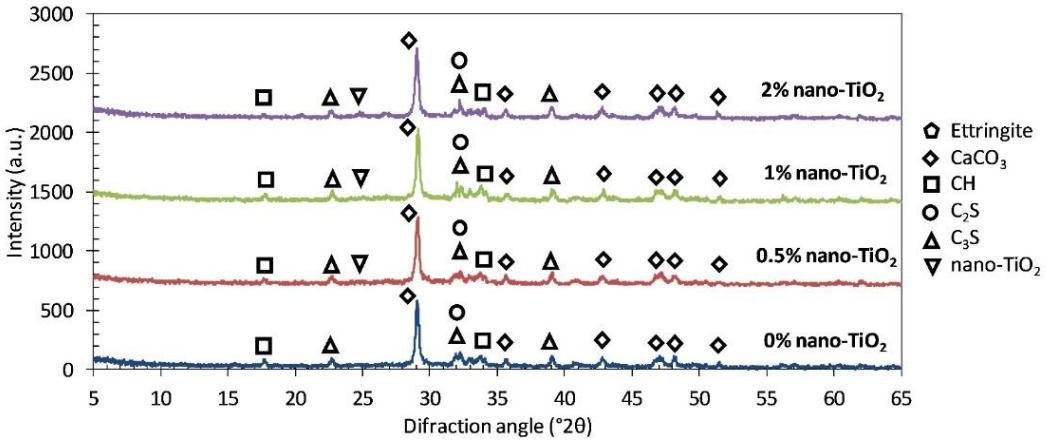

Figure 6.5. XRD pattern of mixtures with CO_2 curing and with different percentages of nano-TiO_2 (0%, 0.5%, 1%, 2%).

Table 6.4 lists the quantitative results from XRD patterns of all studied specimens. The results are displayed in percentages of solid phases, and they only include crystalline structures. In terms of NC samples, the alite (C_3S) percentage was lower in samples with nano-TiO_2 than the reference specimens (P0-NC). Even though fewer cement particles, and therefore fewer alite particles, were used in samples with nano-TiO_2 (due to the partial substitution of cement by nano-TiO_2), the differences in the alite content between samples with and without nano-TiO_2, calculated based on the XRD patterns, were higher than the variations in the mixture proportions. Therefore, this suggests the use of nano-TiO_2 produced an acceleration of the hydration since samples with nano-TiO_2 presented less anhydrate C_3S particles. The acceleration of the hydration was also exhibited with the ettringite percentage since the higher the nano-TiO_2 percentage, the higher the ettringite content in NC samples. Besides, the calcium hydroxide (CH) content was also increased in NC samples using nanoparticles (up to 1%) compared to P0-NC specimens.

In samples with CO_2 curing (CC samples), the use of nano-TiO_2 decreased the anhydrate C_3S content to a lower extent than NC specimens. It suggests that the acceleration of the hydration due to the nano-TiO_2 in CO_2 cured samples is lower than in normal cured samples. As a result, the percentage of anhydrate alite in CC samples was higher than in NC specimens. Besides, CC samples present a remarkably lower anhydrate belite content. These two observations suggest that the CO_2 curing process promoted the carbonation of belite to a greater extent than the carbonation of alite. This observation agrees with previous research showing that belite may be carbonated quicker than alite under the same conditions [200]. It is well-known that alite is consumed in the

first hours of hydration due to its high hydraulic reactivity. Therefore, the CO_2 curing (after 24 hours of hydration) may induce the carbonation of C_2S due to the higher availability of Ca^{2+} ions in comparison to C_3S (which was mostly consumed during the first 24 hours of hydration) [200]. Ibañez et al. [201] also found that the carbonation of belite produced higher carbonation depth than the carbonation of alite.

For CO_2 cured samples, the use of nano-TiO_2 increases the consumption of C_2S, especially in P1 and P2 specimens. This may suggest that the use of nanoparticles promotes the carbonation of belite during accelerated CO_2 curing. Besides, it is also noticeable that results suggest that the addition of nano-TiO_2 promoted carbonation since the higher the nano-TiO_2 percentage, the higher the $CaCO_3$ content.

Furthermore, the ettringite and portlandite content of all studied samples was highly reduced during the CO_2 curing. When nano-TiO_2 was used, the carbonation of ettringite increased. The ettringite content in CC samples with 0%, 0.5%, 1%, and 2% of nanoparticles was reduced a 52%, 70%, 61%, and 83%, respectively, compared to the NC samples with the same percentage of nano-TiO_2.

Table 6.4. Quantitative phase analysis results from XRD patterns for all studied mixtures.

Mixtures		**Phase content (%)**							
		C_3S	**C_2S**	**C_3A**	**C_4AF**	**Ettringite**	**CH**	**$CaCO_3$**	**Minor phases**
Normal curing	**P0-NC**	14.25	15.34	3.59	7.96	13.09	26.46	18.46	0.85
	P0.5-NC	10.46	15.10	3.31	7.74	13.69	28.01	18.84	2.88
	P1-NC	10.65	16.57	3.90	5.95	14.99	29.97	13.88	4.09
	P2-NC	8.76	16.30	4.35	4.31	15.55	27.87	17.14	5.67
CO_2 curing	**P0-CC**	14.53	7.37	4.69	8.77	6.29	3.64	52.93	1.77
	P0.5-CC	12.82	7.70	4.11	9.00	4.10	5.52	54.27	2.49
	P1-CC	11.49	3.71	5.84	8.58	5.87	4.49	56.36	3.67
	P2-CC	13.96	2.33	4.00	10.70	2.64	1.10	61.03	4.25

6.3.3 CH consumption and CO_2 uptake due to CO_2 curing

Figure 6.6 exhibits the TGA curves for normal, and CO_2 cured samples of each studied nano-TiO_2 level (0%, 0.5%, 1%, 2%). Results showed that the higher the nano-TiO_2 dosage, the lower the CH content and the higher the $CaCO_3$ content after the CO_2 curing. These data were analyzed following the procedure described in the Methods section, using the first and second derivatives.

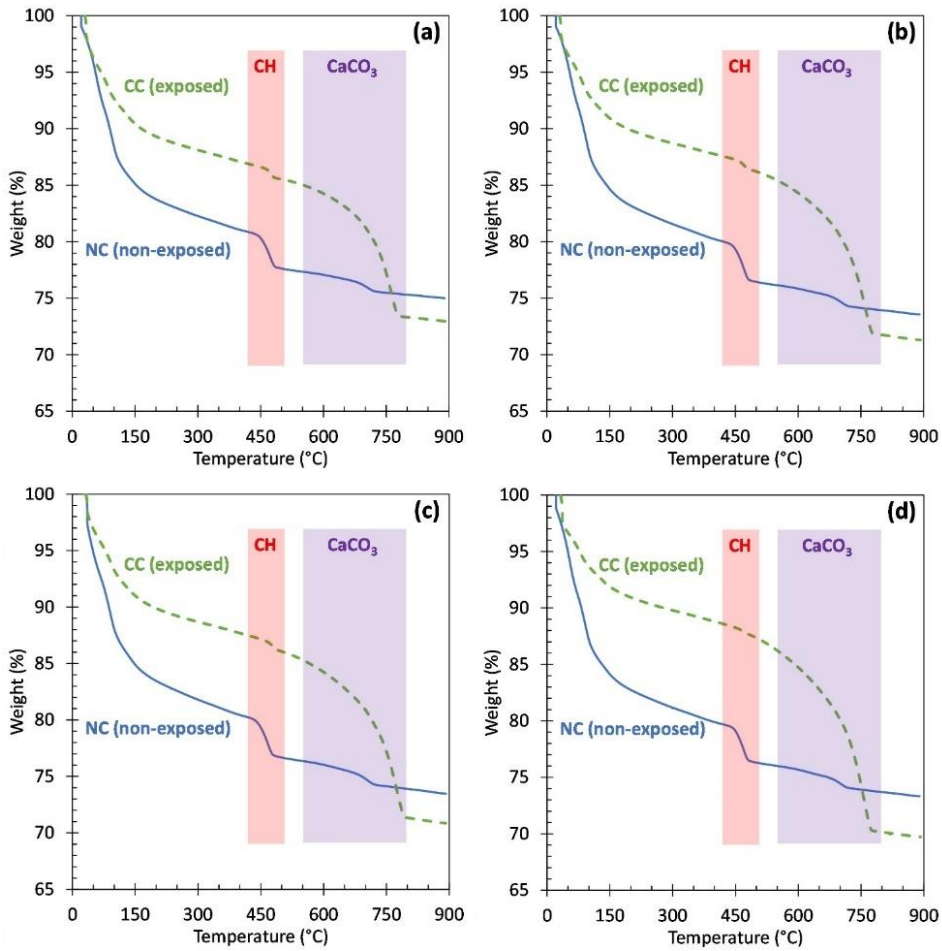

Figure 6.6. TGA curves for normal and CO_2 cured samples. (a) 0% nano-TiO_2. (b) 0.5% nano-TiO_2. (c) 1% nano-TiO_2. (d) 2% nano-TiO_2

Figure 6.7 presents the CH consumption and CO_2 uptake during 12-hour CO_2 curing for all studied mixtures quantified based on TGA results. Results showed that the higher the nano-TiO_2 percentage, the higher the CO_2 uptake. The use of 0.5%, 1%, and 2% of nanoparticles increased 18.5%, 20.5%, and 38.4%, respectively, the CO_2 uptake in comparison to the reference paste (no

nano-TiO_2). A potential explanation is that the TiO_2 nanoparticles increase the CH reactivity due to the reduction of its size, thus increasing its specific surface area without decreasing the total CH amount [29], [44], [47]. CH consumption results agreed with CO_2 uptake results, as shown in Figure 6.7.

The carbonation process produces a reduction of porosity, thus a potential increase of strength. However, even though P2 produced a higher CO_2 uptake than P1, the difference between their compressive strength values (Figure 6.3) was negligible. High dosages of nano-TiO_2 may reduce the beneficial effects of the nanoparticles because it may cause a lack of space available for the hydration products to grow, and this lack of space may produce the hydration process to stop [29], [199]. Consequently, an excess in the nanoparticles' percentage could jeopardize their beneficial effects in the microstructure and thus the compressive strength.

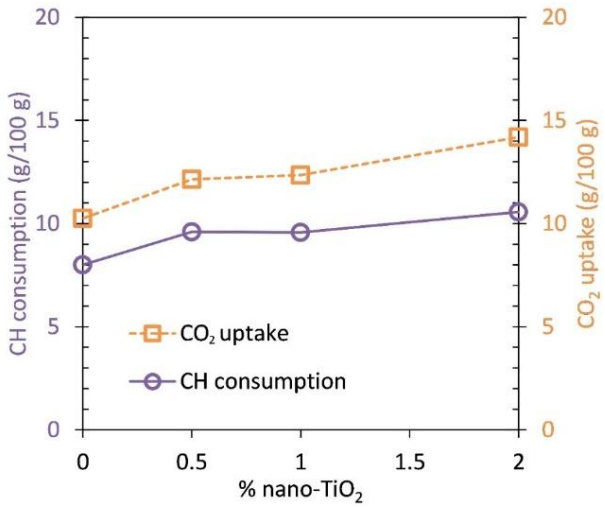

Figure 6.7. CH consumption and CO_2 uptake of all studied mixtures quantified using TGA.

6.3.4 Microstructure (SEM)

Figure 6.8 shows the SEM images for the studied samples. These images exhibit the effect of CO_2 curing in the microstructure of samples without TiO_2 nanoparticles (Figure 6.8.a and c) and with 0.5% nano-TiO_2 addition (Figure 6.8.b and d). As expected, the CO_2 curing produced densification of the microstructure in both 0% and 0.5% nano-TiO_2 mixtures due to calcium carbonate formation, with higher molar volume than calcium hydroxide. This densification and refinement of the microstructure could be the reason behind the enhancement of compressive strength in CO_2 cured samples (Figure 6.3).

Moreover, the greater the densification during CO_2 exposure, the higher the CO_2 uptake. Samples with nano-TiO_2 showed more significant densification of the microstructure due to CO_2 curing (Figure 6.b and 6.d) than samples without nano-TiO_2 (Figure 6.a and 6.c). This suggests that 0.5% nano-TiO_2 addition increased the CO_2 sequestration during the CO_2 curing. This agrees with TGA results (Figure 6.7).

In samples with no nano-TiO_2, the CO_2 curing process did not produce considerable differences in terms of anhydrate cement particles. In contrast, the sample with 0.5% of nanoparticles and CO_2 curing exhibited significantly less presence of anhydrate cement particles than the specimen with the same percentage of nanoparticles and normal curing. It suggests that the use of nano-TiO_2 promotes the reaction of anhydrate cement particles during CO_2 curing.

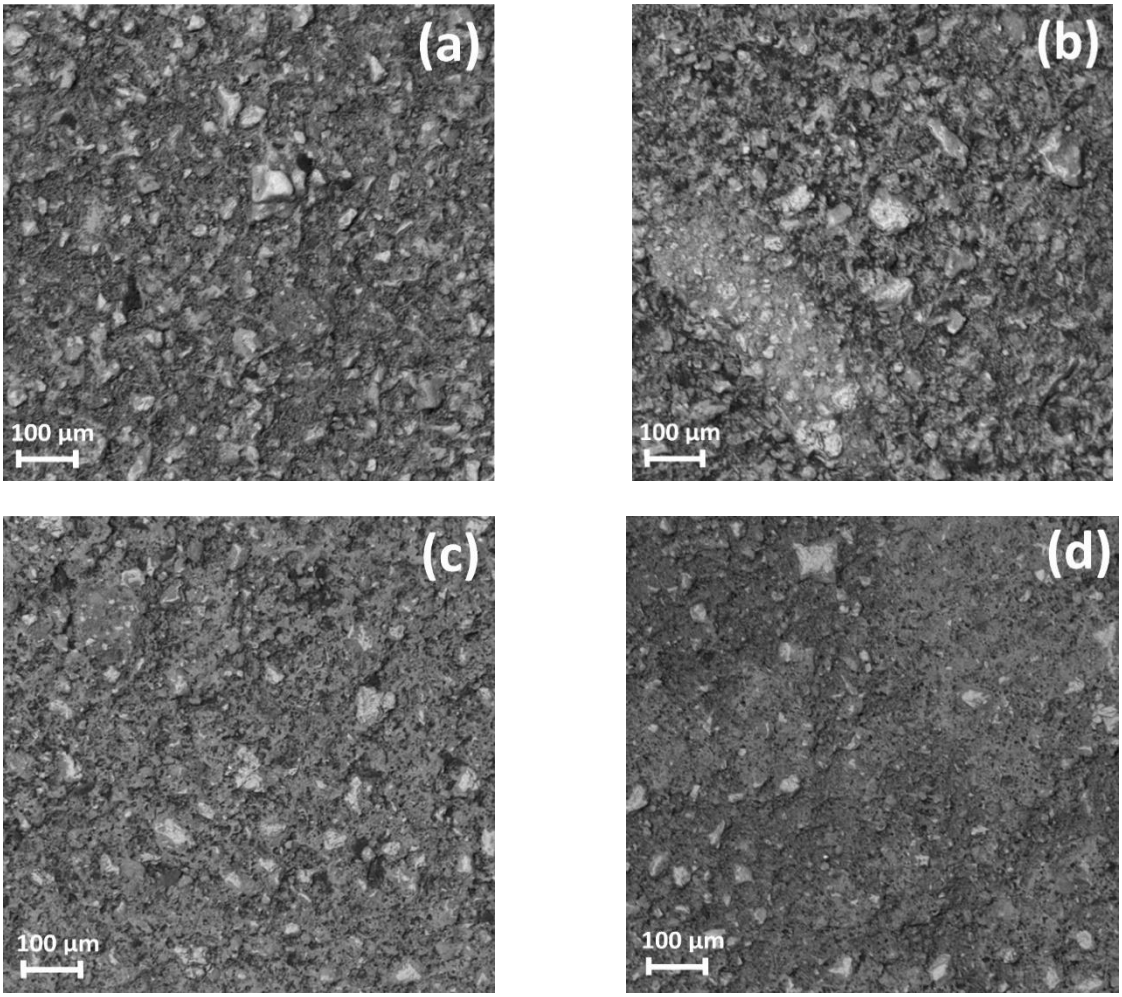

Figure 6.8. SEM images of the studied samples. (a) P0 NC. (b) P0.5 NC. (c) P0 CC. (d) P0.5 CC.

6.3.5 Estimation of CO_2 emissions

Figure 6.9 displays the variation of compressive strength of NC paste with no nano-TiO_2 as a function of binder content per m^3. Each compressive strength value of all studied mixtures correlates with an estimated binder content; in case the paste was made with no nanoparticles and NC. A predicted required binder content for each mixture can be obtained using the difference between the estimated content and the initial content. Then, the predicted required binder content was divided into cement and nano-TiO_2 content, if applicable.

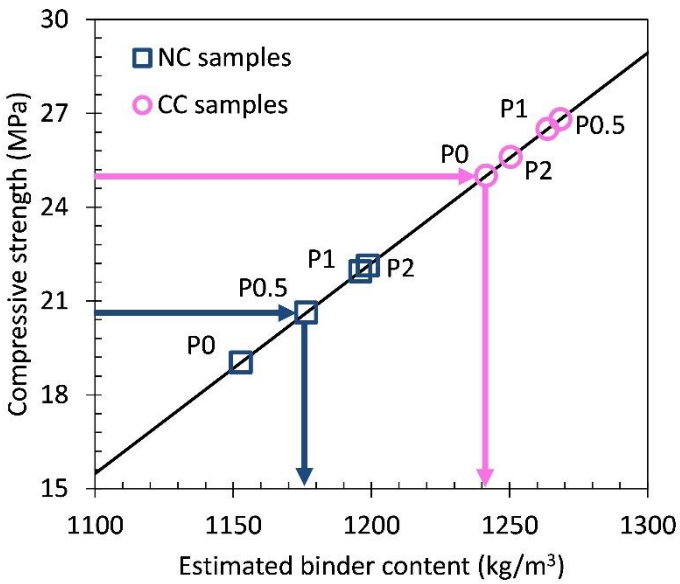

Figure 6.9. Compressive strength as a function of the estimated binder content of the reference mixture (P0-NC).

Table 6.5 lists the results of the estimation of binder content to achieve the same compressive strength as P0-NC for all studied mixtures, considering the effect of nano-TiO_2 addition and/or type of curing (NC or CC). The CO_2 emissions are calculated using LCI data from Table 6.2.

Table 6.5. Binder content required to have the same compressive strength as P0-NC.

Mixture	Compressive strength (MPa)	Initial binder content (kg/m^3) [*Cement - nano-TiO_2*]	Predicted required binder content (kg/m^3) [*Cement - nano-TiO_2*]
P0-NC	19.03	1152.8 [*1152.8-0.0*]	1152.8 [*1152.8-0.0*]
P0.5-NC	20.62	1152.8 [*1147.0-5.8*]	1129.6 [*1124.0-5.6*]
P1-NC	21.94	1152.8 [*1141.3-11.5*]	1111.1 [*1100.0-11.1*]
P2-NC	22.13	1152.8 [*1129.7-23.1*]	1108.5 [*1086.4-22.2*]
P0-CC	25.00	1152.8 [*1152.8-0.0*]	1070.4 [1070.4-*0.0*]
P0.5-CC	26.81	1152.8 [*1147.0-5.8*]	1047.7 [*1042.4-5.2*]
P1-CC	26.50	1152.8 [*1141.3-11.5*]	1051.5 [*1041.0-10.5*]
P2-CC	25.60	1152.8 [*1129.7-23.1*]	1062.7 [*1041.5-21.3*]

FU1 results (Volume)

Figure 6.10 summarizes the net CO_2 emissions of mixtures with all studied percentages of nano-TiO_2 depending on the functional unit used in the analysis. Since neither the compressive strength nor the CO_2 capture were included in FU1, NC and CC samples possessed the same net CO_2 emissions using this functional unit. FU1 results exhibited that the higher the nano-TiO_2 percentage, the higher the net CO_2 emissions since the TiO_2 nanoparticles production is more harmful in terms of CO_2 emissions than the cement production. The net CO_2 emissions increased by 1%, 2%, and 4% with the addition of 0.5%, 1%, and 2% of nano-TiO_2, respectively, when FU1 was used. Therefore, results suggest that the nanoparticles negatively affected net CO_2 emissions when only the volume was included in the functional unit (FU1).

FU2 results (Volume + Compressive strength)

In contrast, results showed different trends when the compressive strength value was added to the functional unit (FU2). In NC samples, the use of nanoparticles reduced the net CO_2 emissions compared to P0 when the compressive strength was considered (FU2). In those specimens, the optimum value in terms of net CO_2 emissions was 1% of nano-TiO_2. A higher amount of nanoparticles (2%) could not overcome the high CO_2 emissions of the nanoparticles production since the compressive strength values of P1-NC and P2-NC were almost the same.

When FU2 was used, CC samples results were different from NC samples results since CO_2 curing increased the compressive strength of samples compared to NC results. Samples with CO_2 curing (CC samples) possessed a lower optimum percentage of nanoparticles than NC samples in terms of net CO_2 emissions with FU2 since the use of nano-TiO_2 produced a higher increase in compressive strength (in comparison to 0% nano-TiO_2 mixtures) in NC samples than in CC samples. Using 0.5% nano-TiO_2 produced the lowest net CO_2 emissions (1.2% reduction compared to P0-CC) of the CC samples using FU2. However, higher amounts of nanoparticles (1% and 2%) increased the net CO_2 emissions obtained with the same functional unit (FU2) in comparison to the P0.5-CC value. Indeed, the P2-CC sample generated 3.2% higher CO_2 emissions than the CC paste with no nano-TiO_2 when FU2 was used.

FU3 results (Volume + Compressive strength + CO_2 uptake)

Finally, FU3 also includes the CO_2 capture of each sample during a 12-hour CO_2 curing process. Considering the definition of the CO_2 capture, FU2 and FU3 results for NC samples were the same since, in this chapter, the CO_2 capture was only estimated during the CO_2 curing.

All CC samples decreased their net CO_2 emissions with FU3 compared to the corresponding FU2 results, especially the samples with TiO_2 nanoparticles that showed a higher decrease of the estimated net CO_2 emissions when FU3 is used.

The optimum dosage of nanoparticles in terms of net CO_2 emissions was 0.5% for CC conditions, considering FU3. The combination of using 12-hour CO_2 curing and the use of 0.5% nano-TiO_2 (P0.5-CC) produced a decrease in the net CO_2 emissions of 20.4% compared to the reference mixture without nano-TiO_2 and normal curing (P0-NC). The CO_2 curing reduced the net CO_2 emissions a 17.7% for the reference mixture (comparison between P0-NC vs. P0-CC). The use of 0.5% nano-TiO_2 produced an additional reduction of 2.7% on the CO_2 emissions. This reduction of the net CO_2 emissions due to the combined use of nano-TiO_2 and CO_2 curing might be even greater than the estimated using FU3 if the functional unit considered their effect on a potential increase in durability (due to reduction of both porosity and CH content).

Figure 6.10 suggests that the use of nanoparticles is beneficial in terms of net CO_2 emissions considering their positive effects (enhancement of compressive strength and promotion of CO_2 uptake). When the compressive strength and the CO_2 capture are included in the functional

unit (FU3), the estimated net CO_2 emissions decreased an 17.7%, 21.2%, 20.9%, and 21.5% for P0, P0.5, P1, and P2 pastes, respectively, in comparison to the corresponding results of each paste using FU1. Thus, not considering the effect of nano-TiO_2 on both compressive strength and CO_2 uptake may lead to an overestimation of the net CO_2 emissions of cement pastes containing nano-TiO_2.

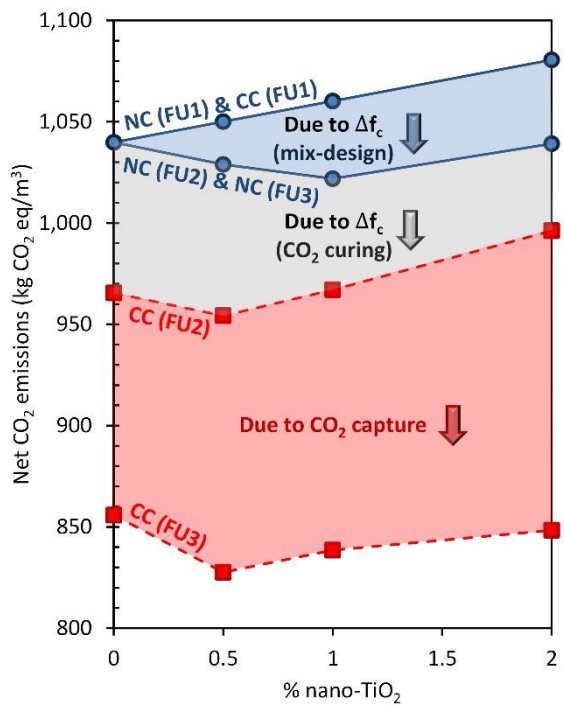

Figure 6.10. Net CO_2 emissions of studied cement pastes, depending on the functional unit used. [Δf_c: variation of compressive strength].

This chapter was focused on studying the effect of nano-TiO_2 on the cement paste's ability to sequestrate CO_2 during a CO_2 curing process. Since cement paste is the matrix of cementitious materials such as mortars and concretes, the findings of this chapter are also important for those materials. However, the addition of aggregates, the scale, and the specific surface of each concrete element to be cured would change the CO_2 diffusion and the nano-TiO_2 addition effect on the overall performance of the composite in terms of net CO_2 emissions.

The present chapter states a first step that indicates a new path towards designing more sustainable concrete elements. The effects and factors that affect the impact of nanoparticles on the CO_2 carbonation of concrete elements should be studied and quantified in future investigations.

In general, the intended applications would be concretes without steel reinforcement, mortars, and plasters. Nonetheless, CO_2 curing may also apply to precast cementitious composites with steel reinforcements [196]. Indeed, the carbonation process may potentially promote the corrosion of the steel bars due to the reduction of the PH. However, curing cementitious composites with CO_2 reduces the porosity of the material. This porosity reduction will decrease water penetration and the easiness of chloride-based salts and other sulfates to penetrate the material, increasing the protection of steel reinforcement against corrosion. In addition, the porosity reduction also increases the strength. This strength enhancement will decrease the risk of cracks and, therefore, the ingress of salts and water or, in other words, the corrosion risk.

6.4 Conclusions

The optimum percentage of nano-TiO_2 in terms of compressive strength depends on the curing process (normal curing vs. CO_2 curing). CO_2 cured samples showed a lower optimum percentage of nano-TiO_2 than samples cured under normal conditions in terms of compressive strength. The initial reduction of the porosity produced by the nano-TiO_2 addition could be the reason behind that. The lower the initial porosity before CO_2 curing, the lower the maximum potential improvement of compressive strength due to carbonation. Besides, a high reduction of porosity at a very early age may stop the hydration due to a lack of space for the hydration products to grow. It may explain the changes in the optimum percentage, in terms of compressive strength, produced by the nano-TiO_2 addition for different curing types.

In terms of CO_2 capture, the higher the nano-TiO_2 dosage, the higher the CO_2 uptake during the CO_2 curing due to the increase of the CH reactivity produced by the TiO_2 nanoparticles. Thus, the use of nano-TiO_2 may increase the early CO_2 uptake of cementitious composites cured with CO_2.

Considering both positive effects of the TiO_2 nanoparticles (enhancement of compressive strength and promotion of CO_2 uptake during CO_2 curing), their use decreases their net CO_2 emissions of cementitious materials compared to samples with no nano-TiO_2. For instance, combining 0.5% nano-TiO_2 addition and CO_2 curing reduces net CO_2 emissions of over 20% in a cement paste with a 0.55 w/c. Otherwise, the net CO_2 emissions could be overestimated since the functional unit would not comprise the nano-TiO_2 effect on cementitious materials properties.

7. MODIFICATION OF SELF-CLEANING ACTIVITY ON CEMENT PASTES DUE TO CO_2 CURING

Part of this work has been submitted for publication as:

C. Moro, V. Francioso, M. Lopez-Arias and M. Velay-Lizancos. *'Modification of self-cleaning activity on cement pastes containing nano-TiO_2 due to CO_2 curing.'* Construction and Building Materials. (Submitted).

7.1 Introduction

Titanium dioxide is a well-known catalyst used for air purification and self-cleaning [14], [39], [40], [202]. The addition of titanium dioxide nanoparticles (nano-TiO_2) to cementitious materials produces a photoactive material with two bands, valence band (with electrons) and conduction band (without them) [203]. The exposure of cementitious composites containing nano-TiO_2 to light, with wavelengths shorter than 415 nm (which corresponds to nano-TiO_2 band gap) [204], may induce an electron promotion from the valence band to the conduction band, leaving a hole on it. These holes can interact with hydroxide ions and produce hydroxyl radicals (OH^-). Conversely, electrons can react with molecular oxygen and form superoxide radical-anion (O_2^-). These components have some beneficial properties, such as degrading some microorganisms [205], [206].

The photocatalytic effect can be divided into two different steps: (i) depollution and (ii) self-cleaning. Depollution is defined as the ability to remove toxic gases (e.g., NO_x, SO_x, VOC_s) from the air [207]. Self-cleaning refers to the ability to eliminate pollutants from the material without the use of manual work [207].

A large and growing body of literature has investigated the influence of nano-TiO_2 addition on the self-cleaning performance of cementitious materials [59], [61], [112], [208]–[215]. The percentage of nano-TiO_2 addition positively influences the effectiveness since the higher the amount of nano-TiO_2, the higher the self-cleaning activity of the material [59], [61], [112], [209]–[214]. Nonetheless, the exposed area of the material could be a key factor regardless of the amount of nano-TiO_2 used. For example, coatings may produce higher degradation of pollutants than mortars with nanoparticles despite having a lower total amount of nanoparticles by volume [210],

[215]. In addition, a rough surface increases the efficacy due to its higher surface area [208]. Previous researchers also observed that samples exposed to accelerated durability tests showed lower self-cleaning activity than the non-exposed specimens [216], [217]. Even though the effectiveness is reduced over time [218], cementitious materials modified with nano-TiO_2 can be effectively reused several times with or without a cleaning process [213], [218].

Apart from its widely known effect on self-cleaning, recent studies showed that nano-TiO_2 might promote the CO_2 uptake of hardened cementitious materials [29], [195]. While one of our previous studies [29] evidenced that using 0.5% of nano-TiO_2 increased the carbonation of mortars during the grinding process, in another study, we have [195] observed that nano-TiO_2 addition might accelerate the CO_2 capture of hardened cement pastes. Previous literature has studied the potential applicability of carbonation technology (CO_2 curing) in conventional cementitious materials [19], [22], [165], [166]. The active or accelerated carbonation of cementitious composites is nowadays a subject undergoing intense study thanks to its promising results in terms of strength, microstructure, sustainability, and durability improvements [25], [164], [167], [171], [172], [174], [175], [186]–[189], [192].

When cementitious composites are exposed to CO_2 at early ages, the CO_2 may react with their cement hydration products [e.g., calcium hydroxide (CH or $Ca(OH)_2$) or calcium silica hydrate (C-S-H or $(CaO)_x \cdot (SiO_2)_y \cdot (H_2O)_z$)] and/or anhydrous cement phases [e.g., alite, C_3S or $3(CaO) \cdot SiO_2$, and belite, C_2S or $2(CaO) \cdot SiO_2$] to produce calcium carbonate ($CaCO_3$), among other compounds [164], [185]. It is well known that the carbonation process promotes the reduction of porosity [167], [175], [186], [187] since the molar volume of the $CaCO_3$ is higher than the molar volume of CH or C-S-H phases, among others [182]. The porosity reduction improves the microstructure [164], [172]. Besides increasing the CO_2 capture and enhancing the microstructure of the cementitious composites, the CO_2 curing may improve other cementitious materials properties (e.g., compressive strength or durability) [26], [170]–[172]. Several studies reported an improvement in compressive strength in samples with CO_2 curing compared to specimens with conventional curing [25], [167], [174], [175], [188], [189]. There are different potential explanations for this effect. Some studies claimed that the CO_2 curing could produce a rapid cement dissolution [190], [191]; others linked the strength improvement with the enhancement of the microstructure [167], [175]. Cementitious materials' durability is also

enhanced, principally due to the improvement of the microstructure [171], [172], [193]. Therefore, the denser microstructure after the CO_2 curing could prevent the ingress of chlorides or sulfates [171], [172].

Furthermore, a recent study has analyzed the influence of nano-TiO_2 on the CO_2 capture in cement pastes during CO_2 curing [219]. The study showed that the use of nano-TiO_2 might increase the CO_2 uptake during CO_2 curing while increasing the material's strength [219]. Both effects (higher CO_2 uptake and strength improvement) could enhance the microstructure made by the nanoparticles [219]. On the other hand, cement pastes' microstructure changes may affect the material's self-cleaning activity [220]–[222]. However, to the best of the authors' knowledge, no investigations have studied the effect of CO_2 curing on the self-cleaning activity of cementitious materials containing nano-TiO_2. Therefore, the main objective of this chapter is to analyze and understand how CO_2 curing may modify the self-cleaning activity of cementitious composites and the link between these potential modifications with changes in the cement paste's microstructure. Furthermore, understanding how CO_2 curing may affect the photocatalytic activity will be critical to assess the sustainability of these two approaches combined (curing with CO_2 at early ages and providing self-cleaning ability).

Finally, the use of supplementary cementitious materials (SCM) such as slag as partial replacement of cement is also one of the main approaches to enhance the sustainability of cementitious composites [223]–[225]. Previous studies showed that the addition of slag might increase the CO_2 uptake of cementitious materials during CO_2 curing [226], [227]. Thus, besides plain cement paste containing nano-TiO_2, this chapter also analyzes the effect of slag addition on the self-cleaning activity before and after CO_2 curing. The aim is to analyze the combination of different sustainable approaches (e.g., the addition of SCM, the use of CO_2 curing, or nanoparticles addition). Studying the interaction of those approaches may be critical to find synergies that enable us to move towards more sustainable construction.

7.2 Materials and methods

7.2.1 Materials

The material characterization of the ordinary Portland cement, slag cement, and nano-TiO_2 used in this chapter is exhibited in *Chapter 2: Materials and general procedures*.

A total of 8 different cement pastes, with water-to-binder ratio of 0.55, were prepared with four different percentages of nano-TiO_2 (0%, 0.5%, 1%, 2%) and two slag cement content; 0% (i.e., 100% OPC), and 30% (i.e., with a substitution of 30% OPC by slag). Both percentages of nano-TiO_2 and % of slag are calculated based on the total weight of the binder. Table 7.1 lists the mixture proportions of each cement paste.

Table 7.1. Mixture proportions of cement paste mixtures.

Mixture	OPC (g)	Slag cement (g)	nano-TiO_2 (g)	w/b
P0-R	1874.8	0.0	0.0	0.55
P0.5-R	1865.4	0.0	9.4	0.55
P1-R	1856.0	0.0	18.7	0.55
P2-R	1837.3	0.0	37.5	0.55
P0-S	1312.4	562.4	0.0	0.55
P0.5-S	1303.0	562.4	9.4	0.55
P1-S	1293.6	562.4	18.7	0.55
P2-S	1274.9	562.4	37.5	0.55

7.2.2 Methods

Self-cleaning activity test

A total of 8 samples with 80 x 80 x 10 mm dimensions were cast for each mixture to perform the self-cleaning activity test. Four samples of each mixture were cured in normal conditions, while the other four samples of each mixture were CO_2 cured. All samples were demolded after 12 hours and left for 12 more hours in an environmental chamber with T = 23°C and RH = 50%. After that, the CO_2 cured samples (named CC samples) were moved to a CO_2 chamber with 20% CO_2 concentration and T = 23°C for 12 hours. The other four samples of each mixture, named as normal cured (NC) samples, were placed in an environmental chamber with T

= 23°C and RH > 90%. CC samples were moved to the same environmental chamber after the 12 hours of carbonation. All samples were left in the environmental chamber (T = 23°C and RH > 90%) for 6.5 days more. Then, the samples were removed from the environmental chamber and air-cured (T = 23°C and RH = 50%) for seven days. Figure 7.1 presents the curing procedure of these samples along with the curing procedure of cubic samples of selected mixtures used for further analysis.

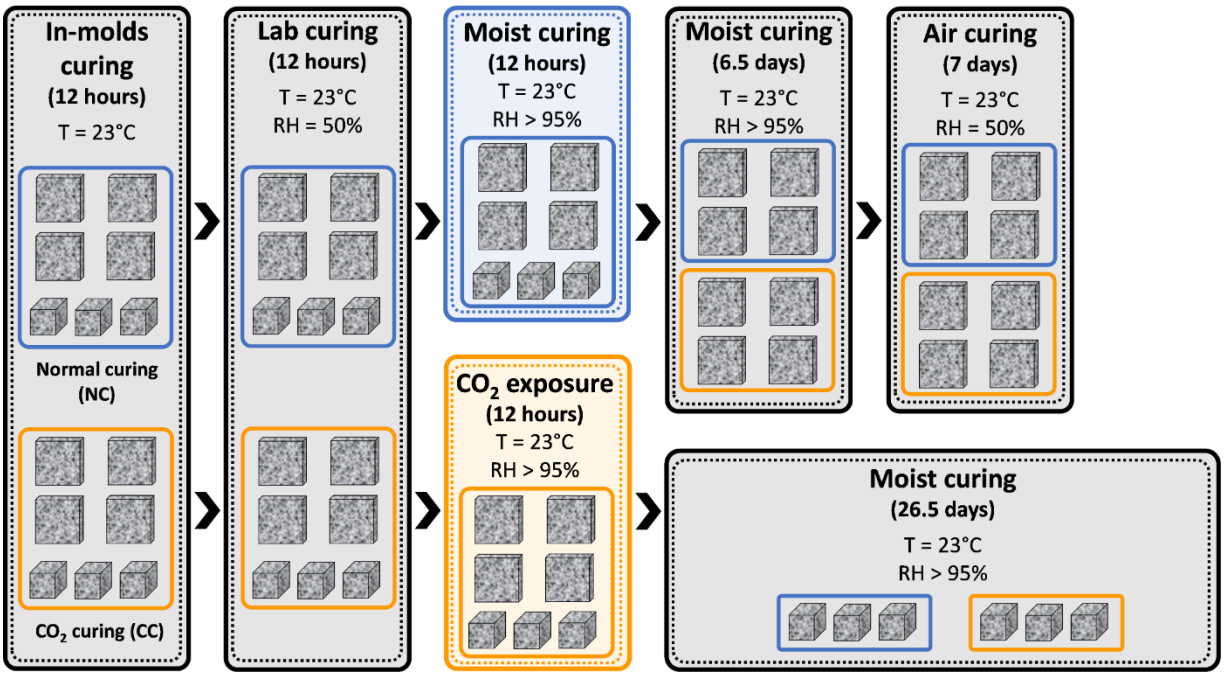

Figure 7.1. Curing procedure diagram.

The changes in the self-cleaning activity of the samples were evaluated based on the Rhodamine B (RhB) degradation under ultraviolet (UV) light. Cement pastes were sprayed with an RhB solution with a concentration of 0.1 ± 0.01 g/l on the top surface of the samples. The specimens remained 24 hours in a dark environment to allow them to dry. The color was then measured using a Ci62 portable spectrophotometer (X-Rite, Grand Rapids, MI). After that, samples were exposed to a UV lamp WTC 36L-110 with an irradiance of 0.28 mW/cm^2 and a wavelength of 368 nm. In some standards, such as UNI 11259 [228], the self-cleaning activity is only measured at certain exposure times (e.g., 4 hours and 24 hours). In this investigation, the color was measured at different exposure times (0 h, 0.5 h, 1 h, 2 h, 3 h, 4 h, 5 h, 6 h, 7 h, 8 h, 24 h) for all samples to study the color degradation over time. Four samples of each mixture were used in

the self-cleaning test. For each sample, four points were employed to measure the color variation. A total of 16 color measurements were obtained per mixture and UV exposure time. The higher the overall color variation (ΔE), the higher the self-cleaning activity of the material.

Color measurements were processed using CIELab (Commission Internationale de l'Éclairage) color space. This space comprises three color coordinates: L* (measuring brightness or, in other words, hues from black to white), a* (measuring hues from red to green), and b* (measuring hues from yellow to blue). The overall color variation (ΔE) was calculated using those color coordinates in Eq. 7.1.

$$\Delta E = \sqrt{(L_t^* - L_0^*)^2 + (a_t^* - a_0^*)^2 + (b_t^* - b_0^*)^2} \qquad 7.1$$

Where: L_t^*, a_t^*, b_t^* = parameters of the color coordinates after the umpteenth hour of UV light exposure; L_0^*, a_0^*, b_0^* = parameters of the color coordinates before the UV light exposure.

Besides, additional self-cleaning activity tests were performed for selected mixtures according to the standard UNI 11259 [228].

Thermogravimetric analysis (TGA)

After the self-cleaning test, samples of the reference mixtures (P0-R and P0-S) and mixtures with higher self-cleaning activity observed (P2-R and P2-S) were used for TGA and XRD analysis. These samples were employed to further investigate the synergistic effects of nano-TiO_2, slag cement, and CO_2 curing. TGA was conducted using the parameters explained in *Chapter 2: Materials and general procedures*.

TGA results were also used to estimate the CO_2 uptake during the CO_2 curing. The CO_2 uptake can be calculated with the difference between the calcium carbonate ($CaCO_3$) content of the CO_2 cured sample (CC) and the normal cured sample (NC). While Eq. 7.2 shows how to calculate the $CaCO_3$ content, Eq. 7.3 displays how to obtain the CO_2 capture based on the $CaCO_3$ content difference.

$$CaCO_3\ (g/100\ g) = 100 \cdot \frac{100.1}{44.0} \cdot \frac{1}{M_c} \cdot \left[\left(M_{start}^{CaCO_3}\right) - \left(M_{end}^{CaCO_3}\right)\right] \qquad 7.2$$

Where $CaCO_3$ is the calcium carbonate content (in g/100 g); 100.1 and 44.0 are the molar mass of $CaCO_3$ and CO_2, respectively; M_C is the initial mass of the sample (in g); and $M_{start}^{CaCO_3}$ and $M_{end}^{CaCO_3}$ are the masses (in g) of the sample at the start and endpoint for $CaCO_3$ decomposition, respectively.

$$\mathrm{CO_2\ uptake\ (g/100\ g)} = \left[\left(\mathrm{CaCO_3^{CC,sample}}\right) - \left(\mathrm{CaCO_3^{NC,sample}}\right)\right] \cdot \frac{44.0}{100.1} \qquad 7.3$$

Where *CO_2 uptake* is the absorbed carbon dioxide content in (g/100 g); $CaCO_3^{CC,sample}$ and $CaCO_3^{NC,sample}$ are the $CaCO_3$ contents (in g/100 g) of the CO_2 and normal cured samples, respectively; and 44.0 and 100.1 are the molar mass of CO_2 and $CaCO_3$ respectively.

X- Ray powder diffraction (XRD)

Powder samples were prepared and employed for X-Ray powder diffraction (XRD) using the same thermogravimetric analysis sample preparation. The parameters of the test are specified in *Chapter 2: Materials and general procedures*.

Density in oven-dry condition

Density and macroporosity examination were conducted in selected mixtures to analyze the effect of slag and CO_2 curing in terms of overall porosity reduction, respectively. For these analyses, reference mixtures (P0-R and P0-S) and the specimens with the highest self-cleaning activity observed (P2-R and P2-S) were selected. Six cubic samples of each selected mixture were cast to obtain the density in oven-dry conditions after 28 days. Figure 7.1 shows the curing timeline of both CC and NC cubic samples. Cubic samples had dimension of 50.8 x 50.8 x 50.8 mm (2 x 2 x 2 in). All the studied specimens were first placed in an oven at 105 °C for at least two days or until their weight was constant. Then, the weight was measured, and the density was obtained using Eq. 7.4.

$$\rho_d = \frac{M_d}{V} \qquad 7.4$$

Where: ρ_d = density in oven-dry condition (in kg/m^3); M_d = oven-dry mass (in kg); V = volume of the samples (in m^3).

Macroporosity examination using image analysis

The cubic samples were also employed for macroporosity examination using 2D cross-sectional images. First, 50.8 x 50.8 x 50.8 mm samples were cut in half using an IsoMet Low-Speed precision cutter (Buehler, Lake Bluff, IL). Then, a 48-megapixel camera was used to photograph the specimens. The captured images were imported to ImageJ software [229] and converted from RGB color feature to 8-bit greyscale (binary pictures). Next, the lower and upper limits of the threshold histogram were manually modified to avoid noise. After that, the image was scaled, considering that the cross-sectional area was 40 x 40 mm. Finally, macroporosity was automatically examined using the software.

7.3 Results

7.3.1 Self-cleaning (RhB degradation)

Figure 7.2 presents the overall color variation (ΔE) from the RhB degradation test for all studied mixtures. Figure 7.2.a exhibits the results for mixtures with no slag, whereas Figure 7.2.b displays the results of mixtures containing slag. Each ΔE data point represents the average of 16 color measurements performed per mixture and UV exposure time. The standard deviation of each of the represented data points is less than 20%. As expected, the use of nano-TiO_2 increased the ΔE. Thus, the higher the nano-TiO_2, the higher the dye degradation and, therefore, the self-cleaning activity. Samples with no nanoparticles showed negligible self-cleaning activity compared to specimens with nano-TiO_2. It is also observed that the CO_2 curing increased the self-cleaning activity of all mixtures containing nanoparticles. Figure 7.2.b shows that the use of slag increased the self-cleaning activity of normal cured cement pastes compared to NC mixtures with 0% slag and the same percentage of nanoparticles.

Results suggest that the combination of nano-TiO_2 addition, slag cement, and CO_2 curing may produce a beneficial synergistic effect in terms of self-cleaning activity. Nonetheless, at low UV exposure time (lower than 2 hours), specimens with 0% slag presented comparable self-cleaning activity or even higher compared to their corresponding mixture with slag.

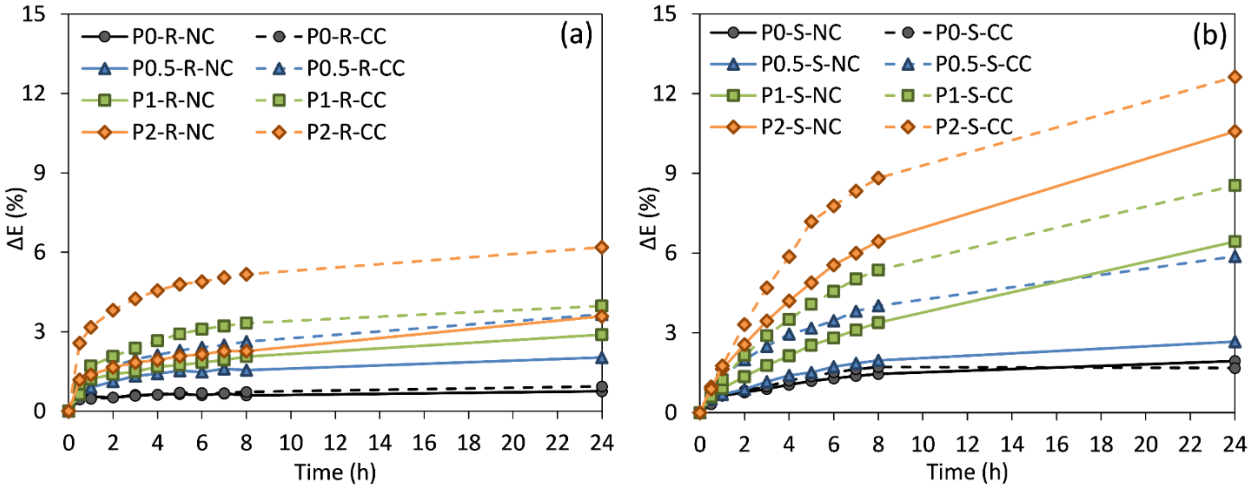

Figure 7.2. Self-cleaning activity after exposure to UV light. (a) 0% slag cement mixtures. (b) 30% slag cement mixtures.

To assess the interrelated effects of CO_2 curing, slag, and nano-TiO_2 addition on the self-cleaning activity, Figure 7.3.a shows the relation between total color variation (ΔE) after 24 hours of UV light exposure vs. nano-TiO_2 percentage. The self-cleaning activity was increased with an increase in the nanoparticles' percentage for all studied mixtures. Likewise, mixtures containing slag presented higher dye degradation than their corresponding mixtures without slag.

According to the results, CO_2 curing increased the self-cleaning activity of all studied mixtures containing nanoparticles. The reason could be the porosity reduction during CO_2 curing. Previous investigations pointed out that the carbonation process during CO_2 curing reduces cementitious materials' porosity [167], [175], [186], [187]. Besides, researchers showed that materials with lower porosity possess higher self-cleaning activity since the pollutants penetrate less into the material and can be easily removed since they are more exposed to UV light [220]–[222]. Therefore, CO_2 curing may be beneficial to increase the self-cleaning activity due to their well-known porosity reduction. In addition, since slag cement used is finer than OPC (Figure 2.1), the use of slag may have produced a decrease in porosity, and this reduction might be the reason behind the observed positive influence of slag in terms of self-cleaning performance, as Figure 7.2 exhibited. Therefore, further experiments were performed to better validate this observation.

Moreover, results suggest that using both materials (nano-TiO_2 and slag cement) may produce a synergistic effect in terms of self-cleaning activity improvement. For instance, in NC

samples, while specimens with 2% nano-TiO_2 and no slag showed degradation of 3.6% after 24 hours, and samples with slag and no nanoparticles showed a value of 1.9%, the samples that combined both slag and 2% nano-TiO_2 the color variation (ΔE) was 10.6%.

Figure 7.3.b exhibits the improvement of ΔE (%) after 24 hours of UV light exposure compared to the mixture with 0% slag and no nano-TiO_2 (P0). The combined use of slag cement and nanoparticles produced a synergistic effect in all samples (except for normal cured samples with 0.5% of nano-TiO_2). That means that, for each nanoparticles' percentage, the effect of combining slag and nano-TiO_2 on the self-cleaning activity is higher than the sum of the single effects on the self-cleaning activity produced by using slag and nanoparticles separately. Figure 7.3.b also shows that the higher the nano-TiO_2 percentage, the higher the synergistic effect of slag and nanoparticles.

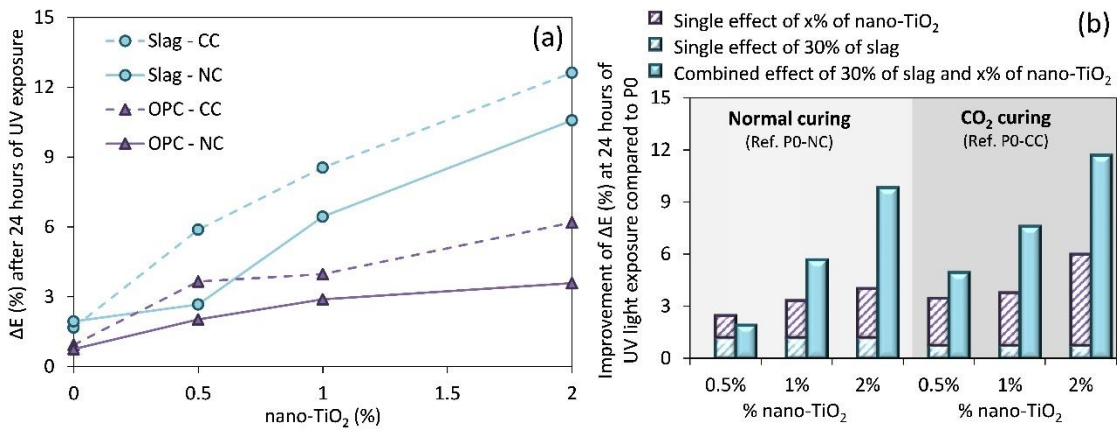

Figure 7.3. (a) Relation between total color variation (ΔE (%)) after 24 hours of UV light exposure vs. nano-TiO_2 percentage. (b) Improvement of ΔE (%) after 24 hours of UV light exposure compared to the mixture with 0% slag and no nano-TiO_2.

7.3.2 Macroporosity examinations using image analysis

Macroporosity examinations were carried out in normal cured samples to analyze the effect of slag in terms of porosity reduction. Samples with no nano-TiO_2 (P0-R and P0-S) and the percentage of nano-TiO_2 that showed the highest self-cleaning activity (P2-R and P2-S) were selected to perform this test. Figure 7.4 shows the cumulative pore volume histogram of normal cured specimens. Each column describes the cumulative volume of macropores lower than the corresponding range of pore sizes.

Figure 7.4.a exhibits the effect of slag addition in the reference mixtures (containing no nanoparticles). When slag cement is added, the total cumulative macroporosity volume decreased 7.6% compared to the reference without slag. Likewise, Figure 7.4.b shows that the use of slag cement in cement pastes with 2% nano-TiO_2 reduced 24% of the total macroporosity volume compared to the mixture with 2% nano-TiO_2 and no slag. Considering the porosity reduction made by the slag cement in all studied mixtures, results suggest that adding 30% slag cement produced a filling effect in those mixtures, reducing the macroporosity.

Moreover, the porosity reduction associated with the slag cement addition was higher in specimens with 2% nanoparticles than samples with no nano-TiO_2. This observation may imply that using both slag cement and nano-TiO_2 may produce a combined effect in terms of porosity reduction. This porosity reduction could be the reason behind the increase of the self-cleaning activity when slag is added. In addition, adding nano-TiO_2 and slag cement may increase the material strength since porosity is the property that influences the strength the most in cementitious composites. This increase in the material strength could also lead to a decrease in the cement content required to obtain a given strength and, therefore, it may imply an enhancement of the material sustainability.

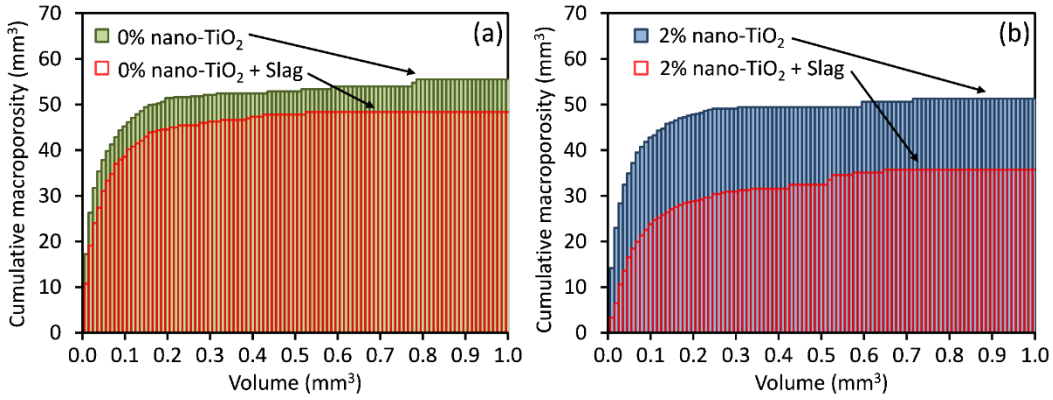

Figure 7.4. Cumulative macroporosity (mm^3) using image analysis. (a) 0% nano-TiO_2 with and without slag. (b) 2% nano-TiO_2 with and without slag.

7.4 Discussion

For every reference studied mixture, it was observed that the higher the percentage of nano-TiO_2, the higher the photocatalysis activity. Thus, to further investigate the effect of CO_2 curing and slag on the self-cleaning activity of cement pastes, additional tests were performed on the samples containing the highest percentage of nano-TiO_2 (2%) of this chapter.

7.4.1 Effect of slag and CO_2 curing on density and CO_2 uptake

Density

The influence of slag addition in terms of macroporosity reduction was assessed in the previous section (Figure 7.4). To further investigate the effect of CO_2 curing on porosity reduction, density measurements in mixtures with 2% nano-TiO_2 and both types of curing (normal curing and CO_2 curing) were performed. Figure 7.5.a shows the density in oven-dry condition (in kg/m^3) for the cement pastes with 2% nano-TiO_2 (P2-R and P2-S).

Results showed that the use of 30% slag cement increased the density in NC samples. This observation agrees with the macroporosity examination results since the slag addition has decreased the macroporosity in normal cured samples.

Regarding the effect of CO_2 curing, results exhibited a density increase of samples cured with CO_2 for both mixtures (with and without slag cement). The formation of $CaCO_3$ during the carbonation could explain the increase in density. It is known that $CaCO_3$ possesses a higher molar volume than the cement hydration products [182]. Therefore, CO_2 would enter the permeable pores of the sample and react with the hydration products, forming denser layers of $CaCO_3$. As a result, the density would increase after CO_2 curing. However, CO_2 curing did not affect density in the same way mixtures with 0% slag than pastes containing 30% slag. While the CO_2 curing increased 7.4% the density in samples with no slag and 2% nano-TiO_2 (P2-R), the mixture with slag cement and 2% nano-TiO_2 (P2-S) experienced a lower density change (3.3%) due to CO_2 curing.

In mixtures containing 2% nano-TiO_2, the CO_2 curing increased the self-cleaning activity of samples with and without slag to a similar extent (Figure 7.3.a). However, density results from Figure 7.5.a evidenced that samples with slag showed a lower increase of density than samples without slag during CO_2 curing. This observation might seem contradictory compared to self-

cleaning activity results. However, in terms of self-cleaning effectiveness, the overall porosity reduction (or increase on overall density in 50.8 x 50.8 x 50.8 mm cube samples) is not as relevant as the reduction of the superficial porosity. Moreover, superficial porosity is a crucial factor in self-cleaning effectiveness. While the use of nano-TiO_2 and slag cement may have a homogeneous effect in each part of the material, the CO_2 curing may be more concentrated on the surface. Nonetheless, a higher CO_2 penetration may imply a higher reduction of the overall material porosity, but it may not correlate with a higher reduction in the surface porosity. Consequently, results exhibited that the lower initial porosity of samples containing slag may induce a more localized and concentrated (due to the lower CO_2 penetration) carbonation of the material's surface, leading to a higher enhancement of the self-cleaning activity.

Thermogravimetric analysis (TGA)

Considering the self-cleaning results, the mixtures with the nano-TiO_2 percentage that possessed the highest activity (P2-R and P2-S) were selected for thermogravimetric analysis to further analyze the synergistic effects of nano-TiO_2, slag and CO_2 curing. TGA samples were prepared using slabs of 80 x 80 x 10 mm to focus on the surface effects of CO_2 curing. Figure 7.5.b displays the thermogravimetric curves of samples with 2% nanoparticles with and without slag cement (P2-R and P2-S, respectively). Whereas the normal cured (NC) samples are represented as solid lines, CO_2 cured (CC) specimens are shown using dashed lines.

Regarding NC samples, the specimen with slag possessed a similar total amount of hydration products but lower CH content than the specimen without slag. In CC samples, the use of slag in samples with 2% nano-TiO_2 slightly increased CO_2 uptake during CO_2 curing (16.3% vs. 16.5%, respectively).

Moreover, even though the use of slag cement reduced the porosity (Figure 7.4), TGA results showed that its use did not reduce the CO_2 uptake during CO_2 curing (Figure 7.5.b). Considering that samples with slag possessed lower initial porosity before CO_2 curing than samples without slag, a lower CO_2 diffusion might be expected through the samples with slag. Therefore, slag samples might have lower carbonation than samples without slag. However, samples with and without slag presented similar CO_2 uptake in 10 mm thickness samples. Therefore, results suggest that samples with slag (P2-S) might have experienced higher and more

localized superficial porosity reduction than P2-R after CO_2 curing due to its lower CO_2 penetration. Thus, even with the same level of carbonation, samples with slag might present a higher enhancement of photocatalytic activity due to the concentration of the porosity reduction on the surface.

This agrees with self-cleaning results (Figure 7.3.b) since the combined effect of 2% nano-TiO_2 , and 30% slag cement produced a synergistic effect in enhancing the self-cleaning activity. As a result, CO_2 cured mixtures containing 2% nano-TiO_2 and slag cement would enhance the self-cleaning activity and increase the CO_2 capture during CO_2 curing. That could imply more beneficial effects, such as strength and durability improvement, due to the lower porosity after CO_2 curing.

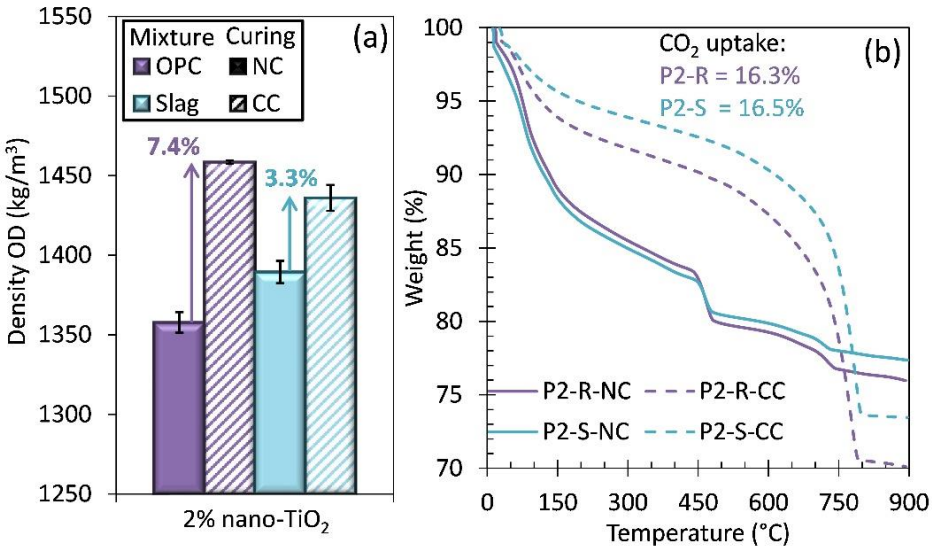

Figure 7.5. (a) Density of mixtures with 2% nano-TiO_2. (b) TGA results of mixtures with 2% nano-TiO_2.

X-ray powder diffraction (XRD)

X-ray powder diffraction tests were performed in samples of the same mixtures used for thermogravimetric analysis (P2-R and P2-S). Figure 7.6 presents the XRD results for samples with 2% nano-TiO_2 and both types of curing (normal curing and CO_2 curing)

Results showed that normal cured (NC) samples with no slag (P2-R-NC) possessed higher CH content than NC specimens with 30% slag cement (P2-S-NC) since the CH peaks are more remarkable in P2-R-NC samples, as expected due to the lower OPC content of mixtures with slag.

Results agree with the TGA data. In CO_2 cured samples (CC), results evidenced that the use of 30% slag cement increased the CO_2 capture since $CaCO_3$ peaks are higher in these samples (P2-S-CC) than in samples with no slag (P2-R-CC). These observations suggest that the use of slag cement may be beneficial in terms of CO_2 uptake after CO_2 curing.

Even though NC samples with slag (P2-S-NC) possessed less calcium hydroxide than NC specimens without slag (P2-R-NC), CO_2 cured samples with slag (P2-S-CC) showed a higher $CaCO_3$ content (and, thus, a higher CO_2 uptake) than CO_2 cured samples with no slag cement (P2-R-CC). This observation suggests that using slag cement in cement pastes with 2% nano-TiO_2 does not reduce the $CaCO_3$ formation during CO_2 curing (i.e., it does not decrease the porosity due to CO_2 curing). This observation again agrees with the self-cleaning activity and TGA results, where the combined use of slag and CO_2 curing produced a cumulative effect in enhancing the self-cleaning activity.

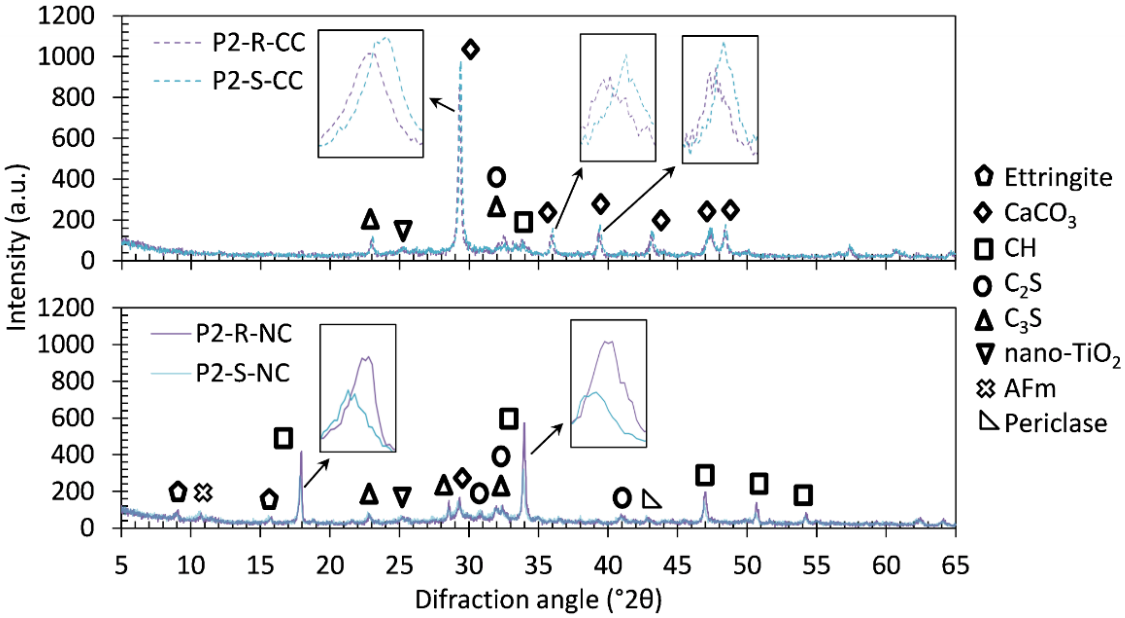

Figure 7.6. XRD results for samples with 2% nanoparticles.

7.4.2 Effect of slag and CO_2 curing on photocatalytic ability according to UNI 11259

The analysis of the photocatalytic properties of cementitious composites containing nano-TiO_2 after standard curing conditions has been widely studied throughout the literature [59], [61], [112], [208]–[215]. Consequently, some standards regulate whether a material could be considered as photocatalytic (e.g., UNI 11259 [228]).

According to UNI 11259, a material can be considered photocatalytic if the variation of the color coordinate a* (Δa*) exceeds 20% after four hours of irradiation and 50% after 24 h irradiation. To analyze whether or not studied mixtures with 2% nano-TiO_2 comply with these thresholds of acceptance, the same photocatalytic test setup is explained in the *Self-cleaning activity test* section, using the irradiance value specified by the UNI 11259 (3.75 ± 0.25 W/m^2).

Figure 7.7 exhibits the results for the standard photocatalytic test of mixtures with 2% nano-TiO_2. This figure shows the Δa* at both 4 and 24 hours of UV light exposure. Results showed that the use of 2% nano-TiO_2 is not enough in conventional cement pastes (P2-R-NC) to provide this material with photocatalytic properties. This was expected since previous literature showed that usually, a minimum of 3% of nano-TiO_2 is needed to make a photocatalytic cementitious composite [211], [218], [230]–[232]. Besides, results evidenced that the use of slag cement is beneficial to increase the photocatalytic properties in all studied mixtures. The use of slag increased the Δa* at both UV light exposure times, even though it was not enough to consider them photocatalytic. Furthermore, samples with CO_2 curing exhibited higher Δa* than their corresponding mixtures with normal curing.

In terms of acceptability thresholds, only the mixture with 2% nano-TiO_2, slag cement, and CO_2 curing met the requirements stated in the standard UNI 11259 [228] to be considered a photocatalytic material. This mixture (P2-S-CC) possessed an average Δa* of 37.4% and 57.6% at 4 and 24 hours of UV light exposure, respectively. In contrast, the same mixture with normal curing (P2-S-NC) exhibited lower values (11.1% and 27.4%, respectively), which means that P2-S-NC cannot be defined as a photocatalytic material. Furthermore, regarding mixtures with no slag, none showed a degradation higher than the acceptability thresholds neither at 4 nor 24 hours of UV light exposure.

Thus, results suggest that the combined use of slag cement and CO_2 curing may become an enabling technology to make photocatalytic cementitious composites with lower percentages of nano-TiO_2.

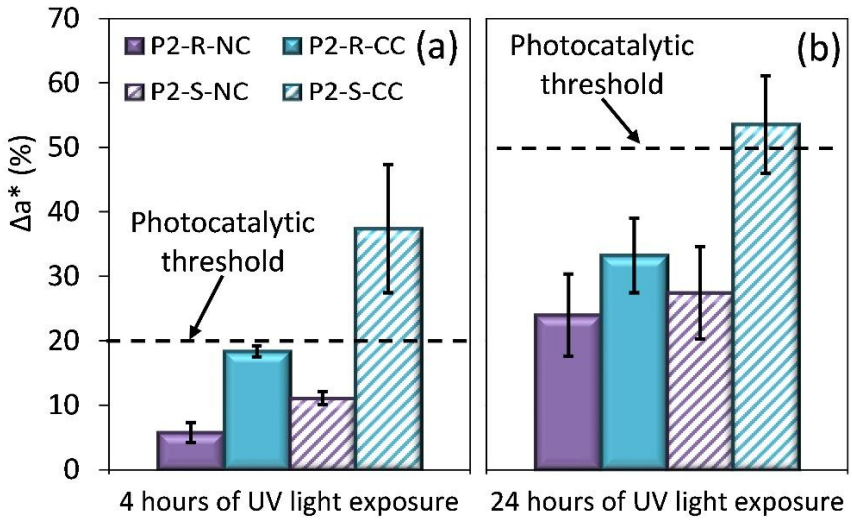

Figure 7.7. Standard photocatalytic test (variation of a* coordinate, in percentage) of mixtures with 2% nano-TiO_2. (a) 4 hours of UV light exposure. (b) 24 hours of UV light exposure.

7.5 Conclusions

This chapter analyzed the single and combined effect of slag cement addition and CO_2 curing on the self-cleaning activity of cement pastes containing nano-TiO_2. Results showed that using slag cement and CO_2 curing reduced the pore volume of cement pastes and, therefore, increased their self-cleaning activity due to the lower penetration of the pollutants.

The production of calcium carbonate during the CO_2 carbonation is very similar in samples with and without slag. Nonetheless, results suggest that the lower porosity of cement pastes containing slag produced higher and more concentrated surface carbonation during CO_2 curing. Thus, CO_2 curing produced a higher reduction of the superficial porosity in samples containing slag than in samples without slag. Consequently, the self-cleaning enhancement of those materials with low initial porosity would be higher than cementitious materials with high initial pore volume.

Moreover, results showed that reference cement pastes with 2% nano-TiO_2 (P2-R-NC) cannot be considered a photocatalytic material, based on the definition of standard UNI 11259. However, the combined use of both slag cement and CO_2 curing produced a synergistic effect on

cement pastes with nano-TiO_2 in terms of porosity reduction of the paste's surface, affecting the self-cleaning activity positively. As a result, the mixture with 2% nano-TiO_2 and 30% slag can be considered a photocatalytic material, according to UNI 11259 test, when cured with CO_2. These results show that the combination of using slag cement and CO_2 curing may enable the production of photocatalytic cementitious composites with lower percentages of nanoparticles.

8. CONCLUSIONS AND FUTURE WORK

8.1 Conclusions

This dissertation has studied the impact of nano-TiO_2 addition on the environmental performance of cementitious composites based on a holistic approach, including: (i) the composite performance, (ii) the impact of material production, and (iii) the effects during the service life.

Regarding the composite performance, this research concluded that the w/b and the testing age influence the optimum percentage of nano-TiO_2 in terms of compressive strength. The higher the w/b, the higher the optimum percentage of nano-TiO_2. Besides, the lower the testing age, the higher the optimum nano-TiO_2 percentage. Thus, mixtures with high initial porosity present a dual beneficial effect of nano-TiO_2 addition, promoting hydration (nucleation effect) and reducing porosity (filling effect). In contrast, in mixtures with low initial porosity, the same level of nano-TiO_2 addition may excessively reduce the porosity, potentially leading to a stop of the hydration due to the lack of space for the hydration products to grow.

In terms of improving the environmental performance of material production, this research has studied the combined effect of nano-TiO_2 and recycled aggregate on the life cycle assessment (LCA) of mortars, using *cradle-to-gate* as the system boundary. The nano-TiO_2 addition on mortar mixtures enhances the sustainability of mortars with recycled concrete aggregates (RCA) to a greater extent than on mortars with natural aggregates. Nano-TiO_2 addition showed a more significant improvement of the compressive strength of mortars with RCA and on mortars with natural aggregate. This enhancement of compressive strength due to nano-TiO_2 reduces the cement content required to make a mortar with a given strength. Indeed, a 0.5% nano-TiO_2 addition highly decreased the GWP in mortars with RCAs, particularly with a total replacement (100% of RCA).

Besides, the benefits of using nano-TiO_2 in terms of sustainability might be even more remarkable when a holistic approach (*cradle-to-grave*) is considered. This approach would account for the potential proactive effects of cementitious composites containing nano-TiO_2 during the service life (e.g., photocatalytic effect, potential enhancement of CO_2 sequestration). Thus, combining nano-TiO_2 and RCAs in cementitious composites may lead to an enormous enhancement of environmental performance.

Furthermore, the effects of nano-TiO_2 during the service life of cementitious composites were also analyzed in this investigation. Besides the well-known NO_x removal property of cementitious composites with nano-TiO_2, the present study has found that nano-TiO_2 may promote the CO_2 sequestration of cementitious materials during service life. This CO_2 uptake is significantly influenced by the initial porosity of the cement paste. The higher the water-to-cement (w/c) ratio, the higher the maximum level of nanoparticles that increases the CO_2 capture of cement paste. In addition, nano-TiO_2 reduces the CH size, making it more reactive and, therefore, increasing the CO_2 uptake. However, the filling effect of the nanoparticles reduces the porosity, reducing the CO_2 penetration into the cement matrix. Both competitive mechanisms (increase of CH reactivity and porosity reduction) may explain why the optimum nano-TiO_2 percentage in terms of CO_2 uptake strongly depends on the w/c and the exposure age.

This research also studied the effect of nano-TiO_2 on the CO_2 capture when cementitious composites are cured with CO_2. CO_2 curing is one of the most promising techniques in the cementitious materials industry to enhance strength while reducing the net CO_2 emissions associated with composite production. After 12-hour CO_2 curing, cement pastes with nano-TiO_2 addition increase both CO_2 uptake and compressive strength compared to mixtures without nanoparticles cured under the same conditions. These effects may produce a significant improvement in terms of the environmental performance of cementitious composites. Furthermore, the nano-TiO_2 addition reduces the net CO_2 emissions of cement pastes when their beneficial effects (promotion of CO_2 uptake and improvement of compressive strength) are considered. For instance, combining 0.5% nano-TiO_2 addition and CO_2 curing reduces net CO_2 emissions of over 20% in a cement paste with 0.55 w/c.

Besides the beneficial effect of CO_2 curing in terms of CO_2 uptake, this investigation analyzed the effect of CO_2 curing on the self-cleaning activity of cement pastes containing nano-TiO_2. The lower porosity of cement pastes containing slag produced higher and more concentrated surface carbonation during CO_2 curing. Thus, CO_2 curing produced a higher reduction of the superficial porosity in samples containing slag than in samples without slag. Consequently, the self-cleaning enhancement of those materials with low initial porosity would be higher than cementitious materials with high initial pore volume. Furthermore, based on the definition of a photocatalytic material stated in the standard UNI 11259, the combination of using slag cement

and CO_2 curing may enable the production of photocatalytic cementitious composites with lower percentages of nanoparticles.

8.2 Future work

8.2.1 The impact of CO_2 uptake rate on the environmental performance of cementitious composites: A new dynamic GWP analysis.

Motivation and goal.

Greenhouse gases (GHG) concentration has dramatically increased a 43% in the last three decades [1]. Carbon dioxide (CO_2) is responsible for 65% of the total GHG concentration [2]. According to the World Meteorological Organization, CO_2 concentration in the atmosphere reached its highest level in the last 3-5 million years [1], leading to numerous global consequences (e.g., global warming and ocean acidification) [3]. Accordingly, identifying long-term decarbonization strategies is crucial to mitigate environmental problems.

Nowadays, cement production produces 8% of the total CO_2 emissions every year [4]. Moreover, cement is one of the essential ingredients of concrete, the most consumed construction material globally [7], with more than 8 billion cubic meters produced each year [8]. Consequently, a small step in enhancing the environmental performance of cementitious composites could lead to a giant leap in global sustainability due to the enormous significance of those materials globally.

Even though cement production is responsible for substantial CO_2 emissions, cementitious composites could also sequestrate enormous amounts of carbon dioxide [19]. For example, a recent investigation showed that the cementitious materials have sequestrated, from 1930 to 2013, almost half of the CO_2 emissions associated with the limestone decomposition in the same period [19]. Thus, not considering this potential CO_2 uptake may overestimate the real environmental impact of cementitious composites. However, the natural CO_2 sequestration of cementitious composites is a slow process that may take decades. Therefore, discounting the total CO_2 that the material would uptake during service life from the initial CO_2 emissions would underestimate the material's real environmental impact.

Nevertheless, the environmental performance of cementitious composites is currently analyzed by traditional life cycle assessment (TLCA) methods [123], [133], [233]. Those TLCA methods are static, with little consideration of significant factors that vary over time. Those TLCA methods report the global warming potential (GWP) as the CO_2 equivalent (CO_2 eq.) emissions in a snapshot in time. The environmental assessment would not account for the time spent for the material to capture CO_2, using traditional system boundaries (i.e., *cradle-to-gate* and *cradle-to-grave*) [131], [132]. This clearly would not represent the actual environmental impact of the material.

The *cradle-to-gate* analysis accounts for all the impacts that the material may have until its production is completed. However, this method does not reflect the potential beneficial effects (e.g., CO_2 uptake) during service life. Therefore, the impact of materials with the ability to sequestrate CO_2 could be overestimated. Likewise, *cradle-to-grave* system boundary possesses limitations in its assessment. It analyzes the material's environmental impact during its whole lifetime (from the extraction of raw materials until its demolition and recycling process). However, it does not consider the different CO_2 uptake rates of those materials. Recent studies showed that the CO_2 uptake rate of cementitious composites could be accelerated by nanomodification of the concrete's matrix [195], [219]. Thus, the imbalance between the CO_2 emitted and the CO_2 uptake during their service life might be even more relevant than in traditional concretes. Even if the final net CO_2 emissions are the same, materials with a higher imbalance between the CO_2 emitted and the CO_2 uptake during their service life would have a higher environmental impact than composites with lower imbalances over their lifetime. Nevertheless, this different imbalance would not be captured by traditional static GWP assessments. High CO_2 concentration in the atmosphere may produce disastrous effects in terms of climate change or global warming [2]. Thus, accounting for the total CO_2 capture and the CO_2 uptake rate is crucial when assessing the sustainability of cementitious composites.

Considering that none of the TLCA methods could effectively estimate the environmental impact of materials with the ability to capture CO_2 during their service life (e.g., cementitious composites), this study proposes a new dynamic GWP method to assess the environmental impact of those materials. This dynamic GWP analysis would be based on an actual environmental assessment from a holistic point of view. This study analyzes and estimates how the CO_2 uptake

rate may modify the environmental performance of cementitious composites based on a dynamic GWP analysis in a 100-year timeframe. Implementing this dynamic GWP method would lead to a realistic analysis of the environmental impact of complex cementitious composites. Using this realistic analysis will be vital to design and assess the new generation of cementitious composites from a sustainable perspective.

8.2.2 Future research lines

This dissertation unveiled several aspects and mechanisms related to enhancing the environmental performance of cementitious composites due to the nanomodification of their microstructure. Based on the findings and limitations of the current investigation, several future lines of research can be followed:

(i) This dissertation showed that the use of nano-TiO_2 may promote the CO_2 uptake of cementitious composites. However, the carbonation of those cementitious materials may increase the risk of corrosion of cementitious composites containing steel reinforcement because the PH may be reduced. Therefore, the analysis of how the extent of carbonation may affect the durability of steel-reinforced materials should be studied in the future.

(ii) Moreover, this dissertation was based on mortars and cement pastes. Cement pastes are indeed the matrix of concretes and, therefore, the studied mechanisms should be directly applicable to concretes. Nonetheless, further research in terms of concrete applicability should be done to understand how these mechanisms work on a bigger scale.

APPENDIX A. MILL CERTIFICATE

Buzzi Unicem USA

MILL CERTIFICATION REPORT
PORTLAND CEMENT - TYPE I

Certification date: 10/15/2019
Cement Type: Type I
Laboratory: Greencastle, IN Plant

We hereby certify that this cement complies with current ASTM C150, AASHTO M85 and CSA-3001_ GU Specifications.
The following data represents the average for the Buzzi Unicem USA cement that was produced in the month of
September-19

ASTM STANDARD REQUIREMENTS		MILL CERTIFICATION VALUES		
CHEMICAL DATA C150				
SiO_2 - %	*	SiO_2 - %	19.54	
Al_2O_3 - %	*	Al_2O_3 - %	5.26	
Fe_2O_3 - %	*	Fe_2O_3 - %	2.71	
CaO - %	*	CaO - %	63.49	
MgO - %	max 6.0	MgO - %	2.18	
SO_3 - %	max 3.0***	SO_3 - %	3.12	
Loss on Ignition - %	max 3.0 (when limestone is not an ingredient)	Loss on Ignition - %	2.85	
Loss on Ignition - %	max 3.5 (when limestone is an ingredient)			
Insoluble Residue - %	max 1.50	Insoluble Residue - %	0.39	
CO_2 in Cement - %	^	CO_2 in Cement - %	1.67	
Limestone - %	max 5.0	Limestone - %	3.94	
$CaCO_3$ in Limestone - %	min 70.0	$CaCO_3$ in Limestone - %	96.7	
Potential Phase Compounds:**		Potential Phase Compounds:**		
C_3S - %	*	C_3S - %	59.5	
C_2S - %	*	C_2S - %	9.0	
C_3A - %	*	C_3A - %	9.0	
C_4AF - %	*	C_4AF - %	7.9	
$C_4AF + 2(C_3A)$ - %	*	$C_4AF + 2(C_3A)$ - %	25.9	
$C_3S + 4.75C_3A$ - %	*	$C_3S + 4.75C_3A$ - %	102.2	
Na_2O Equivalent - %	*	Na_2O Equivalent - %	0.62	
Free CaO - %	*	Free CaO - %	1.05	
PHYSICAL DATA C150				
Fineness- Blaine - m^2/kg	min 260	Blaine - m^2/kg	417	
Fineness- #325 Sieve Passing (%)	*	#325 Sieve Passing (%)	93.2	
Autoclave Expansion % (C151)	max 0.80	Autoclave Expansion % (C151)	0.04	
Time of Set		Time of Set		
Vicat (minutes)	min 45	Vicat (minutes) Initial	101	
	max 375	Final	209	
Air Content %	max 12	Air Content %	10.9	
Compressive Strength:		Compressive Strength:		
1 day - psi (MPa)	*	1 day - psi (MPa)	2480	(17.1)
3 day - psi (MPa)	1740 (12.0)	3 day - psi (MPa)	3850	(26.5)
7 day - psi (MPa)	2760 (19.0)	7 day - psi (MPa)	4730	(32.6)
28 day - psi (MPa)	*	28 day - psi (MPa)	5910	(40.7) Previous Month Avg.

Additional Data

Type	Limestone	I.P.A. Addition Data	Base Cement Phase Composition	
Amount (%)				
SiO_2 - %	3.93	*	**C_3S - %**	62
Al_2O_3 - %	0.82	*	**C_2S - %**	9
Fe_2O_3 - %	0.45	*	**C_3A - %**	9
CaO - %	49.91	*	**C_4AF - %**	8
MgO - %	2.01	*		
SO_3 - %	0.29	*		

** Not applicable.*
*** Adjusted per ASTM C150 Annex A1.6*
**** It is permissible to exceed the values for SO3 content provided that the Mortar Bar Expansion C1038 does not exceed 0.020 % at 14 days.*

ATTN:

Silo	Bill of Lading	Tons	Date

By Marcia L Dyrud Case

BUZZI UNICEM USA, Greencastle Plant
3301 S CR 150W,Greencastle, IN 46135, Phone 765.653.9766

Marcia L. Dyrud Case
Quality Control Manager

STATE OF INDIANA}
COUNTY OF PUTNAM}
Before me the undersigned, a Notary Public for Putnam County, State of Indiana personally appeared Marcia L. Dyrud and acknowledged the the execution of the foregoing instrument this day 2019.

Stephanie A. Richardson, Notary Public
My commission expires March 10, 2024.

APPENDIX B. TGA CURVES OF OTHER NANO-TiO_2 PERCENTAGES (0.5% AND 2%)

Figure B.1 shows the TGA curves of the comparison between the other studied percentages of nano-TiO_2 (0.5% and 2%) and the reference mixtures (no nanoparticles).

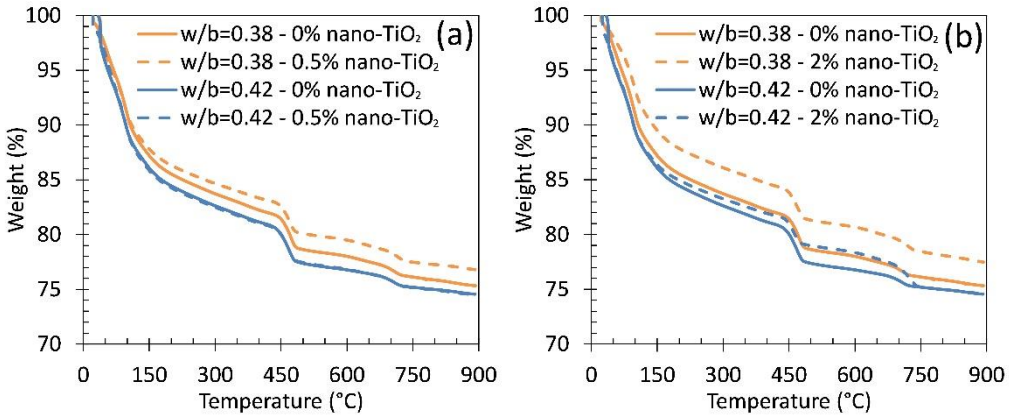

Figure B.1. TGA curves of cement pastes at 7 days two different w/b (0.38 and 0.42). (a) Comparison between 0% and 0.5% of nano-TiO_2. (b) Comparison between 0% and 2% of nano-TiO_2.

APPENDIX C. REPEATABILITY OF TGA TESTS

To test the reliability of the TGA procedure used in this study, instead of conducting this preliminary study at 14 or 28 days, TGA tests at early age (2 days) were conducted. At early age, any minor deviation of the procedure or human mistake may cause more significant differences between the results of two samples of the same mixture and conditions. Figure C.1 displays two TGA curves of two cement paste samples with 1% of nano-TiO_2 (non-exposed to CO_2). Figure C.1 displays two TGA curves of two samples of the same cement pastes after CO_2 exposure. Results showed that the procedure used to perform TGA is reliable and repeatable for both non-exposed and exposed samples.

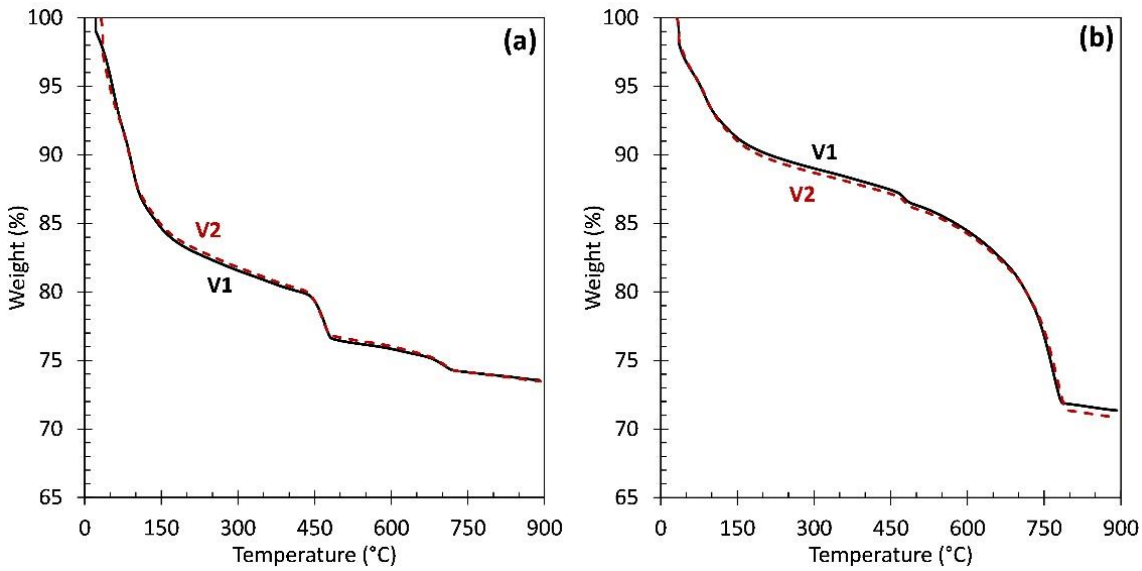

Figure C.1. Two TGA curves of the same mixture with 1% of nano-TiO_2. (a) Non-exposed. (b) Exposed.

APPENDIX D. QUALITATIVE TGA CURVES

Figure D.1 presents the TGA curves of samples with w/c=0.45 at 14 days with four percentages of nano-TiO_2 (0%, 0.5%, 1%, 2%).

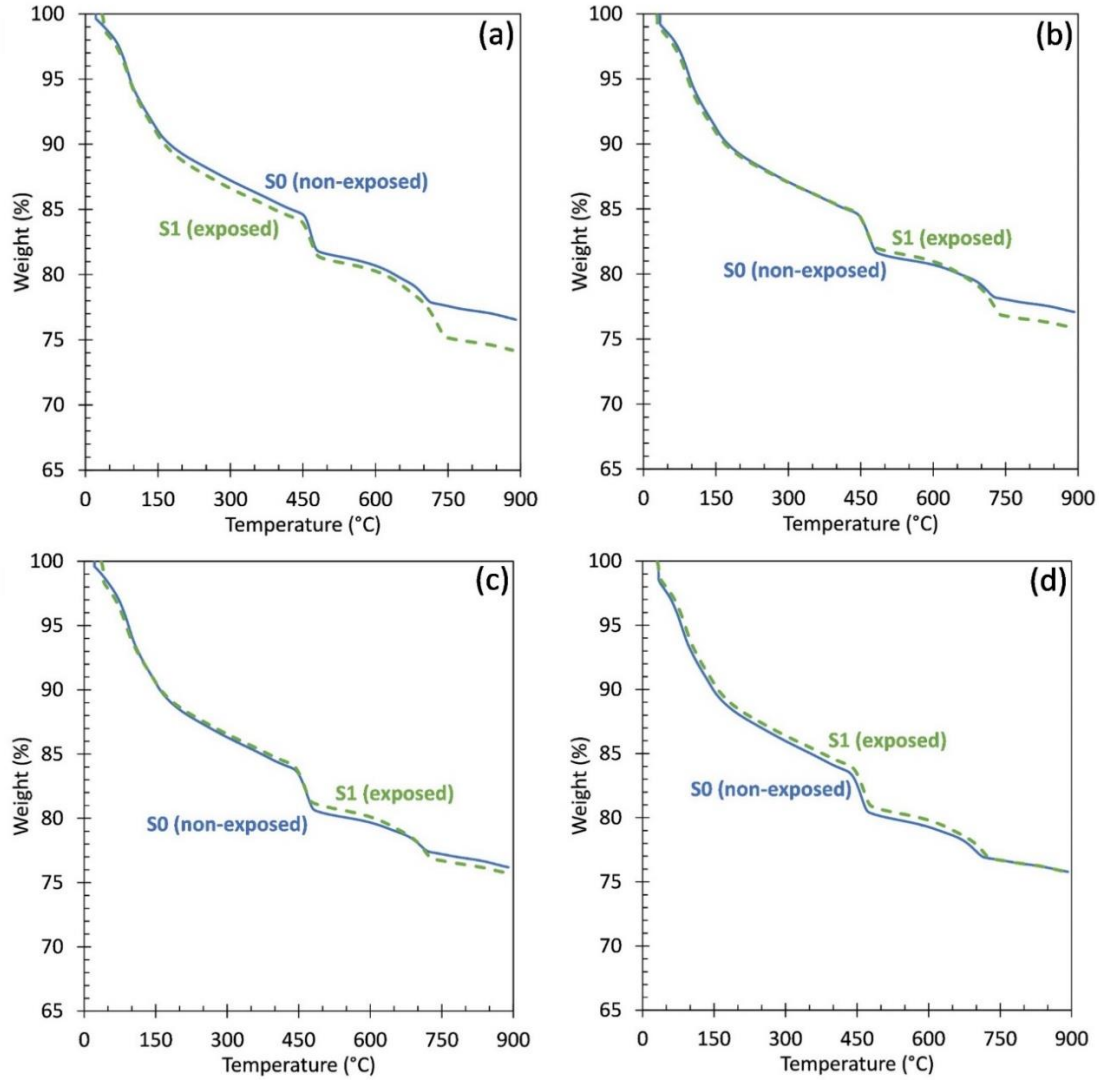

Figure D.1. TGA curves of mixtures with w/b=0.45 at 14 days. (a) P0. (b) P0.5. (c) P1. (d) P2.

Figure D.2. presents the TGA curves of samples with w/c=0.50 at 14 days with four percentages of nano-TiO_2 (0%, 0.5%, 1%, 2%).

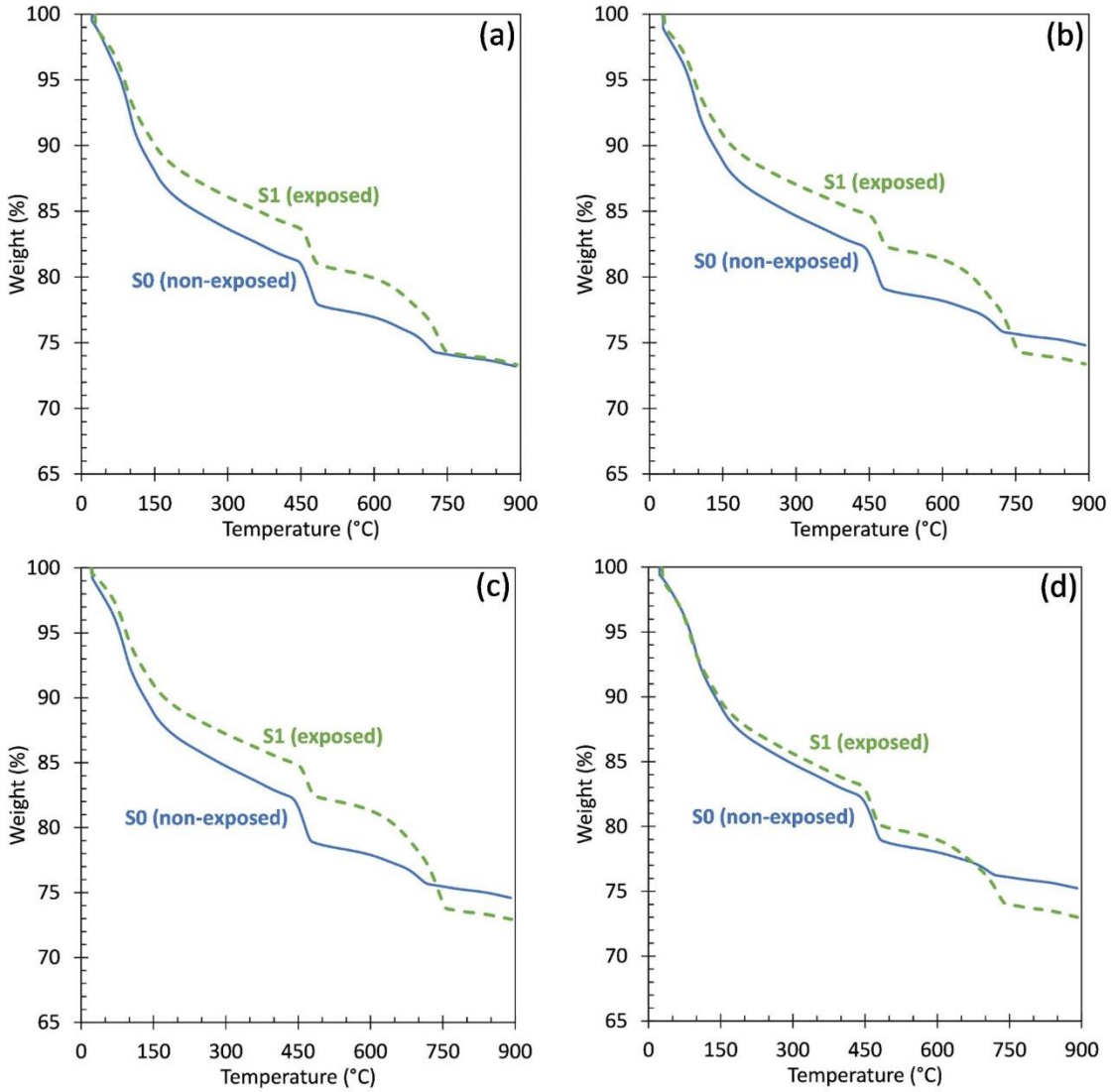

Figure D.2. TGA curves of mixtures with w/b=0.50 at 14 days. (a) P0. (b) P0.5. (c) P1. (d) P2.

Figure D.3 presents the TGA curves of samples with w/c=0.55 at 14 days with four percentages of nano-TiO_2 (0%, 0.5%, 1%, 2%).

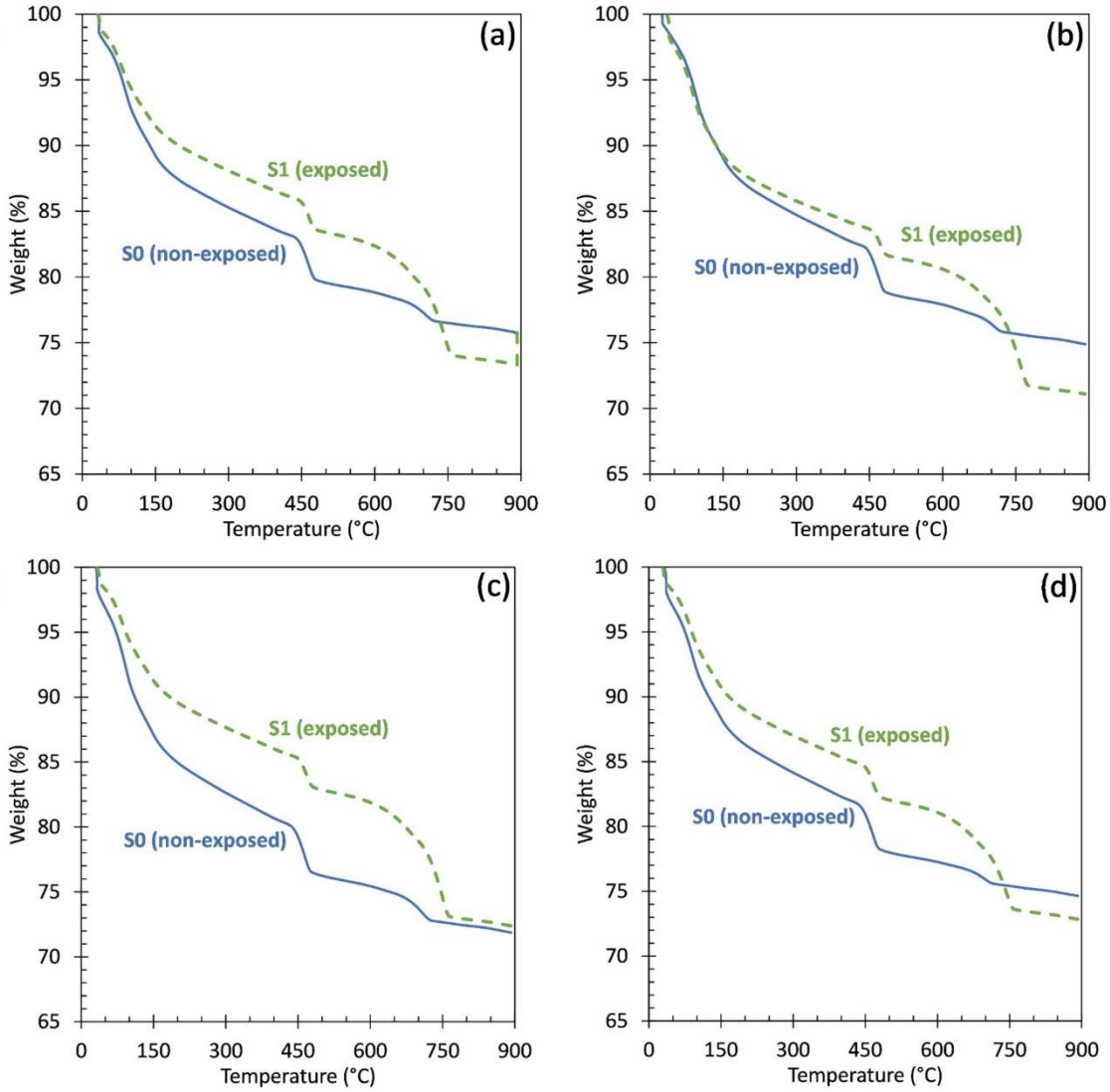

Figure D.3. TGA curves of mixtures with w/b=0.55 at 14 days. (a) P0. (b) P0.5. (c) P1. (d) P2.

Figure D.4. presents the TGA curves of samples with w/c=0.45 at 28 days with four percentages of nano-TiO_2 (0%, 0.5%, 1%, 2%).

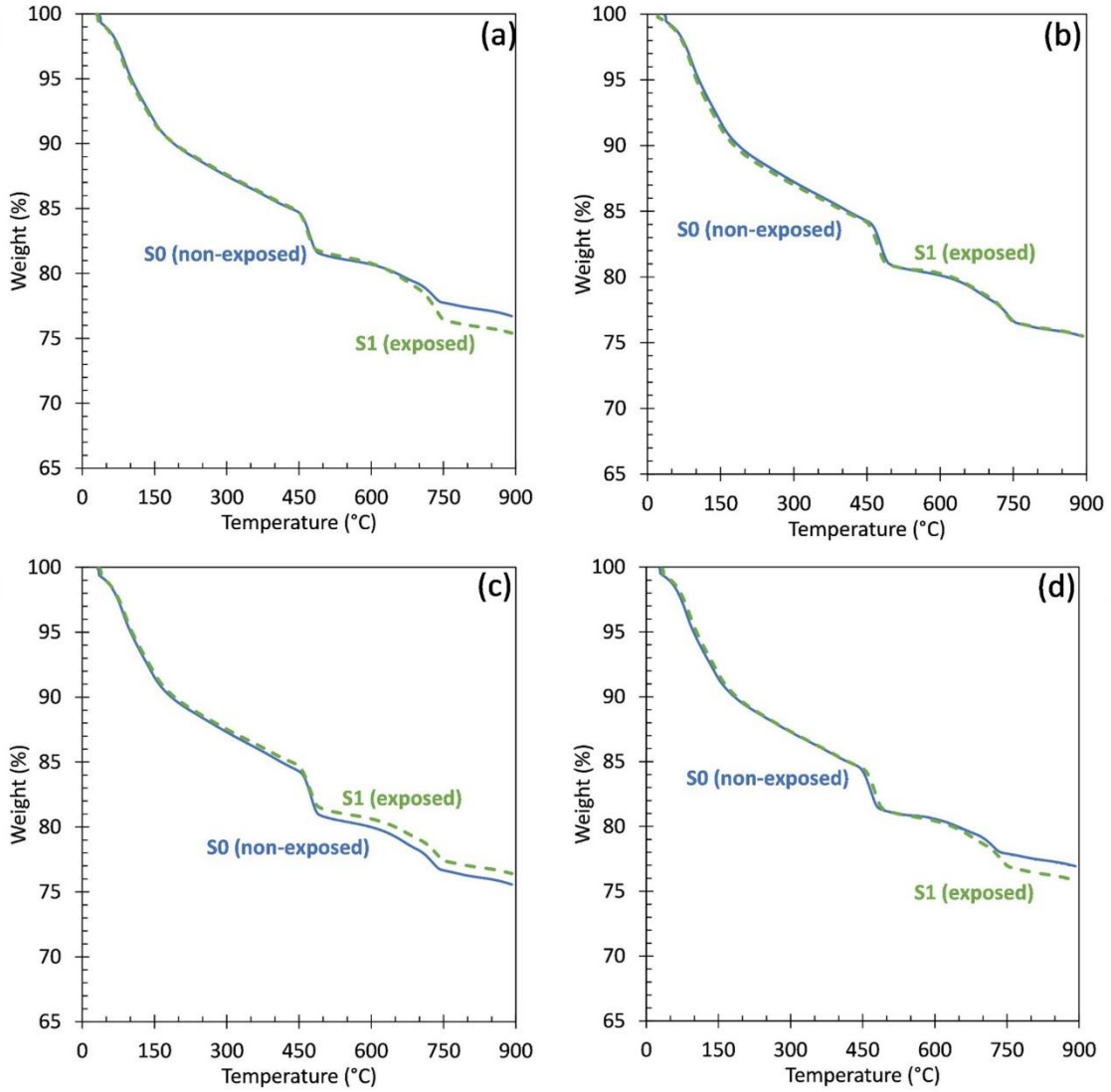

Figure D.4. TGA curves of mixtures with w/b=0.45 at 28 days. (a) P0. (b) P0.5. (c) P1. (d) P2.

Figure D.5. presents the TGA curves of samples with w/c=0.50 at 28 days with four percentages of nano-TiO_2 (0%, 0.5%, 1%, 2%).

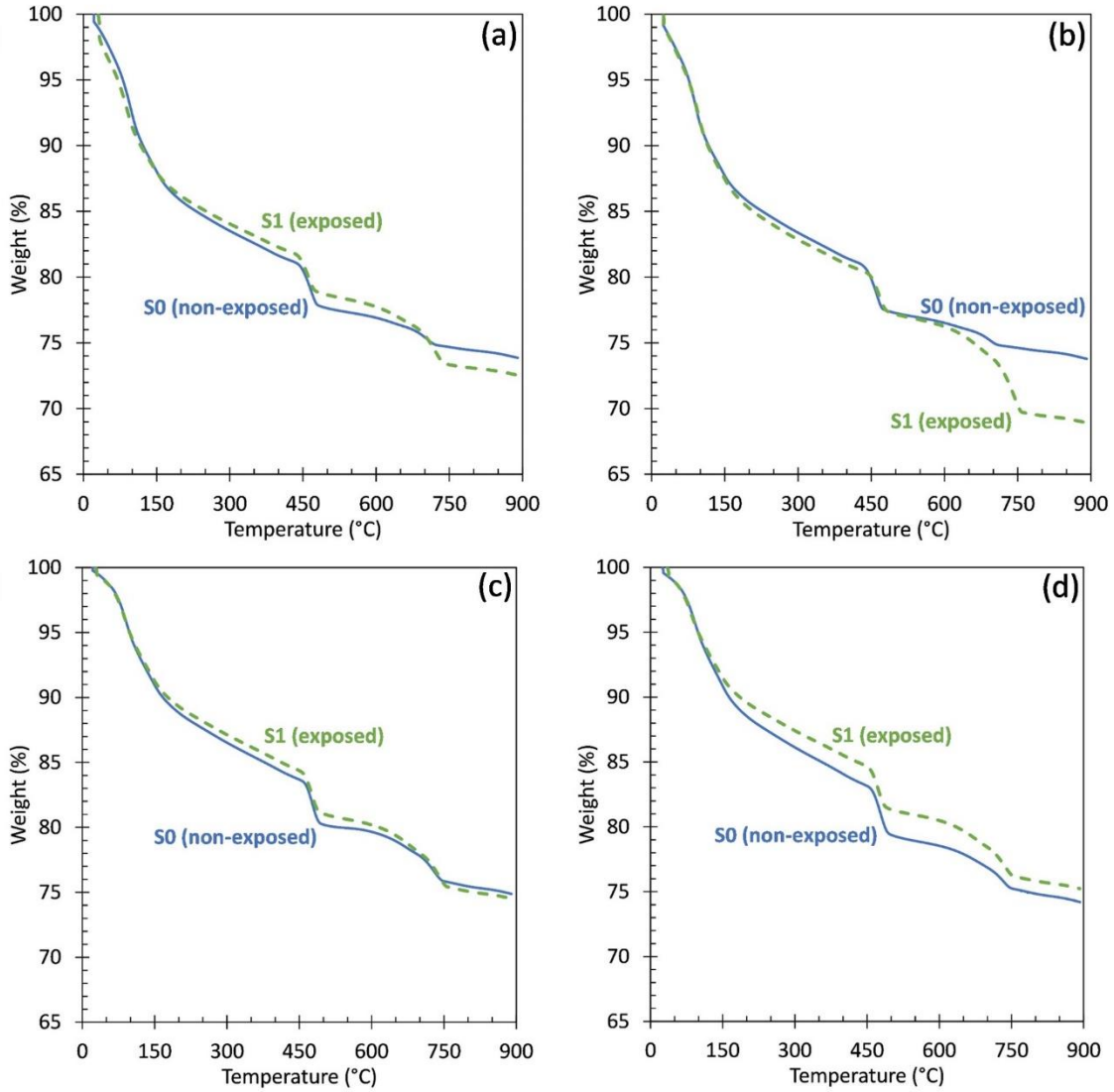

Figure D.5. TGA curves of mixtures with w/b=0.50 at 28 days. (a) P0. (b) P0.5. (c) P1. (d) P2.

Figure D.6. presents the TGA curves of samples with w/c=0.55 at 28 days with four percentages of nano-TiO_2 (0%, 0.5%, 1%, 2%).

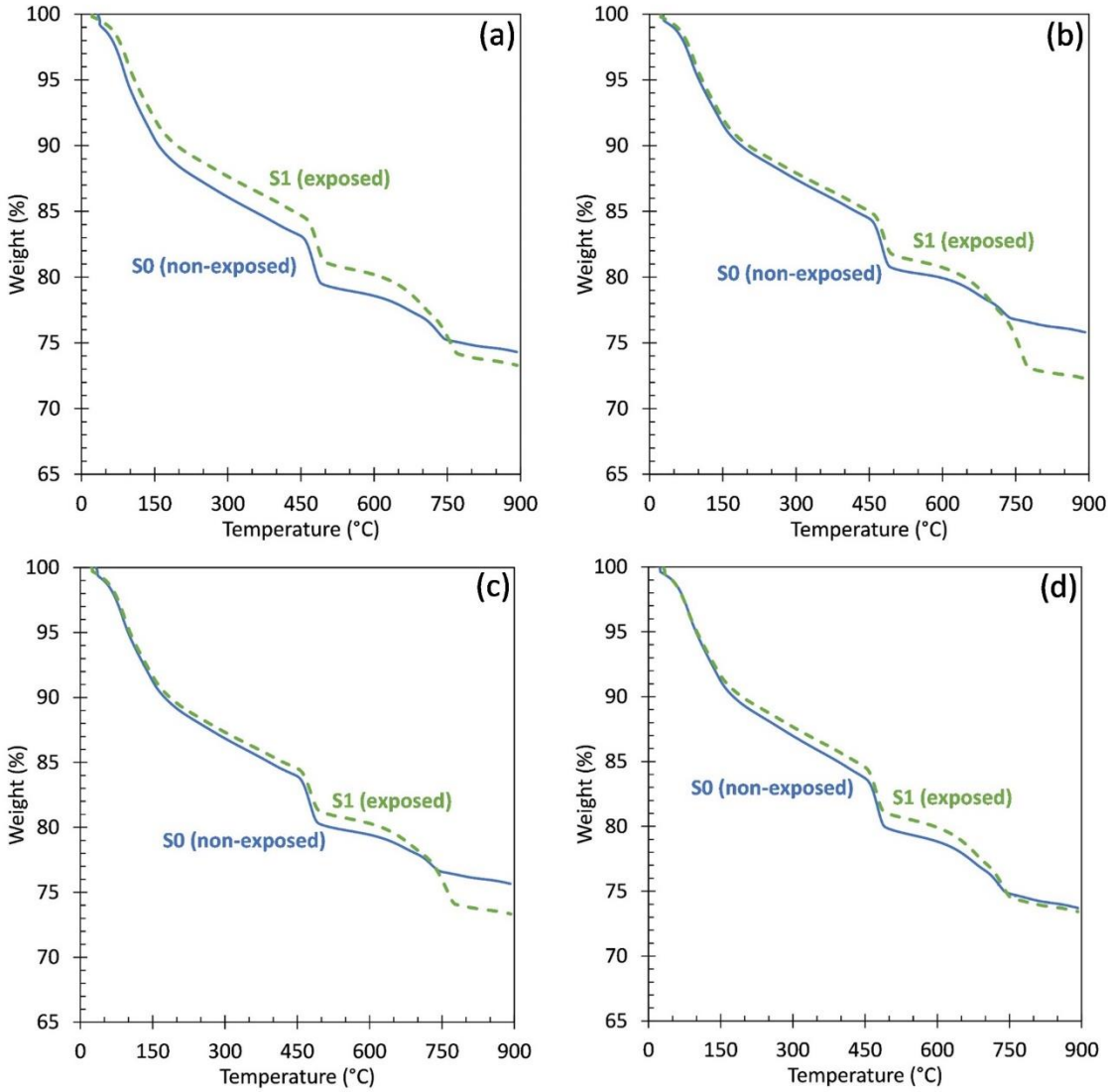

Figure D.6. TGA curves of mixtures with w/b=0.55 at 28 days. (a) P0. (b) P0.5. (c) P1. (d) P2.

REFERENCES

[1] World Meteorological Organization, "WMO Greenhouse Gas Bulletin (GHG Bulletin) - No. 15: The State of Greenhouse Gases in the Atmosphere Based on Global Observations through 2018," 2019.

[2] IPCC 2014, "Climate Change 2014: Synthesis Report. Contribution of Working Groups I, II and III to the Fifth Assessment Report of the Intergovernmental Panel on Climate Change [Core Writing Team, R.K. Pachauri and L.A. Meyer (eds.)]," Geneve, Switzerland.

[3] S. Cooley, J. Mathis, K. Yates, and C. Turley, "Frequently asked questions about ocean acidification," *U.S. Ocean Carbon Biogeochem. Progr. UK Ocean Acidif. Res. Program.*, vol. Version 2, 2012.

[4] R. M. Andrew, "Global CO2 emissions from cement production, 1928 – 2017," *Earth Syst. Sci. Data*, vol. 10, pp. 2213–2239, 2018.

[5] C. Pade and M. Guimaraes, "The CO2 uptake of concrete in a 100 year perspective," *Cem. Concr. Res.*, vol. 37, no. 9, pp. 1348–1356, 2007.

[6] G. Habert and C. Ouellet-Plamondon, "Recent update on the environmental impact of geopolymers," *RILEM Tech. Lett.*, vol. 1, p. 17, 2016.

[7] C. Tam *et al.*, "Cement Technology Roadmap 2009 - Carbon emissions reductions up to 2050," 2009.

[8] P. J. M. Monteiro, S. A. Miller, and A. Horvath, "Towards sustainable concrete," *Nat. Mater.*, vol. 16, no. 7, pp. 698–699, 2017.

[9] S. A. Miller, "Supplementary cementitious materials to mitigate greenhouse gas emissions from concrete: can there be too much of a good thing?," *J. Clean. Prod.*, vol. 178, pp. 587–598, 2018.

[10] K. M. Rahla, R. Mateus, and L. Bragança, "Comparative sustainability assessment of binary blended concretes using supplementary cementitious materials (SCMs) and ordinary Portland cement (OPC)," *J. Clean. Prod.*, vol. 220, pp. 445–459, 2019.

[11] K. H. Yang, Y. B. Jung, M. S. Cho, and S. H. Tae, "Effect of supplementary cementitious materials on reduction of CO2 emissions from concrete," *Handb. Low Carbon Concr.*, vol. 103, pp. 89–110, 2014.

[12] M. Velay-Lizancos, I. Martinez-Lage, M. Azenha, J. Granja, and P. Vazquez-Burgo, "Concrete with fine and coarse recycled aggregates: E-modulus evolution, compressive strength and non-destructive testing at early ages," *Constr. Build. Mater.*, vol. 193, pp. 323–331, 2018.

[13] L. Evangelista and J. de Brito, "Mechanical behaviour of concrete made with fine recycled concrete aggregates," *Cem. Concr. Compos.*, vol. 29, no. 5, pp. 397–401, 2007.

[14] Z. Shayegan, C. S. S. Lee, and F. Haghighat, "TiO2 photocatalyst for removal of volatile organic compounds in gas phase – A review," *Chem. Eng. J.*, vol. 334, pp. 2408–2439, 2018.

[15] J. S. S. Dalton, P. A. A. Janes, N. G. G. Jones, J. A. A. Nicholson, K. R. R. Hallam, and G. C. C. Allen, "Photocatalytic oxidation of NOx gases using TiO2: A surface spectroscopic approach," *Environ. Pollut.*, vol. 120, no. 2, pp. 415–422, 2002.

[16] C. J. Churchill and D. K. Panesar, "Life-cycle cost analysis of highway noise barriers designed with photocatalytic cement," *Struct. Infrastruct. Eng.*, vol. 9, no. 10, pp. 983–998, 2013.

[17] M. Hassan, "Life-cycle assessment of titanium dioxide coatings," *ASCE 2009 Construction Research Congress*, 2009.

[18] A. Baral, S. Sen, and J. R. Roesler, "Use phase assessment of photocatalytic cool pavements," *J. Clean. Prod.*, vol. 190, pp. 722–728, 2018.

[19] F. Xi *et al.*, "Substantial global carbon uptake by cement carbonation," *Nat. Geosci.*, vol. 9, no. 12, pp. 880–887, 2016.

[20] U.S. Geological Survey, "Mineral Commodity Summaries," 2020.

[21] W. Ashraf, J. Olek, and S. Sahu, "Phase evolution and strength development during carbonation of low-lime calcium silicate cement (CSC)," *Constr. Build. Mater.*, vol. 210, pp. 473–482, 2019.

[22] W. Ashraf, "Carbonation of cement-based materials: Challenges and opportunities," *Constr. Build. Mater.*, vol. 120, pp. 558–570, 2016.

[23] W. Ashraf, J. Olek, and J. Jain, "Microscopic features of non-hydraulic calcium silicate cement paste and mortar," *Cem. Concr. Res.*, vol. 100, pp. 361–372, 2017.

[24] J. A. Jain, A. Seth, and N. DeCristofaro, "Environmental impact and durability of carbonated calcium silicate concrete," *Proc. Inst. Civ. Eng. Constr. Mater.*, vol. 172, no. 4, pp. 179–191, 2019.

[25] V. Rostami, Y. Shao, A. J. Boyd, and Z. He, "Microstructure of cement paste subject to early carbonation curing," *Cem. Concr. Res.*, vol. 42, no. 1, pp. 186–193, 2012.

[26] D. Zhang, X. Cai, and Y. Shao, "Carbonation curing of precast fly ash concrete," *J. Mater. Civ. Eng.*, vol. 28, no. 11, pp. 1–9, 2016.

[27] A. Neves Junior, J. Dweck, R. D. T. Filho, B. Ellis, and V. Li, "Determination of CO2 capture during accelerated carbonation of engineered cementitious composite pastes by thermogravimetry," *J. Therm. Anal. Calorim.*, vol. 138, no. 1, pp. 97–109, 2019.

[28] D. Sharma and S. Goyal, "Accelerated carbonation curing of cement mortars containing cement kiln dust: An effective way of CO2 sequestration and carbon footprint reduction," *J. Clean. Prod.*, vol. 192, pp. 844–854, 2018.

[29] V. Francioso, C. Moro, I. Martinez-Lage, and M. Velay-Lizancos, "Curing temperature: A key factor that changes the effect of TiO2 nanoparticles on mechanical properties, calcium hydroxide formation and pore structure of cement mortars," *Cem. Concr. Compos.*, vol. 104, p. 103374, 2019.

[30] ASTM, "ASTM C 150/ C150M-20 - Standard specification for portland cement," *ASTM Int.*, 2020.

[31] AAHSTO, “AASHTO M85-20 - Standard Specification for Portland Cement,” *AAHSTO Int.*, 2020.

[32] ASTM, “ASTM C989/C989M − Standard specification for slag cement for use in concrete and mortars,” *ASTM Int.*, vol. 44, pp. 1–8, 2013.

[33] ASTM, “ASTM C33/C33M - Standard Specification for Concrete Aggregates,” *ASTM Int.*, 2018.

[34] ASTM, “ASTM C136/C136M - Standard Test Method for Sieve Analysis of Fine and Coarse Aggregates,” *ASTM Int.*, 2014.

[35] ASTM, “ASTM C128 - Standard Test Method for Relative Density (Specific Gravity) and Absorption of Fine Aggregate,” *ASTM Int.*, 2015.

[36] ASTM, “ASTM C349 - Standard Test Method for Compressive Strength,” *ASTM Int.*, 2018.

[37] K. Scrivener, R. Snellings, and B. Lothenbach, *A Practical Guide to Microstructural Analysis of Cementitious Materials*. 2015.

[38] N. Doebelin and R. Kleeberg, “Profex: A graphical user interface for the Rietveld refinement program BGMN,” *J. Appl. Crystallogr.*, vol. 48, no. 5, pp. 1573–1580, Oct. 2015.

[39] L. Cassar, C. Pepe, G. Tognon, G. L. Guerrini, and R. Amadelli, “White cement for architectural concrete, possessing photocatalytic properties,” 2003.

[40] L. Cassar, “Photocatalysis of cementitious materials: Clean buildings and clean air,” *MRS Bull.*, vol. 29, no. 05, pp. 328–331, 2004.

[41] L. Cassar, A. Beeldens, N. Pimpinelli, G. L. Guerrini, and S. D. Milanese, “Photocatalysis of cementitious materials,” *Int. RILEM Symp. Photocatal. Environ. Constr. Mater.*, pp. 131–145, 2007.

[42] A. Fujishima and X. Zhang, “Titanium dioxide photocatalysis: present situation and future approaches,” *Comptes Rendus Chim.*, vol. 9, no. 5–6, pp. 750–760, 2006.

[43] B. Ma, H. Li, X. Li, J. Mei, and Y. Lv, “Influence of nano-TiO2 on physical and hydration characteristics of fly ash–cement systems,” *Constr. Build. Mater.*, vol. 122, pp. 242–253, 2016.

[44] J. Chen, S. C. Kou, and C. S. Poon, “Hydration and properties of nano-TiO2 blended cement composites,” *Cem. Concr. Compos.*, vol. 34, no. 5, pp. 642–649, May 2012.

[45] A. Nazari and S. Riahi, “The effects of TiO2 nanoparticles on properties of binary blended concrete,” *J. Compos. Mater.*, vol. 45, no. 11, pp. 1181–1188, 2011.

[46] B. Y. Lee, A. Jayapalan, and K. E. Kurtis, “Effects of nano-TiO2 on properties of cement-based materials,” *Mag. Concr. Res.*, vol. 65, no. 21, pp. 1293–1302, Nov. 2013.

[47] R. Zhang, X. Cheng, P. Hou, and Z. Ye, “Influences of nano-TiO2 on the properties of cement-based materials: Hydration and drying shrinkage,” *Constr. Build. Mater.*, vol. 81, pp. 35–41, 2015.

[48] P. Duan, C. Yan, W. Luo, and W. Zhou, “Effects of adding nano-TiO2 on compressive strength, drying shrinkage, carbonation and microstructure of fluidized bed fly ash based geopolymer paste,” *Constr. Build. Mater.*, vol. 106, pp. 115–125, 2016.

[49] L. Y. Yang, Z. J. Jia, Y. M. Zhang, and J. G. Dai, "Effects of nano-TiO2 on strength, shrinkage and microstructure of alkali activated slag pastes," *Cem. Concr. Compos.*, vol. 57, pp. 1–7, 2015.

[50] K. P. Teixeira, I. P. Rocha, L. D. S. Carneiro, J. Flores, E. A. Dauer, and A. Ghahremaninezhad, "The effect of curing temperature on the properties of cement pastes modified with TiO2 nanoparticles," *Materials (Basel).*, vol. 9, no. 11, pp. 1–15, 2016.

[51] J. Ying, B. Zhou, and J. Xiao, "Pore structure and chloride diffusivity of recycled aggregate concrete with nano-SiO2 and nano-TiO2," *Constr. Build. Mater.*, vol. 150, pp. 49–55, 2017.

[52] M. Jalal, M. Fathi, and M. Farzad, "Effects of fly ash and TiO2 nanoparticles on rheological, mechanical, microstructural and thermal properties of high strength self compacting concrete," *Mech. Mater.*, vol. 61, pp. 11–27, 2013.

[53] D. Wang, W. Zhang, Y. Ruan, X. Yu, and B. Han, "Enhancements and mechanisms of nanoparticles on wear resistance and chloride penetration resistance of reactive powder concrete," *Constr. Build. Mater.*, vol. 189, pp. 487–497, 2018.

[54] E. Mohseni, B. M. Miyandehi, J. Yang, and M. A. Yazdi, "Single and combined effects of nano-SiO2, nano-Al2O3 and nano-TiO2 on the mechanical, rheological and durability properties of self-compacting mortar containing fly ash," *Constr. Build. Mater.*, vol. 84, pp. 331–340, 2015.

[55] Atta-ur-Rehman, A. Qudoos, H. G. Kim, and J. S. Ryou, "Influence of titanium dioxide nanoparticles on the sulfate attack upon ordinary Portland cement and slag-blended mortars," *Materials (Basel).*, vol. 11, no. 3, 2018.

[56] B. Ma, H. Li, J. Mei, X. Li, and F. Chen, "Effects of nano-TiO2 on the toughness and durability of cement-based material," *Adv. Mater. Sci. Eng.*, vol. 2015, 2015.

[57] H. Noorvand, A. A. Abang Ali, R. Demirboga, N. Farzadnia, and H. Noorvand, "Incorporation of nano TiO2 in black rice husk ash mortars," *Constr. Build. Mater.*, vol. 47, pp. 1350–1361, 2013.

[58] J. Ren, Y. Lai, and J. Gao, "Exploring the influence of SiO2 and TiO2 nanoparticles on the mechanical properties of concrete," *Constr. Build. Mater.*, vol. 175, pp. 277–285, 2018.

[59] A. Zhao, J. Yang, and E. H. Yang, "Self-cleaning engineered cementitious composites," *Cem. Concr. Compos.*, vol. 64, pp. 74–83, 2015.

[60] T. Meng, Y. Yu, X. Qian, S. Zhan, and K. Qian, "Effect of nano-TiO2 on the mechanical properties of cement mortar," *Constr. Build. Mater.*, vol. 29, pp. 241–245, Apr. 2012.

[61] R. Khataee, V. Heydari, L. Moradkhannejhad, M. Safarpour, and S. W. Joo, "Self-cleaning and mechanical properties of modified white cement with nanostructured TiO2," *J. Nanosci. Nanotechnol.*, vol. 13, no. 7, pp. 5109–5114, 2013.

[62] S. Rao, P. Silva, and J. De Brito, "Experimental study of the mechanical properties and durability of self-compacting mortars with nano materials (SiO2 and TiO2)," *Constr. Build. Mater.*, vol. 96, pp. 508–517, 2015.

[63] E. Mohseni, F. Naseri, R. Amjadi, M. M. Khotbehsara, and M. M. Ranjbar, "Microstructure and durability properties of cement mortars containing nano-TiO2 and rice husk ash," *Constr. Build. Mater.*, vol. 114, pp. 656–664, 2016.

[64] C. Moro, V. Francioso, M. Schager, and M. Velay-Lizancos, "TiO2 nanoparticles influence on the environmental performance of natural and recycled mortars: A life cycle assessment," *Environ. Impact Assess. Rev.*, vol. 84, p. 106430, 2020.

[65] B. Han *et al.*, "Reactive powder concrete reinforced with nano SiO2-coated TiO2," *Constr. Build. Mater.*, vol. 148, pp. 104–112, Sep. 2017.

[66] Z. Li *et al.*, "Effect of nano-titanium dioxide on mechanical and electrical properties and microstructure of reactive powder concrete," *Mater. Res. Express*, vol. 4, no. 9, 2017.

[67] J. Liu, Q. Li, and S. Xu, "Influence of nanoparticles on fluidity and mechanical properties of cement mortar," *Constr. Build. Mater.*, vol. 101, pp. 892–901, 2015.

[68] A. Nazari and S. Riahi, "The effect of TiO2 nanoparticles on water permeability and thermal and mechanical properties of high strength self-compacting concrete," *Mater. Sci. Eng. A*, vol. 528, no. 2, pp. 756–763, 2010.

[69] R. Zhang, X. Cheng, P. Hou, and Z. Ye, "Influences of nano-TiO2 on the properties of cement-based materials: Hydration and drying shrinkage," *Constr. Build. Mater.*, vol. 81, pp. 35–41, 2015.

[70] H. Noorvand, A. A. Abang Ali, R. Demirboga, N. Farzadnia, and H. Noorvand, "Incorporation of nano TiO2 in black rice husk ash mortars," *Constr. Build. Mater.*, vol. 47, pp. 1350–1361, 2013.

[71] P. Parthiban and J. Karthikeyan, "Artificial neural network to predict the compressive strength of semilightweight concrete containing ultrafine GGBS," *J. Test. Eval.*, vol. 48, no. 2, 2020.

[72] D. C. Feng *et al.*, "Machine learning-based compressive strength prediction for concrete: An adaptive boosting approach," *Constr. Build. Mater.*, vol. 230, p. 117000, 2020.

[73] J. Zhang and Y. Zhao, "The mechanical properties and microstructure of ultra-high-performance concrete containing various supplementary cementitious materials," *J. Sustain. Cem. Mater.*, vol. 6, no. 4, pp. 254–266, 2017.

[74] E. M. Golafshani, A. Behnood, and M. Arashpour, "Predicting the compressive strength of normal and High-Performance Concretes using ANN and ANFIS hybridized with Grey Wolf Optimizer," *Constr. Build. Mater.*, vol. 232, 2020.

[75] J. Y. Park, Y. G. Yoon, and T. K. Oh, "Prediction of concrete strength with P-, S-, R-wave velocities by support vector machine (SVM) and artificial neural network (ANN)," *Appl. Sci.*, vol. 9, no. 19, 2019.

[76] W. S. McCulloch and W. Pitts, "A logical calculus of the ideas immanent in nervous activity," *Bull. Math. Biophys.*, 1943.

[77] L. Fausett, "Fundamentals Of neural network architectures, algorithms, and applications," *Inc., New Jersey*, 1994.

[78] M. M. Alshihri, A. M. Azmy, and M. S. El-Bisy, “Neural networks for predicting compressive strength of structural light weight concrete,” *Constr. Build. Mater.*, vol. 23, no. 6, 2009.

[79] S. Subaşi, “Prediction of mechanical properties of cement containing class C fly ash by using artificial neural network and regression technique,” *Sci. Res. Essays*, vol. 4, no. 4, pp. 289–297, 2009.

[80] V. Chandwani, V. Agrawal, and R. Nagar, “Modeling slump of ready mix concrete using genetic algorithms assisted training of artificial neural networks,” *Expert Syst. Appl.*, vol. 42, no. 2, pp. 885–893, 2015.

[81] H. G. Ni and J. Z. Wang, “Prediction of compressive strength of concrete by neural networks,” *Cem. Concr. Res.*, vol. 30, no. 8, 2000.

[82] C. Moro, V. Francioso, and M. Velay-Lizancos, “Nano-TiO2 effects on high temperature resistance of recycled mortars,” *J. Clean. Prod.*, vol. 263, p. 121581, 2020.

[83] B. B. Han *et al.*, “Reactive powder concrete reinforced with nano SiO2 -coated TiO2,” *Constr. Build. Mater.*, vol. 148, pp. 104–112, Sep. 2017.

[84] M. M. Salman, K. M. Eweed, and A. M. Hameed, “Influence of partial replacement TiO2 nanoparticles on the compressive and flexural strength of ordinary cement mortar,” *Al-Nahrain Univ. Coll. Eng. J.*, vol. 19, no. 2, pp. 265–270, 2016.

[85] T. Kim and J. Olek, “Effects of sample preparation and interpretation of thermogravimetric curves on calcium hydroxide in hydrated pastes and mortars,” *Transp. Res. Rec. J. Transp. Res. Board*, vol. 2290, no. 1, pp. 10–18, Jan. 2012.

[86] S. Brunauer, J. Sklany, I. Odler, and M. Yudenfreund, “Hardened Portland cement pastes of low porosity,” *Cem. Concr. Res.*, vol. 3, pp. 279–293, 1973.

[87] J. Beaudoin and I. Odler, “Hydration, setting and hardening of Portland cement,” in *Lea’s Chemistry of Cement and Concrete*, 2019, pp. 157–250.

[88] I. Odler, M. Rossler, and I. Odler, “Investigations on the relationship between porosity, structure and strength of hydrated Portland cement pastes. II. Effect of pore structure and of degree of hydration,” *Cem. Concr. Res.*, vol. 15, pp. 320–330, 1985.

[89] T. Slamečka and F. Škvára, “The effect of water ratio on microstructure and composition of the hydration products of Portland cement pastes,” *Ceram. - Silikaty*, vol. 46, no. 4, pp. 152–158, 2002.

[90] R. H. Mills, “Factors influencing cessation of hydration in water cured cement pastes,” *Symposium on Structure of Portland Cement Paste and Concrete*, no. HRB Special Report 90, Highway Research Board, Washington. pp. 406–424, 1966.

[91] B. R. Gurjar, T. M. Butler, M. G. Lawrence, and J. Lelieveld, “Evaluation of emissions and air quality in megacities,” *Atmos. Environ.*, vol. 42, no. 7, pp. 1593–1606, 2008.

[92] A. J. Cohen *et al.*, “The global burden of disease due to outdoor air pollution,” *J. Toxicol. Environ. Heal. - Part A*, vol. 68, no. 13–14, pp. 1301–1307, 2005.

[93] B. Ostro, “Outdoor air pollution: Assessing the environmental burden of disease at national and local levels,” *World Heal. Organ. Prot. Hum. Environ. Geneva*, no. Environmental Burden of Disease Series, No. 5, 2004.

[94] S. D. Beevers, E. Westmoreland, M. C. de Jong, M. L. Williams, and D. C. Carslaw, “Trends in NOx and NO2 emissions from road traffic in Great Britain,” *Atmos. Environ.*, vol. 54, no. 2, pp. 107–116, 2012.

[95] S. Rezaei *et al.*, “Investigation of the levels of air criteria pollutants effecting on health in Dogonbadan city and description of air quality using AQI index,” *Acta Medica Mediterr.*, vol. 32, pp. 1449–1455, 2016.

[96] Y. Li, Y. H. Chiu, and L. C. Lu, “Energy, CO2, AQI and economic performance in 31 cities in China: a slacks-based dynamic data envelopment analysis,” *Carbon Manag.*, vol. 10, no. 3, pp. 269–286, 2019.

[97] A. P. Jones, “Indoor air quality and health,” vol. 33, pp. 4535–4564, 1999.

[98] G. D’Amato, L. Cecchi, M. D’Amato, and G. Liccardi, “Urban air pollution and climate change as environmental risk factors of respiratory allergy: An update,” *J. Investig. Allergol. Clin. Immunol.*, vol. 20, no. 2, pp. 95–102, 2010.

[99] A. Singh and M. Agrawal, “Acid rain and its ecological consequences,” *J. Environ. Biol.*, vol. 29, no. 1, pp. 15–24, 2008.

[100] J. Lelieveld, J. S. Evans, M. Fnais, D. Giannadaki, and A. Pozzer, “The contribution of outdoor air pollution sources to premature mortality on a global scale,” *Nature*, vol. 525, no. 7569, pp. 367–371, 2015.

[101] M. Guarnieri and J. R. Balmes, “Outdoor air pollution and asthma,” *Lancet*, vol. 383, no. 9928, pp. 1581–1592, 2014.

[102] UNFCCC, “Kyoto protocol reference manual on accounting of emissions and assigned amount,” 2008.

[103] UNFCCC, “Paris Agreement to the United Nations Framework Convention on Climate Change,” 2015.

[104] C. F. Schleussner *et al.*, “Differential climate impacts for policy-relevant limits to global warming: The case of 1.5°C and 2°C,” *Earth Syst. Dyn.*, vol. 7, no. 2, pp. 327–351, 2016.

[105] C. F. Schleussner *et al.*, “Science and policy characteristics of the Paris Agreement temperature goal,” *Nat. Clim. Chang.*, vol. 6, no. 9, pp. 827–835, 2016.

[106] Z. Zhang and B. Wang, “Research on the life-cycle CO2 emission of China’s construction sector,” *Energy Build.*, vol. 112, no. 92, pp. 244–255, 2016.

[107] P. Alaejos Gutierrez, “Tipos y propiedades de áridos reciclados (Spanish),” *Inf. del CEDEX para el Minist. Medio Ambient.*, 2008.

[108] M. Velay-Lizancos, I. Martinez-Lage, M. Azenha, and P. Vazquez-Burgo, “Influence of temperature in the evolution of compressive strength and in its correlations with UPV in eco-concretes with recycled materials,” *Constr. Build. Mater.*, vol. 124, pp. 276–286, 2016.

[109] V. Corinaldesi, “Mechanical and elastic behaviour of concretes made of recycled-concrete coarse aggregates,” *Constr. Build. Mater.*, vol. 24, no. 9, pp. 1616–1620, 2010.

[110] J. Thomas, N. N. Thaickavil, and P. M. Wilson, “Strength and durability of concrete containing recycled concrete aggregates,” *J. Build. Eng.*, vol. 19, pp. 349–365, 2018.

[111] B. Han *et al.*, “Nano-core effect in nano-engineered cementitious composites,” *Compos. Part A Appl. Sci. Manuf.*, vol. 95, pp. 100–109, 2017.

[112] W. Shen, C. Zhang, Q. Li, W. Zhang, L. Cao, and J. Ye, “Preparation of titanium dioxide nano particle modified photocatalytic self-cleaning concrete,” *J. Clean. Prod.*, vol. 87, pp. 762–765, 2015.

[113] N. Salemi, K. Behfarnia, and S. A. Zaree, “Effect of nanoparticles on frost durability of concrete,” *Asian J. Civ. Eng.*, vol. 15, no. 3, pp. 411–420, 2014.

[114] S. N. Mat Saliah, N. Md Nor, and M. I. Jamaludin, “The effects of TiO2 in the performance of mortar,” *Appl. Mech. Mater.*, vol. 773–774, pp. 1027–1031, 2015.

[115] Z. Li, S. Ding, X. Yu, B. Han, and J. Ou, “Multifunctional cementitious composites modified with nano titanium dioxide: A review,” *Compos. Part A Appl. Sci. Manuf.*, vol. 111, pp. 115–137, 2018.

[116] M. H. Zhang and H. Li, “Pore structure and chloride permeability of concrete containing nano-particles for pavement,” *Constr. Build. Mater.*, vol. 25, no. 2, pp. 608–616, 2011.

[117] N. D. Oikonomou, “Recycled concrete aggregates,” *Cem. Concr. Compos.*, vol. 27, no. 2, pp. 315–318, 2005.

[118] I. S. Jawahir, S. K. Sikdar, and Y. Huang, *Treatise on sustainability science and engineering*. 2013.

[119] J. Sjunnesson, “Life Cycle Assessment of Concrete,” 2005.

[120] S. B. Marinkovic, *Life cycle assessment (LCA) aspects of concrete*. 2013.

[121] G. K. C. Ding, “Life cycle assessment (LCA) of sustainable building materials: An overview,” *Eco-Efficient Constr. Build. Mater. Life Cycle Assess. (LCA), Eco-Labelling Case Stud.*, pp. 38–62, 2013.

[122] NRMCA, “Life Cycle Assessment of Concrete Buildings,” 2011.

[123] D. K. Panesar, K. E. Seto, and C. J. Churchill, “Impact of the selection of functional unit on the life cycle assessment of green concrete,” *Int. J. Life Cycle Assess.*, vol. 22, no. 12, pp. 1969–1986, 2017.

[124] A. M. Braga, J. D. Silvestre, and J. de Brito, “Compared environmental and economic impact from cradle to gate of concrete with natural and recycled coarse aggregates,” *J. Clean. Prod.*, vol. 162, no. 2017, pp. 529–543, 2017.

[125] S. Marinković, V. Radonjanin, M. Malešev, and I. Ignjatović, “Comparative environmental assessment of natural and recycled aggregate concrete,” *Waste Manag.*, vol. 30, no. 11, pp. 2255–2264, 2010.

[126] Y. Zhang, W. Luo, J. Wang, Y. Wang, Y. Xu, and J. Xiao, "A review of life cycle assessment of recycled aggregate concrete," *Constr. Build. Mater.*, vol. 209, pp. 115–125, 2019.

[127] P. Visintin, T. Xie, and B. Bennett, "A large-scale life-cycle assessment of recycled aggregate concrete: The influence of functional unit, emissions allocation and carbon dioxide uptake," *J. Clean. Prod.*, p. 119243, 2019.

[128] I. Martínez-Lage, P. Vázquez-Burgo, M. Velay-Lizancos, I. Lage, P. Vázquez-Burgo, and M. Velay-Lizancos, "Sustainability evaluation of concretes with mixed recycled aggregate based on holistic approach: Technical, economic and environmental analysis," *Waste Manag.*, vol. 104, pp. 9–19, Jan. 2020.

[129] M. Dolatabadi, "Properties and performance of photocatalytic concrete," 2013.

[130] P. Feng, H. Chang, G. Xu, Q. Liu, Z. Jin, and J. Liu, "Feasibility of utilizing recycled aggregate concrete for revetment construction of the lower Yellow River," *Materials (Basel).*, vol. 12, no. 24, pp. 1–20, 2019.

[131] "ISO 14040: Environmental management — Life cycle assessment — Principles and framework," 2006.

[132] "ISO 14044: Environmental management - Life cycle assessment - Requirements and guidelines," 2006.

[133] S. Marinković, J. Dragaš, I. Ignjatović, and N. Tošić, "Environmental assessment of green concretes for structural use," *J. Clean. Prod.*, vol. 154, pp. 633–649, 2017.

[134] M. L. Marceau, M. M. A. Nisbet, and M. G. Vangeem, "Life Cycle Inventory of Portland Cement Concrete," 2007.

[135] T. Kikuchi and Y. Kuroda, *Carbon dioxide uptake in demolished and crushed concrete*, vol. 9, no. 1. 2011.

[136] R. Kurda, J. D. Silvestre, and J. de Brito, "Life cycle assessment of concrete made with high volume of recycled concrete aggregates and fly ash," *Resour. Conserv. Recycl.*, vol. 139, pp. 407–417, 2018.

[137] R. Kurda, "Sustainable Development of Cement-Based Materials: Application to Recycled Aggregates Concrete," Universidade de Lisboa, 2017.

[138] P. Rodrigues *et al.*, "Methodology for the assessment of the ecotoxicological potential of construction materials," *Materials (Basel).*, vol. 10, no. 6, 2017.

[139] U.S. Environmental Protection Agency (EPA), "TRACI methodology characterization factors," 2011. [Online]. Available: https://www.epa.gov/chemical-research/tool-reduction-and-assessment-chemicals-and-other-environmental-impacts-traci.

[140] Leiden University, "CML methodology characterization factors," 2016. [Online]. Available: https://www.universiteitleiden.nl/en/research/research-output/science/cml-ia-characterisation-factors.

[141] M. Ryberg, M. D. M. Vieira, M. Zgola, J. Bare, and R. K. Rosenbaum, "Updated US and Canadian normalization factors for TRACI 2.1," *Clean Technol. Environ. Policy*, vol. 16, no. 2, pp. 329–339, 2014.

[142] A. W. Sleeswijk, L. F. C. M. van Oers, J. B. Guinée, J. Struijs, and M. A. J. Huijbregts, "Normalisation in product life cycle assessment: An LCA of the global and European economic systems in the year 2000," *Sci. Total Environ.*, vol. 390, no. 1, pp. 227–240, 2008.

[143] M. Wijayasundara, P. Mendis, and R. H. Crawford, "Integrated assessment of the use of recycled concrete aggregate replacing natural aggregate in structural concrete," *J. Clean. Prod.*, vol. 174, pp. 591–604, 2018.

[144] G. Azúa, M. González, P. Arroyo, and Y. Kurama, "Recycled coarse aggregates from precast plant and building demolitions: Environmental and economic modeling through stochastic simulations," *J. Clean. Prod.*, vol. 210, pp. 1425–1434, 2019.

[145] A. H. Shekari and M. S. Razzaghi, "Influence of nano particles on durability and mechanical properties of high performance concrete," *Procedia Eng.*, vol. 14, pp. 3036–3041, 2011.

[146] J. V. S. De Melo, G. Trichês, P. J. P. Gleize, and J. Villena, "Development and evaluation of the efficiency of photocatalytic pavement blocks in the laboratory and after one year in the field," *Constr. Build. Mater.*, vol. 37, pp. 310–319, 2012.

[147] M. Pérez-Nicolás *et al.*, "Photocatalytic NOx abatement by calcium aluminate cements modified with TiO2: Improved NO2 conversion," *Cem. Concr. Res.*, vol. 70, no. 2, pp. 67–76, 2015.

[148] C. S. Poon and E. Cheung, "NO removal efficiency of photocatalytic paving blocks prepared with recycled materials," *Constr. Build. Mater.*, vol. 21, no. 8, pp. 1746–1753, 2007.

[149] G. Hüsken, M. Hunger, and H. J. H. Brouwers, "Experimental study of photocatalytic concrete products for air purification," *Build. Environ.*, vol. 44, no. 12, pp. 2463–2474, 2009.

[150] C. Toro, B. T. Jobson, L. Haselbach, S. Shen, and S. H. Chung, "Photoactive roadways: Determination of CO, NO and VOC uptake coefficients and photolabile side product yields on TiO2 treated asphalt and concrete," *Atmos. Environ.*, vol. 139, pp. 37–45, 2016.

[151] C. George *et al.*, "Impact of photocatalytic remediation of pollutants on urban air quality," *Front. Environ. Sci. Eng.*, vol. 10, no. 5, pp. 1–11, 2016.

[152] R. M. Ghantous, Y. Farnam, E. Unal, and J. Weiss, "The influence of carbonation on the formation of calcium oxychloride," *Cem. Concr. Compos.*, vol. 73, pp. 185–191, 2016.

[153] UNFCCC, "United Nations Framework Convention on climate change," 1992.

[154] World Health Organization, "Ambient (outdoor) air pollution," 2018. [Online]. Available: https://www.who.int/en/news-room/fact-sheets/detail/ambient-(outdoor)-air-quality-and-health. [Accessed: 21-Apr-2020].

[155] B. Lagerblad, *Carbon dioxide uptake during concrete life cycle - State of the art*, no. 2. 2005.

[156] G. Villain and G. Platret, "Two experimental methods to determine carbonation profiles in concrete," *ACI Mater. J.*, vol. 103, no. 4, pp. 265–271, 2006.

[157] G. Villain, M. Thiery, and G. Platret, "Measurement methods of carbonation profiles in concrete: Thermogravimetry, chemical analysis and gammadensimetry," *Cem. Concr. Res.*, vol. 37, no. 8, pp. 1182–1192, 2007.

[158] GatesNotes, “A Stunning Statistic About China and Concrete,” 2014. [Online]. Available: https://www.gatesnotes.com/About-Bill-Gates/Concrete-in-China. [Accessed: 21-Apr-2020].

[159] B. Šavija and M. Luković, “Carbonation of cement paste: Understanding, challenges, and opportunities,” *Constr. Build. Mater.*, vol. 117, pp. 285–301, 2016.

[160] NOAA GML, “Trends in Atmospheric Carbon Dioxide,” *Earth System Research Laboratories*, 2020. [Online]. Available: https://www.esrl.noaa.gov/gmd/ccgg/trends/global.html. [Accessed: 16-Jun-2020].

[161] International Organization for Standardization (ISO), “ISO 1920-12: Testing of concrete - Part 12: Determination of the carbonation resistance of concrete - Accelerated carbonation method.,” 2015.

[162] T. Bakharev, J. G. Sanjayan, and Y. B. Cheng, “Resistance of alkali-activated slag concrete to acid attack,” *Cem. Concr. Res.*, vol. 33, no. 10, pp. 1607–1611, 2003.

[163] R. V. Silva, R. Neves, J. De Brito, and R. K. Dhir, “Carbonation behaviour of recycled aggregate concrete,” *Cem. Concr. Compos.*, vol. 62, pp. 22–32, 2015.

[164] D. Zhang, Z. Ghouleh, and Y. Shao, “Review on carbonation curing of cement-based materials,” *J. CO2 Util.*, vol. 21, pp. 119–131, 2017.

[165] M. Fernández Bertos, S. J. R. Simons, C. D. Hills, and P. J. Carey, “A review of accelerated carbonation technology in the treatment of cement-based materials and sequestration of CO2,” *J. Hazard. Mater.*, vol. 112, no. 3, pp. 193–205, 2004.

[166] F. Pacheco Torgal, S. Miraldo, J. A. Labrincha, and J. De Brito, “An overview on concrete carbonation in the context of eco-efficient construction: Evaluation, use of SCMs and/or RAC,” *Constr. Build. Mater.*, vol. 36, pp. 141–150, 2012.

[167] J. Wang *et al.*, “Accelerated carbonation of hardened cement pastes: Influence of porosity,” *Constr. Build. Mater.*, vol. 225, pp. 159–169, 2019.

[168] Z. Tu, M. Z. Guo, C. S. Poon, and C. Shi, “Effects of limestone powder on CaCO3 precipitation in CO2 cured cement pastes,” *Cem. Concr. Compos.*, vol. 72, pp. 9–16, 2016.

[169] H. El-Hassan and Y. Shao, “Early carbonation curing of concrete masonry units with Portland limestone cement,” *Cem. Concr. Compos.*, vol. 62, pp. 168–177, 2015.

[170] V. Rostami, Y. Shao, and A. J. Boyd, “Durability of concrete pipes subjected to combined steam and carbonation curing,” *Constr. Build. Mater.*, vol. 25, no. 8, pp. 3345–3355, 2011.

[171] D. Zhang and Y. Shao, “Effect of early carbonation curing on chloride penetration and weathering carbonation in concrete,” *Constr. Build. Mater.*, vol. 123, pp. 516–526, 2016.

[172] V. Rostami, Y. Shao, and A. J. Boyd, “Carbonation curing versus steam curing for precast concrete production,” *J. Mater. Civ. Eng.*, vol. 24, no. 9, pp. 1221–1229, 2012.

[173] H. El-Hassan, Y. Shao, and Z. Ghouleh, “Reaction products in carbonation-cured lightweight concrete,” *J. Mater. Civ. Eng.*, vol. 25, no. 6, pp. 799–809, 2013.

[174] H. El-Hassan, Y. Shao, and Z. Ghouleh, “Effect of initial curing on carbonation of lightweight concrete masonry units,” *ACI Mater. J.*, vol. 110, no. 4, pp. 441–450, 2013.

[175] S. Siddique, A. Naqi, and J. G. Jang, “Influence of water to cement ratio on CO2 uptake capacity of belite-rich cement upon exposure to carbonation curing,” *Cem. Concr. Compos.*, vol. 111, 2020.

[176] V. S. (Vangipuram S. Ramachandran, *Handbook of thermal analysis of construction materials*. Noyes Publications, 2002.

[177] R. Gabrovšek, T. Vuk, and V. Kaučič, “Evaluation of the hydration of Portland cement containing various carbonates by means of thermal analysis,” *Acta Chim. Slov.*, vol. 53, no. 2, pp. 159–165, 2006.

[178] B. El-Jazairi and J. M. Illston, “A simultaneous semi-isothermal method of thermogravimetry and derivative thermogravimetry, and its application to cement pastes,” *Cem. Concr. Res.*, vol. 7, no. 3, pp. 247–257, May 1977.

[179] L. P. Singh, A. Goel, S. K. Bhattachharyya, S. Ahalawat, U. Sharma, and G. Mishra, “Effect of Morphology and Dispersibility of Silica Nanoparticles on the Mechanical Behaviour of Cement Mortar,” *Int. J. Concr. Struct. Mater.*, vol. 9, no. 2, pp. 207–217, Jun. 2015.

[180] N. Ukrainczyk, M. Ukrainczyk, J. Sipusic, and T. Matusinovic, “XRD and TGA Investigation of Hardened Cement Paste,” *11. Conf. Mater. Process. Frict. Wear MATRIB’06, Vela Luka*, pp. 22–24, 2006.

[181] J. Jain and N. Neithalath, “Analysis of calcium leaching behavior of plain and modified cement pastes in pure water,” *Cem. Concr. Compos.*, vol. 31, no. 3, pp. 176–185, Mar. 2009.

[182] T. Tracz and T. Zdeb, “Effect of hydration and carbonation progress on the porosity and permeability of cement pastes,” *Materials (Basel).*, vol. 12, no. 1, 2019.

[183] R. Kurihara and I. Maruyama, “Influences of nano-TiO2 particles on alteration of microstructure of hardened cement,” *Proc. Japan Concr. Inst.*, vol. 38, no. 1, pp. 219–224, 2016.

[184] M. Thiery, G. Villain, P. Dangla, and G. Platret, “Investigation of the carbonation front shape on cementitious materials: Effects of the chemical kinetics,” *Cem. Concr. Res.*, vol. 37, no. 7, pp. 1047–1058, 2007.

[185] A. Morandeau, M. Thiéry, and P. Dangla, “Investigation of the carbonation mechanism of CH and C-S-H in terms of kinetics, microstructure changes and moisture properties,” *Cem. Concr. Res.*, vol. 56, pp. 153–170, 2014.

[186] T. Chen and X. Gao, “Effect of carbonation curing regime on strength and microstructure of Portland cement paste,” *J. CO2 Util.*, vol. 34, pp. 74–86, 2019.

[187] J. Chang, Y. Gu, and W. S. Ansari, “Mechanism of blended steel slag mortar with CO2 curing exposed to sulfate attack,” *Constr. Build. Mater.*, vol. 251, pp. 1–11, 2020.

[188] A. Neves Junior, R. D. Toledo Filho, E. De Moraes Rego Fairbairn, and J. Dweck, “The effects of the early carbonation curing on the mechanical and porosity properties of high initial strength Portland cement pastes,” *Constr. Build. Mater.*, vol. 77, pp. 448–454, 2015.

[189] Y. Fang and J. Chang, “Microstructure changes of waste hydrated cement paste induced by accelerated carbonation,” *Constr. Build. Mater.*, vol. 76, pp. 360–365, 2015.

[190] J. F. Young, R. L. Berger, and J. Breese, "Accelerated curing of compacted calcium silicate mortars on exposure to CO2," *J. Am. Ceram. Soc.*, vol. 57, no. 9, pp. 394–397, 1974.

[191] W. A. Klemm and R. L. Berger, "Accelerated curing of cementitious systems by carbon dioxide," *Cem. Concr. Res.*, vol. 2, pp. 567–576, 1972.

[192] H. Huang *et al.*, "Carbonation curing for wollastonite-Portland cementitious materials: CO2 sequestration potential and feasibility assessment," *J. Clean. Prod.*, vol. 211, pp. 830–841, 2019.

[193] T. Chen and X. Gao, "Use of carbonation curing to improve mechanical strength and durability of pervious concrete," *ACS Sustain. Chem. Eng.*, vol. 8, no. 9, pp. 3872–3884, 2020.

[194] B. Johannesson and P. Utgenannt, "Microstructural changes caused by carbonation of cement mortar," *Cem. Concr. Res.*, vol. 31, no. 6, pp. 925–931, 2001.

[195] C. Moro, V. Francioso, and M. Velay-lizancos, "Modification of CO2 capture and pore structure of hardened cement paste made with nano-TiO2 addition : Influence of water-to-cement ratio and CO2 exposure age," *Constr. Build. Mater.*, vol. 275, p. 122131, 2021.

[196] D. Zhang and Y. Shao, "Early age carbonation curing for precast reinforced concretes," *Constr. Build. Mater.*, vol. 113, pp. 134–143, 2016.

[197] C. M. Hunt and L. A. Tomes, "Reaction of hardened portland cement paste with carbon dioxide," *J. Res. Natl. Bur. Stand. Sect. A Phys. Chem.*, vol. 66A, no. 6, p. 473, 1962.

[198] G. W. Groves, D. I. Rodway, and I. G. Richardson, "The carbonation of hardened cement pastes," *Adv. Cem. Res.*, vol. 3, no. 11, pp. 117–125, 1990.

[199] C. Moro *et al.*, "Influence of water-to-binder ratio on the optimum percentage of nano-TiO2 addition in terms of compressive strength of mortars: A laboratory and virtual experimental study based on ANN model," *Constr. Build. Mater.*, vol. 267, p. 120960, 2020.

[200] J. G. Jang and H. K. Lee, "Microstructural densification and CO2 uptake promoted by the carbonation curing of belite-rich Portland cement," *Cem. Concr. Res.*, vol. 82, pp. 50–57, 2016.

[201] J. Ibañez, L. Artus, R. Cusco, A. Lopez, E. Menedez, and M. C. Andrade, "Hydration and carbonation of monoclinic C2S and C3S studied by Raman spectroscopy," *J. Raman Spectrosc.*, vol. 38, pp. 61–67, 2007.

[202] J. Mo, Y. Zhang, Q. Xu, J. J. Lamson, and R. Zhao, "Photocatalytic purification of volatile organic compounds in indoor air: A literature review," *Atmos. Environ.*, vol. 43, no. 14, pp. 2229–2246, 2009.

[203] A. Maury and N. de Belie, "State of the art of TiO2 containing cementitious materials: Self-cleaning properties | Estado del arte de los materiales a base de cemento que contienen TiO2: Propiedades auto-limpiantes," *Mater. Constr.*, vol. 60, no. 298, pp. 33–50, 2010.

[204] K. Fujishima, A. and Honda, A. Fujishima, and K. Honda, "Electrochemical photolysis of water at a semiconductor electrode," *Nature*, vol. 238, p. 37, 1972.

[205] T. Saito, T. Iwase, J. Horie, and T. Morioka, “Mode of photocatalytic bactericidal action of powdered semiconductor TiO2 on mutans streptococci,” *J. Photochem. Photobiol. B Biol.*, vol. 14, no. 4, pp. 369–379, 1992.

[206] Z. Huang, P. C. Maness, D. M. Blake, E. J. Wolfrum, S. L. Smolinski, and W. A. Jacoby, “Bactericidal mode of titanium dioxide photocatalysis,” *J. Photochem. Photobiol. A Chem.*, vol. 130, no. 2–3, pp. 163–170, 2000.

[207] J. Chen and C. sun Poon, “Photocatalytic construction and building materials: From fundamentals to applications,” *Build. Environ.*, vol. 44, no. 9, pp. 1899–1906, 2009.

[208] A. Laplaza, E. Jimenez-Relinque, J. Campos, and M. Castellote, “Photocatalytic behavior of colored mortars containing TiO2 and iron oxide based pigments,” *Constr. Build. Mater.*, vol. 144, pp. 300–310, 2017.

[209] J. D. Cohen, G. Sierra-Gallego, and J. I. Tobón, “Evaluation of photocatalytic properties of Portland cement blended with titanium oxynitride (TiO2-xNy) nanoparticles,” *Coatings*, vol. 5, no. 3, pp. 465–476, 2015.

[210] P. Krishnan, M.-H. Zhang, L. Yu, and H. Feng, “Photocatalytic degradation of particulate pollutants and self-cleaning performance of TiO2-containing silicate coating and mortar,” *Constr. Build. Mater.*, vol. 44, pp. 309–316, 2013.

[211] B. Ruot, A. Plassais, F. Olive, L. Guillot, and L. Bonafous, “TiO2-containing cement pastes and mortars: Measurements of the photocatalytic efficiency using a Rhodamine B-based colourimetric test,” *Sol. Energy*, vol. 83, no. 10, pp. 1794–1801, 2009.

[212] I. Karatasios *et al.*, “Photo-induced carbonation of lime-TiO2 mortars,” *Appl. Catal. B Environ.*, vol. 95, no. 1–2, pp. 78–86, 2010.

[213] S. Afshar, S. Pordel, B. Tahmouresilerd, and A. Azad, “Improving the photocatalytic activity of modified anatase TiO2 with different concentrations of aluminum under visible light: mechanistic survey,” *Photochem. Photobiol.*, vol. 92, no. 6, pp. 783–789, 2016.

[214] E. Cerro-Prada, M. Manso, V. Torres, and J. Soriano, “Microstructural and photocatalytic characterization of cement-paste sol-gel synthesized titanium dioxide,” *Front. Struct. Civ. Eng.*, vol. 10, no. 2, pp. 189–197, 2016.

[215] M. Z. Guo, A. Maury-Ramirez, and C. S. Poon, “Photocatalytic activities of titanium dioxide incorporated architectural mortars: Effects of weathering and activation light,” *Build. Environ.*, vol. 94, pp. 395–402, 2015.

[216] M. V. Diamanti, F. Lollini, M. P. Pedeferri, and L. Bertolini, “Mutual interactions between carbonation and titanium dioxide photoactivity in concrete,” *Build. Environ.*, vol. 62, pp. 174–181, 2013.

[217] M. Vittoria *et al.*, “Durability of self-cleaning cement-based materials,” *Constr. Build. Mater.*, vol. 280, p. 122442, 2021.

[218] M. V. Diamanti *et al.*, “Long term self-cleaning and photocatalytic performance of anatase added mortars exposed to the urban environment,” *Constr. Build. Mater.*, vol. 96, pp. 270–278, 2015.

[219] C. Moro, V. Francioso, and M. Velay-Lizancos, “Impact of nano-TiO2 addition on the reduction of net CO2 emissions of cement pastes after CO2 curing,” *Cem. Concr. Compos.*, vol. 123, p. 104160, 2021.

[220] L. Pinho and M. J. Mosquera, “Titania-silica nanocomposite photocatalysts with application in stone self-cleaning,” *J. Phys. Chem. C*, vol. 115, no. 46, pp. 22851–22862, 2011.

[221] L. Pinho and M. J. Mosquera, “Photocatalytic activity of TiO2-SiO2 nanocomposites applied to buildings: Influence of particle size and loading,” *Appl. Catal. B Environ.*, vol. 134–135, pp. 205–221, 2013.

[222] P. Munafò, G. B. Goffredo, and E. Quagliarini, “TiO2-based nanocoatings for preserving architectural stone surfaces: An overview,” *Constr. Build. Mater.*, vol. 84, pp. 201–218, 2015.

[223] Y. Li *et al.*, “Environmental impact analysis of blast furnace slag applied to ordinary Portland cement production,” *J. Clean. Prod.*, vol. 120, pp. 221–230, 2016.

[224] J. R. Prusinski, M. L. Marceau, and M. G. Vangeem, “Life cycle inventory of slag cement concrete,” in *Proceedings of the 8th International Conference on Fly Ash, Silica Fume, Slag and Natural Pozzolans in Concrete*, 2004, pp. 1–33.

[225] P. Van Den Heede and N. De Belie, “Environmental impact and life cycle assessment (LCA) of traditional and ‘green’ concretes: Literature review and theoretical calculations,” *Cem. Concr. Compos.*, vol. 34, no. 4, pp. 431–442, 2012.

[226] Z. Yi, T. Wang, and R. Guo, “Sustainable building material from CO2 mineralization slag: Aggregate for concretes and effect of CO2 curing,” *J. CO2 Util.*, vol. 40, p. 101196, 2020.

[227] A. Dixit, H. Du, and S. D. Pang, “Carbon capture in ultra-high performance concrete using pressurized CO2 curing,” *Constr. Build. Mater.*, vol. 288, p. 123076, 2021.

[228] UNI, “UNI 11259 - Determination of the photocatalytic activity of hydraulic binders - Rhodamine test method.,” 2008.

[229] C. A. Schneider, W. S. Rasband, and K. W. Eliceiri, “NIH Image to ImageJ: 25 years of image analysis,” *Nat. Methods*, vol. 9, no. 7, pp. 671–675, 2012.

[230] M. V. Diamanti, B. Del Curto, M. Ormellese, and M. P. Pedeferri, “Photocatalytic and self-cleaning activity of colored mortars containing TiO2,” *Constr. Build. Mater.*, vol. 46, pp. 167–174, 2013.

[231] Atta-ur-Rehman, J. H. Kim, H. G. Kim, A. Qudoos, and J. S. Ryou, “Effect of leaching on the hardened, microstructural and self-cleaning characteristics of titanium dioxide containing cement mortars,” *Constr. Build. Mater.*, vol. 207, pp. 640–650, 2019.

[232] J. I. Tobón, J. D. Cohen, and L. Dorkis, “Photocatalytic activity under visible light irradiation of cement based materials containing TiO2-xNy nanoparticles,” *Rev. Fac. Ing.*, no. 94, pp. 87–96, 2020.

[233] D. Ravikumar, D. Zhang, G. Keoleian, S. Miller, V. Sick, and V. Li, “Carbon dioxide utilization in concrete curing or mixing might not produce a net climate benefit,” *Nat. Commun.*, vol. 12, no. 1, pp. 1–13, 2021.

PUBLICATIONS

Publications entirely related with the dissertation:

C. Moro, V. Francioso, M. Lopez-Arias and M. Velay-Lizancos. *'Modification of self-cleaning activity on cement pastes containing nano-TiO_2 due to CO_2 curing.'* Construction and Building Materials. (Submitted).

C. Moro, V. Francioso and M. Velay-Lizancos (2021). *'Impact of nano-TiO_2 addition on the reduction of net CO_2 emissions of cement pastes after CO_2 curing.'* Cement and Concrete Composites, vol. 123, p. 104160.
https://doi.org/10.1016/j.cemconcomp.2021.104160.

C. Moro, V. Francioso and M. Velay-Lizancos (2021). *'Modification of CO_2 capture and pore structure of hardened cement paste made with nano-TiO_2 addition: Influence of water-to-cement ratio and CO_2 exposure age.'* Construction and Building Materials, vol. 275, p. 122131. https://doi.org/10.1016/j.conbuildmat.2020.122131.

C. Moro, H. El-Fil, V. Francioso and M. Velay-Lizancos (2020). *'Influence of water-to-binder ratio on the optimum percentage of nano-TiO_2 addition in terms of compressive strength of mortars: A laboratory and virtual experimental study based on ANN model.'* Construction and Building Materials, vol. 275, p. 122131.
https://doi.org/10.1016/j.conbuildmat.2020.120960.

C. Moro, V. Francioso, M. Schager and M. Velay-Lizancos (2020). *'TiO_2 nanoparticles influence on the environmental performance of natural and recycled mortars: A life cycle assessment.'* Environmental Impact Assessment Review, vol. 84, p. 106430. https://doi.org/10.1016/j.eiar.2020.106430.

Manuscripts entirely related with the dissertation:

C. Moro, V. Francioso, M. Lopez-Arias and M. Velay-Lizancos. *'The impact of CO_2 uptake rate on the environmental impact of cementitious composites: A new dynamic GWP analysis.'* (Working paper).

Other publications:

V. Francioso, C. Moro, and M. Velay-Lizancos (2021). '*Effect of recycled concrete aggregate (RCA) on mortar's thermal conductivity susceptibility to variations of moisture content and ambient temperature.*' Journal of Building Engineering, vol. 43, p. 103208. https://doi.org/10.1016/j.jobe.2021.103208

V. Francioso, C. Moro, A. Castillo, and M. Velay-Lizancos (2020). '*Effect of elevated temperature on flexural behavior and fibers-matrix bonding of recycled PP fiber-reinforced cementitious composite.*' Construction and Building Materials, vol. 269, p. 121243. https://doi.org/10.1016/j.conbuildmat.2020.121243.

C. Moro, V. Francioso and M. Velay-Lizancos (2020). *'Nano-TiO_2 effects on high temperature resistance of recycled mortars.'* Journal of Cleaner Production, vol. 263, p. 121581. https://doi.org/10.1016/j.jclepro.2020.121581.

V. Francioso, C. Moro, I. Martinez-Lage, and M. Velay-Lizancos (2019). *'Curing temperature: A key factor that changes the effect of TiO_2 nanoparticles on mechanical properties, calcium hydroxide formation and pore structure of cement mortars.'* Cement and Concrete Composites., vol. 104, p. 103374.

https://doi.org/10.1016/j.cemconcomp.2019.103374.